Characterizing Controlled Low-Strength Materials (CLSM) for Narrow-Trench Reinstatement

by

Mohammad Rezaei

A thesis submitted in partial fulfillment of the requirements for the degree of

Doctor of Philosophy

Department of Civil and Environmental Engineering

University of Alberta

Abstract

Cutting the pavement to install a small diameter utility network, such as flexible pipes, conduits or telecommunication lines, is a common practice in urban areas. The last 200 meters of installation is known particularly difficult to deliver, with obstacles both above and below ground to navigate, and these difficulties increase installation time and cost. Micro-trenching (MT) is a variation of narrow-trenching (NT) in which the trench is as narrow as 25 to 40 mm. Providers have found a considerable saving in project time and cost when MT is employed instead of the traditional open-cut method. Due to its advantages, MT is growing in popularity as a means of quickly, efficiently, and cost-effectively installing the utility networks is in a metropolitan area. Hence, many utility installers are now switching to NT. Despite all the advantages, NT method is not being widely practiced around the world because municipalities are reluctant to accept the risks associated with it, including potential pavement damage, and lack of stability of the buried conduit in shallow depths in freeze-thaw climatic regions. Due to the narrow width of the trench and shallow depth of the installation, the quality of the backfilling plays a crucial role in the durability of the installation. The backfill materials in cold regions are exposed to harsh weather conditions including prolonged winter seasons, short thawing periods and long

summer days. This, as well as lack of available knowledge about the performance of the materials inside a narrow trench, resulted in many distress and failures in surveyed MT projects. This research study aims to improve the overall civil work of the NT projects. To serve this purpose, different backfilling materials and methods were investigated and properties of the three most promising alternatives for NT application, i.e cold-mix-asphalt, lightweight cement-based foams, and alkali-activated foams, studied in detail. Subsequently, the performance of the reinstated trench, as well as its response to the different pavement or narrow-trench designs, were evaluated by a series of physical and numerical models. The result showed the satisfactory performance of lightweight foams as a backfilling material. Lastly, a multi-objective optimization model was developed to minimize project cost and time while using the most levelled resources.

Preface

In all the material presented in this thesis, Mohammad Rezaei is the main student contributor. I was the principal researcher and responsible for all of the research planning, experimental studies, data gathering and analysis and preparation of manuscripts.

Chapter 2 is prepared for submission to the *journal of road materials and pavement design* as "Application of controlled low-strength material (CLSM) for narrow-trench backfill-An overview". Chapter 3 is published as "Rezaei, M., Hashemian, L., Bayat, A., & Huculak, B. (2017). Investigation of rutting resistance and moisture damage of cold asphalt mixes. *Journal of Materials in Civil Engineering*, 29(10), 04017193". Chapter 4 is submitted in the *journal of road material and pavement design* with the title of "Application of Cement-Based Foams for Narrow-Trench Backfilling". Chapter 5 is a summarized version of a study paper that submitted to the *journal of cement and concrete composite* as "Alkali-Activated Fly Ash Foams for Narrow-Trench Reinstatement". Chapter 6 is also a short version of a paper titled as "Freeze-thaw resistance of cement- and alkali-activated-based foams for narrow-trench backfilling in cold regions" and prepared for submission in the *journal of construction and building materials*. Similarly, Chapter 7 is an abridged version of the paper that was prepared for submission in the *journal of construction and building materials* titled as "physical and numerical analysis of distresses associated with

the backfilling in a narrow-trench". A part of the laboratory results on the physical models of Chapter 7 is also published as "Hashemian, L., Rezaei, M., & Bayat, A. (2017). Field and laboratory investigations on pavement backfilling material for micro-trenching in cold regions. *International Journal of Pavement Research and Technology*, 10(4), 333-342". Lastly, Chapter 8 is prepared for submission in the *journal of automation in construction* under the title of "multi-objective time-cost-resource optimization of narrow-trenching projects using linear scheduling method and non-dominated sorting genetic algorithm". Prof. Bindiganavile has supervised the research and assisted in the organization and production of the manuscripts.

Acknowledgements

I would like to begin by thanking my supervisor, Vivek Bindiganavile, for his constant support, deep insights, continuous encouragements, and having confidence in my work. I have been privileged to work under a passionate researcher with immense knowledge. His valuable discussions and suggestions have helped me grow as a researcher and an engineer.

Second, I would like to thank my parents for their selfless love and for always encouraging me to pursue my ambitions in education. Special thanks go to my wife, Elham, for her invaluable support and continuous encouragements, and to my loving sister, Shadi for always being there for me.

I greatly appreciate the help, consideration, and support of Dr. Samer Adeeb, the head of the civil engineering department, Dr. Robin Everall, the associate dean of the faculty of graduate studies and research who patiently supported me during the very hardest moments in my educational path. My sincere thanks go to Ms. Sasha van der Klein, the president of the Graduate Students Association for her time, kind advice and help through my Ph.D. studies at the University of Alberta.

I would like to thank my colleagues and fellow students- Arian, Shiva, Chaofan, Jonathan, Steve- for their insightful discussions and noteworthy assistance in conducting experiments.

I would also like to express my gratitude to my cousin Sadegh, for his warm friendship and generous care during all these years.

I would like to acknowledge the financial support provided by the University of Alberta, Edmonton, Alberta.

Contents

List of Figures

List of Tables

List of Abbreviations

AAF	**A**lkali-**A**ctivated **F**oam
AC	**A**sphalt **C**concrete
AHP	**A**nalytic **H**ierarchy **P**rocess
CBM	**C**ement **B**ased **F**oam
CLSM	**C**ontrolled **L**ow-**S**trength **M**aterial
CMA	**C**old **M**ix **A**sphalt
CS	**C**ompressivce **S**trength
CTE	**C**oefficient of **T**hermal **E**xpansion
DF	**D**urability **F**actor
DG	**D**ense-**G**raded
DOT	**D**epartment **o**f **T**ransportation
DTCRO	**D**iscrete **T**ime-**C**ost-**R**esource **O**ptimization
DTCTP	**D**iscrete **T**ime-**C**ost **T**radeoff **P**roblem
F.S	**F**actor **o**f textbfSafety
FA	**F**ly **A**sh
FBST	**F**lexural **B**ond **S**trength **T**est
FE	**F**inite **E**lement
FO	**F**ibre **O**ptic
FTTH	**F**ibre-**t**o-**t**he-**H**ome
HDD	**H**orizontal **D**irectional **D**rilling
HMA	**H**ot **M**ix **A**sphalt
HWT	**H**amburg **W**heel **T**racking
ISP	**I**nternet **S**ervice **P**roviders
ITS	**I**ndirect **T**ensile **S**trength
LD	**L**ow **D**ensity
LOB	**L**ine-**o**f-**B**alance
LSM	**L**inear **S**cheduling **M**ethod
MQ	**M**arshall **Q**uotient
MSI	**M**oisture-**S**usceptibility **I**ndex
MT	**M**icro-**T**renching
NT	**N**arrow-**T**renching
OD	**O**pen-**G**raded
OG	**O**uter-**D**iameter
PR	**P**recedence **R**elationships

RE	**R**emovability **M**odulus
RLP	**R**esource **L**eveling **P**roblem
SSR	**S**hear **S**tress **R**atio
SSD	**S**aturated **S**urface **D**ry
SST	**S**lant **S**hear **T**est
TSR	**T**ensile **S**trength **R**atio

Chapter 1

Introduction

1.1 Background

Cutting the pavement for installation of various small diameter utility lines, especially telecommunication cables is inevitable in today's urban life. The busy and crowded life in cities also demands the fastest installation method with minimum disruption to city life. On the other hand, the limited budget for these constructions and environmental concerns request a cost-effective construction method with a minimum usage of resources. In general, the small diameter utility installation methods in an urban area can be classified into two major groups: utility sharing and direct buried methods [1]. The former involves installing the new utility line through the existing lines (e.g. sewer, water or gas lines). Despite being fast and cost-effective, these methods require exhaustive long-term collaboration between the new and host utility lines [2]. Moreover, the new utility line may be damaged during the maintenance, renovation, or replacement of the host network. As a result, this method has not been practically

used yet [1]. Direct buried methods include the subsurface installation of the utility line [3]. Among them, the open-cut method is commonly used by the utility network developers. However in crowded urban areas, open-cut is time consuming, costly, and has a high risk of hitting the underground services [4], high indirect cost as a result of disruption to the local traffic or businesses, and an adverse impact on the sound and air quality [5, 6]. It is also reported to reduce the pavement serviceability index of the road [7]. Hence, trenchless or near-trenchless methods have alternatively been practiced in urban areas [1] to reduce the cost and associated impacts of open-cut installation and improve productivity. Mini-horizontal directional drilling (mini-HDD) and narrow-trenching (NT) are the two most popular among these methods. They are fast, cost-effective, and environmentally preferred while exposing minimum impact on the local traffic or businesses [1].

Due to its many benefits, the use of narrow trenches for installation of flexible pipelines or conduits of small diameter is a common technique for the construction of water, electricity, lighting and telecommunication networks. The last 200 m of fibre deployment can be particularly difficult to deliver with obstacles both above and below ground to navigate, and these difficulties increase installation time and cost. Providers have found that construction costs and time may be reduced considerably when employing micro-trenching (MT) procedures compared to other methods [1, 3]. MT is a variation of NT which is commonly used in crowded urban areas because of its tiny dimension of trench. The micro-trench is usually as narrow as 25 to 40 mm wide, and up to 250 mm deep [8, 9].

The narrow-trenching process includes three main steps. The first step is cutting a NT in

the pavement using a dry or wet saw cut. Trench dimension is selected according to the size of conduits, pavement thickness, and regional considerations and commonly consists of three zones, first 2.5-8 cm is conduit height follows by a 10 cm cover or buffer zone and a 5-10 cm municipal grind depth [10]. Cover zone is usually deeper in freeze/thaw climates. The second step is cleaning the trench and laying the cable or conduit inside, and the third and final step is backfilling the trench. The main advantages of this technique include fast and cost-effective deployment (typically 50% faster and upto 75% cheaper than traditional open trenching [10–12]), limited interference with other services and/or traffic during construction, lower environmental impact (less waste creation and disposal, less new material and fewer truck movement and CO_2 emission) and lower impact on the road (less damage to the pavement and sub-base due to the tiny dimension of the trench) [1, 13]. Its simplicity also allows to use of multi-skilled installer teams in the project.

MT is particularly popular for the last mile installation of fibre optic cables [1]. Today's demand for high speed internet and the limited bandwidth of the existing copper-based network made the internet service providers rally to upgrade their network to optical fibres. For instance, TELUS communication has invested one billion dollar only in Edmonton, Alberta to migrate from copper to a fibre optic network by 2021 [3, 14]. MT has been used in many countries, including Australia, Ireland, Germany, France, Norway, Portugal, Israel, Malaysia, and Iran [15].

1.2 Problem statement and motivation

Despite the many benefits of NT over other methods of utility installation in urban areas, most municipalities have not yet been convinced to issue a permit for this method because of its poor quality of reinstatement, lack of deployment standard, and unsolved liability risks of the road and/or FO cable damages [1, 3]. Additionally, in changed weather conditions (e.g., freeze and thaw cycles), MT may result in significantly different backfilling performance, leading to premature failures of restoral materials which may, in turn, degrade the present serviceability index of pavement as well as damage the installed cables or conduits [16, 17].

Monitoring different MT projects in Alberta, Canada by the author [18, 19] revealed that the process and material of backfilling are not engineered, and no follow-up research work was done to improve MT practice. Instead, the narrow-trench is designed merely based on the available equipment and materials. Therefore, many distress (as will be discussed in the next chapter) was observed in the reinstated trench after a few cycles of freezing and thawing which even led to the failure of the reinstatement and up to 18 cm upward movement of the cable (in a 23 cm deep trench) [1, 18]. Interviewing with different MT designers and contractors cleared that the performance of the backfill materials, especially inside a narrow-trench, is not fully investigated and understood. This study is premised on the following hypotheses: (i) that the controlled low-strength materials with their strength and rigidity engineered to be low, but having high dimensional stability shall outperform high strength materials of higher elastic modulus; (ii) that when reinstating a narrow-trench, using bituminous mixtures like

cold-mix-asphalt in asphalt concrete pavement layer and limiting the controlled low-strength materials to the granular base layer, the performance of the backfilling will be superior to using controlled low-strength materials all the way to the top; (iii) that incorporating aggregates in the controlled low-strength materials improves its load-carrying capacity and dimensional stability due to interlocking properties of the aggregates. Also using lightweight aggregates like expanded perlite in the mixtures makes a better backfilling material than using natural sand; (iv) that microfibre improves the mechanical properties, dimensional stability, and bonding of controlled low-strength materials to the asphalt concrete substrate and therefore enhances their performance in the narrow-trench; and (v) that the lower shrinkage and improved strength and bonding of alkali-activated concrete compared to Portland cement concrete make alkali-activated foams better alternatives for narrow-trench backfilling than cement-based foams.

Besides, the effect of the trench dimension, its location in the road, different traffic or environmental loading, or the pavement structure or design on the performance of the reinstatement is not yet explored. On the other hand, the few available standards on MT only provide general guidelines and hence, lack of a detailed and specific guideline for MT is another reason for the poor performance of this method.

Monitoring of the real-life MT projects also exposed the lack of a comprehensive project management plan for these specific types of the project. The current practice involves the daily planning and resource allocation by the superintendent and cost-plus payment which will reduce the productivity and increase the idle time of the crew. This resulted in delayed and over-budget completion of the project [19]. Since the main advantage of MT is to deliver a fast

yet cost-efficient installation in busy urban areas, improper scheduling of the project can lead to a considerable increase in project time, cost, and social impact of the project. Considering the huge investment for fibre optic deployment in cities like Edmonton, a powerful decision support tools for planning and scheduling of MT projects in order to trade-off between time, cost, and usage of the resources of the project is crucial for the successful implementation of this method.

The results of this study is hoped to help the narrow-trench designers by (i) increasing the knowledge about the properties of the backfill materials and their performance inside a narrow-trench, (ii) introducing innovative, environmentally friendly, yet cost-effective alternative for narrow-trenching reinstatement, (iii) investigating the backfill response to different loading, pavement, or environmental condition, and (iv) providing a comprehensive decision support system for planning and scheduling narrow-trenching projects. The results of this study can also be used by utility owners or municipalities to publish a detailed standard for these projects and define the limits and acceptance criteria. Lastly, the application of the findings may be extended to the pavement pothole or crack repair.

1.3 Objectives

The main objective of this research is to study the overall civil work of NT projects, study their applicability in the cold climate of Canada, and to suggest a cost- and time-efficient reinstatement solution for these projects. Considering the recent interest in MT for the last-mile fibre

optic deployment projects, special attention was given to MT projects. Five objectives have been set in this thesis according to the gaps in previous literature:

1. To investigate the lesson learned from the existing real-life NT projects and literature and understand the methods and materials for the reinstatement of narrow-trench through monitoring real-life NT projects and reviewing the existing literature.

2. To evaluate and characterize different ready-to-use cold-mix-asphalts (CMA) and investigate their applicability as a narrow-trench backfill material through different laboratory tests on CMAs and physical models of the narrow-trench.

3. To assess the performance and key fresh, early age and hardened state properties as well as freeze-thaw resistance of the foamed cementitious and alkali-activated grout, in order to identify its potential as a durable yet cheap and environmentally friendly fill material for reinstatement of NT projects in the cold climate of Canada.

4. To investigate the response of the reinstated section to different trench or pavement design as well as loading or environmental condition through physical and numerical modeling of the trench.

5. To presents a decision-support system for the planning and scheduling of MT projects as a linear construction project. The model allows construction planners to generate and evaluate optimal/near-optimal construction scheduling plans that provide a time and cost trade-off while using the most leveled resources profile.

1.4 Outline

Chapter 2 is a quick review of the surveyed literature on the NT reinstatement methods and materials. Special attention is given to the cement- and alkali-activated foams due to their high potential to be used for this purpose. Chapter 3 tests the engineering properties, permanent deformation and moisture resistance of different CMAs to assess their suitability for use as a narrow-trench backfill. Chapter 4 characterizes the mechanical performance, thermal shrinkage, and bonding with the bituminous substrate of different cement-based foams. The same tests and analysis were done in Chapter 5 for alkali-activated foams. Chapter 6 explores the freeze-thaw performance of the cement- and alkali-activated foams. Chapter 7 presents the results of physical and numerical models of the narrow-trench. Chapter 8 introduces a discrete time-cost-resource optimization model which together with linear scheduling model (LSM) tries to select starting time and the number of the crew assigned to each activity satisfying all the project constraints. Chapter 8 is a summary of findings, conclusions, and recommendations for future studies.

Chapter 2

Background

Despite all the advantages, narrow-trenching, and in particular, micro-trenching method is not being widely practiced by Internet service providers (ISP) around the world because municipalities are reluctant to accept the risks associated with NT, including potential pavement damage, lack of stability of the buried conduit in shallow depths in freeze-thaw climatic regions, and possible damages to the FO cable as a result of road rehabilitation. To understand the current practices of NT, different pilot installations in Alberta, Canada were performed and monitored as a part of this research. Result revealed the quality of backfilling material as the main cause of NT failures.

Controlled-low-strength-materials (CLSM) have been used for decade for various construction applications including utility trench backfilling. There have been renewed interest in its structural characteristics in view of its lighter weight, savings in material especially cement and potential for large scale utilization of wastes like fly ash. To overcome the disadvantages of current practice of FTTH projects and to engineer the design and process of these projects,

a comprehensive study started at University of Alberta. Therefore, the focus of this chapter is to provide a summary of the pilot installations and to classify literature on NT backfilling options. Owing to their advantages, a special attention was given to CLSM, foamed CLSM and Alkali-activated (AA) CLSM in terms of constituent materials (foaming agent, cement and other fillers used), mix proportioning, fresh and hardened properties by conducting a comprehensive overview of the previous works carried out on using different CLSM admixtures and additives focusing on the narrow-trench (NT) backfilling application.

2.1 Introduction

In today's urban life, digging the pavement for installing new utilities, rehabilitating, or updating the existing ones has become inevitable. Among these utilities, telecommunication lines has proven to require special attention in modern cities. Internet has become an inseparable part of every aspect of our society, including individual life, national economic growth, business growth, health, education, communication, and entertainment [20–22]. Therefore, the internet's growth has become explosive and the recent demand for high-speed internet cannot be fulfilled through the existing copper networks because of the limited capacity and high attenuation of the copper cables. The fibre optic (FO) network, on the other hand, theoretically have unlimited capacity [23], and can transfer the data at the speed of light with a very small attenuation over a long distance. Currently, only 10% of Canada's total broadband subscriptions are

fibre connections which are increasing with annual growth of 38% [4]. Therefore, CP companies in Canada, has planned to upgrade their existing copper network to a fibre network. As an illustration, Telus communication has invested 4.2 billion CAD through 2019 in Alberta to upgrade their copper network to a FO network [14].

However, constructing FO networks encounters many economical, legal, environmental, and social issues that need to be considered and managed prior to the installations. FO network construction projects in urban area are usually found to be very difficult and more challenging than previously thought [24]. For example, the civil work costs of the construction are reported to be up to 70% of the initial investments [25], beside the fact that it involves disruptive digging on the streets [24]. In urban areas where underground spaces are overcrowded, the risk of damaging existing services, impacts on the environment and social costs related to the community disturbance are substantial [4, 5]. Possible environmental disturbances include contaminant spills, pollutant emissions, and noise [5, 26, 27]. Additionally, the local government sometimes enforces legal difficulties and zoning laws [4], which make obtaining permits and agreements difficult and time consuming [6]. Regardless, the extent of FO construction impact is directly dependent on the choice of installation method.

Generally, the FO deployment method can be classified into two main groups: direct buried and utility sharing methods. A direct buried method involves direct underground installation of FO cable. One of the most common direct buried methods, still in use in many countries is open–cut, which has a high risk of hitting existing underground services [4], high social costs,

negative effect on pavement's long-term life and significant impacts on the air and sound quality [5, 6]. Therefore, to reduce the costs of FO deployment and its negative impacts, trenchless and near-trenchless methods, such as plowing, narrow-trenching, piercing or mini horizontal directional drilling (mini-HDD), can be an effective tool.

The use of narrow trenches for installation of flexible pipelines or conduits of small diameter is a common technique for the construction of water, electricity, lighting and telecommunication networks. As explained in Chapter 1, the last 200 m of fibre deployment is particularly difficult to deliver due to the busy urban environment and crowded underground installations. Due to its fast construction and cost-effectiveness, NT has received considerable attention in recent years. NT requires no utility inspection due to its shallow depth of installation and does not disturb or damage the adjacent subsurface facilities [1]. Its fast construction rate also causes minimal traffic delays and low environmental and social impacts [28]. Solvian [29] studied the life cycle environmental impact of different methods to install fibre optic network and concluded that NT is the most preferred method of fibre installation in asphalt pavement. NT also poses less risk to underground services than mini-HDD [10].

The terms NT and MT are frequently used interchangeably in the literature where in fact, the distinction is evident with respect to their trench dimensions. While the cut in MT is 25-40 mm wide and up to 250 mm deep, it can be considerably wider and deeper in NT. According to Solivan [29], NT is cut normally 80 mm wide and 400 mm deep. Therefore, the micro-trench is usually cut using a blade saw while milling wheels are used for cutting the narrow-trenches.

The narrow-trenching process includes three main steps as explained in Chapter 1. First,

cutting a small trench in the pavement using a dry or wet saw cut. Then, cleaning the trench and laying the cable or conduit inside, and finally backfilling the trench. This method of installation is mainly fast and cost-effective (up to 50% faster and 75% cheaper than open trenching [10–12]), lower disruption of other services and traffic during construction, lower environmental impact and lower damage to the road [1, 13].

However, one of the major challenges urban municipalities face is the quality of trench restoration [30]. Quality of backfilling plays an important role in the resulting performance. It secures the cables and/or conduits in the trench bottom and provides mechanical protection to the cable against traffic loads. Moreover, restoration material and technique directly affect pavement quality and its service life as it has been proven in utility installations that major pavement failures may happen using unsuitable or improperly installed backfilling materials [30]. Several studies have been conducted on using different granular, bituminous material, and concrete for narrow-trench backfilling [31–35]. Granular materials can be easily washed out by water ingress into the trench, resulting in the sinking of the top sealant layer and leaving the cables unsupported. Accordingly, a considerable cable movement was observed in a micro-trench which was backfilled using play sand [1]. Likewise, traditional reinstatement materials like asphalt and macadam were not designed to be used in NT. Placing the hot or cold asphalt inside the trench, maintaining the temperature of hot asphalt, and reaching the optimum compaction are very difficult and time-consuming [18]. Improper compaction results in lack of cohesion in backfilled asphalt which will let the asphalt to be washed out of the trench [1]. Cold mix asphalt also reported having an insufficient bond to the cut asphalt edges [13]. Lack

of cohesion and adhesion will result in water ingress and further deterioration of the trench reinstatement. Achieving the design gradation and compaction of bituminous macadam is also not practical in NT which resulted in the failure of backfilling in a real life project [19]. Filling the trench with neat bitumen is not a solution either, due to the lack of strength and skid resistance. Unlike the asphalt mixture, flowable fills are self -compacting and -leveling and can penetrate the gaps in the trench which makes the backfilling easier and faster. However, cement-based grout and epoxy mortars are stiff and using them in the flexible pavement will result in progressive cracks in the composite structure under the service physical and thermal loading. Considering the lesson learned from the previous pilot installations [19], bonding between the cellular grout fill and existing pavement is another concern. Lack of permeability in these materials can also interfere with the designed subsurface drainage of the pavement [28]. Nevertheless, backfilling of lengthy trenches requires a considerable amount of material, and therefore, resins or specialty cementitious materials are not practical candidates due to the high costs. As an illustration, a commercial non-shrink cement grout, with a unit price of 1$/kg, was used to partially backfill a micro-trench in a real-life project in Alberta, Canada as a part of this research. Final cost analysis of the project revealed that the cost of the cement material is 68% and 20% of the total grouting task and overall MT costs, respectively.

Due to the small dimensions of the narrow-trench, the appropriate backfilling material should be flowable enough to penetrate and completely fill the whole trench depth. The other essential requirements for backfilling materials include: bonding to the existing material, sealing the trench against water intrusion, resisting permanent deformation and supporting the cut

edges of the asphalt, being compatible with flexibility of the pavement, having dimensional stability under service loads and showing no shrinkage strain, being excavatable for future repairs of installed utilities, rapid hardening to allow the road to be reopened to traffic quickly, and being economical and simple to apply by multi-skilled installer teams [13, 36]. For the purpose of narrow-trench backfilling, one common time-, cost-, and quality-effective backfilling alternative is controlled low-strength material (CLSM) [37, 38]. CLSM is a self-compacting and self-leveling cementitious backfill material used instead of conventional compacted fill [39]. The other terms used to describe this backfilling material include flowable fill, controlled-density fill, flowable mortar, self-compacted backfill material, plastic soil-cement or slurry [39, 40]. For the purpose of this study, the definition of CLSM is broadened to include controlled low-strength cement-based slurries, foams, and alkali-activated (AA) foams.

In general, CLSM costs slightly higher than the conventional compacted soil or granular backfill materials; however, it is cheaper than regular cementitious grout. This material requires less on-site labor and equipment, as it is flowable, self-leveling, and can be conveniently placed with no vibration needed. Other potential advantages associated with the usage of CLSM include fast construction speed, potential of usage in narrow trenches (where compacting soil or asphalt is difficult, or in some cases, impossible), and utilizing high volumes of waste or by-product materials in the mixture [37, 41]. CLSM usually possesses a sufficient load-carrying capacity and serves as a strong and durable backfill material for trench or structural fill, as well as pavement applications. More importantly, it can be designed with sufficient early strength to support traffic loads within hours of placement [42–44].

A total of 135 research articles are found for trench backfilling using CLSM in the literature in English dating from 1990 to 2018, 20 of which are published in 2018. In this paper, an overview of CLSM for narrow-trench backfilling applications is presented based on the available literature. The presented study reviews specifications, adopted materials, and the influence of CLSM on the properties of trench backfilling.

2.2 Review of NT reinstatement methods and materials

In general, two backfilling methods have been practiced in real-life projects. First, is the single backfilling in which the trench is filled with a single material. Granular materials, cement slurries, cement-based concrete or foams, epoxy resins, bituminous sealant, and asphalt macadam are among the commonly used materials. Second, dual backfilling, which has been practiced widely for reinstatement of narrow-trenches in flexible pavements and includes filling the trench with one of the aforementioned materials up to the asphalt layer and then using cold or warm-mix-asphalt to completely fill the trench. While NT has been used globally for many years, there are a few follow-up reports on the quality of the narrow-trench reinstatement. To investigate the common practices of NT and monitor the long-term performance of the trench, different pilot installations in Alberta, Canada was performed and monitored by the author. The details of these installations are reported in [19] and [18]. Following is a review on the available literature on NT reinstatement methods and materials.

2.2.1 Single backfilling

Many researchers proposed the single backfilling method in heavy traffic areas [45, 46] because it is faster and easier to apply which results in less traffic disruption and social cost. Plain cement grout is relatively cheap when compared to other specialty mixed products and easy to be made and used on site. Therefore, it has been widely used in many NT projects including a micro-trenching project in South Africa [47], Kula Lumpur, Malaysia [48], Israel [13] and Alberta, Canada [18]. Moreover, many specialty modified cement-based grouts and epoxy resins are available on the shelf for sale. For example, FastPatch DPR [49] is a multi-component polymer modified resin that can be used in narrow-trenches up to 10 cm wide and gain 8 MPa compressive strength in 24 hours. [50], another commercially available product, is a single component fibre reinforced cementitious mortar designed for Micro-trench reinstatement. It can reach a compressive strength of 23 MPa in only 4 hours. In a real-life project, Elephant-armor [50] was placed in a micro-trench perpendicular to heavy truck traffic and after 8 months and undergoing 125 freeze-thaw (F-T) cycles, no visible distress was observed in the micro-trench. Despite the ease of application, using high-strength and rigid cement grout or epoxy resin in NT might not be a sensible engineering solution for many reasons. First, the mortar will become a "beam" in the flexible pavement and overtime, the inflexibility of the reinstated material will break the road [28]. In order to investigate this issue, a physical model of a narrow-trench reinstated with a commercially available epoxy resin was tested under the Hamburg Wheel Tracking device. After 20,000 passes, ruth depth at the center of the trench was only 1 mm and this deformation was disappeared after unloading [51]. The corresponding

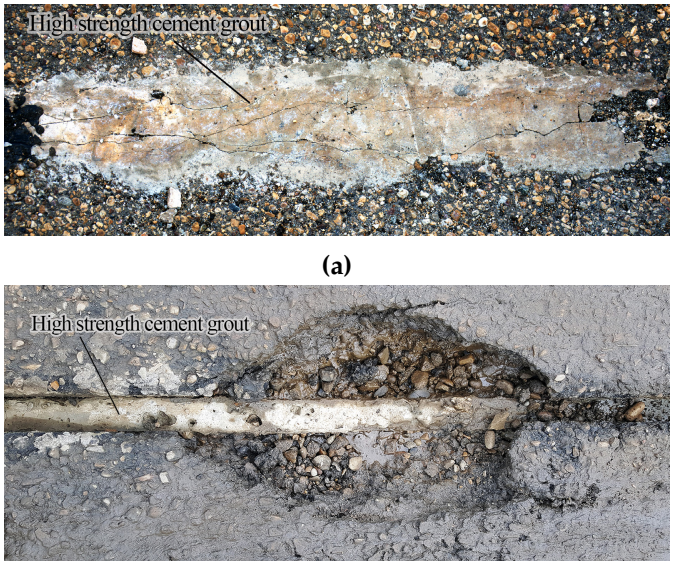

Fig. 2.1. High strength grout in a micro-trench. (a) longitudinal cracks in high-strength cement grout [19], and (b) Damage to the asphalt pavement and debonding between the grout and the cut asphalt surface [19].

ruth depth for hot-mix asphalt (HMA) without a trench is 3 mm [15]. The different behavior of the pavement and the rigid backfill under loading caused cracks around the trench edges (Figure 2.1a, which may cause water ingress into the trench and, consequently, failure of the reinstatement. The same issue was reported by the author [19] in a MT project reinstated with cement grout (Figure 2.1b). Second, due to the lack of permeability, mortar in the road could effectively act as a wall in the road, interrupting the drainage system of the road and diverting water flow and leading to flooding where the trenching ends [28]. Third, using a high strength material in the trench will make access to the buried cables or utilities, for future expansion or repair, difficult. Fourth, using a specialty mixed material or epoxy resin can be economically challenging in a full-scale NT project (see section 2.2.3).

Bitumen joint sealant also has been used to fill and seal a micro-trench [1, 19, 52]. However,

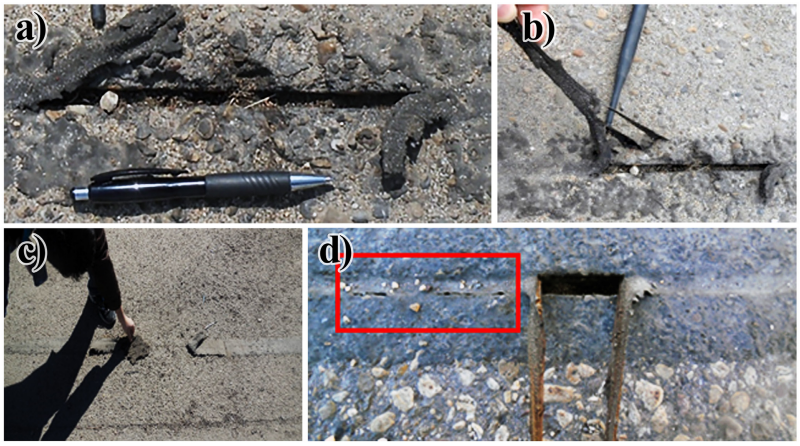

Fig. 2.2. Failures in sealant. (a), (b) and (d) show the sealant is pulled out of the trench. The red rectangle in (d) shows the debonding between the sealant and the trench. (c) shows the poor bonding between sealant and asphalt. [18].

the shape factor must be considered when using bitumen sealant in the trench. The shape factor is defined as the ratio of the sealant width to the thickness. The recommended shape factor of rubberized asphalt is 1:1 [53] and considering the low width-to-height ratio in narrow-trench, using sealant materials to fill the trench is not recommended. On the other hand, the contact surface of the sealant and the pavement must be clear of any dust or moisture to insure a good bonding, which is very difficult in real-life projects. Therefore, sealant was pulled out of the trench after few months (Figure 2.2) in the pilot installations [18, 19].

Regardless of the recommended shape factor of 0.5 [54], Cold lay macadam or asphalt mastic also has been used to backfill a narrow-trench in Dublin, Ireland [13] and in an MT pilot project in Alberta, Canada [18]. In this method, either the trench will be reinstated with flowable asphalt mastic or it will be filled with an engineered gradation, and then the cold bitumen emulsion will be poured on top of the aggregates. While this method has been reported as one

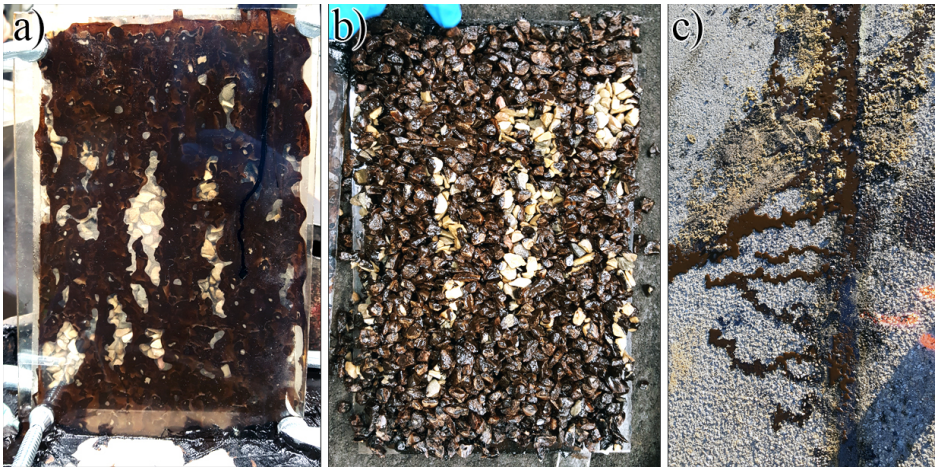

Fig. 2.3. Cold bitumen emulsion freshly poured on aggregates in a physical model of narrow-trench in (a) and a week after (b). Ununiform coverage of aggregates can be seen in (a) and (b). In (c), cold bitumen emulsion escaped from a micro-trench with dense aggregate gradation [18].

of the fastest and cost-efficient backfilling methods [18], there are many concerns about the performance of reinstatement. Sealant and macadam will not withstand heavy traffic, solvents or harsh environmental conditions. Due to the lack of lateral stability, movement of the pavement faces toward the trench will force the asphalt mastic out of the trench slot in hot weather. The mastic can also be knocked off the trench by traffic, and as the weather becomes colder and the joint slot opens there will not be enough mastic in the slot and failure will occur. In the areas of failure, dirt and other foreign matter will settle into the trench and in time, the trench will become so full of non-mastic material that the pavement will break due to the lack of lateral support. Due to the narrow width of the trench and absence of compaction, reaching the desired gradation inside the trench is not possible. This will result in an un-uniform gradation along the trench. As a result, bitumen emulsion will flush down the trench where the gradation is more open and flow out in the dense areas, remaining the aggregates uncoated (Figure 2.3).

2.2.2 Double backfilling

In the double backfilling method, the trench is filled with a filler, including granular or recycled aggregates or cement-based grout, up to the existing pavement and then a compatible material with the existing flexible pavement, usually cold- or hot-mix asphalt is used on top of the filler and in asphalt layer to fill the trench to the top. This method is commonly used in many NT projects including [55] (double backfilling of beach sand and cold-mix asphalt to reinstate a 24 $\times$ 305 mm micro-trench), [56] (used concrete slurry and cold-mix asphalt to reinstate a 40 $\times$ 250 mm micro-trench), [57] (concrete slurry and cold-mix asphalt), [19] (high strength, non-shrink cement grout and cold-mix asphalt), [1] (play sand and cold-mix asphalt) and, [18] (different fillers including cement grout, polymer modified high strength cement grout and, cement-based foam were tested as filler and trench was filled to the top using a commercially available cold-mix asphalt). Real field NT projects and laboratory studies revealed that fine granular materials are washed out of the trench in presence of water [1, 15]. This will leave the upper cold-mix asphalt unsupported and prone to settlement. The author [15] compared the ruth depth of two physical models of a micro-trench under the Hamburg wheel tracking device. The first and second trench was backfilled up to the asphalt layer with play sand and cement grout, respectively. Both trenches then filled by compacting cold-mix asphalt on top of the first layer. The test results in the dry condition revealed a 22% higher ruth depth in MT sample backfilled with sand than the sample backfilled with grout. This result was expected since sand densifies and deforms more under wheel loading compared to grout. Moreover, after soaking the samples under water and subjecting them to one F-T cycle, the sample backfilled with sand

Fig. 2.4. Distresses of cold-mix asphalt in a micro-trench. (a) Backfilling settlement and cold-mix asphalt washed out, (b) lack of cohesion and (c) lack of bonding between cold-mix asphalt and the existing pavement [1].

underwent 30% more deformation than its results in dry condition test while no considerable change was observed in the trench backfilled with grout. Settlement, raveling, lack of cohesion and adhesion to existing asphalt layer are other concerns with using cold-mix asphalt in narrow trenches (Figure 2.4).

2.2.3 Material cost

Since the trench albeit narrow is yet quite long in length, the volume of the required material to reinstate the trench is relatively high. Cost analysis of the MT project in Alberta, Canada by the author showed that the cost of material required for double backfilling of the trench with high-strength, non-shrink grout, and cold-mix asphalt can be as high as 65% of the main trench installation cost and 25% of the total project cost [19]. Despite the considerable cost of the reinstatement materials, there are few studies that considered this cost. Table 2.1 compared the material cost of different backfilling options based on analysis of [18] and [19]. In general, the material cost of double backfilling is higher than single backfilling and the difference will be higher if the equipment and labor cost are taken into consideration. With the cement-based

Table 2.1. Cost and productivity of different reinstatement options for narrow-trenching [18, 19].

	Double backfilling			Single backfilling		
	$CMA^* + Grout^1$	$CMA + Grout^2$	$CMA + CBF^*$	$Grout^2$	CBF	$Macadam$
Material Cost (CAD/m^3)	2990	1964	678	1945	300	713
Productivity (m/hr)	8	8	9	22	8	9

[1]High-strength, polymer modified cement grout; [2] high-strength, non-shrink cement grout. [*]Abbreviations: CMA, cold-mix asphalt; CBF, Portland cement-based foam.

foams, a considerable saving in weight of cement can be achieved. Cost of the foaming agent is also negligible when compared to the cement cost. Therefore, cement-based foams are preferred over the other reinstatement options from the financial and environmental perspective. All the backfilling options deliver almost the same productivity of 8 m per hour except for single backfilling with plain high-strength grout which has considerably higher productivity. However, it must be noted that the pilot project in [18] was done by unprofessional workers and without proper industrial equipment. for instance, the rate of production and placement of cement-based foam inside the trench is expected to be much higher if a proper foam making machine, industrial mixer and a grout pump are used.

2.3 Proportioning and preparation of CLSM

2.3.1 Constituent of the base mix

Table 2.2 exhibits typical mix proportions for different materials being used in CLSM for trench backfilling. As may be inferred from this table, CLSM is usually a mixture of small amounts

of Portland Cement (PC), Fly Ash (FA), fine aggregate or other waste materials, water, and in some cases, aerated foam. Rapid hardening [58, 59], high alumina, and Calcium Sulfoaluminate cement [60] have also been used to reduce the setting time and improve the early strength of the mixture. Moreover, many researchers have studied the application of by-products in CLSM. As a cement replacement, FA and ground granulated blast furnace slag (GGBFS) have been used commonly in the range of 15-25% [59, 61–64] and 50-70% [65–67], respectively. Silica fume is another cement replacement that commonly replaces up to 10% mass of cement to intensify its strength [68–70]. Coarse FA and ponded ash (PA) have also been used as fine aggregate in CLSM [71, 72]. A large amount of PA reported to be successfully used in the fabrication of regular [73] and foamed CLSM [74].

Several studies have been conducted in the past few decades to produce cement-free CLSM. Cement-free CLSMs use industrial byproducts or natural aluminosilicate materials activated by an alkali activator and then combined with fine aggregates to form an AA CLSM [75]. Major aluminosilicates, which are used as precursors, include GGBFS [76, 77], FA [78–80], and metakaolin [81]. Caustic alkali, silicate, carbonate, and sulfate are also among the main activators [82]. However, there is still a lack of research focusing on the actual field performance of CLSMs made with these byproducts in a NT.

Table 2.2. Typical mixture proportions of standard CLSM for NT backfilling.

Constituent	IOWA DOT [43]	Dockter [43]	Maher and Balaguru [83]	Samadi and Herbert [84]	Pierce and Blackwell [85]	British Cement Association [86]
Cement (kg/m^3)	59	5.9	29.5	23-69	30	300
Fly Ash (kg/m^3)	178	163	236	91-136	360	-
Sand (kg/m^3)	1544	1650	1575	1293	1500	-
Water (kg/m^3)	346	247	342	227	300	600
Foam Volume (%)	-	-	-	-	-	78
Compressive strength (MPa)	0.69-1.03	0.83	0.55	Not Specified	Not Specified	0.5-1

2.3.2 Foam

As noted earlier, the aerated foam can be added to the CLSM mixture to create small and enclosed air bubbles in the mix. It produces a lightweight material which reduces the cost, compressive strength, modulus of elasticity and increases the dimensional stability and F-T resistance when compared to the plain cement grout. The reduced rigidity of foamed CLSM has also made it a good backfilling option of flexible pavements [44, 87–89].

Two common types of foaming agents, natural material-based and synthetic, are studied in different research studies [90–94]. [95] reported that the foaming agent type has a considerable effect on sorptivity and thermal conductivity of foamed CLSMs. Protein-based foaming agent results in smaller isolated air bubbles compared to synthetic agents. A decrease in the wet density of synthetic foaming agents, on the other hand, results in an increase in the number of the connected pores and therefore, increase in porosity. This increased capillary pore volume is least suited for narrow-trench backfilling which is exposed to moisture, chemicals, and F-T cycles. Thermal conductivity of the foamed CLSMs that produced with a synthetic foaming

agent is generally lower than the ones with a protein-based agent. Foaming agents with higher wet densities, regardless of their type, will result is higher compressive strength and modulus of elasticity [95]. [96] suggested using synthetic surfactants for densities more than 1000 kg/m^3 and protein-based surfactants for densities of 400 to 1600 kg/m^3.

Foamed CLSM can be produced by either of pre-foaming (i.e., compressed-air) or mixed-foaming (i.e., high-speed mixing) methods [68, 97]. The pre-foaming method usually costs more but offers better foaming quality and efficiency [95]. There is also a close relationship between the volume of the foam and air content of the mix in the pre-foaming method [96, 98].

Regardless of the foaming method, the foam must be stable enough to resist the mixing loads as well as the pressure of the mortar until the mortar sets [99]. [100] introduce three parameters to evaluate the performance of the foaming agent that can be useful in the field. These parameters are, foaming capacity, that is the ratio of final volume of aerated foam to volume of the foaming solution; bleeding rate, or the volume of water seeping from the aerated foam in an hour; and collapse rate, which is the collapsed length of the aerated foam in a standard test tube within an hour. Foaming agents also needed to conform to the requirements of [101] and [102].

2.3.3 Mix design

Limited information is available in the literature about the methods of CLSM mixture proportioning based on requirements of various applications. Considering the particular composition

and properties of CLSM, common methods used for proportioning of the regular concrete mixtures cannot be followed. Generally, net water content, as well as the percentage of foam and binder content of the CLSM mixture are chosen based on rules-of-thumb from either past experience or trial-and-error [103–105]. Therefore, the existing mixtures do not necessarily comprise optimized ratios of constituent materials. In this regard, [38] have proposed a deterministic model for optimizing the CLSM mixture design specifically for narrow-trenches. In this method, numerical simulations were availed to define the required compressive strength of the product, following which the mixture constituent materials were optimized through an experimental procedure based on the required strength. However, the carried methodology is not theoretically rigorous, and cannot be generalized to all work-sites. In order to overcome these shortcomings, and to provide a general approach to rational mixture-proportioning, [106] has proposed a new methodology. The method presented in [106] satisfies the flowability and compressive strength requirements of the material to achieve the optimal composition. The novelty of their methodology lies in considering all solid particles at once, instead of calculating the solid or cement content separately, to estimate the required water content. Therefore, the compressive strength can be modified without sacrificing the flowability which is beneficial in the narrow-trenching application.

Currently, workability in fresh-state and compressive strength in the hardened-state are considered as the two main requirements of a CLSM. Therefore, the common design targets are high flowability (>200 mm spread) and low compressive strength (<2.1 MPa), which allow for re-excavation in future, and yet are strong enough for backfilling needs [37, 39, 42, 107].

However and as stated before, other performance criteria, like modulus of elasticity, bonding strength, dimensional stability and durability of the mix must be considered in the calculation.

There is also no standard method for calculating the desired foam content of the foamed CLSM, and therefore, trial-and-error methods such as net water content, content of foam by percentage, and binder content are commonly used [108, 109]. The amount of foam required in cement-based slurries to meet the design density depends on the cast density, type of the admixtures, cement substitution ratio, and types of foaming agents used [110, 111]. [111] reported that even in the presence of pozzolanic admixtures, the foam content decreases as the required density increases. When FA with higher substitution ratios is used in the mix, the foam demand increases because of high fluid consistency of the base mix, as well as the high residual carbon in the ash [112]. Similarly, higher foam demand was discerned when silica-fume was used with higher substitution ratio, likely because of the fine particle size of silica-fume [113]. However, in contrast to the above cases, using Metakaolin in higher portions reduces the foam demand, because of the size and high water absorptive property of Metakaolin as reported by [113, 114].

For a given mix proportion and density, [115] proposed a rational mix design method based on solid volume calculation. Founded on McCormick's study and the design guide of [116], which relates plastic density and compressive strength, the cement and water contents can be estimated for a desired strength and density. [117] has also furnished a method to calculate the required foam volume so as to achieve a cement slurry with a predetermined water-to-cement ratio and target density. Moreover, there are many equations developed to calculate the required foam volume for a specific design. One of these equations was proposed by [118] to

calculate the required mass of foam based on the mass and density of the base mix along with the target density [119]. In another study, [120] derived a set of equations to calculate the foam volume and cement content based on the base mix composition and the target density in high FA mixtures. Knowing the required compressive strength and fresh density of the mix, typical mix design equations of [121] can also be used to determine the volume of constituent materials of the mixture, including the foam volume. In contrast to the design methods based on the target density of the mix, [122] have proposed a volumetric design approach that considers the 50-200 kg/m^3 desorption value of the foamed concrete, the targeted plastic density, and specific density values of all corresponding constituent materials. The results of [122] have been used by several other researchers including [123–125]. This volumetric approach also seems more practical for on-site NT projects.

2.4 Properties of CLSM

A successful narrow-trench reinstatement dictates a specific characterization for the CLSM both in fresh and hardened states. Due to the small width of the trench, the backfilling material should be flowable enough to fill all the voids inside the trench without bleeding, subsidence or the need for compaction. It also needs to set fast in order to minimize traffic interruption. Hardened CLSM in a narrow-trench is expected to be strong enough to undergo the traffic load and provide the lateral support for the existing pavement, however not too strong to stand out the strength of the pavement layer and make the future excavation impossible. Bonding of the

CLSM to the cut asphalt surface is another factor that directly affects the performance of the reinstatement. It is also important that the reinstated layer has dimensional stability. Moreover, it should be permeable enough to avoid interruption in the drainage of the pavement.

Table 2.3 summarizes the fresh and hardened properties studied by researchers. The hardened properties are classified into mechanical (compressive and tensile strength, modulus of elasticity, re-excavatability, and prediction models), physical (re-excavatability, stiffness, settlement, permeability, shrinkage, and thermal deformation), and durability properties.

2.4.1 Fresh CLSM properties

Flowability

One of the most important attributes of CLSM is its capacity to easily flow into confined areas, self-leveled, and obtain required strength and/or density without the need for conventional placing and compacting equipment. Due to its self-leveling and high flowability, no compaction is required at the bottom of the trench, making it easier to maintain the conduit alignment as well as less chance for settlement [43, 44, 143]. In addition, it increases the construction speed, minimizes the working area required within the trench and, more importantly, can reduce the required trench width [39, 44, 107].

Because the enhanced flow properties of CLSM are critical to successful placement and performance, flowability is measured regularly as an important quality-control parameter [144].

Table 2.3. literature and properties of CLSM investigated

Study	Ingredients	Fresh Properties	Physical and mechanical properties								Others
			Strength	re-excavatability	Stiffness	Settlement	Permeability	Shrinkage	Thermal Deformation	Durability	
[90]	C/L/CM		✓				✓	✓			Thermal, fire and acoustical properties
[126]	C		✓	✓			✓				Thermal properties, Cryogenic applications
[127]	NA	✓									
[128]	FA/BA/SD	✓	✓								
[129]	FA/SLG/SD	✓	✓								
[64] [130]	FA/BA/L	✓	✓								Thermal conductivity
[131]	PC/FA/SA	✓	✓		✓						Long-term excavatability
[125]	PC/CSA/FA/SA/F	✓	✓		✓		✓	✓	✓	✓	Modulus of Elasticity, Temperature Development, Thermal, Sound insulation, Environmental, Microstructure Analysis
[132] [133]	PC/FA/SA/F	✓	✓				✓			✓	Sulfate resistance
[59] [134] [69]	C/FA/F	✓	✓					✓			Air-void analysis
[71] [121] [135]	PC/FA/SA/F	✓	✓				✓	✓			Density-Strength, empirical model
[136]	PC/FA/SA/F	✓	✓		✓	✓				✓	Resillient modulus, F-T and Frost Heave
[115]	PC/SA/F		✓		✓						Modulus of Elasticity
[137]	PC/FA/SA/F		✓								Effect of Curing
[37]	PC/FA/SA/F	✓	✓								Effect of Curing, Corrosion Susceptibility, Environmental Impact
[138]	GBFS/FA/NaOH /H3PO4	✓	✓				✓				Acid Resistance
[139]	Sl/FA/NaOH /SiO2	✓	✓				✓				Modulus of Elasticity, Compressive and Tensile Strength
[140]	PC/PA/SA/F	✓	✓								Environmental Impact
[140]	PC/FA/F	✓									In-situ Setting behaviour (Ultrasonic Pulse)
[141]	PC/FA/SA	✓		✓	✓		✓			✓	PH and Toxicity, Compressive and Tensile Strength
[142]	RM/GGBFS/NaOH	✓	✓								Microstructure, Optimal Mixture Analysis

C: Cement, PC: Portland Cement, CSA: Calcium Sulfo-aluminate Cement, FA: Fly-Ash, PA: Ponded-Ash, RM: Red-Mug Slag, GGBFS: Ground-Granulated Blast Furnace Slag, Sl: Slag, SA: Sand, F: Air-Foam

NA: Not available.

Depending upon application and placement requirement, flow characteristic of CLSMs designed for narrow-trench can vary considerably from plastic to fluid; therefore their flowability can be measured using either concrete or grout test methodologies. Slump cone test [145], flow cone test [146], and open-ended flow cylinder [147] are frequently used for assessing the flowability of CLSM. The slump cone is designed for conventional concrete, which is stiffer than CLSM [148]. However, when a stiffer mixture is required, for instance for filling the narrow-trenches on a slope, [145] becomes a useful indicator of consistency [149]. [150] defines flowability of high, normal and low associated with slump ranges of greater than 200 mm, 150 to 200 mm and less than 200 mm, respectively. The flow cone test is used for neat cement grout but can also be used for CLSM with high flowability and aggregate size less than 6 mm [87]. However, even with small size aggregate, the funnel tends to clog [148]. [87] also reported an increase in efflux time in flow cone test when the density of the foamed CLSM decreases. Considering that the flow cone test is not recommended if the efflux time is more than 35 seconds, it cannot be used for foamed CLSM with low unit weights (lower than 800 kg/m^3 in [87] study). Several state DOTs have used flow cone test method for CLSM; the Florida and Indiana Departments of Transportation requires an efflux time of 30 $\pm$ 5 seconds in this test [151]. Open-ended flow cylinder is specifically designed for CLSM and has become the most common test to measure the flow consistency of CLSM since its adoption by ASTM [144]. [147] specifies lifting a 75 $\times$ 105 mm cylinder, filled with CLSM and open at both ends, and measuring the diameter of the spread CLSM as a measure of consistency. A spread diameter of 200 to 300 mm is considered flowable and acceptable for most narrow-trench reinstatements [39]. Nevertheless, [152]

reported that the test method is not as sensitive to consistency as the conventional slump test. For CLSMs with higher aggregate ratios, Water and fine material may also run out of the cylinder, leaving a sand cylinder standing. Inverted slump cone is a variation of slump cone test that can be used on site to measure the consistency of the CLSM. In this method, the slump cone is inverted and the material is allowed to flow out of the smaller diameter. The spread diameter is a measure of the flow consistency of the mixture as specified in [146]. While the spread diameter in inverted slump cone test often exceeds the diameter of the flow cylinder, [87] conclude a linear correlation between the result of the two tests as expressed in Equation 2.1.

$$Flow_{inverted\ slump} = 2.9 \times Flow_{cylinder} - 120 \tag{2.1}$$

There are many factors that influence the flowability of CLSM, including its components, aggregate, gradation, shape, air content, water content, fly ash type and quantity, to name a few. For example, [97] observed that when coarse fly ash was used as filler, it exhibited 2.5 times higher spread compared to cement–sand slurry, and when sand was replaced with fine fly ash by mass, the consistency of the mix was reduced due to higher fine content. Increase in the foam content in general, reduces the flowability, mainly because of the greater cohesion resulting from higher air content [127], and extra adhesion between the bubbles and solid particles in the mix [97]. Fly ash mixes were also reported to affect foam stability, necessitating larger foam volume to achieve the desired plastic density, which was attributed to the high fluid

consistency in the base mix as well as high residual carbon in the ash [132]. Nevertheless, to achieve the desired flowability for a specific application, trial mixtures should be performed. [141] reported that the proper amount of constituent materials is critical in determining the required amount of water for the desired flowability. Flowability of AA systems highly depends on the activator modulus [153]. Higher activator modulus results in a sticky paste with low flowability. However, when using the low modulus activator, the possibility of segregation and bleeding must be considered [154].

Segregation and bleeding

Gravity-induced homogeneity of cementitious materials is commonly divided into two categories, that is bleeding and segregation [155]. Bleeding is a result of water migration through a dense network of interacting cement grains as a consolidation process [156], whereas segregation is the movement of coarse particles [154]. Because of the high-water content requirement for the high fluidity of CLSM mixtures for use in narrow-trench, there is the potential for excessive segregation and bleeding [157]. This problem is more critical in narrower trenches like micro-trenching which demand high flowability to ensure a complete fill of various cavities deep in the trench. All components of CLSM are in suspension when being placed, and therefore, it is natural for segregation and bleeding to occur when mixtures consolidate. Another reason for the likelihood of segregation and bleeding is that water is the main flow-enhancing ingredient, and there is not sufficient surface area (fines). Generally, the use of fly ash and air-entraining agents increase cohesion and reduces the demand for water, thus minimizing

the potential for segregation and excessive bleeding. Using [158], [159] found that the 30% air-modified mix had 0% bleed water, while the non-air-modified CLSM mixture yielded 2.4% bleed water at the top of the sample.

In general, both the static and dynamic viscosity of AA systems are larger than that of normal Portland cement concrete [154, 160–162]. [154] also reported that AA systems are also less susceptible to segregation than cement-based concrete due to their higher cohesiveness. Nevertheless, high flowing AA systems are still at the risk of segregation. Amount of activator solution is known as one of the factors controlling cohesiveness of the AA system [154]. [163] show that more than 18% of activator results in heavy segregation. Effect of aggregates on the cohesion of AA systems is similar to that of cement-based concrete [164]. [165] suggested the AA paste to the aggregate ratio of 0.33 for a homogeneous distribution of aggregate particles and avoid segregation. Following this recommendation, [166] obtained a highly workable AA concrete with a slump of 240 mm without segregation.

Bleed of the CLSM can be measured by monitoring the height reduction in an undisturbed sample or measuring the amount of bleed water at the surface of the undisturbed sample according to [167], or by measuring the visual stability index as specified in [168]. The test methods for assessing the likelihood of segregation are also include [169], [168], and the sieve stability test [170].

Subsidence

Subsidence or volume reduction of CLSM results from loss of water (through bleeding and absorption into surrounding soil) and/or loss of entrapped air. Due to the high water content of CLSM, subsidence of up to approximately 20 mm/m [37] or 1 to 2 percent of the fill depth [171] has been reported whereas CLSM with lower fluidity shows little or no subsidence [172, 173]. When considering the narrow-trench backfilling, even a small subsidence is noticeable by the road users and reduces the quality of the road. Moreover, water and dirt accumulated in the gap over the trench will damage the backfilling which eventually can end in a complete failure of the backfilling after a few F-T cycles [19]. Subsidence mainly occurs during CLSM placement and can take up until the fresh material sets [39]. Considerable subsidence in foamed CLSM can occur if the foam stability is low, the mixing method is not appropriate, and if the material is subjected to vibration. Therefore, it is recommended to insert the foamed CLSM in the NT using a grout pump with a nozzle to avoid loss of entrained airs [174]. Regardless of the production method, it has been reported that the ultra-low density ($\leq 500 kg/m^3$) foamed concrete are greatly susceptible to instability and subsidence [132, 133, 175]. It has been previously noticed that the average bubble size increases as the density decreases [124, 176, 177]. Increase in buoyancy force of these bigger bubbles and reduce in confinement force of the paste because of the increased air content, will float the entrained air bubbles out of the fresh mix and cause complete separation of the gas and solid [178]. Accelerating admixtures or high early-strength cement may decrease subsidence by reducing bleed water and avoid escaping the air bubbles in foamed-CLSM. Currently, little information is available on subsidence.

Hardening time

[151] defines hardening time as the approximate period of time required for CLSM to develop from the plastic state to a hardened state, with sufficient strength to support the weight of an average person. In the double backfilling method where CLSM will be placed inside the narrow-trench up to the asphalt layer, the traffic is allowed over the trench right after placement of the CLSM [19]. Even though the trench is not fully reinstated, the vehicles can pass the narrow width of the trench without disturbing the filled CLSM. However, in single backfilling setting time of the CLSM mainly controls the re-opening time of the road [18]. Therefore, rapid hardening of CLSM is a desired characteristic that allow the road to be re-opened quickly [179].

Hardening time can be as short as one hour but is usually close to three to five hours under normal conditions [180]. There are many factors affecting the hardening of CLSM, including binder type and content, aggregate type, drainage conditions, proportioning of CLSM, temperature, humidity, and depth of fill. Hardening time, as defined above, is approximate and likely originated from the concept of "Standing-On Time" in concrete technology. The most common and easy approach is to use penetration resistance as an index of hardening. The standard in [181] has been frequently utilized for this purpose [41, 140, 142]. The soil pocket penetrometer has also been used to study the hardening of CLSM. Terzhaghi's bearing-capacity equation of a circular footing is the theoretical basis of this method [141]. Resistance values from the soil pocket penetrometer generally correlate well with those of [181]. Ball drop test [182] is used preliminary in the field as a quality control test to evaluate the mixtures setting time [136]. However, the big size of the ball makes its application impractical for most of the narrow-trench

projects. [183] have used the Vicat needle test to investigate the initial and final setting times of foamed CLSMs, and has compared the results by the values of Ultrasonic Pulse Velocities test. They concluded that while initial and the final setting times can be used to describe arbitrarily chosen stages of setting in practice, the ultrasonic method gives a more continuous and complete picture of the setting process. It is also more suitable for micro-trench where the very narrow width of the trench affects the reliability of other test methods.

Hydration reaction rate will increase with an increase in curing temperature, while the reverse phenomenon is observed when pre-foamed foam and fly ash are incorporated [183]. Based on [140], the setting time will reduce when higher cement or ponded ash contents are used. The molarity of the NaOH solution, water glass, and especially, the curing temperature are also inversely proportioned with the setting time of AA CLSM [139]. According to [138, 184], the setting time decreases with the increase in slag content in AA FA/slag CLSMs. The proper slag content in the mixture was determined to be 15–20% considering the setting, slump, and strength [139].

2.4.2 Hardened CLSM properties

Compressive strength

Like any other applications, compressive strength is one of the most important characteristics of CLSM in narrow-trench backfilling because it determines the load carrying capacity of the reinstatement. However, due to the narrow size of the trench, the existing pavement contributes

to support the traffic load and therefore, only a portion of the service load will be transferred to the CLSM. Numerical study of [38] showed maximum compressive stress of 1.12 MPa in the NT under heavy traffic load. They concluded that the compressive strength of 2-2.5 MPa will ensure stability and excavatability of the CLSM in NT. Nevertheless, there are also different recommendations for compressive strength of CLSM in flexible pavements. For example, [37, 39, 107], specified the upper and lower limits for 28 days unconfined compressive strength of CLSM as 8.3 MPa and 0.3 MPa respectively. [185] also recommended a $7-$day compressive strength of $4-10$ MPa for foamed CLSM as a backfill material. Choosing a high compressive strength for CLSM in NT will make the reinstatement "over designed" and will make the future access to the buried utilities, for repair or development, impossible. Moreover, it might cause trouble in regular maintenance of the road. Therefore, many municipalities require the reinstatement to be stable under traffic load and advised contractors to design a proper compressive strength with regard to the traffic load, pavement condition and future maintenance or reconstruct of the road [8].

The strength of CLSM can be considered in terms of particulate and non-particulate components [157]. The non-particulate component of strength results from the cementitious (and pozzolanic) reaction of cement and fly ash with water. The particulate component of strength is composed of pure friction and dilatancy, similar to granular soil. For unconfined compressive strength, the non-particulate component is dominant, as granular soil has no shear strength without confining pressure. Moreover, there is usually no coarse aggregate in CLSM, especially for the purpose of NT backfill. Water$-$cement ratio is considered as the single, most important

parameter that determines the unconfined compressive strength of CLSM mixtures [141]. Some researchers have deemed cement content as a more convenient index of strength development, possibly because of the insensitivity of strength to water-cement ratio variations at high levels ($\geq$3) [186].

Many mixture proportions have been studied in laboratory testing [137]. Because of the variety of component materials in CLSM, it is difficult to develop a general model to predict the strength development of CLSM mixtures. For a given density, a mix with fine sand resulted in higher strength than another mix with coarse sand, and the variation is higher at higher densities. This higher strength-to-density ratio is attributed to the comparatively uniform distribution of pore in foam concrete with fine sand, while the pores were larger and irregular for mixes with coarse sand [71, 115]. Similar behavior was observed when sand was replaced with fine fly ash [121]. The type and amount of fly ash (if used) also possess important effects on the strength development of CLSM mixtures. [37] found that the use of Class C fly ash increases the strength considerably (up to 78%) when compared with CLSM containing Class F fly ash, mainly due to differences in chemical composition and reactivity. Study on the effect of replacing large volumes of cement with fly ash on the strength of foam concrete reports that up to 67% replacement can be achieved without any significant reduction in strength [59]. When the cement is replaced with silica fume, higher compressive strength is obtained in the long term, due to their pozzolanic reaction and filler characteristics, with a more marked effect at high foam concrete densities [97]. The compressive strength decreases exponentially with a reduction in the density of foam concrete [69]. [187] examined various cellular solids and concluded

that the crushing strength is a function of the relative density and scales according to the power of 1.5. The exponent is a measure of the sensitivity of cement-based foam to density. For dry densities between 500 and 1000 kg/m^3, the compressive strength decreases with an increase in void diameter. For densities higher than 1000 kg/m^3, as the air-voids are far apart to have an influence on the compressive strength, the composition of the paste determines the compressive strength [134]. It has also been reported that small changes in the water−cement ratio do not affect the strength of foam concrete as in the case of normal weight concrete [133]. At higher water−cement ratios (within the consistency and stability limit), an increase in strength is observed with an increase in water−cement ratio [58, 188], just opposite to the trend usually noted for conventional concrete/mortar, where the entrapped air content is only a few percentages by volume. [189] found that the curing effects on the strengths of CLSM mixtures largely depend on the constituent materials and mixture proportioning. However, in general, compressive strength of water−cured foamed concrete is reported to be higher than that cured in air [190]. However, higher strengths are reported for humid air curing at temperatures around 40 $^{\circ}C$ as compared to normal water-cured specimens [191].

AA systems have a considerably lower early strength than cement-based CLSM, which can be a drawback in their application for narrow-trench backfilling. However, their long-term strength can exceed that of cement-based CLSM and even after thermally curing, a compressive strength of 60 MPa can be achieved [192, 193]. [194] reported that polypropylene micro fibres can increase the early age strength of AA systems while decrease the 28 days strength and improve compressive strength after 50 F-T cycles, which is beneficial for narrow-trench

backfilling. It is reported that the concentration of NAOH solution has the most significant effect on the strength of AA systems [195, 196]. However, there is an ideal concentration of activator and beyond that, the presence of free OH^- will change the AA structure and reduce the strength [197]. [198] concluded that the elevated temperature curing considerably accelerates the strength development of AA systems, but at later ages, the compressive strength of the materials is reduced compared with the room temperature cures samples. In practice, AA CLSM in narrow-trench can be heat cured by running hot water into the conduits installed inside the trench. The same method was used by [19] to prevent cement-based CLSM from freezing in a micro-trenching project. Superplasticizer can also be used in AA CLSM to increase early and long-term compressive strength as reported by [199–201].

The standard in [202] was adopted in 1995 and has gained acceptance with state agencies and commercial testing laboratories. The relatively low strength of CLSM may cause potential problems, such as damaging the test cylinder when stripping of CLSM cylinders from plastic molds. Because large-capacity concrete compression machines typically offer poor accuracy in the required low load ranges, the results often show significant variations [203]. The capacities of many load frames used to test CLSM specimens in research laboratories are typically in the range of 1,300 kN to 2,220 kN. To fail a 150 $\times$ 300-mm CLSM specimen with a compressive strength of 1 MPa, a load of only about 18 kN is required. This load is only about one percent of the load frame capacity in a typical concrete compression machine. According to one survey, most state DOTs used concrete machines in the testing of CLSM compression specimens [203]. Researchers using a loading rate of 0.24 MPa/sec failed CLSM specimens in a few seconds, and

could not satisfy the minimum requirement of two-minute failure time specified in the ASTM standard [141].

Re-excavatability

Re-excavatability is one of the critical properties for backfilling utility trenches. Strength of the reinstatement material should allow the future excavation with the purpose of maintenance of the installed utilities or the road itself. Researchers often use unconfined compressive strength of CLSM as the index of excavatability [204, 205]. Generally, CLSM with an unconfined compressive strength of 0.35 to 0.69 MPa have similar bearing capacities as well-compacted granular soil [157], and can be excavated manually [39, 107]. On the other hand, the strength of 2 MPa in France [206] and 1.4 MPa in USA [151] is defined as a differentiator between excavatable and non-excavatable materials using a backhoe. However, those yield values appeared to be insufficient in some cases [131, 207, 208], and too restrictive in others [209]. On the same subject, [205] tried to link the mix proportions of cementitious material to its excavatability using a new punching test apparatus. Engineers in Hamilton County [210] also specify a Removability Modulus (RE) to estimate future excavation of CLSM. According to Equation 2.2, RE is a function of both the thirty-day UCS and the dry unit weight [211]. RE is specified at a maximum one and if the calculated value of the Removability Modulus is less than 1.0, the specific mixture is deemed to be removable in the future.

$$RE = \frac{W^{1.5} \times 104 \times C^{0.5}}{10^6} \tag{2.2}$$

where:

W=in-situ unit weight (pcf) and C=28-day compressive strength

A more sophisticated formula, equation 2.3 , is proposed by [212] which considers the strength of the backfill, equipment used and direction of excavation. CLSM with RF value of 0-20 are considered not-removable, 20-60 difficult to remove and 60-100 are easy to remove.

$$RF = \frac{5.27 \times T \times J \left(1 + \left(\frac{I \times P - D^3}{\sqrt{I \times P \times D}}\right)\right)}{S \times A} \tag{2.3}$$

where:

RF = removeability factor; T = equipment type; J = cutting edge used on the excavating equipment; I = Impact factor; P = power factor based on the equipment used; D = direction of excavation; A = area under the stress-strain curve; and S= density.

A special concern is always needed when the CLSM mixtures are prepared with a high volume of fly ash, as they can keep gaining strength even after a year [39, 107].

Stiffness

As noted earlier, it is critical for reinstatement materials to have a stiffness close to the surrounding pavement to guarantee the compatible deformation of the composite structure under the load. While there is no standard recommended range for modulus of elasticity and Poisson's ratio of CLSM in the NT, they should be high enough to restrict the deformation of the

backfill but not too high to cause micro-cracking due to the high stiffness. As the elastic modulus of the CLSM increases, the stress in the backfilled section due to the traffic load increases and compressive stress in the surrounding soil and pavement, stress in the buried utilities and the displacement in the pavement decreases [38]. On the other hand, resilient modulus of asphalt pavement changes from 700 MPa at 38 $^{\circ}C$ to 14,000 MPa at -1 $^{\circ}C$ [213]. In the pilot installation by [18], an 800 kg/m^3 foamed CLSM with 28−days modulus of elasticity of 700 MPa was used to backfill a micro-trench and no visible distress was observed in the trench after a year. According to [38], this value results in a maximum deformation of 0.6 mm in the trench that can barely be noticed by the traffic.

The static modulus of elasticity of CLSM is reported to be significantly lower than that of normal- or light-weight concretes [122] so that the E-values of normal weight concrete is up to four times larger than that of equivalent strength foam concrete. For brittle cellular solids, [187] also showed that the modulus of elasticity scales according to the square of the relative density. It has been reported that using fine aggregates in higher portions compared to that of coarse aggregate increases the elastic modulus in 28 days [109]. Foamed CLSM with fly ash as a fine aggregate is reported to exhibit lower E-value than that of foam concrete with fine sand, due to the increased interaction between paste and the porous aggregates [122, 214]. [215] has reviewed an empirical model for foamed concrete modulus of elasticity determination. These empirical equations indicate that foamed concrete with high dry density results in higher compressive strength as well as higher modulus of elasticity. In general, the prediction models of

Table 2.4. The regression equations for predicting the modulus of elasticity of cellular foams.

Model	Reference	Equation	Comments
Cement-based foam	[122]	$E = 420 \times f_c^1.18$	when sand is used as fine aggregate [97]
		$E = 990 \times f_c^0.6$	when Fly-ash is used as fine aggregate [97]
	[115]	$E = 33000 \times \gamma^{1.5} f_c^0.5$	Pau's equation [97]
Alkali-activated based foam	[216]	$E = 374.3 \times f_c^{0.671}$	R^2 =0.95 and Correlation coefficient=0.98
		$E = 0.5 \times \gamma \times f_c^{0.561}$	R^2 =0.92 and Correlation coefficient=0.96
	[217]	$E = 580.0 \times f_c^{0.5}$	-

Note: γ is the dry density (kg/m^3), f_c is the compressive strength (MPa) and E is the modulus of elasticity (MPa).

E-modulus can be expressed in one of the following forms:

$$E = a \times f_c^b \tag{2.4}$$

$$E = a \times \gamma \times f_c^b \tag{2.5}$$

in which a and b are fitting constants, γ is the dry density (kg/m^3) and f_c is the compressive strength (MPa).

Table 2.4 summarized some of the regression equations for predicting the E-modulus of cement-based or alkali-activated based foams.

CBR is a penetration-type test developed by California State Highways Department to evaluate the strength of subbase and subgrade materials. Through years of development, [218], is now a standard method to measure the California Bearing Ratio. Researchers have frequently evaluated CLSM mixtures by measuring their CBR values [143], mainly as a subbase

or subgrade material [219–221]. The resilient modulus is another measure of material stiffness. This test was initially used to evaluate pavement subgrades. The work in [222] showed that the resilient modulus of CLSM is usually higher than those of subgrade soils, which are typically within the range of 30–60 MPa. The higher resilient modulus could reduce the post-construction deflection, as well as the pressure exerted on the conduits or pipes by moving traffic load [223], which is beneficial for the loading condition of the installed utilities or conduits. They also found a good linear relationship between the resilient modulus and compressive strength of CLSM. Currently, the method in [224] is commonly used to measure the resilient modulus of CLSM. However, there have been very few studies on the resilient modulus of CLSM mixtures.

Although the compressive strength and modulus of elasticity of conventional cellular concrete are well-established, there is very little data on their Poisson's ratio. The latter is an important parameter in this application as there is considerable lateral stress developed due to the traffic.

Bond strength

Narrow trenches are usually open to traffic right after the backfilling material is set and are thus expected to meet their normal operational loads within a short time post backfilling. Therefore, the bond strength of the CLSM with respect to the surrounding asphalt layer, especially at an early age post filling becomes an important criterion in the mix design.

Among all the tests available to characterize bond between two media, mainly three tests are generally used to evaluate the bond between concrete and asphalt. The most commonly used is the direct tensile test. Tensile failure stress, especially in a composite mix of two different materials like CLSM and asphalt in this study, can be a measure of the bond failure. [225] and [226]; have reported tensile bond strengths of 0.5 MPa and 0.8 MPa (tests performed after 28 days). However tensile tests do not correctly reproduce the stresses existing at the CLSM interface with asphalt. Therefore, the direct shear test, based on the shear Iowa device is also widely used. For instance, [227] and [228] obtained failure shear stresses around 1 MPa for site cored, and laboratory manufactured samples respectively.

Lastly, the compressive slant shear test is also mainly used to characterize the bond between repair material to the substrate. It submits the bond interface to a combined state of shear and compression. [229] have worked on this aspect and have given a theoretical assessment formula for the ratio of bond/compression strengths depending on the angle of the interface between the materials. The Slant shear test (according to [230]) is claimed to provide a realistic representation of stress state in the composite structure [231, 232]. The test is also sensitive to variation in bond strength [231] and therefore, produces consistent results [233]. Nevertheless, Failure is pre-eminently dependent on the angle of the interface plane, which is fixed in the standard test, that is 30 $^{\circ}$ in [230]. Therefore, the failure is not necessarily occurring on the plane with the most critical combination of compressive and shear stresses [234]. Moreover, the results are reported to be insensitive to surface roughness, especially at steeper interface angles [229, 235]. The test is also sensitive to differences to the modulus of elasticity of the materials

which can cause stress concentrations. Lastly, Slant shear test yields much higher values for bond strength than the other tests [229, 234] and therefore, the combined state of shear and compression in Slant shear test might overstate the actual bond strength.

Failures in the composite of the asphalt-concrete structure occur as delamination between layers because of cracking in concrete layer. This phenomenon arises under the combined influence of normal and shear stresses. In flexible pavements, flexural bonding tests are used to account for this combined stress [226]. The flexural bond test allows measurement of the adhesion capacity, or resistance to tearing, of CLSM to the asphalt substrate. Flexural bond test according to [230] is designed to measure the bonding strength the masonry by physical testing of each joint of masonry prism. The small thickness of the CLSM joint between asphalt concrete blocks can be a good representative of the CLSM in NT.

Permeability

The transportation of liquids into CLSM depends on its permeation characteristics, that is permeability, water absorption, and sorption [177]. The permeability is defined as a measure of the water flow under pressure in a saturated porous medium [236]. Since the CLSM in an NT could be in a saturated environment, especially after heavy rain, ingress of water in CLSM is governed by its permeability. Therefore, drainage characteristics, F-T resistance, and leaching potential of CLSM are influenced by its permeability. In NT application, CLSM must be also permeable enough to comply with the natural drainage of the surrounding environment. Otherwise, it will act as a wall in the middle of the road, diverting the flow and in turn lead to

flooding at the end of the trench [28].

Many authors have investigated the relationship between porosity and permeability of mortar and concrete. If the porosity is high and the pores are interconnected the permeability is also high, but if the pores are discontinuous the permeability of the concrete is low although the porosity is high [237]. In general, the water absorption of foamed CLSM is almost twice the normal CLSM at a similar water-to-binder ratio [59]. However, it seems to be insensitive to the volume of air entertainment [237]. Water absorption of foamed concrete is also relatively higher than other types of concrete [238, 239]. Many parameters affect the permeability of CLSM including air-void distribution [97, 240, 241] and mineral admixtures. It was investigated that the increase in ash/cement ratio in foam concrete mixtures proportionally increased the water vapor permeability, especially at the lower densities [237]. It also slightly increases sorptivity [132]. However, it was also reported that when the fly ash was used as 75% of cement replacement, the degree of permeability was demonstrated to be relying on the volume of foam agent to a higher extent than that of mixes with no fly ash [237, 242].

The approach in [243] is often adopted for CLSM mixtures. In an experimental work by [141], a back-pressure of around 550 kPa was applied and maintained to calculate the "B" value as the ratio of pore water pressure to confining pressure change under undrained conditions. However, it must be considered that the pore structure of CLSM specimens can be damaged by such high pressure.

Settlement and consolidation

CLSM may reduce its volume as it releases its free water and entraps air through consolidation of the mixture. The consolidation of soil consists of primary and secondary consolidation. Primary consolidation is mainly caused by seeping of water. Secondary consolidation is caused by rolling, slipping, sliding, crushing at the particle contact points to some extent, and elastic distortions. Similarly, the initial settlement of CLSM mixture within several hours after placement may be regarded as primary consolidation. The further reduction of CLSM volume due to the applied load is similar to the secondary consolidation of soil. Because of the relatively strong and rigid skeleton of CLSM after hardening, consolidation is expected to be very small, and corresponding settlement of backfill will be negligible [157].

The method in [244] can be used to measure the consolidation of CLSM mixtures. The above-mentioned test estimates both the rate and total amount of settlement of CLSM used in various applications. For high-air-content CLSM, the coefficient of volume compressibility is in the range of compacted dense gravel fill [159]. For non-air-modified CLSM mixtures, the coefficients are expected to be significantly smaller [157]. Therefore, lightweight fill was used by [245] to mitigate the settlement in buried utilities.

Drying shrinkage

High water-cement ratio and high water content are two factors known to cause excessive drying shrinkage in concrete. CLSM usually has higher water-to-cement ratios and higher water contents than concrete, therefore shrinkage is one of the main concerns when using CLSM in the

NT. Accordingly, shrinkage can result in the formation of micro-cracks in foamed concrete. Water ingress into these micro-cracks can even result in the failure of trench backfilling, especially under frequent F-T cycles in Canada.

Typical reported linear-shrinkage values of CLSM are in the range of 0.02 to 0.05 %, which is similar to concrete with low drying shrinkage [151]. On the other hand, drying shrinkage is reported as one of the main drawbacks of foamed CLSM in the absence of aggregates, and usually levels off between 3rd and 10th weeks of casting time [246, 247]. Drying shrinkage typically ranges between 0.1% and 0.35% of the total volume of the hardened foamed CLSM [248]. Shrinkage of foamed CLSM is reported to be higher than regular concrete [249] and lower than regular cementitious mortar [135]. The main factor that contributes to the higher shrinkage of foamed-CLSM compared to normal concrete is reported as the use of little or no aggregate in foamed-grout [249]. According to [250], it is the aggregate that restrains shrinkage. Therefore, by increasing the sand-to-cement ratio from 1 to 3, the shrinkage of foam concrete considerably decreases from 0.125% to 0.075% [135]. Drying shrinkage also depends on the curing condition. Autoclaving is reported to reduce the drying shrinkage significantly (by 12–50%) compared to that of moist-cured concrete, due to a change in mineralogical compositions [90, 251]. Moreover, air storage at 70% relative humidity [252] or heat curing [198] significantly reduces the drying shrinkage of AA concrete, making it comparable with shrinkage of cement-based concrete. In relative humidity of 33 and 50%, the drying shrinkage is considerably higher [252, 253]. Furthermore, the shrinkage of foam concrete reduces with density for a fixed solid content [97, 112, 254], which is attributed to the lower paste content affecting the shrinkage in low-density mixes.

The drying shrinkage of AA foamed mortars is reported to be less than regular cementitious mortar [255].

There are several studies on the effect of foamed concrete mix design on drying shrinkage. Some researchers also suggested empirical equations to determine the value of drying shrinkage theoretically based on the mix design constituents [135]. However, there is still a lack of knowledge about the effect of each mix constituent on drying shrinkage of foamed-grout and AA mortars [215]. The water-reducing property of fly-ash can be advantageously used for achieving a considerable reduction in the drying shrinkage of concrete mixtures [256]. However, as reported by [135], using aggregate in the mix reduces drying shrinkage more than using fly-ash. Moreover, using polypropylene microfibre also found to be more effective in reducing drying shrinkage than fly-ash or sand alone [248].

The shrinkage and expansion of CLSM tend to continue varying throughout testing. [257] has found that the maximum shrinkage and expansion values of CLSM were generally less than the acceptable limit established for concrete. The work in [258] also showed that shrinkage of CLSM was minimal when a shrinkage-ring method was used. A shrinkage ring is often used to measure the cracking of concrete cast around a steel ring. This approach represents 100% restraint and can be used to assess different materials and mixtures. Most published studies have used the conventional concrete method to measure the shrinkage of CLSM specimens [257]. This method specifies embedding gage studs at both ends of the prisms of sizes $25 \times 25 \times 160$ (or 285) -mm in accordance with the recommended practice of [259], and measures the length change. Careful handling of the shrinkage prisms is required during the form removal as well

as subsequent measurements. CLSM specimens could be damaged when using this approach because of the lower strengths of CLSM. Thus, this approach may not be appropriate for CLSM. Therefore, [260] suggested using the $25 \times 25 \times 300$ -mm bar specimens for measuring the drying shrinkage of foamed concrete in order to reduce the chance of the specimen damage when demolding, and provide more reliable measurements. Other researchers like [258] have also used the shrinkage ring method, which is not an adopted standard. Since the microstructure of cement-based foam is very similar to that of autoclaved aerated concrete, the standard method for measuring drying shrinkage of autoclaved aerated concrete, that is BS EN 680:2005 [261], has been suggested for foamed CLSM [125].

Thermal expansion

Investigations about the deformation behavior of CLSMs are mostly focused on drying shrinkage after curing [262, 263]. So far, thermal deformations (e.g. during heat curing) have barely been investigated. Specifically, since alkali-activated CLSMs with low-calcium fly ash binders harden slowly at ambient temperatures, they are normally heat cured to improve strength development. Therefore, studying the thermal deformation properties of these materials is of great importance [192].

The coefficient of thermal expansion (CTE) of asphalt concrete mixtures is reportedly between 20-63 $\mu\epsilon/^{\circ}C$ [264, 265]. That for plain mature cement paste is about 11-20 $\mu\epsilon/^{\circ}C$ [250, 266] and develops over a period as the hydration proceeds [267, 268]. While the CTE of lightweight

concretes is between 7-13 $\mu\epsilon/^{\circ}C$ [269, 270], there is very limited data on the CTE of cement-based foams. As reported by [125, 271–273], the values range from 8.1 to 41.7 $\mu\epsilon/^{\circ}C$.

[274] has stated that the CTE of concrete is the resultant of the individual values for hydrated cement paste and aggregates, as they have dissimilar thermal expansion values. It was reported that neat cement has a much higher CTE than concrete containing sand, with the thermal expansion coefficient decreasing as the sand content increases. This is due to the inherently lower CTE of aggregates than cement pastes [275]. Moreover, for 500 kg/m^3 autoclaved aerated CLSM containing fly ash, [276] reported the CTE as 9.4 $\mu\epsilon/^{\circ}C$. While there was no information available about the influence of sand or fly−ash combinations on thermal expansion, [277] stated that fly ash does not really affect the coefficient of thermal expansion. Therefore, it can be concluded that the lower the aggregate content (to restrain the expansive strains), the higher the coefficient of thermal expansion value. As there is a lower amount of aggregates (or no aggregates) in lightweight CLSM than normal weight concrete, thermal expansion is expected to be higher in lightweight CLSM. However among the foamed CLSM, it is generally to be expected that the more porous the material, the lower the CTE. This is because porous solids are inherently less conductive thermally. In contrast to the study of [277], [278] relate CTE to porosity and portlandite (Ca(OH)2) content of the hardened cement paste. Portlandite has a much higher CTE than that of normal cement paste and therefore, any reduction in portlandite content will result in a reduction in CTE. Since replacing Portland cement with fly-ash reduces the portlandite content and increase porosity, it reduces the coefficient of thermal expansion.

Principally, the methods for the determination of the CTE can be classified into two groups [279]:

1. The "saw-tooth temperature" method, in which the sample is subjected to cycles of heating-(holding)-cooling [280–284]. The CTE is calculated based on the change in the volume of samples [280], or their length [281–284]. In this method, the autogenous deformation during the temperature cycles is not considered, and is regarded as the consequence of the change in temperature.

2. The "maturity concept" method in which two samples from the same mortar batch are subjected to two temperature histories [285]. The maturity of the samples is expressed by the equivalent time calculated using the Arrhenius equation. It is assumed that at the same equivalent time (maturity), the autogenous deformation of both samples is the same. The difference in total deformation between the samples is thus the difference in thermal deformation caused by their temperature deviation. In the literature, this method is much less used than the "saw-tooth temperature" method.

Many studies measure the CTE following the assumptions of the standard in [286]. This standard covers the determination of the CTE of hydraulic cement concrete cores and cylinders by measuring the length change of the specimen due to a specified temperature change. To make the procedure more compatible for the lightweight CLSM specimens, few modifications to [286] was suggested by [125]. Following this procedure, specimens will be kept saturated for 24-hours in 20 $^{\circ}C$ water bath to reach the maximum expansion caused by water saturation.

Any further expansion (during testing) can then be assumed to be solely caused by the increase in temperature. Length of the specimens will be measured and immediately after, two of the specimens will be put in a 50 $^{\circ}C$ water bath, and the other two specimens will be kept in a 20 $^{\circ}C$ water tank as control specimens. Following a further 24-hours of submersion, the length changes of the specimens will be measured in both 50 and 20 $^{\circ}C$ water tanks. Length changes of the control specimens were then subtracted from the test specimens. CET is then calculated as the ratio of the strain in test samples caused by temperature change, over the change in the temperature.

Freeze-thaw resistance

Freezing-and-thawing resistance is an important durability parameter for construction materials. There have been several laboratory and field studies on the freezing and thawing resistance of CLSM [222, 287–290]. Low cement, high fly ash content CLSM broke into pieces about the size of a hand when it was placed in a zone of total water saturation and subjected to severe winter freezing and temperatures below –18 $^{\circ}C$ [287]. Without water saturation, this type of CLSM appears to perform well under freeze-and-thaw conditions in the field [287]. [291] investigated the effect of the aggregate type and plastic density on the freeze–thaw resistance behavior of foam CLSM. Results revealed that the Foamed CLSM with both sand and coarse fly ash exhibits a good F-T resistance performance compare to the mixes with only sand or fly ash. Lower densities also result in higher FT expansion. Although the large expansion, the strength of specimens did not show a significant decrease. In narrow-trenching, this frost heave can

push the top sealant layer out of the trench which can consequently be pilled off by the traffic over the trench. In this regard, [289] proposed that the top 5 to 150 mm of CLSM mixture fill be replaced by a frost heave-compatible material for a uniform heaving of pavement and trench, after 24 hours of CLSM placement. Foamed CLSM with a high cement content (10%) is recommended for construction applications where severe freezing is expected [157]. According to [159], regular CLSM specimens failed in only five cycles during the testing process of [292] while high air content CLSM mixtures with 21% and 30% air contents performed satisfactorily in the test. [136] studied the effect of different replacement levels of cement by fly ash on F-T resistance of ultra-low strength mixtures. Results revealed that CLSM with fly ash had a high susceptibility to frost heave, which increased with an increase in fly ash content. These mixtures had low freeze–thaw durability, which was demonstrated by a significant reduction in their stiffness modulus after repeated freeze–thaw cycles while Air-entrained CLSM without fly ash had negligible frost heave.

F-T resistance of AA CLSM has not been fully studied yet [293, 294]. According to the limited studies available, AA concrete has a superior performance in F-T resistance over Portland cement concrete [295]. [296] also reported that AA concrete withstands 2.2 times more F-T cycles than cement concrete.

Conventional concrete test methods for freezing-and-thawing resistance have been found to be severe for CLSM [157]. The low strength and the high permeability of CLSM make it susceptible to damage under testing conditions for concrete. The high permeability allows water to enter CLSM samples easily and ice lenses to form inside the specimens. As a result, the material

is damaged internally. This phenomenon is very similar to the frost heave of soil. The internal hydraulic pressure generated during water freezing also damages the skeletal structure of CLSM. [288] have modified existing concrete test methods by exposing CLSM specimens to less severe environments to simulate field conditions. [292] is a method to measure the ability of soil-cement mixtures to resist freezing-and-thawing cycles. Because of the similarity of CLSM and soil-cement, the method is beginning to gain acceptance in the research community [74, 297]. This method is much less severe than those for concrete and requires only 12 freezing-and-thawing cycles. A modification of [298] Method B, which comprised of freezing specimens in the air and thawing them in the water, was also used as a representative freeze–thaw test due to the absorption and failure characteristics of cellular concrete [136, 290, 291]. However, ASTM C666 provides no provisions for normalizing the moisture content of specimens. Moisture content at the time of freezing is an important parameter governing cellular concrete freeze–thaw behavior. A saturation procedure to normalize the moisture content is suggested by [290] to account for natural absorption characteristics.

2.5 Specification of CLSM

Cement-based grouts have been used for utility trench backfilling over decades. Different specifications are available for flowable-fill or CLSM. Table 2.5 summarizes some of the requirements of the flowable-fill, shows the test methods (mainly from ASTM), and the acceptance criteria of a quality CLSM mixture specified in the document. The [39] document is not only

Table 2.5. Summary of requirements for CLSM materials

Source	City of Winnipeg	National ready mixed concrete association	City of Colorado Springs	NCHRP report 597	ACI 229R	FHWA-RD-97-148
Application	Flowable-fill	General construction backfills	Cellular flash-fill	General construction backfills	General construction backfills	Flowable-fill
Compressive Strength (28 days)	1.5- 2.5 Mpa (CSA A23.2-3C)	$<$ 8 MPa (ASTM D4832)	0.7- 2 Mpa (ASTM D4832)	$>$ [0.2 Mpa] (AASHTO X1)	0.1-2.1 Mpa	$<$2.1 Mpa
Slump/flow (ASTM D6103)	$>$ 200 mm	$>$ 150 mm	$>$ 200 mm	$>$ 200 mm	-	[150-250 mm]
Air-content	$>$ 20% (CW 2160.1)	- (ASTM D6023)	$>$ 15% (ASTM C231)	$>$ 6%	-	-
Removability Modulus	-	-	$<$1.5	-	-	-
Permeability Coefficient (k)	-	-	-	$1 \times 10^{-}4$ mm/s (AASHTO X7)	-	-

the main guideline used in the USA but also has been widely referenced by many countries. To the best of our knowledge, except the USA there is no specific standard and CLSM specification published by other countries. It has clearly described the properties of CLSM in its fresh and hardened state and provides useful advice to purchasers of ready-mixed and site mixed concrete on how CLSM should be specified in relation to specific ASTM standards. However, its recommendations might not be applied for the specific use of CLSM in narrow-trenching in the flexible pavement. Due to the growing popularity of narrow-trenching in the urban area, various recommendations are published by municipalities [8, 36, 185]. However, they only deal with the general recommendations and lack specific advice for the properties of the reinstated materials.

2.6 Conclusion

1. Rheology of CLSM, especially foamed CLSM, which is one of the most important parameter affecting the developing behaviour of the backfill and its performance in the practical

applications, needs to be studied in detail.

2. In general, there is limited information on the behaviour of different cement substitute blends. Therefore, analysis of the behaviour of such cement systems, including its effects on CLSM properties (fresh, early age, hardened and insulation), needs to be carried out.

3. Composite performance of the CLSM with its surrounding materials in narrow-trench requires more attention.

4. Durability properties of CLSM, especially F-T resistance and frost heave, over a range of densities would value from further research. The analysis needs to be carried out in respect to foamed concrete density, type of constituents, hardened properties like stiffness, bubble size and microstructural properties such as porosity and tortuosity.

5. Full scale trials of CLSM in narrow-trench need to be designed and tested, specifically in micro-trenching application which the width of the trench can be only 4 cm, to evaluate the fresh and hardened properties along with excavatability of flowable fill and examine the effects of surrounding environments and local climate conditions on these properties compared to laboratory results.

6. Considering the advanced computer simulation tools available, a structural model should be created using advanced software for different backfilling applications with CLSM to computationally understand the behavior of material and structure as a whole component. In absences of the standard recommendations for reinstatement materials based

on experiment, simulation results can be useful for performance evaluation of different narrow-trenching backfills.

Chapter 3

Rutting Resistance and Moisture Damage of Cold Asphalt Mixes

Cold mix asphalt (CMA) is considered a convenient and rapid solution for pavement pothole repair as well as narrow-trenching reinstatement projects. Despite the wide use of CMAs, reliable procedures for quality control and screening of different types of these mixes are still not available. This chapter studies and compares the engineering properties, permanent deformation and moisture resistance of nine types of CMAs. For this purpose, three different well-known experiments, namely Marshall stability, indirect tensile strength, and the Hamburg wheel tracker tests, were performed on each oven-cured and ambient-cured CMA sample. The results mainly showed that the rutting resistance of densely-graded CMA samples is considerably higher than the open-graded samples. However, moisture susceptibility of dense-graded CMAs is commonly higher than open-graded CMAs. The dust-to-binder ratio seemed to have a high correlation with the moisture susceptibility of dense-graded CMAs, while the percentage

of coarse aggregates plays an important role in that of open-graded CMAs.

3.1 Introduction

Pavement repairs and trench reinstatement can be time- and cost-consuming, so the durability and quality of asphalt repair materials are of great importance. One of the most common and environmentally friendly approaches in constructing and rehabilitating pavements is the use of cold mix asphalt (CMA). As explained in Chapter 2, CMA is also commonly used for the purpose of narrow-trenching (NT) backfilling. CMA is produced by blending aggregates with special bitumen emulsion or cutback, thereby eliminating the need to use a hot asphalt binder. As a result, CMA aggregate does not require heating or drying, which saves a significant amount of energy [299]. It can also be stockpiled, and it has a longer working life [300]. CMA can also be used in the winter, a time when hot mix asphalt (HMA) is not practical [300, 301].

However, the performance of CMA is usually weaker than HMA, especially with rutting and moisture-damage resistance. Rutting is an accumulation of permanent deformation caused by repeated loads at high temperatures that mainly occurs in the asphalt layers. Rutting affects the pavement's ride quality and can lead to serious safety issues. Moisture damage is defined as the progressive loss of mechanical characteristics of asphalt mixtures due to moisture exposure under mechanical loading [302]. Moisture damage can also be accelerated after rutting or other significant pavement defects as a later-stage distress [303].

Various laboratory tests have been developed to mark the rutting resistance of asphalt mixtures, including Marshall stability and flow [304, 305], indirect tensile strength (ITS), and Hamburg wheel tracking (HWT) [306]. Both the ITS and HWT tests can be used as an indicator of moisture damage in asphalt concrete surfaces by testing the specimens under wet conditions. The HWT test could be a potential substitute for the widely used ITS test since it can simulate the dynamic effect of vehicle load [307, 308]. While Maher et al. [309] reported that no significant correlation could be made with the Marshall stability test, ITS, or field performance, HWT test results have been proven to generally correlate with other wheel tracking tests, such as the asphalt pavement analyzer [310], as well as field performance [311, 312]. The HWT device is designed for HMA; it can be harsh on CMA, resulting in premature failure of specimens [313]. Nevertheless, different researchers have used it to determine engineering properties and performances of CMA materials [314–316].

Despite the few specifications regarding the production and placement of CMAs [313, 317, 318], the evaluation methods and indicators related to CMA materials are not very clear. Generally, open-graded (OG) CMAs with a naturally higher void content allow a quick escape of volatiles when fully compacted, but this results in reduced deformation resistance and stiffness. Dense-graded (DG) CMAs may provide better durability and stability when installed, but have reduced workability for stockpiling and handling [314, 315, 319, 320].

Based on the foregoing information, this chapter provides a direct comparative evaluation

of nine ready-to-use CMAs to characterize their resistance to permanent deformation and moisture damage. Toward this goal, materials are tested in two different curing conditions to simulate their early life and long-term behavior. The Marshall stability and flow test is used to measure the cold mix samples' resistance to permanent deformation, and the results are compared to the HWT test results under dry conditions. The moisture-damage resistance of each of these CMAs is also evaluated by ITS and HWT tests under wet conditions.

3.2 Materials and experimental procedures

For the purpose of this study, nine popular ready-to-use CMAs in the US and Canada were collected. Among them, six were proprietary cold mixes available for purchase, and three were conventional CMAs applied for local use. In this chapter, the CMAs tested were named as CMA-1 to CMA-9, which CMA-1 to CMA-5 are DG and CMA-6 to CMA-9 are OG. The mixtures' properties, based on the information provided by the manufacturers, are summarized as below:

- **CMA-1** is specifically formulated for pothole and crack repair over 25.4-mm wide in asphalt pavements. CMA-1 mixture consists of sand, stone, proprietary additives, and cutback bitumen (Generally 3.5% of PG64-22).

- **CMA-2** is a special blend of cutback bitumen (4-6.5%) and graded limestone. It can be used when surface temperatures are as low as -40 $^{\circ}C$ to as high as 76 $^{\circ}C$. As claimed

by the manufacturer, it is the only rapid-curing asphaltic concrete patching material in existence.

- **CMA-3** mixture is made by mixing mineral aggregate, filler, and emulsified bitumen. A coating test, according to the ASTM D2489 standard, reported 90% of coated aggregates.

- **CMA-4** is a high-float emulsion mixture used for pothole patching. It is a DG conventional cold mix, and the design procedure is similar to the cutback asphalt mixture.

- **CMA-5** is a mixture of cutback bitumen, graded aggregates, and polymer additives. The bituminous material is a liquid asphalt blend prepared from a base asphalt stock of either AC-5, AC-10, or AC-20 with an approved blending formula. The aggregates consist of 85% mainland sand and gravel and 15% washed sand.

- **CMA-6** is produced from crushed aggregate and 5-6.5% of cutback bitumen binder. An aggregate coating test reported more than 95% coated aggregates. The US federal government also named this mixture as one of its control materials in the Strategic Highway Research Program [321].

- **CMA-7**'s modified cutback bitumen is formulated using liquid asphalt cement, cutter stocks, binding adhesives, and anti-stripping agents. The mixture aggregates consist of 100% crushed stone. It has a stripping resistance of 95% retained coating. It is also usable from -20 $^{\circ}C$ to 40 $^{\circ}C$. CMA-7 is Department of Transportation (DOT) approved in all US states and is being used throughout Canada.

- **CMA-8** is a proprietary formula composed of cutback bitumen, special aggregate, polymer additive, and pressure-sensitive plastics. It sets up by compaction rather than by evaporation.

- **CMA-9** is another cutback asphalt. Aggregate consists of a minimum 80% crushed, washed, or screened limestone or approved equivalent. The mix can be applied in sub-zero temperatures and will adhere in wet conditions.

The testing procedure of this study is divided into three major steps. In the first step, the physical properties of the CMA materials were determined by ignition testing, followed by gradation analysis to further investigate the mixtures' designs. In the second step, the rutting and stripping performance of materials were examined through a series of laboratory tests. In the third step, the results of each test were analyzed to quantify and compare rutting and moisture susceptibility of CMA materials.

3.2.1 Binder content and gradation

Manufacturers present the gradation and binder content of the CMAs as an expected range. In order to obtain accurate information about the mixtures' compositions, the binder content and gradation of each sample were tested according to AASHTO T308 [322] and T30 [323], respectively. After determining the moisture content of the CMAs according to AASHTO T329 [324], two 1,200 g samples of each CMA were burned in an ignition furnace set to 587 °C. The binder content was then calculated as the difference between the initial mass of the sample

and the final mass of the residual aggregates after applying the correction factors. Then, the gradation test can be run on the remaining aggregates.

Figure 3.1 shows the aggregate gradation curves and binder content of the DG and OG asphalt samples. The average binder content of DG and OG CMAs are close (4.66% vs 4.39%), while the highest binder content belongs to CMA-6 (6.71%) and the lowest to CMA-8 (2.44%), both of which are OG mixes.

Gradation is noted as one of the main factors affecting load-bearing and rutting resistance of asphalt mixtures [325]. The stone-to-stone contact of coarse aggregates is considered to be the main source of internal resistance [326]. On the other hand, the dust content can affect the properties of the asphalt concrete mixtures' mastic (asphalt binder and dust) and will reduce the percent of voids in aggregates. Hence, dust content is considered to be a remarkable mixtures parameter that affects the workability and deformation resistance of asphalt concrete [327]. In this study, the percentage of particles smaller than 0.08 mm is considered "dust content", and "percent of coarse aggregates" is the cumulative percentage of retained particles on the 5-mm sieve (Figure 3.1). The nominal maximum aggregate size is 12.5 mm for all CMAs except CMA-7 and CMA-9, which are both 10 mm. CMA-4 and CMA-5 have the finest gradation, and CMA-2 has the coarsest gradation out of the DG CMAs with almost 34% coarse aggregates. Among the OG aggregate particle size distribution curves, CMA-9 has the coarsest uniform distribution, and CMA-6, CMA-7, and CMA-8 have almost the same distribution.

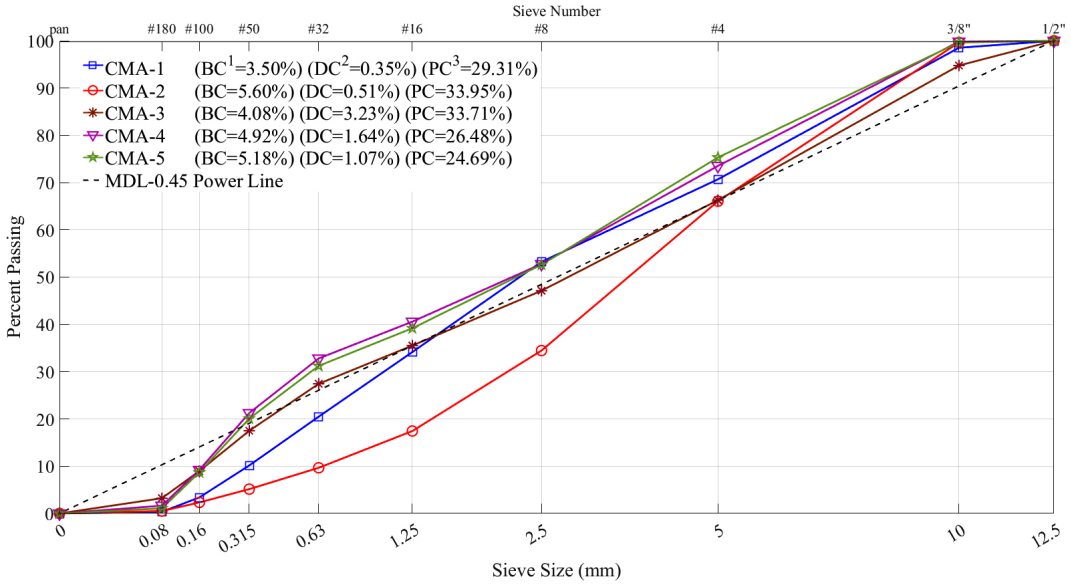

(a)

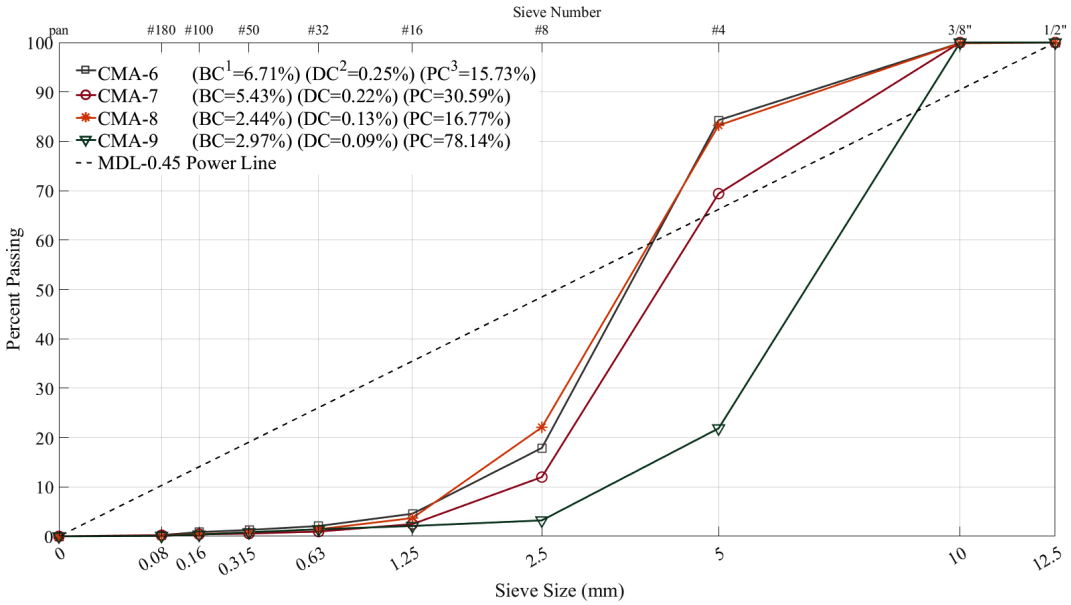

[1] Binder Content; [2] Dust Content (<0.08mm); [3] Percent of Coarse Aggregates (>5mm)

(b)

Fig. 3.1. Gradation curves, binder content and percent of dust and coarse aggregates for the DG (a) and OG (b) samples

3.2.2 Marshall stability and flow test

The stability of asphalt concrete determines performance. Asphalt concrete with low stability can result in various types of pavement distress [328, 329], including rutting and shoving [330]. Marshall flow is also defined as the vertical deformation of the sample, and high flow value generally marks a plastic mix, which is susceptible to rutting under traffic load [331, 332]. The majority of the laboratory tests are designed for HMA, so CMA must be oven-cured to add strength for further testing. The accelerated curing process is also proven to be a reliable approach to forecast the ultimate strength of the CMAs at their mature states [316]. According to [333], materials were cured overnight at 135 $^{\circ}C$. Then the specimens were prepared by applying 75 blows on each side using a standard Marshall Hammer. This procedure follows recommendations by the [334] and proposed test methods by [316].

A Marshall stability and flow test was conducted on cured specimens conforming to ASTM D6927 [335]. After conditioning at 60 $^{\circ}C$ in a water bath, the peak load on the specimens was observed at a loading rate of 50.8 mm/min. Load-deformation values are recorded over time to determine specimen stability and flow.

The Marshall stability numbers of all CMA samples are reported in Table 3.1 and 3.2. As Table 3.1 indicates, all DG specimens had high stability values. With the exception of CMA-1, all DG CMAs had a higher stability value than the recommended stability of 11,500 N for HMA. Among the OG mixes and according to Table 3.2, CMA-6 had a stability close to HMA. The rest of the OG mixes had a low stability, which can be a result of their high air-void contents.

The Marshall Quotient (MQ) is defined as the ratio of stability to flow (rigidity ratio). Higher

Table 3.1. Marshall Stability and Flow Test Results and MQ Values of DG CMAs

Laboratory Test	Tested Parameter	CMA-1	CMA-2	CMA-3	CMA-4	CMA-5
Marshall Stability and Flow	Stability (N)	6,800	18,950	16,600	15,000	13,700
	MQ (N/mm)	3,886	12,633	8,300	7,500	6,850

Note: MQ= Marshall Quotient; these data are each the average of at least three test replicates.

Table 3.2. Marshall Stability and Flow Test Results and MQ Values of OG CMAs.

Laboratory Test	Tested Parameter	CMA-6	CMA-7	CMA-8	CMA-9
Marshall Stability and Flow	Stability (N)	10,100	5,450	5,400	3,400
	MQ (N/mm)	8,080	4,360	4,320	2,720

Note: MQ= Marshall Quotient; these data are each the average of at least three test replicates.

MQ values portray higher mixture stiffness, which can be interpreted as a material's higher resistance to permanent deformation in service [305, 336] . The average MQ value of DG CMAs is higher than that of OG mixes, which implies higher resistance to shear stress and rutting. The MQ value of CMA-2 is almost twice the upper recommended range for HMA, which means it has high stiffness and low workability.

3.2.3 Indirect tensile strength test

In this study, an ITS test was performed on all cured samples following the AASHTO T 283 [337] guideline. According to the standard, the long-term stripping potential of an asphalt mixture is determined by measuring the change in ITS of samples subjected to water saturation, then compared with the same properties of dry samples.

Following the same curing process as the Marshall stability and flow test, two sets of samples consisting of three specimens each were prepared from each material. The first set was

tested for ITS in dry conditions, and the second set was saturated in a 25 $^{\circ}C$ water bath to reach a 70-80% degree of saturation before being tested for ITS. Cylindrical specimens were subjected to compressive loading at 50 mm/min at a temperature of 25 $^{\circ}C$. The load was applied along the vertical diameter plane of the specimen, causing failure by splitting along the vertical diameter. Peak load at failure was measured, and the tensile strength of the conditioned specimens was compared to the dry specimens to determine the tensile strength ratio (TSR), which shows the susceptibility of the material to moisture damage.

The results of the ITS testing are included in Table 3.3 and 3.4. Except for CMA-2, CMA-3, and CMA-5, the ITS values of all other cold mix specimens were smaller than the minimum specified value of 800 kPa for HMA [314]. The average ITS of the DG mixes is also considerably higher than the OG asphalts. Nonetheless, to assess the performance of an asphalt mixture, tensile strength should be considered along with the TSR value [338]. Despite the high ITS value of CMA-3 in the dry test, its tensile strength reduced considerably in the wet test. CMA-3's TSR value of 0.66 marks its high moisture-damage susceptibility. On the other hand, CMA-2 assumedly has a high deformation and moisture-damage resistance based on its high tensile strength and TSR value. Excluding CMA-9, the TSR of all OG CMAs was higher than the minimum recommended value of 0.8 for HMA [338]. The tensile strength of CMA-9 was the least among all studied CMAs, and its TSR value of 0.64 made this asphalt mixture the most susceptible to moisture damage.

Table 3.3. Indirect tensile strength test results for DG CMAs.

Laboratory Test	Tested Parameter	CMA-1	CMA-2	CMA-3	CMA-4	CMA-5
ITS	ITS (kPa), Dry	790	1,568	1,070	498	883
	TSR (Saturation)	1.05	1.06	0.66	0.77	0.86

Note: These data are each the average of at least three test replicates.

Table 3.4. Indirect tensile strength test results for OG CMAs.

Laboratory Test	Tested Parameter	CMA-6	CMA-7	CMA-8	CMA-9
ITS	ITS (kPa), Dry	592	546	522	370
	TSR (Saturation)	0.89	0.85	0.95	0.64

Note: These data are each the average of at least three test replicates.

3.2.4 Hamburg wheel tracking test

An HWT test measures the rutting and moisture susceptibility of asphalt mixtures by rolling a steel wheel over the sample inside a temperature-controlled chamber according to AASHTO T324-11 [339]. In this research, two CMA cylindrical samples fitted in a 60-mm deep high-density polyethylene mold were inserted beneath the wheel. The wheel moved back and forth at a rate of 52 passes/minute, boring on the CMA samples. The wheel moved along the surface of the CMA specimens at a standard loading of 705 ± 4.5 N. The vertical deformation induced at the middle of the sample versus the number of passes was recorded to characterize the rutting resistance of the CMAs.

The number of passes should be adjusted appropriately so the moisture damage of the samples can be observed in immersed conditions. In a study by the City of Hamburg, it was observed that when the samples were subjected to 19,200 passes, the effect of moisture damage could be observed just after 10,000 passes [340]. Therefore, the literature suggested performing

more than 10,000 wheel passes to reveal the effect of moisture damage [340, 341]. Hence, in this research, the test was terminated after 20,000 passes or when vertical deformation of the samples reached 12 mm.

Three variations of the wheel tracking test were used to evaluate CMA characteristics. The first wheel tracking test was performed at 25 $^{\circ}C$ air temperature to evaluate the rutting characteristics of CMA under dry conditions. The second wheel tracking test was conducted on CMA samples submerged in 25 $^{\circ}C$ water to evaluate the effect of moisture on rutting performance. The third test was performed on CMA samples submerged in 50 $^{\circ}C$ hot water to further investigate the moisture susceptibility of the samples, all of which performed well in the 25 $^{\circ}C$ wet test. Even though previous researchers have used both 40 $^{\circ}C$ and 50 $^{\circ}C$, 50 $^{\circ}C$ is the most common test temperature [342, 343].

To prepare the HWT specimens, loose CMA was placed inside a cylindrical mold with a diameter of 150 mm and loaded into a Superpave Gyratory Compactor (SGC). A compactor arm was lowered into the mold, compressing the sample with an applied pressure of 600 kPa. The specimens underwent 200 gyratory revolutions at this pressure, resulting in a height of 62 mm. For each wheel tracking test, two SGC cylindrical specimens were prepared and mounted on a wheel tracker mold. To investigate the early-life rutting potential of asphalt samples, one set of samples was compacted at ambient temperature and then cured at 25 $^{\circ}C$ for 24 hours. To investigate the effect of curing on the rutting susceptibility, another set of samples was compacted after curing for 18 hours at 135 $^{\circ}C$ [309, 333, 344]. In this study, the first sets are referred to as ambient-cured and the second set as oven-cured samples. The curing procedure helps to

Table 3.5. Summary of air voids measurement results

		DG					OG			
		CMA-1	CMA-2	CMA-3	CMA-4	CMA-5	CMA-6	CMA-7	CMA-8	CMA-9
AC[a]	Rep.[1]	4	4	10	6	5	NA	NA	NA	NA
	%AV[2]	6.8	10.7	7.3	6.5	6.5	NA	NA	NA	NA
	STD[3]	0.51	0.29	0.6	0.07	0.34	NA	NA	NA	NA
OC[b]	Rep.	12	10	6	6	9	8	8	8	8
	%AV	8.4	10.5	7.9	7.8	7.2	9.3	9.9	16.9	12.2
	STD	0.51	0.58	0.99	0.45	0.36	0.23	0.6	0.67	0.3

[a] Ambient-cured samples; [b] Oven-cured samples.
[1] Number of test replicates; [2] Average air voids; [3] Standard deviation.
NA: Not available.

add stability to the samples and simulates the field condition after several weeks of mix compaction. Physical properties of the tested samples are also calculated according to AASHTO T209 [345] before each test, and the average values for ambient-cured and oven-cured samples are included in Table 3.5.

HWT on ambient-cured samples

The HWT device was originally designed to test HMA samples and might be too intense for ambient-cured CMA specimens. CMA samples that are compacted after a short curing time or at a low temperature are reported to collapse right after compaction or under the HWT device [346]. Based on Chatterjee et al. [347], the cold-mix specimens should have air voids close to 10% to have enough density under the HWT test. Most of the CMAs tested had an air void close to 10% excluding CMA-8, which had a higher value of 17%. After compaction, all ambient-cured OG samples collapsed, but ambient-cured DG samples were stable enough to

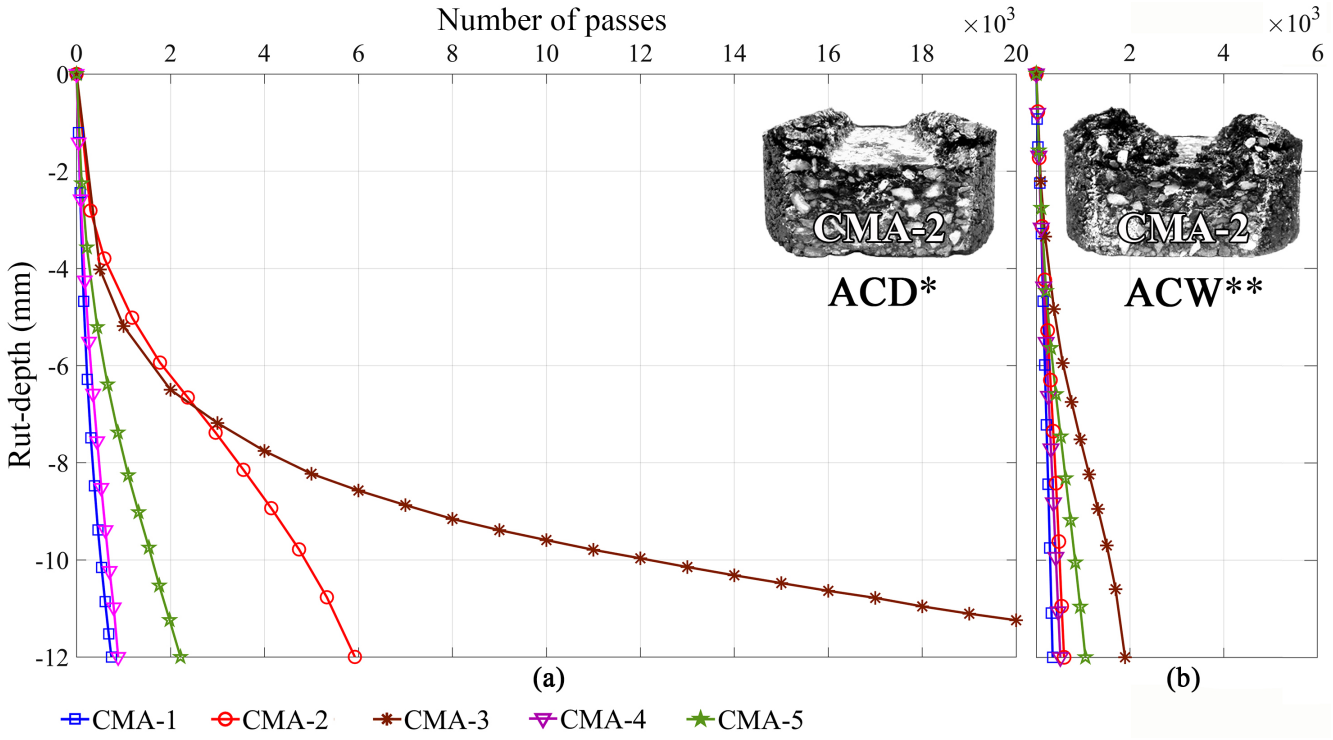

* Ambient-cured sample tested under dry condition; ** Ambient-cured sample tested under wet condition.
Note: Each curve represents an average of at least two test replicates.

Fig. 3.2. Rut-depth curves for ambient-cured-DG CMAs tested under dry (a) and wet (b) conditions.

be tested in dry and wet conditions with an HWT device. Each test was repeated at least twice to ensure the validity of the results. Figure 3.2 shows the average rut-depth curves of each DG CMA studied in this research under dry (ACD) and wet (ACW) conditions.

As the ACD and ACW curves reveal, all samples failed prematurely except CMA-3 ACD. The curve for CMA-3 ACD shows a rapid increase in rut depth in its first 2,000 passes and then displays a slight increase at a constant rate until reaching the test termination of 20,000 passes. Despite this strong performance of CMA-3 under dry conditions, it failed with a steep rate of rutting under water. Presence of water also increased the rutting rate of CMA-2 and CMA-5 but

did not have a considerable effect on the CMA-1 and CMA-4 samples. Based on the results of the HWT test on wet ambient-cured samples, it can be concluded that the ambient-cured CMA patching materials are highly susceptible to moisture damage in their early lives.

HWT test on oven-cured samples

The oven-cured CMA samples were first tested in dry conditions at 25 $^{\circ}C$ to evaluate their rutting resistance. Solid-line curves in Figure 3.3a present the average rut-depth curves of oven-cured DG CMAs tested under dry conditions (OCD). The deformation curves for CMA-1, CMA-2, and CMA-5 remain almost constant after the primary consolidation. The rut-depth curve for CMA-3 shows a superior performance until 15,000 passes, but then the rut depth starts to increase with an accelerated rate. CMA-4 shows the least resistance to rutting among the DG CMAs studied here. Considering the fact that the air void contents of CMA-1, CMA-3, and CMA-4 are almost the same, the lower rutting resistance of CMA-4 could be a result of the lower quality of its emulsified binder. The values of Table 3.3 also confirm that CMA-4 has lower tensile strength compared to other DG mixes.

Among the oven-cured OG CMAs tested under dry conditions (dashed-line curves in Figure 3.3a), only CMA-9 withstood 20,000 passes with a rut depth of 9 mm. CMA-8, CMA-7, and CMA-6 reached the ultimate 12-mm rut depth with almost similar rates of rutting.

With the second series of tests on oven-cured CMAs, the effect of moisture on rutting resistance of CMAs was investigated by testing them under 25 $^{\circ}C$ water. Figure 3.4 shows the rut-depth curves of DG and OG samples (OCW). As the solid-line curves for DG CMAs show,

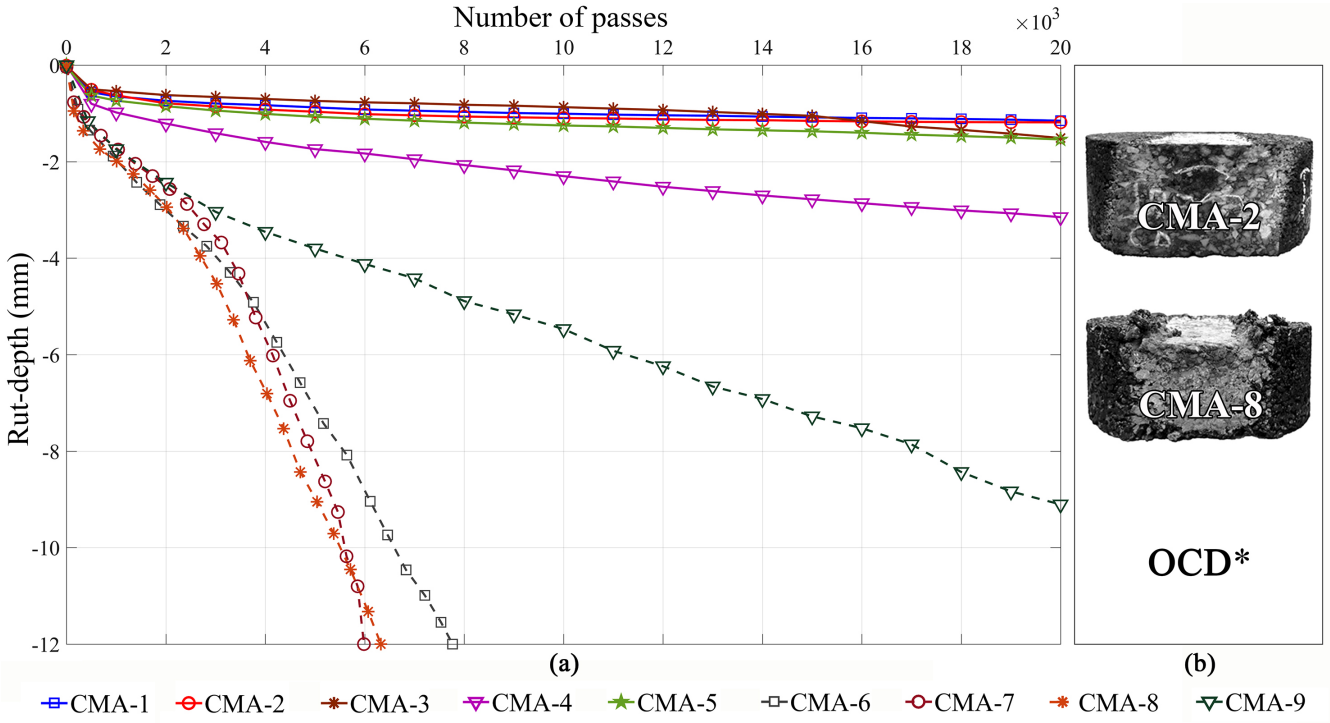

* Oven-cured sample tested under dry condition.
Note: Each curve represents an average of at least two test replicates.

Fig. 3.3. (a) Rut-depth curves for oven-cured CMAs tested under dry conditions. (b) HWT results on one CMA-2 and CMA-8 specimen cuts.

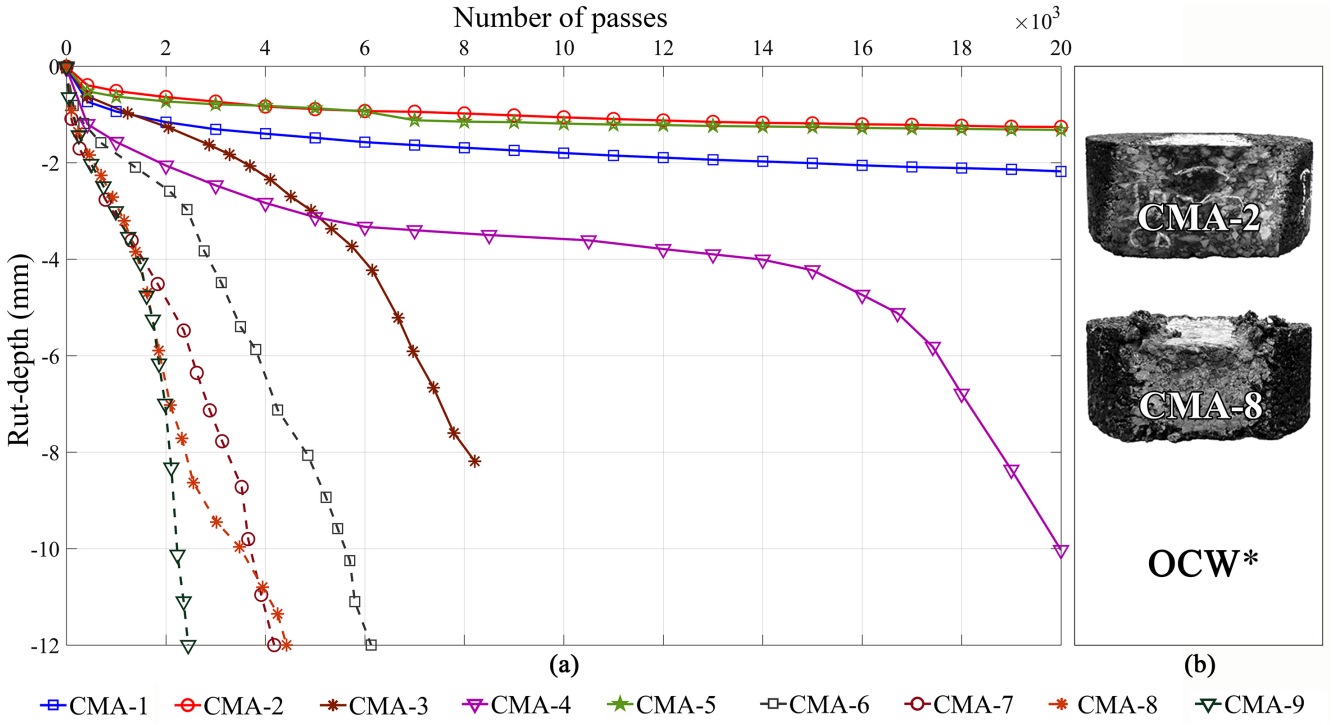

* Oven-cured sample tested under wet condition.
Note: Each curve represents an average of at least two test replicates.

Fig. 3.4. (a) Rut-depth curves for oven-cured CMAs tested under wet conditions. (b) HWT results on one CMA-2 and CMA-8 specimen cuts.

the presence of water did not have any visible effect on the rut-depth curves for CMA-2 and CMA-5. CMA-1 still had a strong resistance to rutting, but the final rut depth increased almost 90% compared to its OCD test result. CMA-4 OCW showed a similar trend as the dry condition test, exhibiting good performance until 17,000 passes when it started to show a steep rate of deformation. The test on CMA-3 stopped at 8,000 passes due to the complete failure of the sample. CMA-3 OCW has a larger deformation than the CMA-3 OCD tested under dry conditions, which clearly indicates high moisture susceptibility of CMA-3.

Based on Mehrara and Khodaii [348], coarse OG mixtures are less susceptible to moisture damage than DG mixtures. Dashed-line curves in Figure 3.4(a) present the results of an HWD

test on oven-cured OG CMAs. It can be observed from this figure that CMA-6 OCW, CMA-7 OCW, and CMA-8 OCW curves portray almost the same behavior compared to their OCD test results. The total number of passes for these three CMAs before reaching 12-mm rut depth decreased by only 30% on average. However, CMA-9 displays an intense moisture susceptibility that caused it to fail in less than 2,500 passes (an almost 90% decrease compared to the CMA-9 OCD curve).

In order to compare the stripping potential of DG-CMAs, CMA-1, CMA-3, and CMA-5 were chosen to be tested under hot water. The first two performed well in dry and immersed (25 $^{\circ}C$ water) tests. Figure 3.5(a) shows the average curves of the HWT test results under 50 $^{\circ}C$ water (OCHW). The creep part of the CMA-5 OCHW curve has a relatively flat slope, but after 12,000 passes, it changed into a steep stripping slope. Despite the good performance of CMA-1 specimens under 25 $^{\circ}C$ water, the CMA-1 OCHW curve displays early stripping, which leads to 12-mm rut depth after 2,840 passes. The CMA-3 OCHW curve also shows premature failure with a much steeper rate of rutting than its OCW curve.

3.3 Discussion

3.3.1 Rutting resistance

The rutting resistance of samples tested with an HWT device can be expressed by their rutting rate (RR). Here, RR is defined as rut depth (millimeters) divided by the logarithm of the total number of passes. Figure 3.6 shows that the RR of DG samples under dry conditions was much

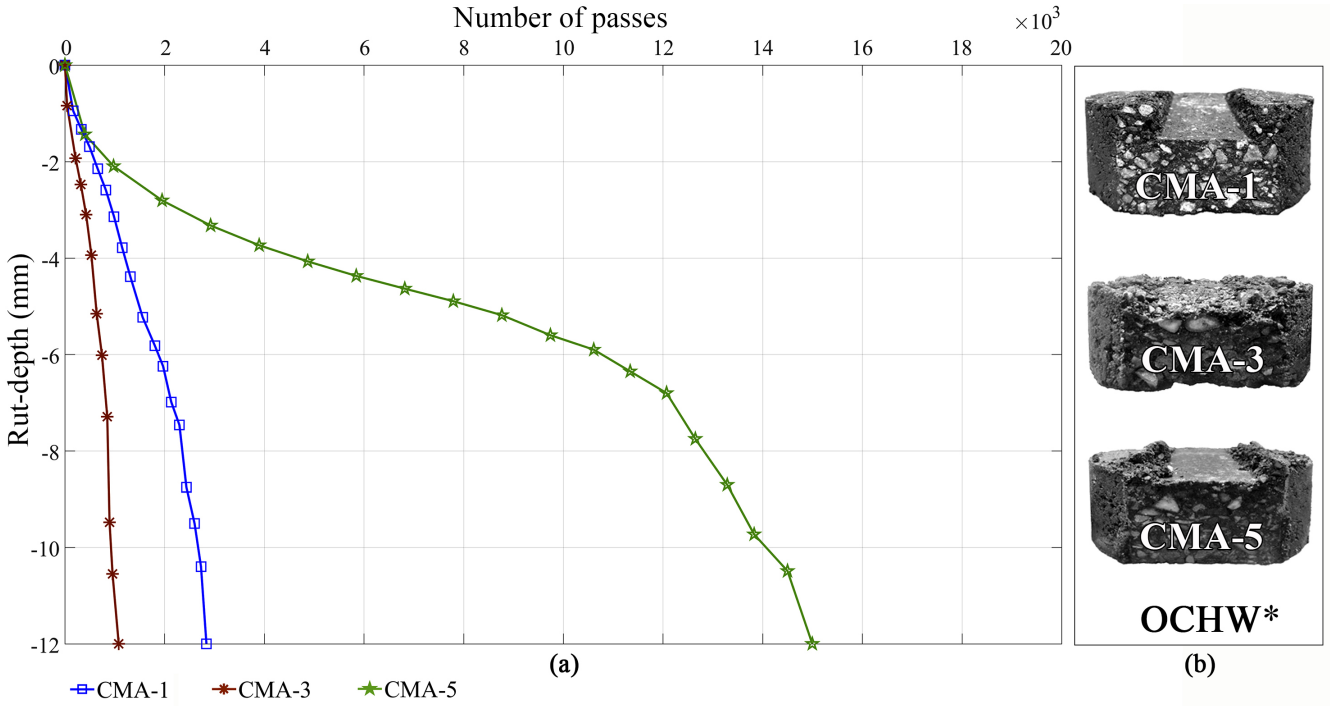

* Oven-cured sample tested under 50 °C wet condition.
Note: Each curve represents an average of at least two test replicates.

Fig. 3.5. (a) Rut-depth curves for three CMAs tested under hot water. (b) HWT results on one specimen cut of each sample.

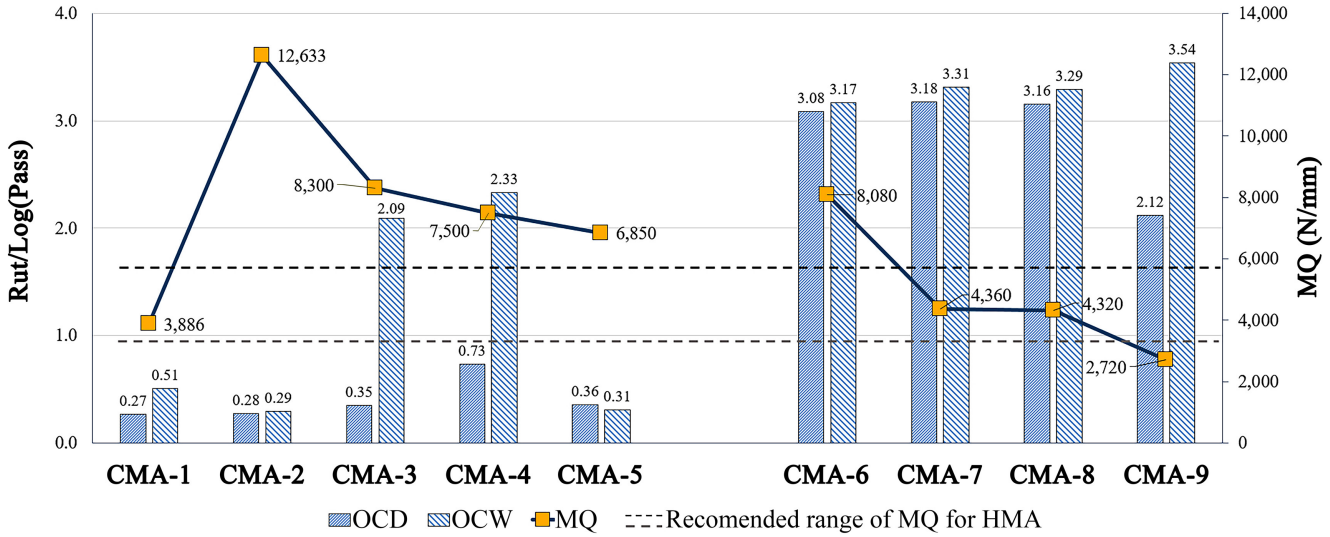

Fig. 3.6. Rutting rate vs Marshall quotient.

smaller than the RR of OG samples, which reflects a higher rutting resistance of DG CMAs compared to OG samples. This is well matched with Marshall stability test results that showed high MQ values for DG samples and a relatively low MQ of OG ones, except for CMA-1. The low value of MQ induces a relatively lower rutting resistance for CMA-1, while based on HWT test results, CMA-1 is the most resistant CMA to rutting in dry condition. The same disparity can be seen comparing the RR and MQ values of CMA-6 and CMA-9.

3.3.2 Moisture damage resistance

The RR in the OCW test depicted in Figure 3.6 shows that only CMA-1, CMA-2, and CMA-5 had acceptable rutting resistance in the water. Despite the high rutting of CMA-6, CMA-7, and CMA-8, their RRs in the OCD and OCW tests are roughly the same, which implies a very low moisture susceptibility.

In analyzing the results of the HWT test, the stripping inflection point (SIP) is mostly used as a measure of the moisture-damage susceptibility of asphalt mixtures [349] and is defined as the number of passes at the intersection of the creep and stripping slope of the rut-depth graph. Since CMAs can have an early failure, it is not meaningful to distinguish between the creep and stripping portions of the graph. Hence, the SIP measurement could be subjective and difficult to scale. In this study, moisture-susceptibility index (MSI) is defined as the ratio of the wet test RR to the dry test RR. An MSI close to one shows approximately the same performance of the cold mix in dry and wet conditions and is therefore an indication of less susceptibility to moisture damage.

Figure 3.7 depicts the values of MSI vs TSR of CMAs. Despite the fact that DG CMAs have much better rutting performances than the OG mixes, their MSI is higher than OG samples on average, so they are more susceptible to moisture damage. Results of the TSR test also show that the specimens that had an MSI value close to one have an acceptable TSR (TSR > 0.8) by the AASHTO T 283 [337] method as well.

3.3.3 Statistical analysis

To investigate the significance of different variables, such as bitumen content and aggregate gradation on rutting and moisture susceptibility, an analysis of variance (ANOVA) with a significance level of 0.05 was performed on the test results. Considering a level of confidence of 95%, the ANOVA null hypothesis (H0) is that all population means are equal. H0 is rejected if the P-value obtained from the analysis is lower than 0.05, which indicates that the sample

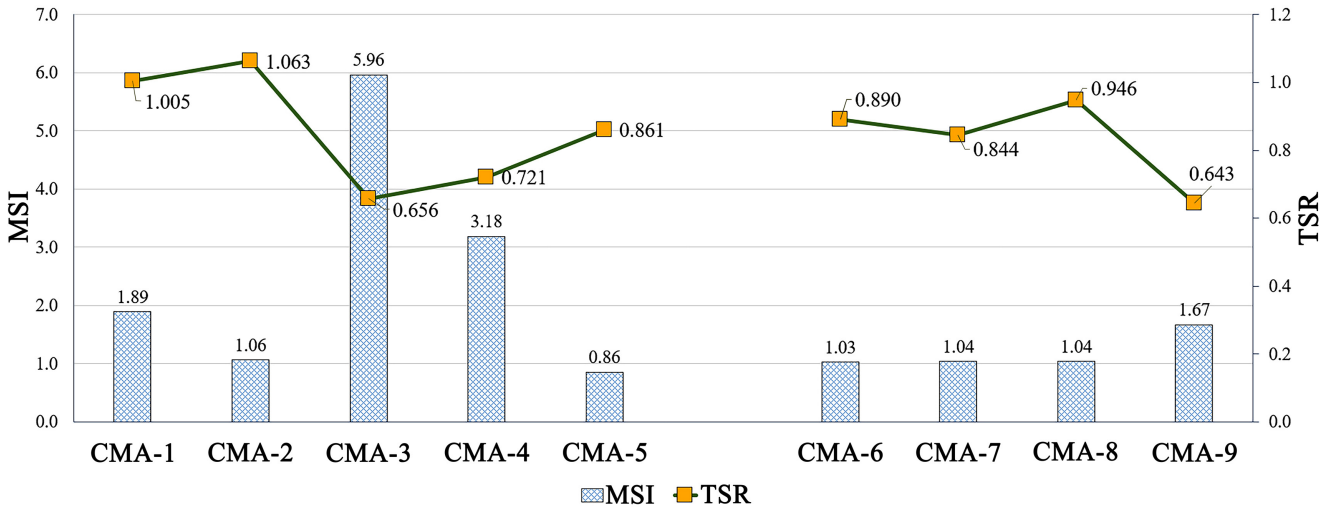

Fig. 3.7. Moisture-susceptibility index vs tensile strength ratio.

means between different groups are not equal. Mixes were divided into two OG and DG groups to analyze the effect of aggregate grain size distribution on the results. To evaluate the effect of bitumen content, mixes were separated into low bitumen content (less than 4.1%) and high bitumen content (more than 4.1%) groups. The ANOVA results are summarized in Table 3.6 and Table 3.7. As concluded from Table 3.6, rutting potential can be significantly affected by grain size distribution of the mixes; however, bitumen content alone does not have a significant effect on the rutting (Table 3.7). DG mixes with different bitumen contents always showed lower rutting values compared with OG ones. It is also revealed in Table 3.6 and Table 3.7 that none of the bitumen content and aggregate grain size distribution parameters affected the mixes' moisture sensitivity results. Other influential variables could be bitumen type, additives, and their compatibility with mix aggregates. For the studied CMA mixes, no information was available on these parameters.

Previous studies also indicated that the wheel tracking tests seem to be more sensitive to

Table 3.6. Summary of the ANOVA of the effect of grain size distribution on rut depth and moisture susceptibility of CMAs

Independent variable: Grain size distribution						
Dependent variable	SS	df	MS	F	P-value	F crit
Final rut depth	203.4848276	1	203.4848276	157.9718268	**4.65734 E-06**	5.591447851
MSI	4.326905	1	4.326905	1.6991	0.233637	5.591448

Table 3.7. Summary of the ANOVA of the effect of bitumen content on rut depth and moisture susceptibility of CMAs

Independent variable: Bitumen content						
Dependent variable	SS	df	MS	F	P-value	F crit
Final rut depth	0.002508053	1	0.002508053	8.26186 E-5	0.993001368	5.591447851
MSI	3.239169	1	3.239169	1.198814	0.309796	5.591448

the effects of dust-to-binder ratio than either asphalt binder content or dust content alone [350]. As realized from Figure 3.8, moisture susceptibility of DG CMAs seems to be highly related to dust-to-binder ratio with a 0.95 coefficient of correlation. CMA-3 has the highest amount of particles smaller than 0.08 mm (3.23%) and is the most susceptible mix to moisture damage. On the other hand, CMA-1, CMA-2, and CMA-5, with less than 1% dust, have a strong resistance to moisture damage. Contrarily, MSI values of OG CMAs are positively correlated to the amount of coarse aggregates (with a coefficient of correlation equal to 0.98). This means mixes with a higher percentage of coarse aggregate are more susceptible to moisture damage. Another perfect correlation on OG cold mixes can be observed between the percentage of coarse aggregates and slope of the stripping part of the rut-depth graph. It denotes that the higher percentage of coarse aggregates would cause a higher stripping rate.

Previous studies stated that HWT test results are not very sensitive to air void contents

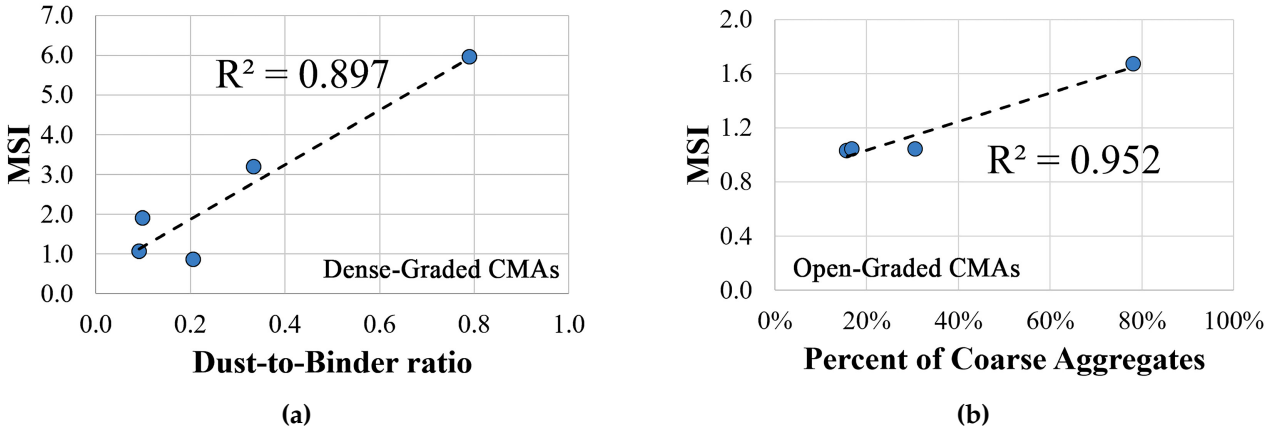

Fig. 3.8. Correlation between (a) MSI of DG CMAs and dust-to-binder ratio of CMAs; (b) MSI of OG CMAs and percentage of coarse aggregates of the mix.

of samples [308, 351, 352]. Similarly, no significant correlation between air void contents and rutting or moisture susceptibility of samples was observed in this research.

3.4 Conclusion

This chapter presents a laboratory evaluation on the engineering properties and performance of nine ready-to-use CMA patching materials in North America. The most important results obtained from this study can be summarized as follows:

1. The Marshall stability and flow test is effective in distinguishing rigidity of CMA materials. The average MQ value of DG CMAs is higher than OG mixtures, reflecting DG mixtures' higher stiffness and lower workability.

2. Rutting resistance of ambient-cured cold mix samples is low, and a wheel tracking test was found to be too harsh to test deformation resistance in the early life of cold mixtures.

On the other hand, the accelerated curing process at 135 $^{\circ}C$ for 18 hours appears suitable to predict the eventual strength of the CMAs.

3. Despite few disparities observed, the MQ value can reflect the rutting resistance of cold mix materials. Cold mixtures with higher MQs are expected to show higher rutting resistance when tested under dry conditions in an HWT device.

4. MSI seemed to be a better indicator for moisture damage susceptibility in CMAs than SIP. CMA-3 and CMA-9 had the highest MSI and lowest TSR among DG and OG CMAs, respectively, which mark them as the most susceptible cold mixtures to moisture.

5. Statistical analysis indicated that the aggregate grain size distribution has a significant effect on rutting resistance of CMAs. However, moisture susceptibility is not a function of bitumen content or grain size distribution alone; and

6. Moisture susceptibility of DG CMAs is found to be strongly correlated to the percentage of fine particles, while in OG mixtures, the amount of coarse aggregates in the mix shows significant correlation with rutting and moisture susceptibility.

Chapter 4

Application of Cement-Based Foams for Narrow-Trench Backfilling

In modern urban traffic scene, it has become a necessity to cut the trenches for carrying service lines, especially cables for various uses, as narrow as possible in order to keep the disturbance to the traffic to the minimum. The rising cost of construction also demands that the time for, and cost of, such service line laying be kept to the minimum. These demands are well met by resorting to narrow trench cutting alongside the roads in use. However, the backfilling of such very narrow trenches requires that the backfilling material must satisfy certain engineering properties as opposed to the traditional earthfills.

Cement based foams are considered to be a good backfill material. This study characterises their mechanical performance, thermal shrinkage, and bonding with the bituminous substrate. Nine different mixtures ranging in density from 600-1100 kg/m^3 were considered here. The hardened cement-based foam mixtures were tested first to ascertain their strength, modulus

of elasticity and Poisson's ratio. This was followed by evaluating their drying shrinkage and coefficient of thermal expansion (CTE). Lastly, these mixtures were assessed for their bond performance with the asphalt concrete. Aside from showing immense promise as a backfill material for narrow trenches, the results now constitute a valuable database to be used by future researchers for simulating and designing the back fills of narrow trenches as a composite structure.

4.1 Introduction

The practice of laying service lines ˇ especially cables ˇ alongside existing roads is an increasingly common feature in modern urban areas. Owing to the need for quick restoration of roads to regular traffic after such an operation, narrow-trenching (NT) has become a popular method to accommodate the laying of cables and conduits. It involves creating a narrow trench in or alongside the road pavement. Micro-trenching (MT) is a variation of NT in urban areas wherein the cut is often as low as only 25 to 40 mm wide and up to 250 mm deep [8, 9]. The process of narrow trenching involves three main steps. Firstly, a narrow trench is cut in the pavement. The trench dimension is usually dictated by the size of conduits, pavement thickness, and any climate considerations (usually deeper when exposed to freeze/thaw cycles). Secondly, this trench is cleaned, and the cable or conduit is placed inside. Finally, the trench is backfilled with a suitable material that has requisite strength, and bonds well with the asphalt of the pavement. This backfilling material must have good thermal insulation to prevent any damage due

Fig. 4.1. Narrow-trenching using a micro-trencher. First a narrow-trench is cut (a), then the cables are laid at the bottom of the trench and secured in place by metallic clamps (b), and lastly, the cut is reinstated using a flowable fill (c). (d) shows the final reinstated trench. A cored section is also shown in (e).

to freeze-thaw cycles in the Canadian climate. Given the small dimensions of the trench, it is extremely critical that the backfill material flows easily and fills the trench thoroughly, penetrating even small voids in the cut (see Figure 4.1). Real-life performance of different backfilling options was investigated earlier by a series of pilot installations in Alberta, Canada by the first author [19]. Different types of distress were observed in the reinstated trenches within these pilot installations after a few freeze-thaw cycles. Such distress includes the erosion of granular fill and raveling, settlement, lack of cohesion and adhesion in cold-mix asphalt or sealant backfill. The results concluded that using traditional backfilling material such as plain sand was not adequate for the Canadian cold regions [1]. Accordingly, this demands a flowable, self-compacting material that can bond well with asphalt concrete.

Since the trench albeit narrow is yet quite long in length, the volume of such a flowable

filling material is relatively high so as to warrant an inexpensive material. Using resins or special cement is seen to make the cost prohibitive. As an illustration, a commercial non-shrink cement grout, when used to partially backfill a micro-trench in a real-life project in Alberta, Canada led to the material cost alone to be as high as 20% of the total project cost, [18]. Between a desire for economy, ease of process and the necessary performance criteria, cement based foam presents itself as a viable alternative to conventional fillers. Besides, cement based foams are easily excavated and possess adequate permeability to allow water to flow through. The latter is important for otherwise, it will act as a wall in the middle of the road, diverting the flow and in turn lead to flooding [28].

Cement-based foams are prepared using a cementitious binder, water, and a pre-formed foam. The foam is obtained by agitating either a liquid surfactant or through the production of gas [175]. While the lower densities are essentially aerated paste, the higher densities do sometimes incorporate fine aggregate. The higher densities ($> 800\ kg/m^3$) are intended for applications that are mainly structural ($f_c{}' > 8\ MPa$). On the other hand, the lower densities ($300 - 800\ kg/m^3$) are attractive for their self-consolidation, good thermal and sound resistance, controlled low-strength, and ease of re-excavation [175]. The spherical air-void network provides superior thermal and acoustic insulation values, but strengths lower than that for normal-weight concrete [353]. Therefore, this suite of properties makes cement-based foam uniquely suitable for backfilling narrow trenches.

4.2 Research significance

Although eminently suited for narrow-trench backfill, there is a lack of information to describe properties of cement-based foams in the context of this application. The composite behavior of the bituminous substrate and the backfilling material is required information to facilitate trench design and execution. Lessons were learned from a recently completed pilot project by the first author, illustrating the importance of the adequate bond between the backfill and the existing pavement, dimensional changes and hygro-thermal effects. Therefore, this study was undertaken to experimentally evaluate these aforesaid parameters and their variations due to the composition. It is expected that the findings shall provide guidance for future backfilling of narrow-trenches.

4.3 Experimental program

4.3.1 Materials

A Type GU (General Use) Portland cement, conforming to [354] was used as the principle binder. Its chemical composition is shown in Table 4.1. Additionally, a subset of the mixtures incorporated fly ash. It is particularly useful to improve strength, reduce thermal conductivity [355] and the autogenous shrinkage [356] in cement based foams. This was a Class C fly ash, sourced from the Genesee Power Generating Station in Warburg, Alberta, Canada and conforms to [354, 357]. The oxide composition is presented in Table 4.2. The particles, mostly

Table 4.1. Chemical composition of cement type GU

Major element	SiO_2	Al_2O_3	Fe_2O_3	CaO	MgO	Na_2O	K_2O	LOI
Mass%	20.65	5.6	4.13	61.87	2.6	0.14	0.83	1.39

Table 4.2. Chemical composition of class C fly-ash.

Major element	SiO_2	Al_2O_3	Fe_2O_3	CaO	MgO	SO_3	Na_2O	K_2O	TiO_2	P_2O_5	LOI
Mass%	55.53	23.24	3.62	10.97	1.22	0.24	2.83	0.76	0.68	0.1	0.54

spherical in shape, ranged in size between 10 to 100 microns. Upon wet-sieving, about 20.5% was retained on the 45 μm (#325) mesh sieve and the moisture content was 0.05%.

A synthetic foaming agent was used, which conformed to [101] and [102], with composition as per Table 4.3 below. It leads to a predominantly closed-cell structure. A pre-formed foam was prepared at a 3% dilution (by volume) of the foaming agent mixed with water which was then aerated to a density of 40 kg/m^3. This stable foam was later added to the cementitious slurry in increments until the target cast density was achieved. The foaming capacity ratio (the ratio of final foam volume to the volume of the foaming solution before air entrainment) and bleeding rate (water seeping from the aerated foam per hour) [100] were calculated as 30 and 5 kg/hr respectively.

In the case of cement-based foams, it is well known that microfibres provide resistance to shrinkage cracking at early age and fracture resistance to the hardened composite [61, 358].

Table 4.3. Composition of the foaming agent provided by the local manufacturer.

Ingredient	Fatty alcohol	Alcohol	Fatty acid
Weight (%)	1-10	6.5-35	10-65

Accordingly, polypropylene microfibres were introduced at a volume fraction of 0.2% to select mixtures to form a companion series of fibre reinforced cement-based foams. This amount has been successfully used in the studies of Kearsley and Mostert [359] and Mamun and Bindiganavile [360]. Laboratory experiments on different fibre fractions confirm that higher fibre fractions (than the selected 0.2%) adversely affect the flowability of the mixtures. Physical and mechanical properties of these microfibres are shown in Table 4.4. The reinforcement efficiency of fibres increases with fibre length. However, at a certain fibre volume fraction, an increase in the fibre length will result in fewer number of fibres in the mix and reduce the uniformity of fibre distribution in the mixture [361]. As discussed in Chapter 2, the trench width can be as narrow as 25 mm. Using longer fibres than the trench width will increase the chance of fibres clumping inside the mix. This reduces the effective bond area between fibre and cement paste [362]. As well, it makes the placement of the fibre reinforced CBF inside the narrow trench difficult. Considering the reasons above and based on prior research [360], the fibre length of 20 mm was found practical (for ease of application) and effective. Denier is also a direct measure of linear density of fibres. In textile industry, denier is defined as the mass (grams) of 9,000 m of a single strand of fibre [363]. Smaller denier translates into finer fibres, more fibre per unit weight of the material, and higher total fibre surface area. Similarly, Tex is defined as the gram per kilometer of a single strand of fibre in SI unit.

While some mixtures were prepared with regular concrete sand, others were made with expanded perlite, as fine aggregate. Figure 4.2 shows the gradation of the various aggregates used in this study. It can be seen that this gradation was identical for both the natural sand and

Table 4.4. Properties of polypropylene microfibre.

properties	Value
Length	20 mm
Tex (Denier)	0.33 (3)
Specific gravity	0.91
Elastic modulus	3500 MPa
Ultimate tensile strength	550 MPa

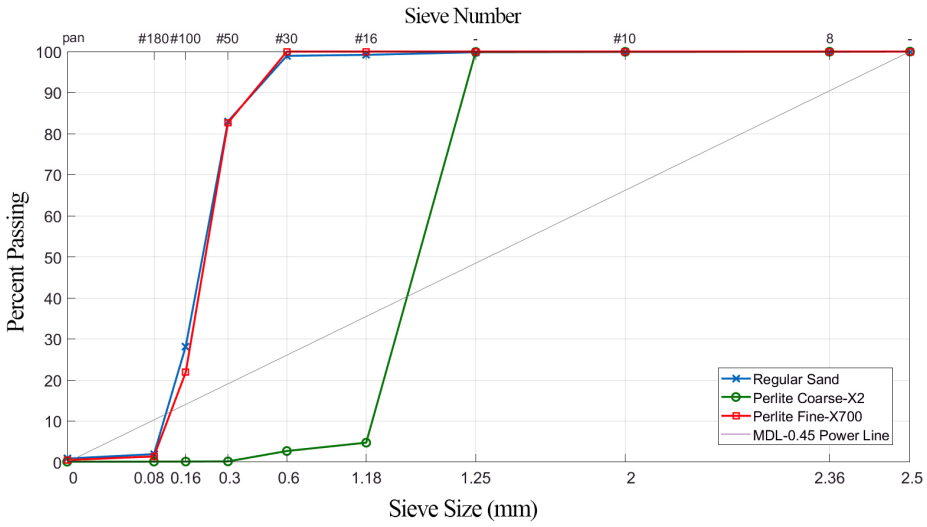

Fig. 4.2. Gradation of aggregates used in this study.

the fine expanded perlite.

4.3.2 Mixture design and sample preparation

The composition and proportion are summarized in Table 4.5. A test plan was designed to explore the effect of different mixtures on the strength, modulus of elasticity, Poisson's ratio, shrinkage, coefficient of thermal expansion and bonding with the asphalt concrete. Accordingly, the mixtures in this study were divided into two groups, designated herein as Group I

(Low Density) and Group II (High Density) such that the cast densities were held nearly constant within each group. Within Group I, the measured dry densities for mixtures designated as PA, PB, PD, PE, and PI lay between 644 to 666 kg/m^3. Mixture PC was significantly lighter at 502 kg/m^3. Within Group II the mixtures designated as PF, PG, and PH ranged in dry density from 921 to 980 kg/m^3. The mixtures so designed were intended to allow for multiple comparisons to illustrate the following:

(i) Effect of fly ash, between mixture PA and PB and again, between mixtures PF and PH.

(ii) Effect of perlite as fine aggregate, between mixtures PA and PD and/or PI.

(iii) Effect of aggregate gradation, between mixtures PD and PI.

(iv) Effect of polypropylene microfibre, between mixtures PA and PE.

(v) Effect of using natural sand as fine aggregate by comparing mixture PG with the reference mixture PF.

(vi) Effect of density, between mixtures PA, PC and PF.

A minimum water-to-binder ratio is suggested at 0.35, below which the binder tends to draw water from the foam leading to its instability [364]. Guidelines for flowable fill [103, 151] specifies an efflux time of (30 $\pm$ 5 seconds) in flow cone tests done as per [146]. Therefore, and in order to ensure the self-flowable characteristic of cement-based foams for easy placement

Table 4.5. Mixture proportions (kg/m^3).

Mix code	Target density[1]	Cast density[2]	Cement	Water	Fly-ash	Aggregate	Microfibre	Dry density[3]	Test density[4]
Group I-Low density									
PA	800	850	706	353	0	0	0	650	810
PB	800	852	424	328	283	0	0	666	832
PD	800	840	462	360	0	96[a]	0	648	760
PE	800	840	563	333	0	0	21.3	652	801
PI	800	831	531	279	0	155[b]	0	644	798
PC	600	649	450	225	0	0	0	502	615
Group II-High density									
PF	1100	1163	871	435	0	0	0	926	1031
PG	1100	1135	355	257	0	710[c]	0	980	1069
PH	1100	1135	261	365	610	0	0	921	1068

[1]Target cast density; [2]cast density of fresh CBF; [3]oven dried density; [4]24 hours air-dried density at test.
[a]Perlite coarse; [b]perlite fine; [c]natural sand.

inside the narrow-trench, water to solid ratio was chosen by trial-and-error to fulfill the aforementioned requirements as tabulated above. [19] also confirmed the good performance of the selected water to cement ratio of mixture PA in a real-life MT project.

To prepare the cement-based slurries, first the solids were mixed in an electric barrow concrete mixer and then water was added, and the mixing continued until a smooth paste was obtained.The pre-formed foam was then added to the mix until the target cast density is achieved.

A total of 12 cylindrical specimens, each 75 mm in diameter and 150 mm in height were cast for each of the nine mixtures. They were examined in compression at 3 days, 7, 28 and 90 days. Drying shrinkage and the co-efficient of thermal expansion (CTE) were measured using six prisms of $50 \times 50 \times 300$ mm per mixture. An asphalt-concrete mixture, commonly employed by the City of Edmonton, was used to prepare the concrete substrate used to examine the bond

Table 4.6. Design properties and gradation of asphalt concrete (AC) specimens.

Design properties	Value	Sieve size (mm)	Combined gradation (%)
A.C. (% of total mix)	5.83	12.5	100.0
Gmm (kg/m^3)	2423	10.0	98.1
Gmb (kg/m^3)	2350	8.0	88.3
Air voids (%)	3.0	6.3	75.5
V.M.A. (%)	15.0	5.0	64.7
V.F.A (%)	80.0	2.5	48.2
Dust/AC (%)	1.1	1.25	38.3
TSR (%)	89.5	0.63	31.5
Combined aggeregate Gsb	2.603	0.315	20.3
Asphalt absorption (%)	0.61	0.16	11.2
AC grade	PG 58-28	0.08	5.7
AC specific gravity	1.032	-	-
Mixing temperature ($^\circ C$)	150	-	-
Compaction temperature ($^\circ C$)	140	-	-

strength. Its mixture design is shown in Table 4.6. Cylinders were cast at 75 mm in diameter and 150 mm in height, compacted by 25 blows in 3 layers using a 24.5 N rammer dropped from a height of 305 mm. The compacted specimens were left for at least 24 hours to cool down to room temperature. Then, the cylinder was cut at a slant angle of 30 degrees to the vertical. Each such half-cylinder was completed by casting a cement-based foam mixture onto it, resulting in a composite cylinder specimen as shown in Figure 4.3a.

While the cylindrical specimens served as a substrate in the shear-bond test, a separate set of prismatic specimens was cast using the same asphalt concrete mixture towards the flexural-bond test. Each prism was 105 mm $\times$ 250 mm $\times$ 300 mm in dimension and was roller-compacted.

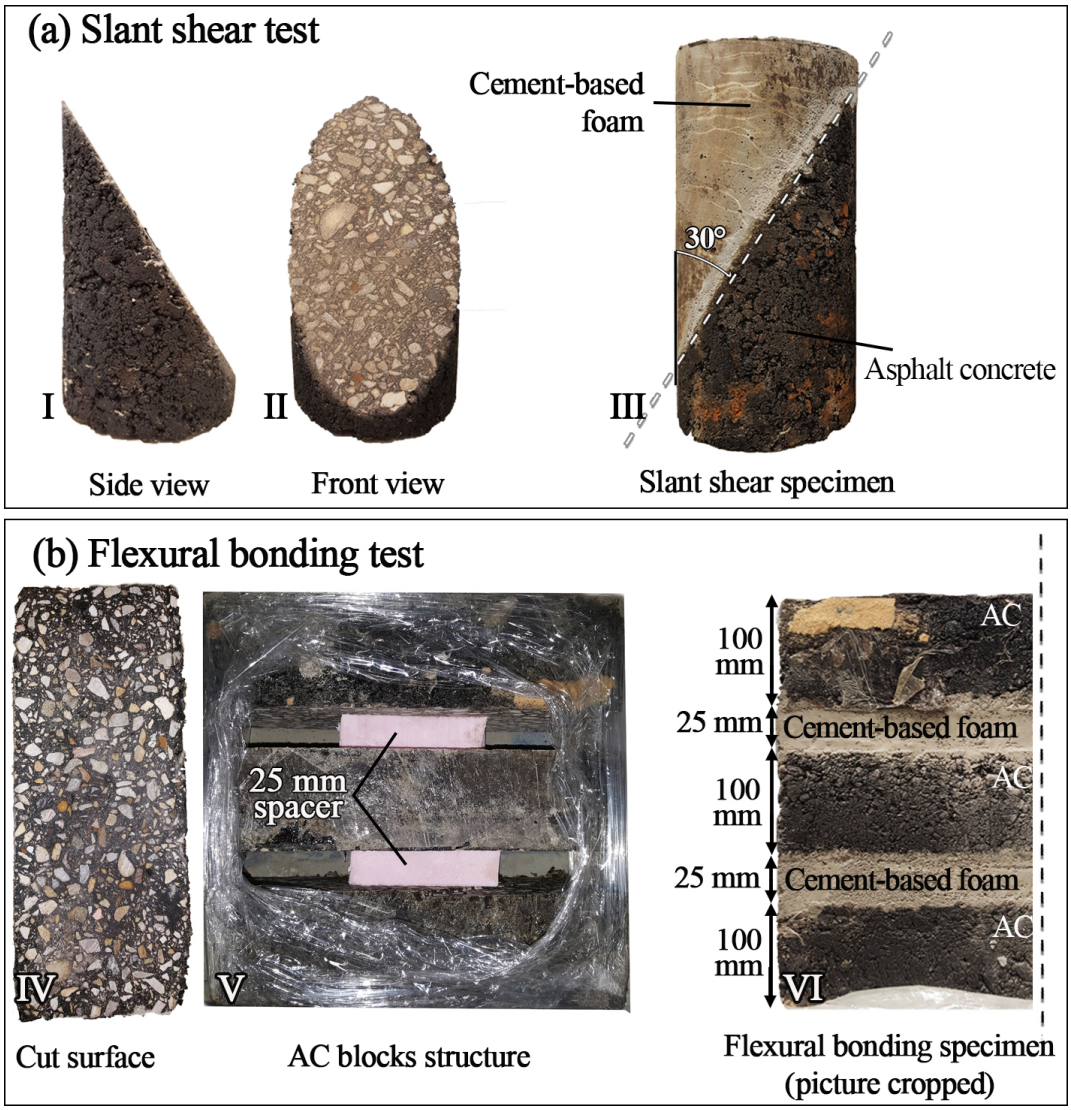

Note: I and II are views of cut asphalt cylinders to the angle of 30 ° to vertical. III is the final slant shear test specimen which is made by casting CBF on top of the II. IV shows the cut surface of an asphalt block used in flexural bond test. V shows the asphalt blocks structure sealed with shrink wrap and ready for introduction of cement foam. Before pouring the foam cement into the two 25 mm gap between blocks in order to form the final specimen in VI, the spacer will be removed.

Fig. 4.3. (a) Specimen preparation for slant shear test and (b) flexural bonding test.

The asphalt concrete (AC) blocks were allowed to cool to room temperature and then 100 mm thick blocks were cut from the 300 mm thick block, using the same saw blade as used for cutting the cylindrical samples. These smaller blocks spaced at 25 mm apart as shown in Figure 4.3b. Afterward, the blocks were held in place and sealed using plastic stretch wrap. Next, the spacers were removed, and the 25 mm trenches were filled variously with one of the nine mixtures of CBF to form a composite unit.

4.3.3 Test details

Mechanical testing

The compressive strength was determined per ASTM C495 [365] in a universal testing machine. A displacement rate of 0.8 mm/min was chosen for all tests. Three specimen replicates were tested at the age of 3, 7, 28 and 90 days. Further, for those specimens tested at 28 and 90 days, they were fitted with a digital compressometer prior to the test, which allowed the measurement of the modulus of elasticity and the Poisson's ratio per ASTM C469 [366].

Drying shrinkage

The drying shrinkage in these cement-based foam mixtures was determined in accordance with BS EN 680 [261], in a manner described therein addressing autoclaved aerated concrete (AAC). Note that the microstructure of cement-based foam is very similar to that of AAC [125]. As mentioned earlier, 4 prismatic bars, each 50 mm $\times$ 50 mm $\times$ 300 mm, were cast and sealed for 28 days. At which point, ball bearings were fixed onto the ends using an epoxy adhesive.

After recording the mass of the samples, both with and without the ball bearings, the specimens were then conditioned in a bath of water for 72 hours as shown in Figure 4.4a. During the first 24-hour period of conditioning, only one-third of the thickness was immersed. In the second 24-hour period, 2/3rd of the thickness was submerged in water. Finally, during the last 24-hour period, the entire bar was submerged in water. Following this "conditioning", the specimens were kept sealed for a further 24 hours in order to maintain an even distribution of moisture. The initial length measurements were taken by a length comparator, capable of measurements to 0.001 mm accuracy in accordance with ASTM C490 [367]. As shown in Figure 4.4d and e, the specimens were then left to dry in a controlled environment (20 $^{\circ}C$, 10 $\pm$ 5% RH). The length and corresponding mass measurements (to the nearest 0.1 gram) were made on a weekly basis from the foregoing instrumentation. Equation 4.1 is then used to calculate the drying shrinkage strain.

$$\epsilon = \frac{(l_n - l_1)}{l_d} \times 10^6 \tag{4.1}$$

Where :

ϵ is drying shrinkage strain ($\mu - strain$), l_1 is the first reading of length, l_n is the length reading after nth days of test, and l_d is the original length of the specimen.

Coefficient of thermal expansion (CTE)

The coefficient of thermal expansion (CTE) was evaluated per a modification to AASHTO T336 [286] suggested by [125]. Considering the unavailability of the apparatus required, the test

Fig. 4.4. Drying shrinkage and CTE testing apparatus. a) conditioning in 20 °C water bath; c) conditioning in 50 °C water (for CTE test); b) length comparator; d and e) drying shrinkage chamber.

method could not be followed strictly, however, the assumptions made in the standard are obeyed. In this instance, six prisms were cast and cured for 28 days in the same process as that of the drying shrinkage specimens. Once again, ball bearings were secured to both ends of the specimens as was done for specimens tested for drying shrinkage. The specimens were then placed in a 20 $^{\circ}C$ water tank for 24 hours in order to allow expansion due to water absorption and saturation (see Figure 4.4a). Using the length comparator (Figure 4.4b), the specimens were monitored for any change in length. After which any further expansion is assumed to be wholly due to the thermal effect. Immediately after taking these initial length measurements, three of the specimens were put in a separate 50 $^{\circ}C$ water bath (see Figure 4.4c) whilst the other three specimens remained in the bath at 20 $^{\circ}C$ to serve as reference specimens. Following a further 24-hour of submersion in their respective water baths, the change in the length of the specimens was measured once again. After subtracting the change in length as measured for the reference specimens, from those seen in the prisms left in the hot bath, one arrives at the change in length due to the temperature alone. The coefficient of thermal expansion was calculated per AASHTO T336 using Equation 4.2.

$$\alpha = \frac{\Delta L}{L_0 \Delta T} \tag{4.2}$$

Where:

α is coefficient of linear thermal expansion, μ-strains/°C; ΔL is change in length after soaking in hot water, mm; L_0 is the initial length of specimens at temperature T_1, mm, and ΔT is the

change in temperature from temperature T_1 to T_2, $^{\circ}C$.

Bond strength evaluation

Narrow trenches are usually open to traffic right after the backfilling material is set and are thus expected to meet their normal operational loads within a short time post backfilling. Therefore, the bond strength of the cement-based foam with respect to the surrounding asphalt layer, especially at an early age post filling becomes an important criterion in mix design.

Among all the tests available to characterize bond between two media, mainly three tests are generally used to evaluate the bond between concrete and asphalt. The most commonly used is the *direct tensile test*. Tensile failure stress, especially in a composite mix of two different materials like CBF and asphalt in this study, can be a measure of the bond failure. [225, 226] have reported tensile bond strengths of 0.5 MPa and 0.8 MPa (tests performed after 28 days). However tensile tests do not correctly reproduce the stresses existing at the CBF interface with asphalt. Therefore, the *direct shear test*, based on the shear Iowa device is also widely used. For instance, [227] and [228] obtained failure shear stresses around 1 MPa for site cored, and laboratory manufactured samples respectively.

Lastly, the *compressive slant shear test* is also mainly used to characterize the bond between repair material to substrate. It submits the bond interface to a combined state of shear and compression. [229] have worked on this aspect and have given a theoretical assessment formula for this ratio bond/compression strengths depending on the angle of the interface between the materials. The slant shear test is claimed to provide a realistic representation of stress state in the

composite structure [231, 232]. The test is also sensitive to variation in bond strength [231] and therefore, produces consistent results [233]. Nevertheless, failure is pre-eminently dependent on the angle of the interfacial plane, which is fixed in the standard test. Therefore, the failure is not necessarily occurring on the plane with the most critical combination of compressive and shear stresses [234]. Moreover, the results are reported to be insensitive to surface roughness, especially at steeper interface angles [229, 235]. The test is also sensitive to differences in the modulus of elasticity of the materials which can cause stress concentrations. Lastly, slant shear test yields much higher values for bond strength than the other tests [229, 234, 368] and therefore, the combined state of shear and compression in SST might overstate the actual bond strength.

Failures in the composite of the asphalt-concrete structure occur as delamination between layers because of cracking in concrete layer. This phenomenon arises under the combined influence of normal and shear stresses. In flexible pavements, flexural bonding tests are used to account for this combined stress [226]. Flexural bond test allows measurement of the adhesion capacity, or resistance to tearing, of CBFs to the asphalt substrate.

Considering the above, in this study, the flexural bond strength and the slant shear tests were both chosen to measure the bond strength between CBFs and asphalt concrete substrate.

Flexural bond strength To this end, three-asphalt concrete blocks were prepared and arranged with a 25 mm spacing. The gaps then filled with cement-based foam to form a composite unit. After 7 days of curing, the unit was subjected to bending test as per ASTM C1072

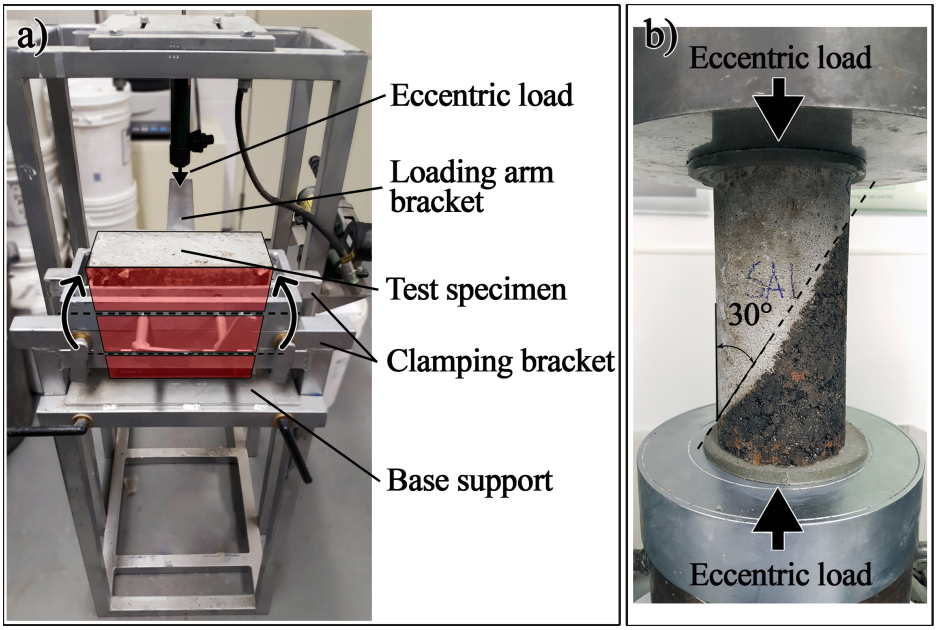

Fig. 4.5. Flexural bond (a) and slant shear (b) test setup.

[230] at 20 $\pm$ 5 °C. The test setup is shown in Figure 4.5a. The prism was supported on a rigid bottom and clamped firmly into a locked position using the lower clamping bracket. The load was applied to the top-most brick of the prism by the loading arm at a uniform rate so that the entire test took between 1-3 minutes [230]. After the failure happened, the rigid support will be raised and this time, the load will be applied to the middle asphalt prism in order to test the bond strength of the CBF in the bottom joint to the asphalt concrete. As the load causes a moment in the masonry unit, a flexure failure results between the asphalt concrete block and the cement-based foam. Accordingly, the flexural bond strength was calculated using Equation 4.3 as specified in [230]:

$$F_g = \frac{6(PL + P_l L_l)}{bd^2} - \frac{(P + P_l)}{bd} \tag{4.3}$$

Where:

F_g is flexural tensile strength, MPa; P is the maximum applied load, N; P_l is the weight of loading arm, N; L is the distance from centre of prism to loading point, mm; L_l = distance from centre of prism to centroid of loading arm, mm; b is the cross-sectional width of the mortar-bedded area measured perpendicular to the loading arm of the upper clamping bracket, mm; d is the cross-sectional depth of the mortar-bedded area, mm. The latter is measured parallel to the loading arm of the upper clamping bracket (see Figure 4.5a).

Slant shear test for bonding As with the flexural bond test, here too the specimens were tested at 7 days with emphasis on the early age resistance to debonding. The test was performed at 20 $\pm$ 5 $^{\circ}C$ and according to ASTM C882 [369] whereby the composite cylinder is subject to compression as illustrated in Figure 4.5b. The shear bond strength of the specimen was then calculated as:

$$\tau_n = \frac{1}{2}\sigma_0 \, sin(2\theta) \tag{4.4}$$

Where:

τ_n is the shear stress acting on the bond plane, σ_0 is the applied vertical stress required to produce a failure along the bond plane, and θ is the bond plane angle, i.e. 30 $^{\circ}$.

4.4 Results and discussions

4.4.1 Compressive strength and elastic properties

The mechanical properties of cement-based foams examined in this study were characterized by means of their compressive strength, modulus of elasticity and Poisson's ratio. Although the compressive strength and modulus of elasticity of conventional cellular concrete are well-established, there is very little data on their Poisson's ratio. The latter is an important parameter in this application as there is considerable lateral stress developed due to the traffic.

Figure 4.6 illustrates the evolution in compressive strength with time up to 90 days of curing. As expected, the higher the porosity, the lower the strength of the cement-based foam [274]. This was in line with a decrease in the plastic density, as reported by prior research [61, 97, 353]. Note that as early as at 3 days, the plain foam mixtures, i.e. PC, PA, and PF, gained a strength that is 50% of their strength at 90 days. Among them, PC gains most of its 90 days strength (almost 99%) during the first 28 days. The strength of PF, on the other hand, increases considerably (almost 46%) after 28 days while that of PA increases approximately linearly with age.

The mechanical properties of CBFs are generally modeled as a function of relative density (ρ_f/ρ_s), defined as the ratio of the density of cement foam, ρ_f, to density of solid cement, ρ_s which was found to equal 1900 kg/m^3 for plain CBFs (i.e. PA, PC and PF). [187] examined various cellular solids and concluded that the crushing strength is a function of the relative density and scales according to the power of 1.5. The exponent is a measure of the sensitivity

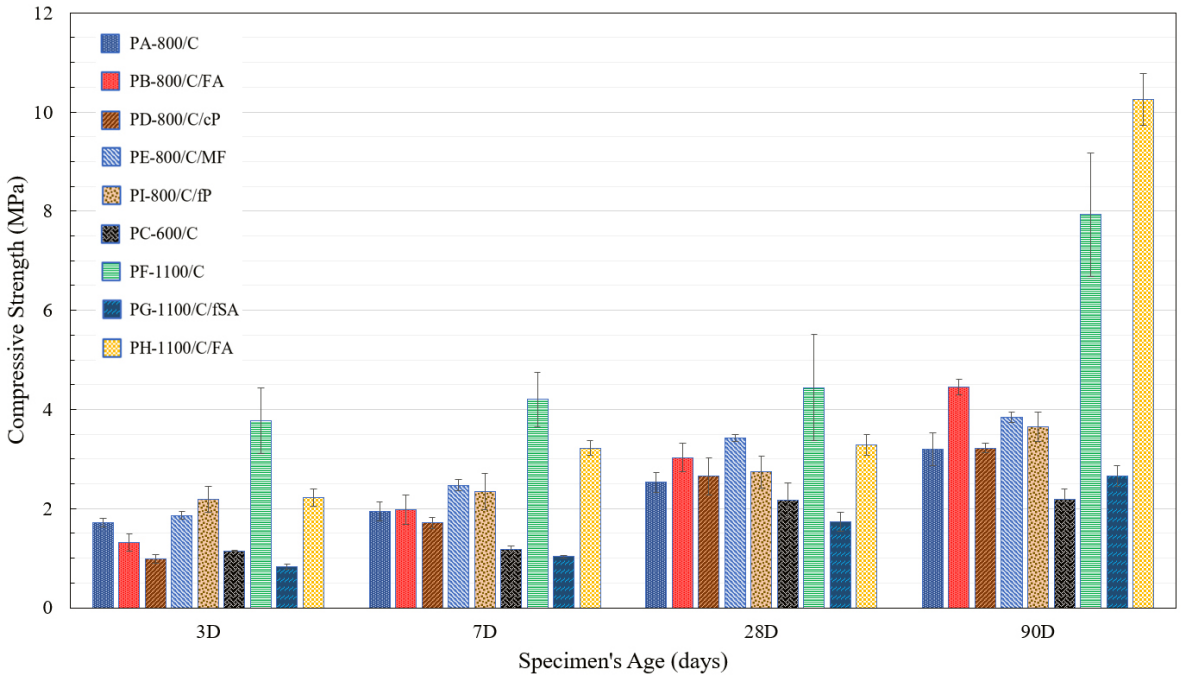

Fig. 4.6. Effect of age on compressive strength of CBFs.

of CBFs to the density. A similar relationship was plotted in Figure 4.7 for 28 and 90 days compressive strength and compared to the results of other studies. Note that, while the results of all the CBFs in this study are presented in Figure 4.7, only those mixtures without any filler, i.e. PA, PC, PE and, PF, were considered in presenting the trendline.

While there is no standard specification as yet for controlled low strength materials used in narrow trench backfill, the numerical study of a narrow-trench by [38] shows a maximum compressive strength of 1.12 MPa in the backfilling under a heavy traffic loading. They confirmed that the strength of 2 MPa would ensure stability and excavatability. Since the trench is open to traffic at early ages, the minimum strength requirement for CBFs is set as 1.5 and 2 MPa at 3 and 7 days respectively. On the other hand, maximum strength of 8.3 MPa is recommended to ensure ease of re-excavatability [221]. Also, if the backfilling material possesses high strength,

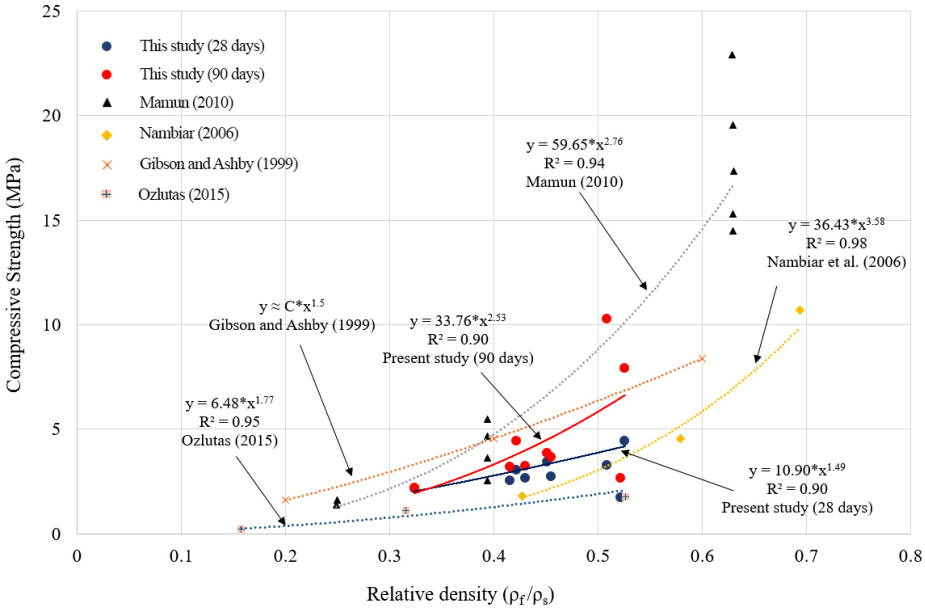

Note 1: The solid lines show the power trendlines of mix PA, PC, PE, and PF.
Note 2: Mamun et al. [370]; Nambiar et al. [71]; Ozlutas [125]; Gibson and Ashby [187].

Fig. 4.7. Effect of relative density on compressive strength of CBFs.

there is every possibility that it could effectively become a beam in the road; i.e. the cementitious fill could be stronger and stiffer than the surrounding road surface, and over a period of time, this inflexibility could break up the road. According to Figure 4.6, compressive strength of PA, PB, PE, PI, and PF fits in the aforementioned acceptable range.

The elastic modulus, E, and the Poisson's ratio of the 9 cement-based foams are presented in Figure 4.8. The elastic moduli measured in this study were found to be mostly similar to values as reported in the literature [125, 371]. So that, for densities ranging from 300 to 1000 kg/m^3, the modulus varied from 200 to 1100 MPa. As with compressive strength, the elastic modulus is proportional to the density [61, 371]. Modulus of elasticity of these three plain CBFs, PA, PC, and PF, is found to be well correlated to their 28-and 90-days compressive strength with

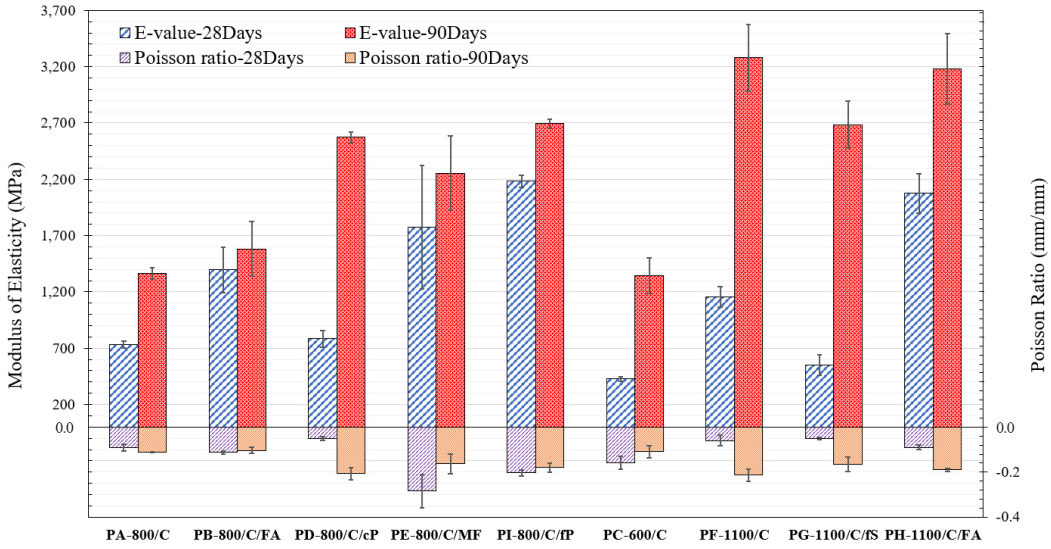

Fig. 4.8. Modulus of Elasticity and Poisson Ratio of cement-based foams.

correlation coefficients of 0.96 and 0.99, respectively. In higher density foams, that contain sand, the elastic modulus is higher than a companion mixture without sand. This is due to the interlocking between the sand particle and the paste [109]. The same is seen here with adding perlite to the reference mixture (see mixtures PD and PI). However, at higher sand-to-cement ratios, as witnessed in mixture PG, the modulus of elasticity was lower by 18% when compared to mixture PF. Thus, the results underline the fact that there is an optimum sand-to-cement ratio for maximum E. It is well known that micro-fibres improve the tensile strength and elastic modulus in cement-based systems [372]. Incorporating them into mixture PE led to a 65% increase in E over that in mixture PA.

The modulus of elasticity of CBFs is plotted against relative density in Figure 4.9. For the sake of comparison, only plain foams, PA, PC, and PF, are considered to fit the power curve. As suggested by [187] and supported by other studies, modulus of elasticity of brittle cellular

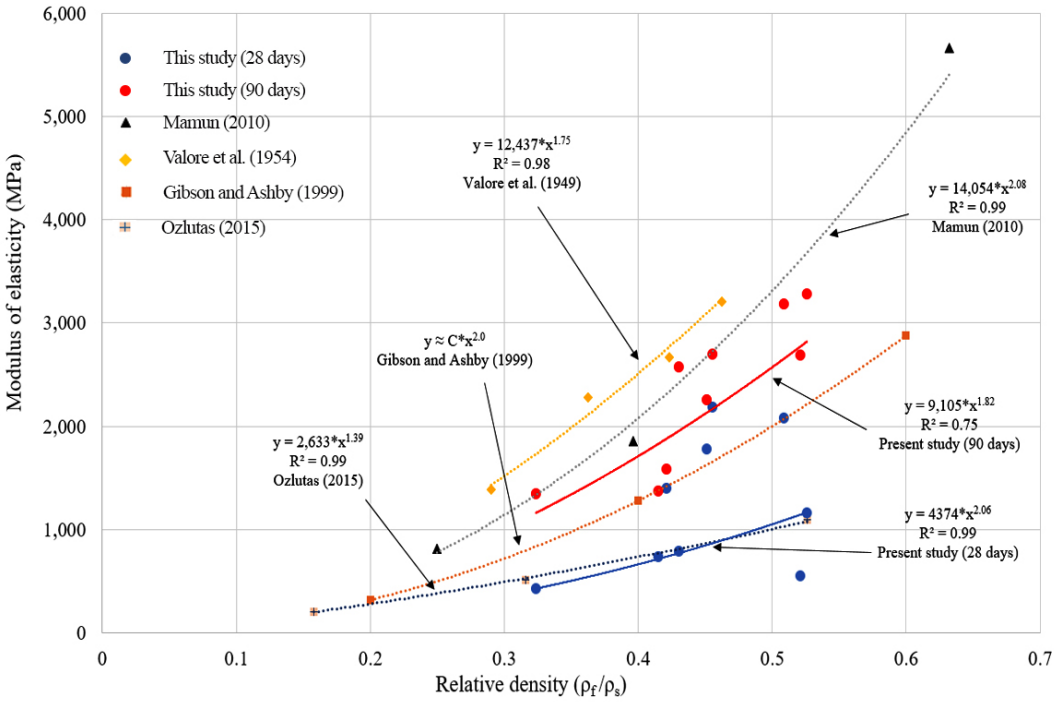

Note 1: The solid lines show the power trendlines of mix PA, PC, and PF.
Note 2: Mamun [370]; Valore et al. [373]; Gibson and Ashby [187]; Ozlutas [125].

Fig. 4.9. Effect of relative density on modulus of elasticity of CBFs.

solids scales according to the square of the relative density.

Prior studies have shown that the Poisson's ratio of cement-based foams containing no sand ranges from 0.13 to 0.16 at 1000 kg/m^3 and rising up to 0.18-0.19 for 1400 kg/m^3 [374]. Normal weight concrete depicts a Poisson's ratio between 0.15 - 0.22 [274]. For lower densities, the values range from 0.14, 0.19, and 0.08 for 300, 600 and 1000 kg/m^3 foamed concretes respectively [125]. In the current study, Poisson's ratios evaluated are also in the same range or slightly lower. This variation in the value of Poisson's ration is due to possible localized crushing of the contact points between the test frame and the specimen during testing, Therefore, taking into the above possibility the Poisson's ratio of foamed concretes in this study can be said to be 0.05

to 0.28 at the age of 28 days and 0.1 to 0.21 at 90 days for mixes with densities ranging from 600 to 1100 kg/m^3.

While there is no standard recommended range for modulus of elasticity and Poisson's ratio of CBFs in the narrow trench, they should be high enough to restrict the deformation of the backfill but not too high to prevent micro-cracking due to the high stiffness. As the elastic modulus of the CBFs increases, the stress in the backfilled section due to the traffic load increases and compressive stress in the surrounding soil and pavement, stress in the buried utilities and the displacement in the pavement decreases [38]. On the other hand, the resilient modulus of asphalt pavement changes from 700 MPa at 38 $^{\circ}C$ to 14,000 MPa at -1 $^{\circ}C$ [375]. As mentioned before, mix PA has been previously tested in a field project and after a year, no visible distress was observed in the trench. Considering all the above, the minimum required 28 days modulus was set to 700 MPa. According to [38], this value results in a maximum deformation of 0.6 mm in the trench that can barely be noticed by the traffic. All the CBFs except PC and PG meet this requirement (See Figure 4.8).

4.4.2 Drying shrinkage

Cement-based foams are known to undergo high drying shrinkage strains, up to 10 times greater than those observed in normal weight concrete [90, 112]. This is mainly due to the absence of coarse aggregates that otherwise restrain the volumetric changes [97]. High water contents of the mixtures and the high paste-to-fine aggregate concentration further contribute to this high shrinkage strains in cement-based foams [247]. On the one hand, [97] and [376] have

reported lower drying shrinkage strains in lightweight cement-based foams. They attribute this to the lower paste content. On the other hand, [247] and [371] report that the shrinkage increases with a drop in the density. In the absence of aggregates, lightweight cement-based foams are highly prone to drying shrinkage strains and corresponding crack growth. In a narrow trench, such cracks can let water in and rapidly lead to failure after only a few freeze-thaw cycles. Besides, letting water in can seriously damage the service cables.

Figure 4.10 shows the drying shrinkage profiles of the nine cement-based foams. Considering the reference mixture at each density range, the drying shrinkage strains vary widely from 67 to 3995 μ-strain for PC, 434 to 4171 μ-strain for PA and 431 to 4515 μ-strain for PF. The variation of the reported shrinkage strains of CBFs in the literature is high. For instance, μ-strains as low as 250 [125] and as high as 4000 [254, 358], 5000 [248] or even 62000 [87] have been observed for densities between 300-1000 kg/m^3 across different mix designs. The values measured in the present study falls closer to the upper bound of the range. This high variation can be attributed mainly to the difference in the test methods and specimen size used by different researchers, error in calibration and reading of the length comparator and emergence of drying micro-cracks during the test.

At lower density, cement-based foams develop an open-cell structure, while those cast to higher densities tend towards a closed-cell structure. [377] concluded that the shrinkage of cellular concrete is a function of volume and specific surface of micropores. However, [378] reported that the removal of water from comparatively bigger pores will not contribute to shrinkage. Since large entrained air voids do not change the structure of the fine pores [379], it can

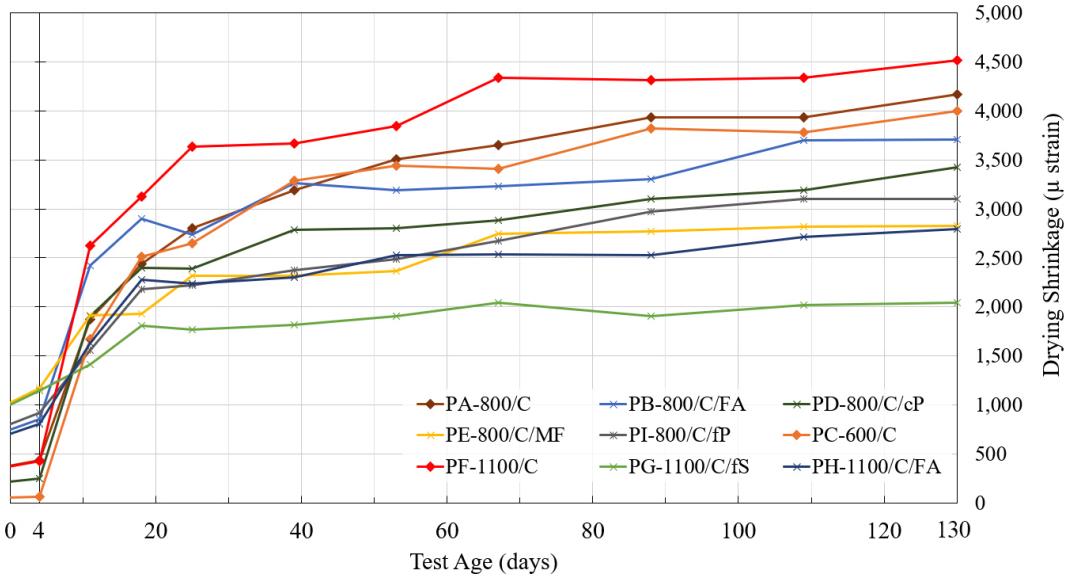

Fig. 4.10. Drying shrinkage versus test age.

be concluded that the micro-pores that control the shrinkage are related to the paste content in the CBF in such a way that the lower paste content will result in lower shrinkage [135]. This explains the current observation that the shrinkage strains increased proportionally with an increase in density of mixtures PC, PA and PF. Further, [246] and [247] point out that the drying shrinkage levels off between the 3^{rd} and 10^{th} week.

In order to investigate the relative effect of different mixture compositions on shrinkage as compared to the reference mixtures, i.e. PA and PF, the shrinkage ratio (SR) of the different mixtures was plotted against the age at test and the relative density in Figure 4.11. SR is defined as the shrinkage strain of the mixture to that of the corresponding reference mixture in that particular density group. Foams that contain aggregates are expected to depict lower shrinkage strains [380, 381]. It was so with mixtures PD and PI that contain coarse perlite and fine perlite, respectively. Both depict lower shrinkage strains with respect to the reference mixture PA after

130 days (82% and 74% of the strain in the reference mix, PA; see Figure 4.11c). One notes from Figure 4.10 that between the two gradations, fine perlite led to consistently lower shrinkage strains. Again, fine sand had the same effect in reducing the shrinkage strain in the high-density cement-based foam mixture, PG. Being stiffer than perlite, sand was seen more effective in reducing the shrinkage strain by 53%, as opposed to the fine and coarse perlite, which resulted in 37% and 28%, respective drop in the shrinkage strain when compared with the reference mixture PA. Although all the mixtures show a shrinkage strain less than the reference mixtures after 25 days (see Figure 4.11b), at early ages, their shrinkage is higher than the reference except for mixture PD which shows only 57% of the shrinkage of the reference mixture, PA. This is due to the coarse gradation of perlite in the mixture PD, which provides relatively bigger voids to facilitate the escape of water at early ages without causing much shrinkage strains.

Clearly, the water-reducing property of fly-ash can be advantageously used for achieving a considerable reduction in the drying shrinkage of concrete mixtures [256]. Drying shrinkage relatively reduces in PB to 89% and in PH to 62% of the reference mixes (Figure 4.11b). This improvement in reduction of shrinkage strains is much stronger in PH which contains a higher percentage of fly-ash than PB (70% in PH vs 40% in PB). However, as reported by [135] and can be seen in Figure 4.11b, using aggregate in the mix reduces drying shrinkage more than using fly-ash.

Polypropylene microfibre in PE also reduced the drying shrinkage to 68% of the reference mix, PA (see Figure 4.11b). Microfibre also found to be more effective in reducing drying shrinkage than fly-ash or sand which is in line with the result of [248]. Another observation from the

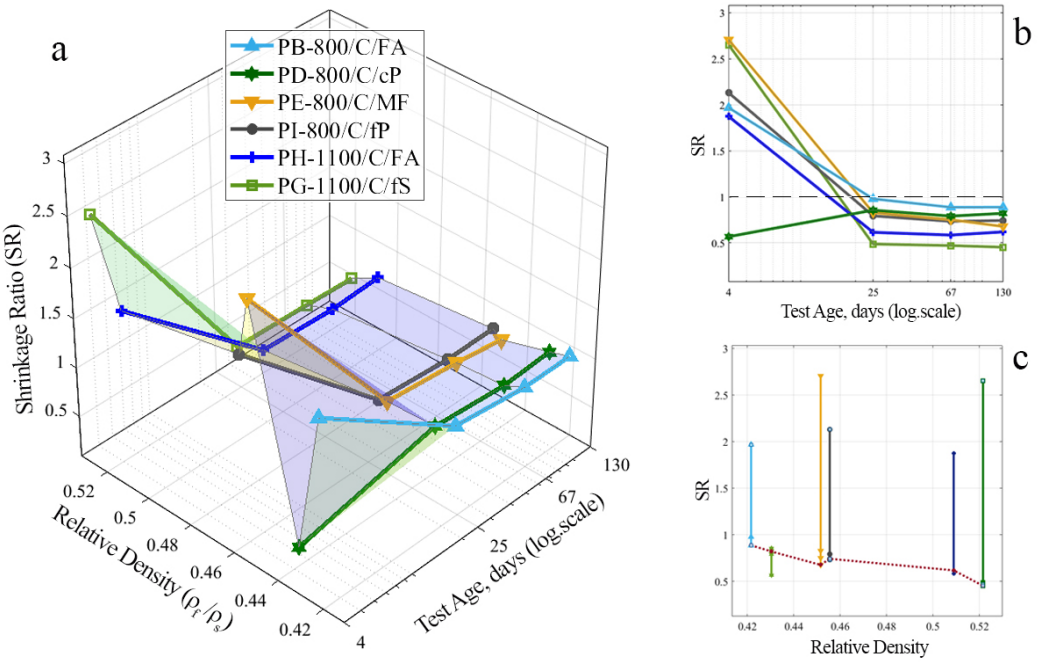

Fig. 4.11. Influence of test age and relative density on shrinkage. The dotted line in (c) connects the values of shrinkage ratio at the age of 130 days.

Figure 4.11c is that at the later ages, SR reduces almost linearly with the slope of -3.54 as the relative density increases (R^2=0.89).

Figure 4.12 shows the variation of shrinkage with moisture content. Based on the plateau achieved by the age of 130 days, the specimens are considered 100% dry at that age. According to [135], the air-voids inherent in the cementitious cell-wall do not contribute to a loss in moisture. So that, only the cellular voids as resulting from the foaming agent are responsible for moisture sorption. In ultra-low density CBF, PC (600 kg/m^3), there is very little shrinkage as the moisture loss occurs from the cells and not from the hydrated cementitious paste in the walls. For very low moisture contents ($< 4\%$), all mixtures exhibited a steep increase in shrinkage, consistent with the literature [135, 251]. Note that the autogenous shrinkage, associated

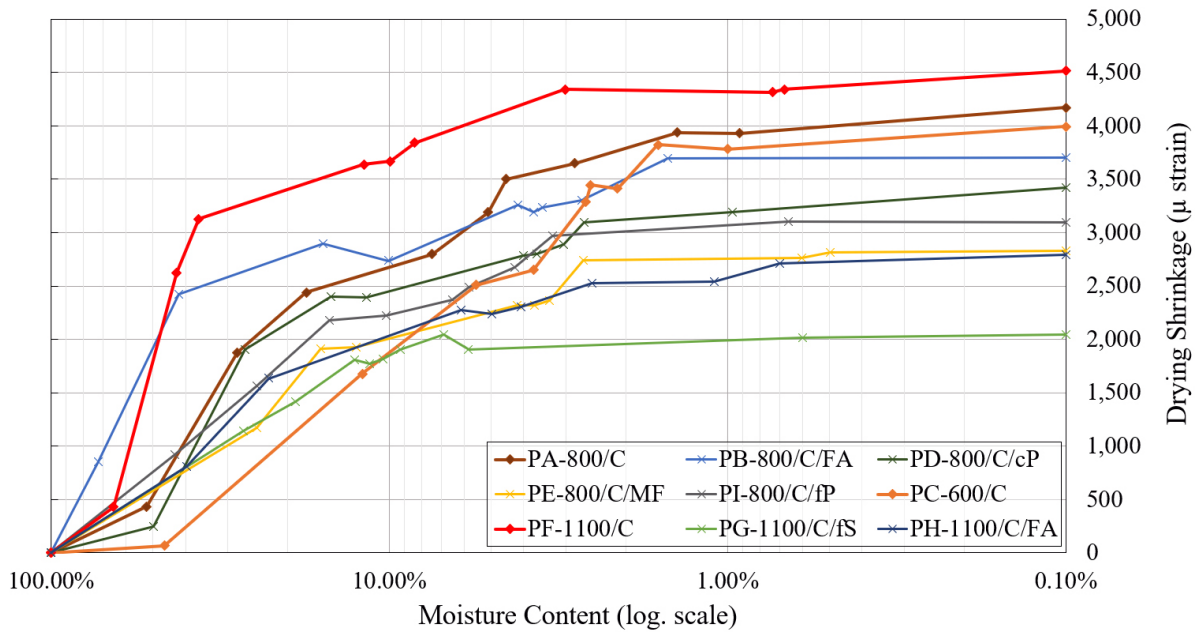

Fig. 4.12. Effect of moisture content on drying shrinkage of cement-based foams.

with a moisture conservative system occurs as a result of self-desiccation during cement hydration [250]. It is significant even when the water-binder ratio is low. However, at higher water-to-binder ratios, the autogenous shrinkage is negligible [382].

4.4.3 Thermal expansion

The CTE of asphalt concrete mixtures is reportedly between 20-63 $\mu\epsilon/^{\circ}C$ [264, 265]. That for plain mature cement paste is about 11-20 $\mu\epsilon/^{\circ}C$ [250, 266] and develops over a period as the hydration proceeds [267, 268]. While the CTE of lightweight concretes is between 7-13 $\mu\epsilon/^{\circ}C$ [269, 270], there is very limited data on the coefficient of thermal expansion of cement-based foams. As reported by [125], the values range from 8.1 to 41.7 $\mu\epsilon/^{\circ}C$. It is seen from Table 4.7 that the CTE of the cement-based foams in this study were between 5.21 to 9.88 $\mu\epsilon/^{\circ}C$. Although lower

Table 4.7. CTE values of CBFs. Values in parentheses are standard errors.

Mix code	PA-800/C	PB-800/C/FA	PD-800/C/cP	PE-800/C/MF	PI-800/C/fP	PC-600/C	PF-1100/C	PG-1100/C/fS	PH-1100/C/FA
CTE $\mu\epsilon/^{\circ}C$	9.43 (0.89)	8.36 (1.18)	7.27 (0.91)	8.84 (1.19)	6.98 (0.89)	5.21 (1.02)	9.84 (0.51)	7.03 (1.11)	5.46 (0.98)

in value, the CTE obtained here follow identical trends as reported in the literature.

It is generally to be expected that the more porous the material, the lower the CTE. This is because porous solids are inherently less conductive thermally. The CTE of the ultra-lightweight reference mixture, PC, is 81% lower than that of the medium-lightweight mixture, PA. Although the CTE of PA is smaller than that of the high-density mixture, PF, the difference is not appreciable. Adding fly ash is known to reduce the thermal expansion, particularly at early age [268, 278]. [278] relate CTE to porosity and portlandite, Ca(OH)2, content of the hardened cement paste. It is known that CTE reduces when porosity increases. Portlandite also has a much higher CTE than that of normal cement paste and therefore, any reduction in portlandite content will result in reduction in CTE. Since replacing Portland cement with fly-ash reduces the portlandite content and increase porosity, it reduces the coefficient of thermal expansion. In the present study, 40% cement replacement by fly-ash in PB and 70% in PH resulted in 11% and 44% reduction in CTE when compared to reference mixes PA and PF respectively.

Aggregates have inherently lower CTE than cement pastes [275]. As reported by [383], concrete mixtures containing a higher volume fraction of aggregates will, therefore, have lower CTE. For cement-based foams, the CTE of the aggregate appears to significantly decide the CTE of the foamed composite. In this study, it was found that adding sand, reduced the CTE substantially by 29%, while fine perlite and coarse perlite caused a reduction in CTE by 26%

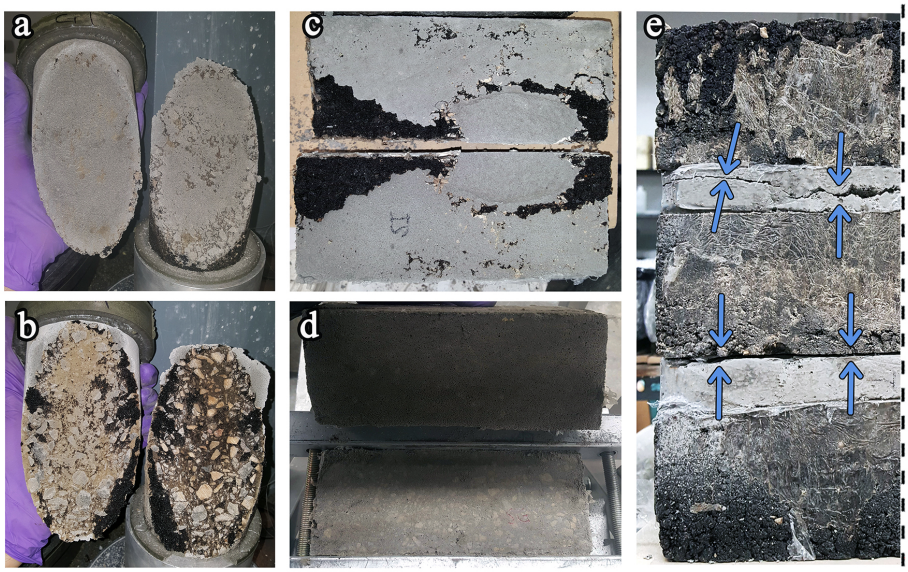

Fig. 4.13. Types of failure: adhesive, in (a), (d) and (e-bottom); cohesive, partially in (b), (c) and in (e-top). Arrows in (e) point to the debonded surface.

and 23%, respectively. Adding microfibres saw only a marginal drop in CTE by 6%.

4.4.4 Bonding characteristics

As seen from Figure 4.13, the typical failure during debonding was part cohesive and part adhesive. All the mixtures tested failed predominantly in adhesion, while in the mixture PF, cohesive failure was considerable. However, it did not account for more than 30% of the debonded surface.

As seen in Figure 4.14, the flexural bond strength was predominantly lower than the bond strength obtained from the slant shear test. The bond strength in flexure varied from $0.15-0.35$ MPa while the shear bond strength varied from 0.33 to 0.63 MPa.

The present study shows that the bond strength regardless of the test method was higher

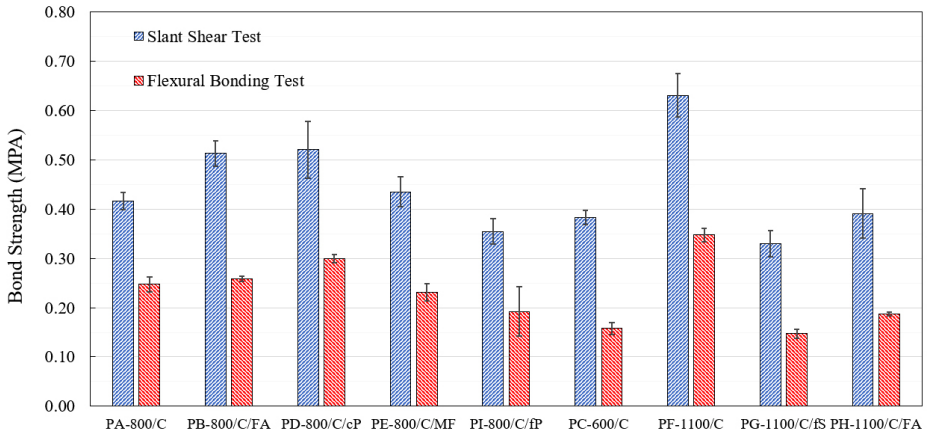

Fig. 4.14. Bond strength of cement-based foams after 7 days of curing.

with an increase in the density of the cement-based foam. However, contrary to expectation, the flexural bond strength was more sensitive and records a 56% increase for a change in the density from 600 to 800 kg/m^3. On the other hand, the shear bond strength registered a mere 10% increase over this change in density. Adding fly ash at 40% replacement of cement results in a 20% increase in the shear bond strength, but only a mere 4% in the flexural bond strength. This may directly be attributed to the pozzolanic outcome that results in superior overall strength [384, 385]. Very high cement replacements, however, cause a drop in the early compressive and tensile strength of the foam and this, in turn, reflect in a drop in the bond strength by 38% in mixture PH compared to mixture PF, for shear bond strength and 46% as obtained via flexural bond strength. Bond strength of PB and PH is yet expected to increase over time due to the age-hardening characteristic of fly-ash. In regard to the aggregates, adding coarse perlite led to a slightly higher bond strength whereas, both fine sand and fine perlite led to a drop in the bond strength. Despite the benefits of microfibres in crack growth resistance and reducing shrinkage, it is reported not to affect the compressive strength of CBFs considerably at a lower dosage [359,

370]. Accordingly, low dosage of polypropylene microfibre in this study did not significantly alter the bond strength of the cement-based foam with asphalt concrete.

Unfortunately, there is no recommendation for the required bond strength of CBF to the asphalt pavement. In the pilot project by [19], no bonding defect was observed in narrow-trenches filled with mixture PA after a year while debonding occurred in the trench that was reinstated by cold-mix asphalt. Interlayer shear strength of the freshly placed CBF against the old hot-mix asphalt was reported to be 0.24-0.4 MPa while this strength is expected to be considerably lower when cold-mix asphalt is used inside a narrow trench with smooth cut faces. Considering this, a threshold of 0.4 MPa in SST or 0.25 MPa in flexural bond strength test can be set. In this case, PA, PB, PD, PE, and PF could be considered to meet this threshold. It must be noted that the values reported here are 7 days strength and the long term bond strength of these mixtures are expected to be higher.

4.5 Selecting the best CBF mixture for narrow-trench reinstatement

Given the lack of a universally accepted recommendation or standard for materials that enable narrow-trench reinstatement, the authors employed the analytic hierarchy process (AHP) [386], which is a powerful and flexible decision-making process to help the user set priorities and arrive at the best decision after taking into account both tangible and nontangible aspects of the activity. The hierarchy of the proposed AHP model is shown in Figure 4.15. The ranking

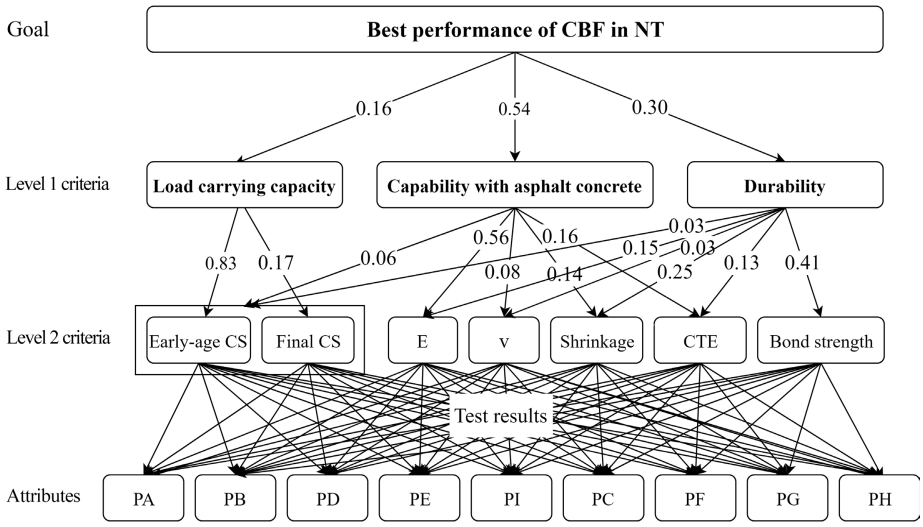

*Abbreviations: CBF, cement-based foam; NT, narow-trenching; CS, compressive strength; E, modulus of elasticity; v, Poisson's ratio; CTE, coefficient of thermal expansion.

Note: Numbers on arrows represent the average importance of each criterion towards the higher level criterion or the goal, by experts.

Fig. 4.15. Hierarchy of the decision support system.

was based on three criteria namely, load carrying capacity, compatibility of the CBF with an asphalt substrate, and its durability as defined by resistance to cracks in this study. Each of the criteria in the two levels namely, level 1 and level 2 were selected and ranked by a series of one-on-one comparison. This exercise aims to build a decision support system that will help future designers of narrow-trenches in ranking different mixture compositions on the basis of their performance. Note that the criteria mentioned above were defined only qualitatively in the present study. It is hoped that municipalities when using the findings from this study shall define quantitative limits to these criteria according to the specific needs of the reinstatement.

Figure 4.16 shows the benefit, in the form of the AHP score for the performance of the CBF mixtures in the trench, versus the material cost per cubic meter. As seen therein, mixtures PC

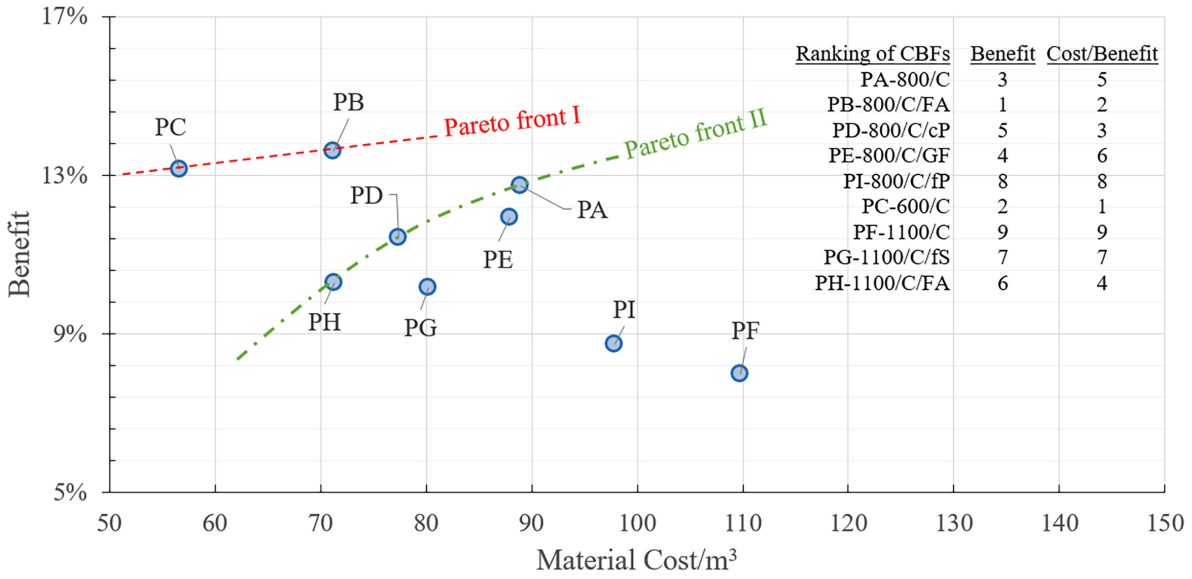

Fig. 4.16. Cost-benefit of nine CBFs in this study. Ranking of the CBFs based on their benefit and cost per benefit is also included at the top right corner of the figure.

and PB are the "Pareto-frontiers", which means that no other mixture composition can supersede them. Note that although mixture PB depicts a marginal improvement in performance over mixture PC, it is also costlier by 26%. Therefore, one with a limited budget might select the mixture PC, which delivers the best performance on cost. On the other hand, if the performance of the CBF, especially its strength be the priority, the mixture PB, which contains fly ash in lieu of Portland cement, emerges as the best option. Mixtures PA, PD and PH are on the second Pareto front, which means that except for mixtures PB and PC, no other option can better them. This exercise shows that the mixture PF was the least favourable option, since it delivers the lowest benefit-cost ratio.

4.6 Concluding remarks

This study was undertaken to investigate the suitability of cement-based foams for narrow-trench backfilling. They were cast to achieve a density between 600 kg/m^3 − 1100 kg/m^3 and were examined for mechanical performance, shrinkage, and coefficient of thermal expansion. Further, their bond strength with an asphalt concrete substrate was studied using the slant shear and the flexural bonding tests. The mixtures designed in this study were ranked per their benefit-cost ratio, based on their load-carrying capacity, compatibility with asphalt concrete and durability. The results show that the lightest mixtures perform best, and also that fly ash substitution of Portland cement is favourable. Based on the findings, the following specific conclusions may be drawn:

- The compressive strength of cement-based foams is affected by the aggregate. Whereas fine perlite resulted in higher compressive strength than coarse perlite, a higher percentage of sand to cement ratio reduces the compressive strength. Both fly ash and fibre reinforcement led to an increase in the compressive strength. As expected, the modulus of elasticity followed closely the trends for the compressive strength above.

- The drying shrinkage of cement-based foams was seen to drop with a decrease in the density. As expected, replacing the cement with fly ash and the addition of aggregates or fibres led to a substantial drop in the drying shrinkage strain.

- The coefficient of thermal expansion (CTE) was seen to drop with a decrease in the density. A higher percentage replacement of Portland cement with fly ash reduced the CTE significantly. Adding aggregates and fibres also led to a reduction in this coefficient.

- Between them, the slant shear test yielded a higher bond strength than the flexural bond test. The bond strength was seen to improve for an increase in the density. At early ages of curing, a smaller dosage of fly ash raised the bond strength, while a higher dosage led to its drop. This may be attributed to the rate of pozzolanic reaction. Whereas coarse perlite led to a higher bond strength, fine perlite led to a drop. No perceptible change was observed as a result of fibre addition.

Chapter 5

Alkali-Activated Fly Ash Foams for Narrow-Trench Reinstatement

This chapter identifies eight mixtures using Fly Ash to prepare alkali-activated foams, cast to densities between 600-1100 kg/m^3. These systems were examined for their mechanical performance, dimensional stability, and bond with the asphalt substrate. The hardened foams were first tested for their strength, modulus of elasticity, and Poisson's ratio. This was followed by evaluating their drying shrinkage and the coefficient of thermal expansion. Lastly, these mixtures were cast against asphalt concrete to assess both slant shear and flexural bond strength. The results show such alkali-activated foams have immense promise as a backfill material for narrow trench reinstatement.

5.1 Introduction

In modern urban areas, the major consideration while placing service lines alongside existing roads is how to restore functionality and keep the disturbance to traffic at a minimum. The first part of this problem is largely achieved by cutting very narrow trenches that are only 25−40 mm in width and no more than 250 mm deep [8]. The second part to this solution requires a suitable material that has satisfactory engineering properties, including adequate strength, water tightness, flowability, bond with the asphalt concrete (AC) substrate and dimensional stability [9].

In a recent report, the on-field performance of different backfilling options was investigated through a series of pilot installations in Alberta, Canada by the first author [19]. Different types of distress were observed in the reinstated trenches within these pilot installations after a few freeze-thaw cycles. The most significant distress among them include (i) the erosion of granular fill or raveling, (ii) settlement, and (iii) a lack of cohesion and adhesion with the cold-mix asphalt or sealant backfill. These findings point out that traditional backfilling materials such as plain sand was not adequate for the Canadian climate [1]. Instead, the colder regions of North America demand a flowable, self-compacting material that is compatible with the AC pavement.

The present authors showed that foamed cementitious systems are aptly suitable as a strong and dimensionally stable backfill that adheres well with the AC substrate [18, 387, 388]. Such foams can be prepared using combustion ash as a precursor for alkali-activation and, in the

process, eliminate the Portland cement altogether [80]. Based on the alumino-silicate used as the precursor, alkali-activated systems have significantly lower production cost [294], improved resistance against frost [389] and chemical attack [390]. Besides, cementitious foams are easily excavated and allow water transpiration. The latter is important to avoid the backfill from behaving like a wall in the middle of the pavement, which otherwise could divert water flow and result in flooding where the trench ends [28].

Alkali-activated foams are composed of three components namely, a precursor, an activator, and a preformed foam. The precursor is a finely dispersed amorphous powder, rich in alumino-silicates and/or calcium silicates [80, 391]. They are commonly sourced as industrial waste or combustion ash including, Fly Ash (FA), Ground Granulated Blast Furnace Slag and Metakaolin. The activators are commonly either Sodium or Potassium Hydroxide and Sodium Silicate solutions [80]. The challenge is to keep the alkaline concentration as low as possible, to promote user safety. The foam is obtained by agitating either a liquid surfactant or through the production of gas [175]. While the lower densities are essentially aerated paste, the higher densities do sometimes incorporate fine aggregate. The higher densities (800 kg/m^3) are intended for applications that are mainly structural ($f'_c > 8$ MPa). On the other hand, the lower densities ($300-800\ kg/m^3$) are attractive for their self-consolidation, good thermal and sound resistance, controlled low-strength, dimensional stability, and ease of re-excavation [175]. The spherical air-void network provides superior thermal and acoustic insulation values, but strengths lower than that for normal- weight concrete [353]. Therefore, this suite of properties makes alkali-activated foam uniquely suitable for backfilling narrow trenches.

5.2 Research significance

Flowable fills are proven to be both fast and cost effective to reinstate narrow trenches after cuts made to install service-utility lines. While there is ample evidence to support alkali-activated foamed systems for insulation, their suitability for narrow-trench backfill is yet to be ascertained. Aside from examining their mechanical performance, it is equally important to characterize the bond behavior against the AC substrate. Therefore, this study was undertaken to prepare a series of alkali-activated FA based foams and to experimentally evaluate their strength, stiffness, dimensional stability, as well as adhesion with the AC. It is expected that the findings reported here shall provide guidance for future reinstatement of narrow-trenches especially in flexible pavement.

5.3 Experimental program

5.3.1 Materials

A same class C Fly-Ash [354, 357] as described in section 4.3.1 was used as the alkali-activated binder. Using X-ray fluorescence, the chemical composition of this FA was determined as reported in Table 4.2.

Sodium hydroxide ($NaOH$) and sodium silicate (Na_2O_3Si) were used as the alkaline activators. The sodium hydroxide solution was prepared by dissolving solid sodium hydroxide pellets in distilled water to achieve 8M concentration [80].This lower concentration of $NaOH$

Table 5.1. Composition of Sodium Silicate solution used in this study.

Water (%)	Sodium silicate (%)	Molar ratio	Density (g/cm^3)	Si (g/lit)	Na (g/lit)
60[a]	40[a]	3.2[a]	1.4[a]	58.65[b]	2.38[b]

[a]According to the supplier safety data sheet (SDS); [b]determined by atomic spectroscopy by [392].

has been previousely used by Stolz et al. [80], which benefit the on-site production of the material by making it safer to produce. A commercially available sodium silicate solution was acquired with a composition as shown in Table 5.1. The method of mixing the activators and FA is explained in following section.

In order to produce the aerated foam, a synthetic foaming agent conformed to [101] and [102] and with the composition as per Table4.3 was used. The foaming method is explained in section 4.3.1.

Similar to cement-based foams, polypropylene microfibres were introduced at a volume fraction of 0.2% to selected mixtures to form a companion series of fibre-reinforced alkali-activated FA based foams. The physical and mechanical properties of these microfibres are shown in Table 4.4.

In order to evaluate the effect of aggregates, two types of fine aggregates, (i) a natural sand and (ii) expanded Perlite, were used to prepare additional alkali-activated foam (AAF) mixtures. Figure 4.2 shows the gradation of the various aggregates used in this study. Note that the gradation of natural sand and that for the fine expanded perlite are nearly identical.

Table 5.2. Mixture proportions (kg/m^3).

Mix code	Target density[1]	Cast density[2]	Fly ash	Sodium silicate	Sodium hydroxide	Water	Aggregate	Microfibre	Dry density[3]	Test density[4]
GA	800	814	600	133	67	20	-	-	680	730
GC	800	807	500	111	56	35	113[a]	-	674	700
GD	800	810	470	104	52	40	70[b]	-	679	705
GE	800	775	510	113	57	50	-	26	645	685
GH	800	780	600	133	67	20	-	-	654	750
GB	600	627	460	102	51	15	-	-	510	590
Group II-High density										
GF	1100	1144	890	198	99	30	-	-	960	1070
GG	1100	1095	350	78	39	65	700[c]	-	980	1045

[1]Target cast density; [2]cast density of fresh AAF; [3]oven dried density; [4]24 hours air-dried density at test.
[a]Perlite coarse; [b]perlite fine; [c]natural sand.

5.3.2 Mixture design and sample preparation

The components and their proportions employed for the mixtures in this study are summarized in Table 5.2. Based on their cast density, the mixtures were grouped into categories namely, Group I (Low Density) and Group II (High Density) such that the cast densities were held nearly constant within each group. Within Group I, the measured oven-dry densities for mixtures designated as GA, GC, GD, GE, and GH lay between 645 to 680 kg/m^3. Here, the mixture GB was significantly lighter at 510 kg/m^3. Within Group II, the mixtures designated as GF and GG had oven-dry densities of 960 and 980 kg/m^3, respectively. Mix GH had a similar composition to GA but was cured at an elevated temperature of 50 $^\circ C$ instead of the room temperature (20 $^\circ C$). The mixtures so designed were intended to allow for multiple comparisons to illustrate the following:

(i) Effect of perlite as fine aggregate, comparing mixtures GA and GC and/or GD.

(ii) Effect of aggregate gradation, comparing mixtures GC and GD.

(iii) Effect of polypropylene microfibre, comparing mixtures GA and GE.

(iv) Effect of curing temperature, comparing GA and GH.

(v) Effect of using natural sand as fine aggregate by comparing mixture GG with the reference mixture GF.

(vi) Effect of density, comparing mixtures GA, GB and GF.

Mindess [364] suggested a minimum water-to-binder ratio of 0.35 in cellular concretes, below which the binder tends to draw water from the foam leading to its instability. Guidelines for flowable fill, [39, 103], specifies an efflux time of (30±5 seconds) in flow cone tests done as per [146]. In order to ensure self-compaction for easy placement of these foams inside the narrow-trench, the water-to-solid ratio was determined through trial-and-error to fulfill the aforementioned requirements as tabulated in Table 5.2. Rezaei [18] also confirmed the good performance of the selected efflux time in a real-life MT project backfilled with cement-based foam.

The process of composing the alkali-activated slurries started with mixing two parts sodium silicate and one part sodium hydroxide solutions (by mass) in an electric barrow concrete mixer. Then, the mix was left to cool down to the room temperature. Next, FA was gradually added to and mixed with this solution. Based on the results of Stolz et. al. [80], the FA to activator ratio was selected as 3:1. After a smooth paste was formed, any additional water was added to the paste. Finally, the aggregates or microfibres were introduced to the paste until a homogeneous slurry was produced. The pre-formed foam is added now to the mix. The density of the

mixtures was checked periodically by means of a small sample and more foam was added to the mixture until the desired target cast density was reached. It is a common practice in manufacturing the alkali-activated concrete to cure them in an elevated temperature environment to accelerate the alkali-activation and improve early mechanical properties of the material. It is also practical in NT application by running hot water through conduits inside the narrow-trench as experienced by Rezaei [18]. However, this practice will increase the time and cost of the project. Therefore, all the alkali-activated specimens were ambient cured for the ease of practical use except for GH. This mixture was immediately moved to an oven set to 50 $^{\circ}C$ and cured for 4 hours. The specimens were left to cool down to the room temperature for 24 hours and then unmolded and stored in a humidity room for the rest of the curing period as will be explained in the test procedure

A total of 12 cylindrical specimens, each 75 mm in diameter and 150 mm in height were cast for each of the eight mixtures. They were examined in compression at 3, 7, 28, and 90 days. Drying shrinkage and the coefficient of thermal expansion (CTE) were measured using six separately cast prisms of $50\times50\times300$ mm per mixture. An asphalt-concrete mixture, commonly used for pavements by the City of Edmonton, was used to prepare the AC substrate to test the bond strength. Its composition and proportions are shown in Table 4.6. The AC cylinders, 75 mm in diameter and 150 mm in height, were compacted, cured and cut as explained in section 4.3.2. Each such half-cylinder was completed by casting an AAF mixture onto it, resulting in a composite specimen as shown in Figure 4.3a.

A separate set of prismatic specimens was cast using the same AC mixture by following the same procedure as described in section 4.3.2. The final composite unit is shown in Figure 4.3b.

5.3.3 Test procedure

Mechanical testing

The compressive strength (CS), modulus of elasticity (E-modulus) and the Poisson's ratio (ν) of the samples were obtained as explained in section 4.3.3.

Drying shrinkage

The drying shrinkage for the foamed systems was examined as per the method described in section 4.3.3 and illustrated in Figure 4.4. The drying shrinkage strain coefficient of the samples was also calculated using Equation 4.1.

Coefficient of thermal expansion (CTE)

The procedure of the coefficient of thermal expansion test is explained in section 4.3.3 and shown in Figure 4.4. The CTE was also calculated using Equation 4.2.

Bond strength evaluation

Among the available test methods to evaluate the bond strength between a backfill and the substrate (discussed in section 4.3.3), the slant shear and the flexural bond strength tests were employed in this chapter in order to measure the bond strength between AAFs and the AC

substrate. The Flexural bond strength test was performed on the prismatic assembly of AAF and AC following the test procedure of section 4.3.3. The slant shear test was also performed as per the instructions explained in section 4.3.3. The flexural bond strength F_g and the shear bond strength in slant shear test were then calculated by using equations 4.3 and 4.4, respectively.

5.4 Results and discussion

5.4.1 Compressive strength and elastic properties

In this study, the CS, E-modulus and ν of AAFs were measured first. Unlike the cement-based foams, there is very little data on the elastic constants of AAFs. The latter is an important parameter in designing backfill materials for narrow trench reinstatement, as there is a considerable lateral stress developed due to the traffic [393].

Figure 5.1 illustrates the effect of curing time on compressive strength of AAFs. Prior research reports a compressive strength between 1-10 MPa, for AAF designed to achieve a density between 360-1400 kg/m^3 [249, 394]. In the present study, the 28-day compressive strength of AAFs was between 0.35 MPa in mixture GG to 5.74 MPa in mixture GF. Some studies have reported an increase in the strength beyond 28 days of curing [79, 395] while others have reported a plateau [396–399]. This contradiction is clearly due to variation in the alumino-silicate precursor or the alkali activator. This study saw a linear increase in strength with age, regardless of mixture compostion (Figure 5.1), also found by Goncalves et al. [79].

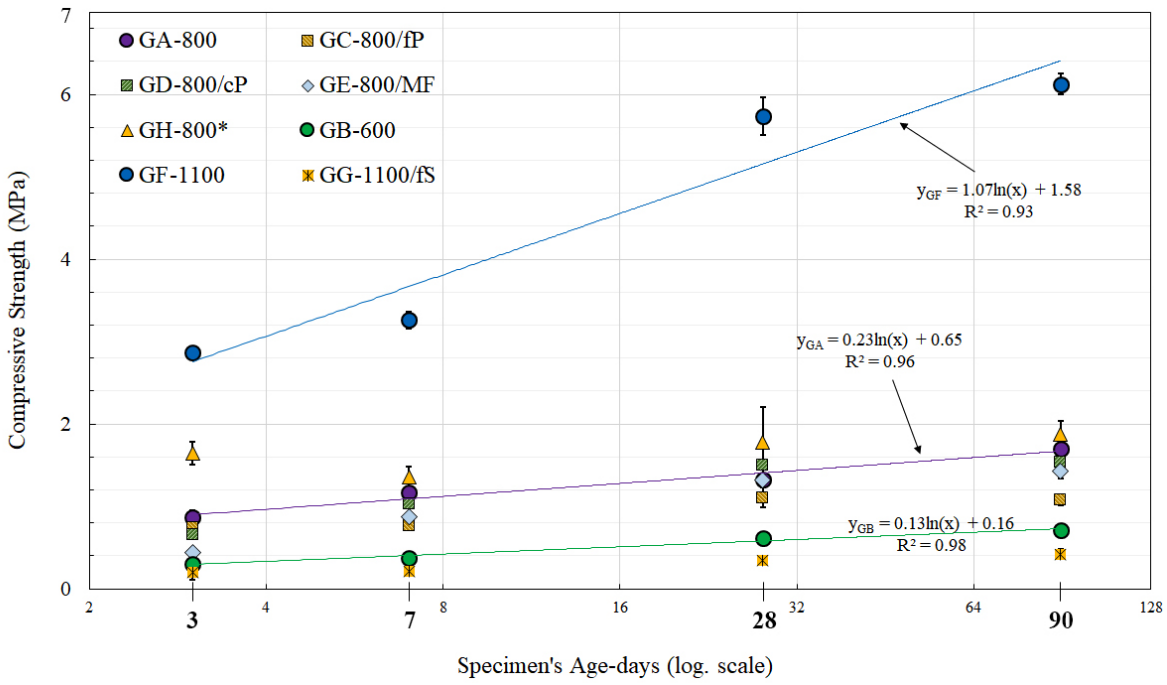

Fig. 5.1. Effect of age on compressive strength of AAFs.

As expected, the higher the porosity, the lower the strength [274, 400, 401]. This is in line with the relationship between the relative density and the compressive strength as seen not only for cementitious foams, but also for cellular solids in general (Figure 5.2). The relative density (ρ_f/ρ_s), is defined as the ratio of the dry density of the AAF, ρ_f, to the dry density of the solid phase,ρ_s. The latter was found experimentally as 1370 kg/m^3 for plain AAFs (specifically, mixtures GA, GB and GF). Gibson et al. [187] examined various cellular cement-based solids and concluded that the crushing strength is a function of the relative density and scales according to the power of 1.5. This exponent is a measure of parametric sensitivity to the change in density of the foamed composite. A similar relationship was found in Figure 5.2 for 28 and 90 days. Note that, while the results of all the AAFs in this study are presented in Figure 5.2, only

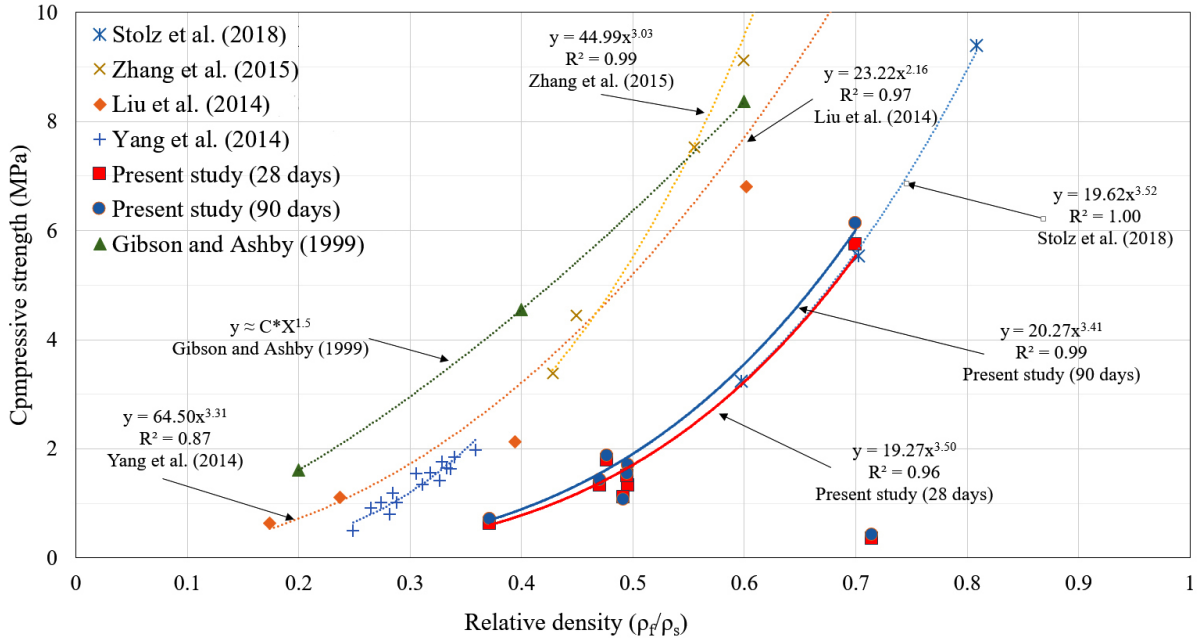

Note 1: The solid lines show the power trendlines of mix GA, GB, GE, GH, and GF.
Note 2: Stolz et al. [80]; Zhang et al. [402]; Liu et al. [403]; Yang et al. [404]; Gibson and Ashby [187].

Fig. 5.2. Effect of relative density on compressive strength of AAFs.

those mixtures without any filler, i.e. GA, GB, GE, GH and, GF, were considered in obtaining the trendline. The exponent for the fitted plots was much higher than that suggested by [187] which suggests the higher sensitivity of the AAFs to the change in density than cement-based foams. Note that the strength of AAFs in this study was expectedly lower than the results of [402, 403], as the latter used a higher concentration of NaOH along with curing at elevated temperatures.

While there is no standard specification as yet for controlled low strength materials used in narrow trench backfill, a numerical analysis of a narrow-trench shows a maximum compressive stress of 1.12 MPa in the backfilling under a heavy traffic loading [38]. A compressive strength of 2 MPa should ensure both stability and excavatability. Since the narrow-trench is

open to traffic at early ages, the minimum strength requirement for AAFs is set as 1.5 at 3 days. Also, a maximum strength of 8 MPa is recommended to ensure ease of re-excavatability [221]. Note from Figure 5.1 that the compressive strength of GH and GF fits in the aforementioned acceptable range.

The elastic modulus, E, and the Poisson's ratio of the 7 AAF mixtures are presented in Figure 5.3. Keeping with the trend reported in prior studies [80, 125, 255, 405, 406], the modulus of elasticity of alkali-activated systems is about 15-30% lower than that of cement based concrete. The elastic moduli measured in this study were found to be mostly similar to values reported by Stolz et al. [80] for AAFs and lower than modulus of elasticity of cement-based foams [125, 387]. So that, for densities ranging from 600 to 1100 kg/m^3, the modulus varied from 205 to 1260 MPa and 310 to 2000 MPa for 28 and 90 days, respectively. As with CS, the elastic modulus is proportional to the relative density [216]. Again, Figure 5.4 compares the results of the present study with those from other reports. Note that in general, the modulus of elasticity in cellular solids varies as the square of the relative density. Once again, the present study reveals a higher sensitivity.

For the sake of comparison, regression equations are fitted for the E-modulus of AAFs in this study and results are tabulated in Table 5.3. Comparing this results with the regression models in the literature (Table 2.4) reveals that the CS regression equation in Table 5.3, complies best to the regression model of the reference [216].

While the density of the AAFs has a significant influence on the modulus of elasticity, there was limited significance to the type of fine aggregate. In the low-density group, the elastic

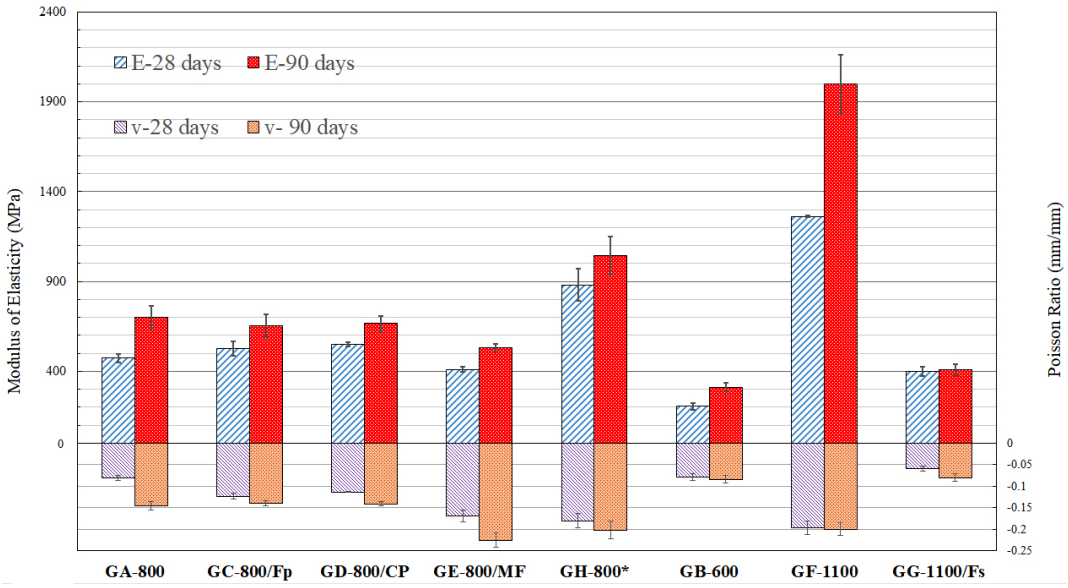

Fig. 5.3. Modulus of Elasticity and Poisson Ratio of AAFs.

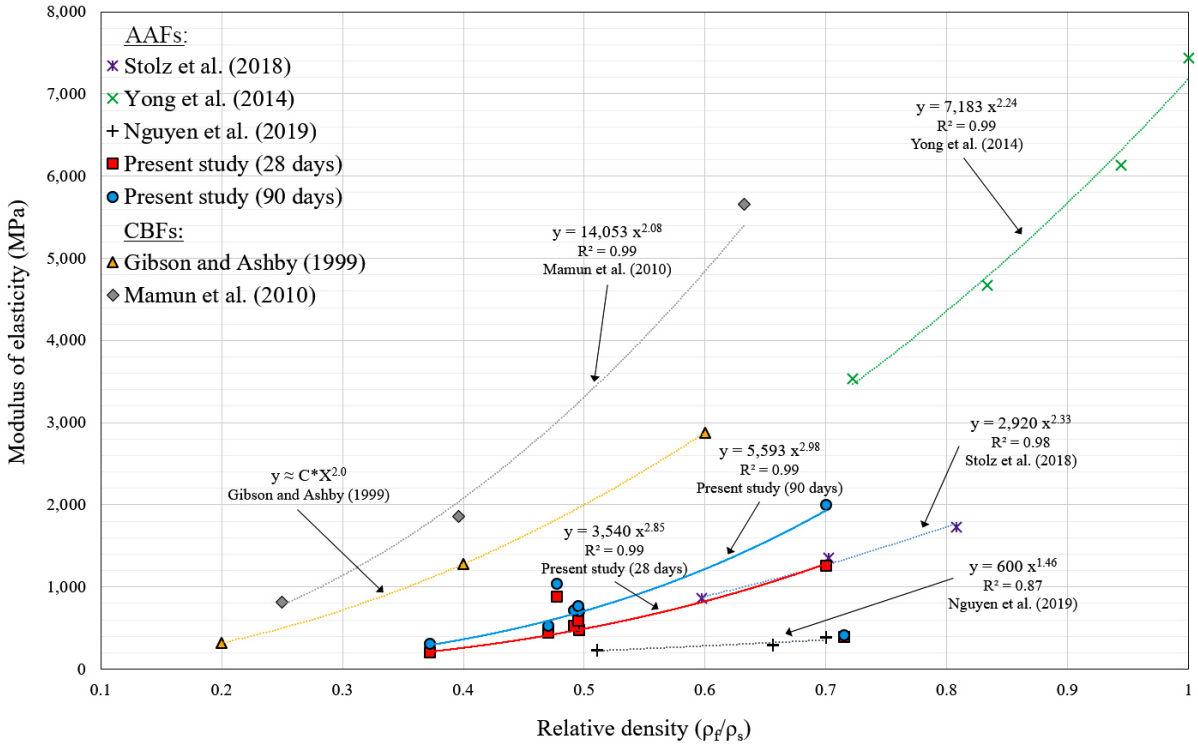

Note 1: The solid lines show the power trendlines of mix GA, GB, GE, and GF.
Note 2: Stolz et al. [80]; Liu et al. [407]; Nguyen et al. [408] Mamun et al. [370]; Gibson and Ashby [187].

Fig. 5.4. Effect of relative density on compressive strength of AAFs.

Table 5.3. The regression equations for predicting the modulus of elasticity of AAFs.

Model	Equation	R^2	Correlation coefficient
CS	$E_{28} = 445.9 \times f_c^{0.607}$	0.87	0.93
	$E_{90} = 492.5 \times f_c^{0.776}$	0.93	0.96
CS-γ	$E_{28} = 0.726 \times \gamma \times f_c^{0.355}$	0.87	0.93
	$E_{90} = 0.832 \times \gamma \times f_c^{0.511}$	0.93	0.96

Note: γ is the dry density (kg/m^3), f_c is the compressive strength (MPa) and E is the modulus of elasticity (MPa).

modulus of the mixtures that contain fine perlite was slightly higher than that of the mixture with the same density but without perlite. This increase may be credited to the aggregate particle interlocking with the paste [109]. However, at higher sand-to-binder ratios, as witnessed in mixture GG, the E-modulus was lower by 70% when compared to the mixture GF. Thus, the results underline the fact that there is an optimum sand-to-binder ratio for maximum E. Adding discrete randomly oriented fibre reinforcement into the mix is known to improve the post-peak response of concrete after cracking [409–411]. The polypropylene fibres have a low modulus of elasticity compared to the cementitious materials and so, easily deform. A decrease in compressive strength [412–414] and modulus of elasticity [194, 409, 415] is expected as a result of incorporating polypropylene fibres. Here too, while the 28 days modulus of elasticity of mixture GE is almost the same as that for the reference mixture, GA, it was 25% lower by the 90^{th} day. The mixture, GH, was cured at higher temperatures, which expectedly promotes the alkali-activation process and resulted in an 85% increase in the modulus of elasticity over the reference mixture, GA.

Prior studies have shown that the Poisson's ratio of AAFs containing no sand ranges from

0.13 to 0.16 at 1000 kg/m^3 that rises up to 0.18 to 0.19 for 1400 kg/m^3 [374]. For lower densities, the values range from 0.14, 0.19, and 0.08 for 300, 600 and 1000 kg/m^3 foamed concretes respectively [125]. Normal weight concrete depicts a Poisson's ratio between 0.15 to 0.22 [274]. As against this, alkali-activated concrete is reported to have a wider range, from 0.08-0.22 [217]. The Poisson's ratios evaluated in this study were in the same range. In foamed concrete, there is likely some localized crushing of the cells during testing, which causes the instantaneous density to change over the course of this test. Based on the specimen density, the Poisson's ratio at 28 days for the alkali-activated foams in this study was between 0.06 to 0.20, which rose only slightly at 90 days to between 0.08 to 0.22.

There is as yet no standard recommended range for either the modulus of elasticity or the Poisson's ratio for backfill in narrow trenches. However, it is clear that the modulus should be high enough to limit deformation in the backfill and at the same time, not so high that the material turns too stiff. According to the numerical model of the reference [38], the stress in the backfilled section for a given traffic load increases with an increase in the elastic modulus. However, this will translate into lower compressive stress in the surrounding soil and pavement. Also, the corresponding stress in the buried utilities and the displacement in the pavement decreases. Note that the E-modulus of asphalt pavement varies with the ambient temperature, reportedly from 700 MPa at 38 $^{\circ}C$ to 14,000 MPa at -1 $^{\circ}C$ [416]. This is significant to the Canadian climate. In a recent field examination [18], cement-based foam cast at 800 kg/m^3 was used as the backfill. It had a modulus of elasticity of 700 MPa at 90 days. After one

year of temperature cycles, no visible distress was observed in the trench. For this elastic modulus, the maximum deformation is noted to be 0.6 mm in the trench (according to [38]), a value that can barely be noticed by the traffic. Therefore, the minimum required 90 days modulus was set to 700 MPa. Of the alkali-activated foams examined in this study, the following three mixtures, namely GA, GH, and GF, met this criterion while the E-modulus of GC and GD was very close to 700 MPa (see Figure 5.3).

5.4.2 Drying shrinkage

The presence of coarse aggregates will restrain the volumetric changes in normal weight concrete [97, 417]. By virtue of their absence in foam concrete, the drying shrinkage strains are up to 10 times greater than those observed in normal weight concrete [112, 271, 418]. Besides, the water content is usually higher in the foams as is the paste-to-fine aggregate ratio. They contribute further to high shrinkage strains in foamed concrete [247]. On the other hand, a higher volume of foam results in lower shrinkage, as the leaner mix is better able to withstand drying shrinkage despite the lower strength [97, 135, 376]. which attributes to the lower paste content. Whereas, shrinkage cracks shall let water in and rapidly lead to failure after only a few freeze-thaw cycles, letting water into a narrow trench is detrimental to the service cables.

Figure 5.5 shows the drying shrinkage profiles for the various mixtures examined in this chapter. Considering only the reference mixtures within each range of target density, the drying shrinkage strains vary widely from 213 to 4246 μ-strain in mixture GB, 594 to 4731 μ-strain with mixture GA, and 601 to 5353 μ-strain for mixture GF. There is a wide variation in the

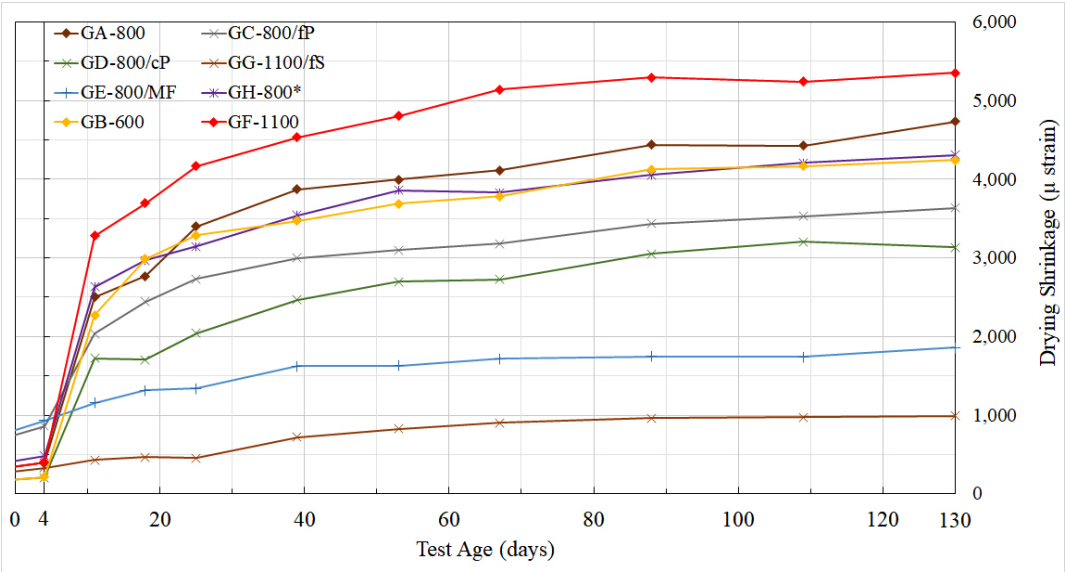

Fig. 5.5. Drying shrinkage versus test age.

shrinkage strains of cement-based systems, as reported in the available literature. And it was noted to be as low as 250 μ-strain [125] and as high as 4000 [254, 358], 5000 [248] or even 62000 [87]μ-strain over a range of cast densities lying between 300 to 1000 kg/m^3 across different mixture compositions. The limited reports on alkali-activated foams note a similar variation in shrinkage strain. For plain alkali-activated foams, Hajmohammadi et al. [418] reported shrinkage strain of 3000 μ-strain. Abdollahinejad et al. [417] observed a μ-strain of 1300 in an alkali-activated foam with sand-to-binder ratio of one. When cured at room temperarure, alkali-activated systems undergo substantially higher drying shrinkage than Portland cement systems [419]. The values measured in the present study lie closer to the upper bound of those reported in the literature.

24 hr curing the alkali-activated concrete at elevated temperature is known to reduce the

drying shrinkage considerably compared to the ambient cured samples [419–421]. This is attributed to the fact that the elevated temperature will accelerate drying of the alkali-activated concrete and therefore, there will be less pore water to cause shrinkage [154].

With cellular concrete, the lower cast density promotes an open-cell structure, while those cast to higher densities tend towards a closed-cell structure [249]. Ziembicka [377] noted that shrinkage in cellular concrete is a function of volume and specific surface of micro-pores. However, Georgiades [378] reports that the removal of water from comparatively bigger pores will not contribute to shrinkage. Since large entrained air voids do not change the structure of the fine pores [379], it can be concluded that the micro-pores that control the shrinkage are related to the paste content in the hardened paste in such a way that the lower paste content will result in lower shrinkage [135]. As noted with Portland cement foams, the shrinkage strains increase proportionally with an increase in the density of mixtures GB, GA and GF. Also, the drying shrinkage levels off between the 3^{rd} and 10^{th} week, as noted elsewhere with alkali-activated systems [419, 421].

The shrinkage strain was normalized against that observed for the reference mixtures at a particular density, i.e. GA and GF, as the shrinkage ratio (SR). It is plotted against the age at test in Figure 5.6. As expected, those foams that contain aggregates, mixtures GC and GD, depict lower shrinkage strains. Between the two gradations, fine perlite led to consistently lower shrinkage strains than coarse perlite. Sand being stiffer than perlite, the former was twice as effective in reducing the shrinkage strain than fine and coarse perlite. As expected, the polypropylene microfibres reduced the drying shrinkage in alkali-activated foams.

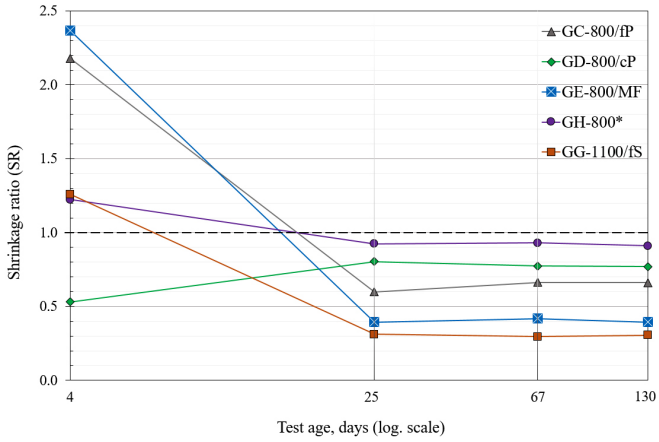

Fig. 5.6. Shrinkage ratio versus test age.

Table 5.4. CTE values of AAFs. Values in parentheses are standard errors.

Mix code	GA-800	GC-800/fP	GD-800/cP	GE-800/MF	GH-800*	GB-600	GF-1100	GG-1100/fS
CTE	14.4	7.39	7.89	12.38	8.46	5.46	16.24	7.67
$\mu - strain/°C$	(0.64)	(0.65)	(0.71)	(1.11)	(0.75)	(0.39)	(0.69)	(0.91)

5.4.3 Thermal expansion

The CTE for asphalt concrete mixtures is between 20-63 $\mu - strain/°C$, while that for plain cement mortar is about 11-20 $\mu - strain/°C$ [250, 264–266]. In Portland cement systems, this develops over time as the hydration proceeds [267, 268]. While the CTE of lightweight concrete lies between 7-13 $\mu - strain/°C$ [269, 270], that for Portland cement foams varies from 8.1 to 41.7 $\mu - strain/°C$. As listed in Table 5.4, the CTE for the various alkali-activated foams in this study was somewhat lower, lying between 5.46 to 16.24 $\mu - strain/°C$.

It is generally to be expected that the more porous the material, the lower the CTE, since porous solids are inherently less thermally conducting. Between the foams examined here, the CTE of the lightest mixture, GB, was 60% lower than that of mixture, GA. The CTE of mixture

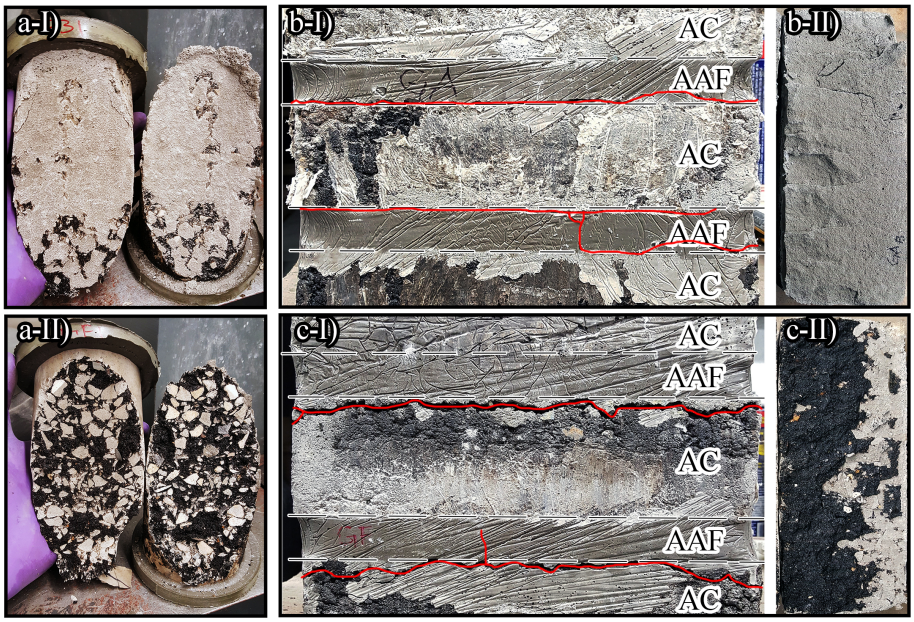

Fig. 5.7. Types of failure in Slant shear test (a) and flexural bonding test (b and c); adhesive failure in a-I and b; cohesive failure in a-II and c.

GA was in turn 10% lower than that of the densest mixture, GF. Given that aggregates have inherently lower CTE than the bulk cement paste [422], their presence significantly decides the CTE of the foamed composite. In comparison with the plain reference foam, sand reduced the CTE by nearly 55%, while the fine and coarse perlite led to a respective drop by 50% and 45%. Note that mixture GH was cured at an elevated temperature, which led to a drop in the CTE by 35% over the reference mixture GA.

5.4.4 Bonding characteristics

The representative failure surface after debonding between the AAFs and the asphalt substrate is shown in Figure 5.7. Whereas mixtures GH and GF display cohesive failure, all others displayed adhesive failure.

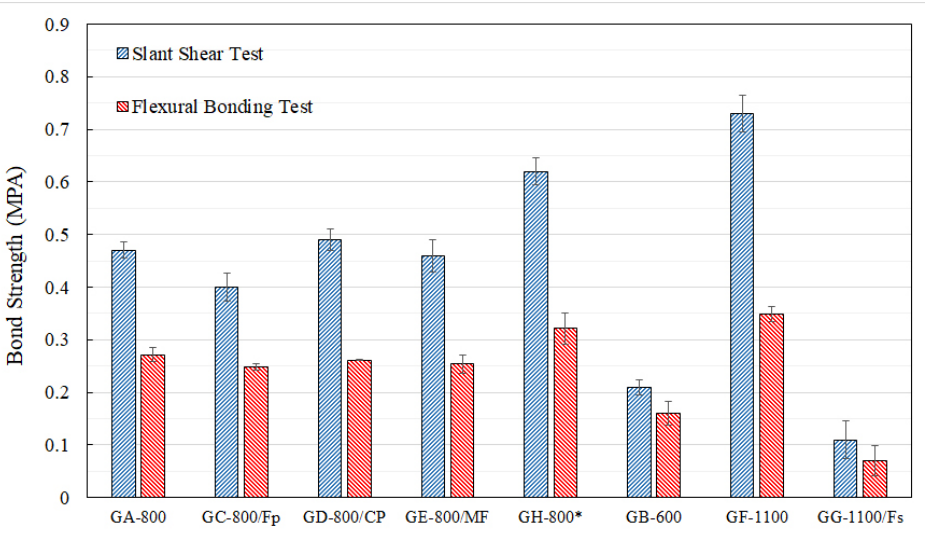

Fig. 5.8. Bond strength of AAFs after 7 days of curing.

It is clear from Figure 5.8, that the flexural bond strength was considerably lower than the bond strength obtained from the slant shear test. The bond strength in flexure varied from 0.07 to 0.35 MPa while the shear bond strength varied from 0.11 to 0.73 MPa. As expected, the higher the density, the higher the bond strength. Also, the flexural bond was about 3 times more sensitive to the density of the AAF, compared to the shear bond strength.

A study by Shuguang et al. [423] concluded that compared to Portland cement mortar, alkali-activated mortar bonds stronger with a concrete substrate. In a prior study, the present authors had examined Portland cement foams as potential backfill [387]. Despite being weaker in compression, the alkali-activated foams described here achieved stronger bond with the asphalt substrate than the Portland cement foams at similar density, aggregate type, and content. Whereas coarse perlite led to a slightly higher bond strength, both fine sand and fine perlite led to a drop in the bond strength. This follows the trend observed among cement-based

foams. Similar to cement-based foams, the addition of polymer microfibres did not alter the bond strength in this study. As found elsewhere [424], the present study confirms that curing the alkali-activated system at elevated temperatures improves the bond strength at early ages (7-days), but according to [424] the effect is not appreciable at 28-days.

There is as yet, no recommendation available for the bond strength required of backfill with asphalt pavement to serve in narrow trench reinstatement. In a pilot project conducted by the first author [18], no bond related defect was observed after 1 year in narrow-trenches filled with a cement based foam that possessed a 7-day slant shear bond of 0.42 MPa (flexural bond of 0.25 MPa). On the other hand, a companion backfill using cold mix asphalt saw debonding in that same period. If a similar threshold were set for the mixtures in the present study, (i.e. 0.4 MPa in shear and 0.25 MPa in flexure), then mixtures GA, GC, GD, GE, and GF are seen to exceed this threshold. It must be noted that the values reported here are 7 days strength and the long term bond strength of these mixtures are expected to be higher.

5.5 Selecting the best AAF mixture for narrow-trench reinstatement

Considering the lack of a comprehensive standard for materials used for narrow-trench reinstatement, an Analytic Hierarchy Process (AHP), was established to rank the mixtures for backfilling, on the basis of the present laboratory test results. AHP [386] is a structured decision support technique, which can help designers to decompose the problem into a set of more

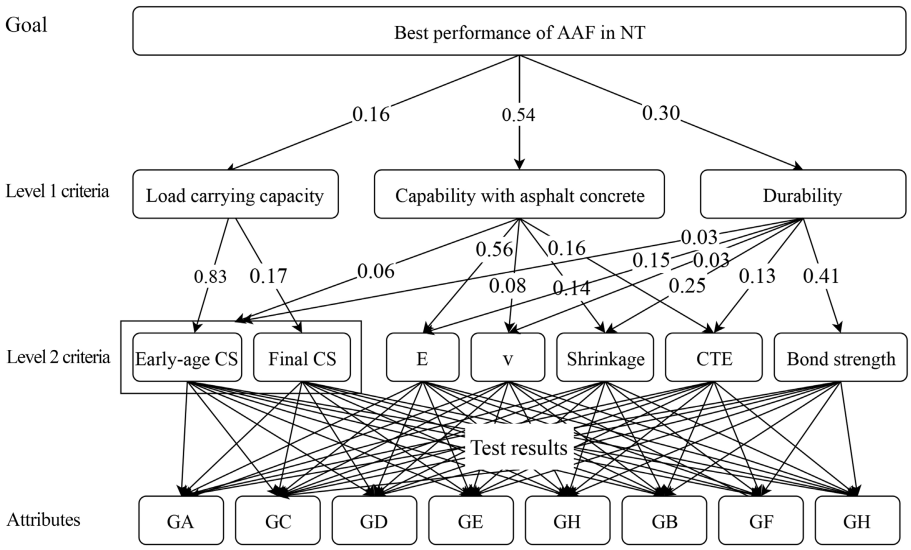

*Abbreviations: AAF, alkali-activated based foam; NT, narow-trenching; CS, compressive strength; E, modulus of elasticity; v, Poisson's ratio; CTE, coefficient of thermal expansion.

Note: numbers on arrows represent the expert's opinion on the average importance of each criterion towards the higher level criterion or the goal.

Fig. 5.9. Hierarchy of the decision support system.

easily comprehensible sub-problems. It assigns priorities to each decision criterion, considering both tangible and intangible aspects of the project, which in turn lead to the best decision towards the overall goal.

The structure of the problem as regards the AHP in this chapter is shown in Figure 5.9. This hierarchy is structured by questioning the experts in narrow-trenching as explained in Section 4.5. The final score or benefit as found through AHP for each AAF mixture in this chapter also calculated following the same steps as discussed in Section 4.5. It is hoped that this decision support model can help narrow-trench designers in ranking different mixture design options, which shall in turn allow for innovative materials in backfilling narrow trenches worldwide.

In Figure 5.10, the performance of each AAF mixture in this study is presented against the

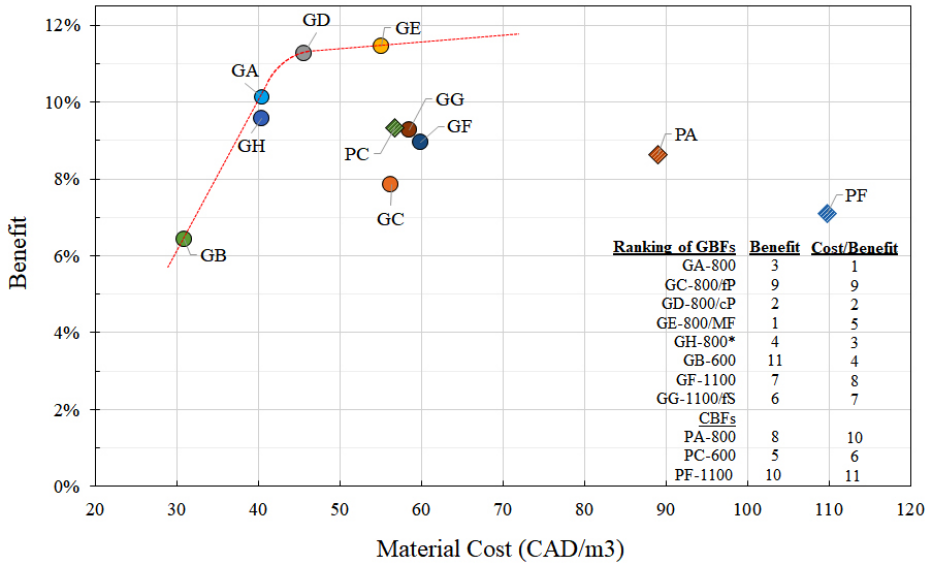

Fig. 5.10. Cost-benefit of AAFs in this study. Ranking of the AAFs based on their benefit and cost per benefit is also included at the bottom right corner of the figure.

cost-per-cubic-meter of the material. These results were compared further with three plain cement-based foams, namely PA, PC, and PF. Recall that these mixtures were cast to densities of 800, 600 and 1100 kg/m^3, respectively. In comparison, the present study confirms that AAFs deliver a higher benefit-to-material cost ratio. As depicted in Figure 5.10, mixtures GB, GA, GD, and GE are "Pareto frontiers" meaning that no other mixture composition can dominate them if both the benefit and material cost be considered. When the performance of the reinstatement material is the first priority, mixture GE should be selected. However, it comes at a greater cost. So that, one with a limited budget might select mixture GA, which offers an average benefit and material cost.

5.6 Concluding remarks

A series of alkali-activated foams was characterized for their suitability as backfill in narrow-trench reinstatement in Canadian climes. Eight mixtures were cast to achieve a target density between 600-1100 kg/m^3. These mixtures were examined to evaluate their mechanical performance, drying shrinkage, coefficient of thermal expansion, and their bond with an asphalt concrete substrate. The bond was evaluated using both a slant shear test and a flexural test. Using these experimental results, the mixtures were ranked on the basis of their performance parameters for deployment as backfill, by means of an Analytic Hierarchy Process (AHP). Based on the findings, the following specific conclusions may be drawn:

- The compressive strength of alkali-activated foams is sensitive to cast density, curing temperature and aggregate type. While higher densities result in higher compressive strength, heat curing improves the strength at early ages. However, no appreciable effect was observed beyond 90 days. Among the aggregates examined here, coarse perlite outperformed fine perlite or ordinary sand. An improvement to the compressive strength resulted in an expected rise in the modulus of elasticity.

- There was a drop in drying shrinkage of AAFs with a decrease in cast density. Adding aggregates and polypropylene microfibres uniformly reduced the shrinkage strain. As well, curing at elevated temperatures resulted in lower shrinkage strain.

- The coefficient of thermal expansion drops with a decrease in the cast density. At the same time, adding aggregates and polypropylene microfibres and curing at elevated temperatures also reduced the CTE.

- The slant shear test witnessed higher bond strength than the flexural bond test. An increase in the cast density of the AAF and heat curing further increased the bond strength. Whereas adding sand to the AAF resulted in a weaker bond, neither perlite nor microfibres appear to affect the bond strength either way.

Chapter 6

Freeze-Thaw Resistance of Cement- and Alkali-Activated-Based Foams Used for Narrow-Trench Backfilling in Cold Regions

Cement-based slurries have shown promising results in narrow trench reinstatement. As have alkali-activated-based foams, in a recent study. Further, alkali-activated-based foams offer a more environmentally friendly alternative by using industrial by-products/waste and thus, reducing the CO_2 emission. However, the performance of these foams in cold regions with frequent freeze-thaw cycles is a concern. The study reported here assessed the performance of cement- and alkali-activated-based foams for reinstating narrow-trenches in cold climates. Accordingly, foam samples with densities ranging from 600-1100 kg/m^3 and different admixtures were prepared in the laboratory and their mechanical performance was assessed after several freeze-thaw cycles following a test procedure, closely based on ASTM C666. Based

on the findings, recommendations are made regarding the production of freeze-thaw resistant reinstatement for narrow-trenching application. The results of this study revealed a better resistance of the cement-based foams to freeze-thaw cycles than alkali-activated foams. The durability of cement-based foams was found to be negatively correlated to their relative density, while this correlation was positive for alkali-activated foams. That said, the low-density cement based foam delivered the highest resistance to freeze-thaw cycles among cement- and alkali-activated-based foams.

6.1 Introduction

Considering the necessary performance criteria of cement-based foam (CBF) for NT application, their low cost, and ease of the process, they have been used as an alternative to conventional fillers [19, 388]. Alternatively, the environmental and performance benefits of alkali-activated binders made them a good candidate for replacing Portland cement. They are sourced from the industrial and agricultural waste and have a significantly lower production cost [294], improved frost [389] and chemical attack [390] resistance, and lower CO_2 emission and therefore, lower environmental impact [294] when compared to Portland cement. Cement- or alkali-activated based foams are also easily excavated and are permeable enough to let the water to flow through. The latter is important since it prevents the backfilling to act as a wall in the middle of the road and interfere with the natural drainage of the pavement and in turn, lead to flooding [28].

CBFs are prepared by mixing a cementitious binder, water, and preformed-foam. The foam is produced by agitating either a liquid surfactant or through the production of gas [175]. Similarly, alkali-activated foams (AAFs) are generally composed of an alkali-activated binder, activator, and preformed-foam. The alkaline binder is finely dispersed amorphous and rich in aluminosilicates or calcium silicates [80]. Alkaline activators are relatively costly and are responsible for about 80% of the cost of the alkali-activated concrete [425]. Therefore, the cost of alkali-activated concrete is slightly higher than Portland cement concrete but lower than the high-performance concrete [293]. The density of the CBF or AAF is typically controlled by the volume of the foam in the mix. Lower densities (300-800 kg/m^3) are essentially aerated paste while higher densities ($\geq$ 800kg/m^3) can incorporate fine aggregates. Higher strength in higher densities makes the structural applications possible while the self-consolidation, good thermal and sound resistance, controlled low-strength, ease of re-excavation, and the superior thermal insulation [175, 353] have made the lower density foams an outstanding option for backfilling the narrow-trench.

6.2 Research significance

Even though foamed, flowable fills are recognized as a quick and cost-effective material for backfilling utility cuts, they have not been used in practice for narrow-trench backfilling, citing durability concern. This is particularly so in regard to the Canadian climate. Examination of some options in a recent pilot study by the first author highlighted distress attributed mainly to

freeze-thaw activity. Prior studies on cementitious foams provide assurance as to their thermo-mechanical performance as well as their bond with the asphalt concrete substrate. Therefore, this study was undertaken to experimentally evaluate the freeze-thaw durability of foamed fills made with Portland cement and alkali-activated binders. It is expected that the present findings shall provide guidance for the design and test of a durable reinstatement for narrow-trenches in cold climates.

6.3 Experimental program

6.3.1 Materials

The properties of the materials used to prepare the CBF and AAF samples are explained in Section 4.3.1 and 5.3.1, respectively.

6.3.2 Mixture design

The composition and proportion of CBFs and AAFs studied here are summarized in Table 4.5 and 5.2, respectively. A test plan was designed to explore the effect of different densities and mix compositions on freeze-thaw resistance of cement and alkali-activated foams. Accordingly, the different mixtures in this study divided into two groups, namely low-density (LD) and high-density (HD) groups. For the LD group, a target cast density of 800 kg/m^3 was selected except for the ultra-low-density mixtures, PC and GB, which targeted for a cast density of 600 kg/m^3. Within HD group, the mixtures were designed with a considerably higher cast density

of 1100 kg/m^3. The mixture design was intended to allow for the following parametric effects upon the freeze-thaw resistance of the foams:

- Effect of incorporating FA in CBFs, between mixture PA and PB and again, between mixtures PF and PH.
- Effect of perlite as fine aggregate between mixtures PA and PD and/or PI in CBFs and between GA and GC and/or GD in AAFs.
- Effect of aggregate gradation between mixtures PD and PI and between GC and GD.
- Effect of fibre reinforcement, between mixtures PA and PE and between GA and GE.
- Effect of using natural sand as fine aggregate by comparing mixtures PF and PG and between GF and GG.
- Effect of density between plain foams, i.e PA, PC and PF among CBFs and GA, GB and GF among AAFs.

Moreover, a direct comparison between cement- and alkali-activated foams is also made by comparing the performance of mixtures in Table 4.5 and 5.2.

The procedure of production of CBF and AAF is explained in Sections 4.3.2 and 5.3.2, respectively.

6.3.3 Test method

Background

While there are a few studies on the freeze-thaw performance of AAFs, three general test methods have been used by Senbu and Kamada [426] and other researchers to evaluate that of cement foams. In the first test method, namely the critical degree of saturation [427, 428], the specimens are brought to different levels of saturation before being subjected to a certain number of freeze-thaw cycles. The level of saturation which caused the deterioration is then called the critical level and is compared to the expected level of saturation in the practical application of the material. The second method is called the top surface freezing test [429, 430] in which the cylindrical specimens are subjected to a temperature gradient varying from below to above freezing temperature, similar to the real-life gradient. The time required for the specimens to crack under this temperature gradient is then considered as a measure of freeze-thaw performance. Last and the most commonly implemented test method in literature is a modified version of ASTM C666 [298]. This test is originally designed for normal-weight concrete and its procedure involves freezing and thawing the specimens in water (method A) or freezing in air and thawing under water (method B).

The difference between the microstructure of cellular and normal-weight concrete leads to a two-phase deterioration [290, 431]: one is the tensile forces caused by the restrained freezing water [432] which results in progressive cracks and the other is surface scaling which happens because of different freeze-thaw induced forces in the saturated surface and unsaturated inner

zones [429]. Unlike the top surface freezing and the critical degree of saturation method, ASTM C666 can provide a full measure of freeze-thaw durability and account for both deterioration phases, i.e. micro-cracking and surface scaling [290, 426, 429, 433].

Modified ASTM C666

Freeze-thaw failure in cellular concrete occurs in larger air voids than the capillary voids in case of normal weight concrete and hence, the failure is not possible if the air voids are not saturated enough [290, 433]. Since ASTM C666 does not account for normalizing the moisture content of the specimens, a modification to the standard is required to be suited for cellular concrete. Therefore, a modified ASTM C666 method B procedure, suggested by Tikalsky et al. [290] based on the results of Senbu and Kamada [433] and Roulet [428], was selected in this study.

Following the recommended specimen size by ASTM C666, prisms of $50 \times 50 \times 300$ mm were first tried in the freeze-thaw test. Since the testing procedure involved frequent displacement and conditioning of the samples, micro-cracks emerged on the slender lightweight foam prisms as a result of this frequent handling. This was more critical in the case of more fragile AAFs, which even led to their premature failure. Therefore, cylindrical specimens, each 75 mm in diameter and 150 mm in height, were used instead of the fragile prisms. For each mix design in Table 4.5 and 5.2, 24 cylindrical specimens were cast, unmolded after 24 hours, and cured in a humidity room with the temperature of 21 $^{\circ}C$ and relative humidity of 95% for a period of 28 days. Then, 18 out of a total of 24 specimens were weighted and then submerged under 2 cm

of water at the room temperature. The saturated surface dry (SSD) weight of specimens was measured at 24 hours intervals. The saturation process continued until the weight gain was less than 1% of the previous reading for a maximum of 28 days.

Following the curing and saturation process, the specimens were sealed immediately after weighing and moved to an industrial walk-in freezer for freeze-thaw cycling. The freeze-thaw cycle consisted of air freezing at the temperature of $-18 \pm 4^{\circ}C$, un-sealing, and thawing under water at room temperature (Figure 6.1). This higher thawing temperature than the recommended temperature of ASTM C666 (i.e. $4^{\circ}C$) was selected because of the bigger size of the specimens in this study and the lower thermal conductivity of foam concrete compared to regular concrete. A thermocouple was inserted into a control specimen to allow the continuous monitoring of the internal temperature of specimens. It was observed that the internal temperature reaches below and above zero temperature after about 8 hours after the start of the freezing and thawing process. This allows for one freeze and thaw cycle per day and the test terminated after 150 cycles.

To quantitatively measure the freeze-thaw resistance of the mixtures, four parameters were measured. First mass loss was monitored every 10 cycles by measuring the SSD weight of the cylinders after the thawing process. The remaining three parameters, compressive strength, modulus of elasticity and Poisson's ratio, were measured after 10, 30, 60, 90, 120, and 150 cycles. The compressive strength of the specimens was obtained using a universal testing machine according to ASTM C495 [365]. As reported elsewhere [434, 435], the static modulus of elasticity and dynamic elastic moduli, acquired from the resonance frequency test, are well correlated.

Fig. 6.1. Freeze-thaw test procedure: a) sealed specimens are freezing inside a walk-in freezer; b) thawing in temperature controlled water bath; and c) uniaxial compression test apparatus.

Due to the unavailability of the resonance frequency test setup, the static modulus of elasticity of the specimens was measured instead of the dynamic modulus, as is suggested by ASTM C666 [298]. For this purpose, the compressive strength test specimens were fitted to a digital compressometer before the test to record their longitudinal and lateral strains for calculation of static modulus of elasticity and Poisson's ratio as per ASTM C469 [366]. Each test was done on three randomly selected specimens. Accordingly, the remaining 6 specimens were kept in the moist room to be tested at the age of 28 and 90 days in order to serve as the reference, unconditioned specimens.

6.4 Results and discussions

The physical and mechanical properties of the unconditioned CBFs and AAFs in this study are shown in Table 6.1. Saturated moisture content shows the percentage of the volume of the samples that was filled with water after the saturation process. As inferred from the table, the absorption of AAFs is marginally higher than their companion CBFs. On the other hand, the compressive strength of CBFs is higher than their corresponding AAFs. This is mainly due to the low concentration of sodium-hydroxide and ambient curing of AAFs in this study. The strength of the foam samples also decreases with density. Adding Perlite slightly improved the strength of CBFs while reduced that of AAFs. This reduction is more pronounced when fine perlite is used. An increase in E modulus was also observed when perlite is introduced to the mix. A higher percentage of natural sand in high-density groups drastically reduced the strength and elastic response of both cement and alkali-activated foams. The fibrous CBFs showed an improvement in compressive strength, modulus of elasticity and Poisson's ratio while in AAFs, no appreciable change was observed. Replacing cement with FA in CBFs also increased the strength and E modulus.

Following the calculation method of ASTM C666 and in order to quantitatively compare the freeze-thaw deterioration of different mixtures, relative value (PR_c) and durability factor (DF) are defined as per Equations 6.1 and 6.2, respectively.

$$PR_c = \frac{n_c^2}{n_0^2} \times 100 \tag{6.1}$$

Table 6.1. Properties of unconditioned cement- and alkali-activated-based foams.

Mix code	Dry density[1]	Saturated density[2]	Saturated moisture content[3]	Compressive strength[4]		Modulus of elasticity[4]		Poisson's ratio	
				28d	90d	28d	90d	28d	90d
Cement-based foams-LD									
PA-800/C	647	1008	36%	2.53	3.20	733	1367	-0.09	-0.11
PB-800/C/FA	668	961	29%	3.03	4.45	1396	1582	-0.11	-0.10
PD-800/C/cP	588	892	30%	2.65	3.22	785	2573	-0.05	-0.20
PE-800/C/GF	642	989	35%	3.43	3.84	1777	2255	-0.28	-0.16
PI-800/C/fP	644	964	32%	2.74	3.65	2183	2693	-0.20	-0.18
PC-600/C	520	985	47%	2.17	2.18	427	1344	-0.16	-0.11
Cement-based foams-HD									
PF-1100/C	857	1153	30%	4.44	7.93	1156	3279	-0.06	-0.21
PG-1100/C/fS	982	1179	20%	1.73	2.65	551	2686	-0.05	-0.17
PH-1100/C/FA	881	1161	28%	3.29	10.26	2076	3179	-0.09	-0.19
alkali-activated-based foams-LD									
GA-800	680	1065	39%	1.33	1.70	473	701	-0.08	-0.15
GC-800/fP	674	1003	33%	1.11	1.07	525	713	-0.12	-0.14
GD-800/cP	679	1060	38%	1.50	1.54	589	767	-0.11	-0.14
GE-800/MF	645	1072	42%	1.32	1.43	440	531	-0.17	-0.23
GH-800*	654	1019	37%	1.78	1.87	880	1044	-0.18	-0.20
GB-600	510	1094	59%	0.62	0.71	205	311	-0.08	-0.08
alkali-activated-based foams-HD									
GF-1100	960	1311	35%	5.74	6.13	1262	1999	-0.20	-0.20
GG-1100/Fs	980	1399	42%	0.35	0.42	397	411	-0.06	-0.08

[1]Oven dried density (kg/m^3); [2]saturated surface dry density (kg/m^3); [3]percent volume; [4]MPa

$$DF = PR_c \times \frac{C}{150} \tag{6.2}$$

In which n_0 and n_c are the measured values before the start of the freeze-thaw conditioning and after c^{th} freeze-thaw cycles, respectively; and C is the number of cycles at which the measured value reaches its minimum, or 150 cycles, whichever occurs first.

The freeze-thaw resistance of alkali-activated concrete is reportedly higher than Portland cement concrete [160, 293, 436–439]. Accordingly, as reported by Yunsheng and Wei [296], alkali-activated FA concrete can withstand 2.2 more freeze-thaw cycles than concrete made with Portland cement. Surface scaling due to freeze-thaw cycles is considerably high in plain cement concrete. As with conventional concrete, it is reported that air entraining agent (0.25-2.5% by mass of FA) improves substantially the freeze-thaw resistance in alkali-activated fly ash concrete [440]. Still, the limited studies on their freeze-thaw performance indicate that alkali-activated systems suffer more damage than CBFs [82, 154, 438, 441]. According to Brooks et al. [438], this is mainly due to the reduced compressive strength and a lack of stable, uniform porous network in the former.

6.4.1 Surface scaling

Relative mass of the cement- and alkali-activated-based foams are calculated using Equation 6.1 and presented in Figure 6.2. It can be inferred that surface scaling and deterioration are more substantial in AAFs than in the CBFs. This may directly be attributed to the lower compressive

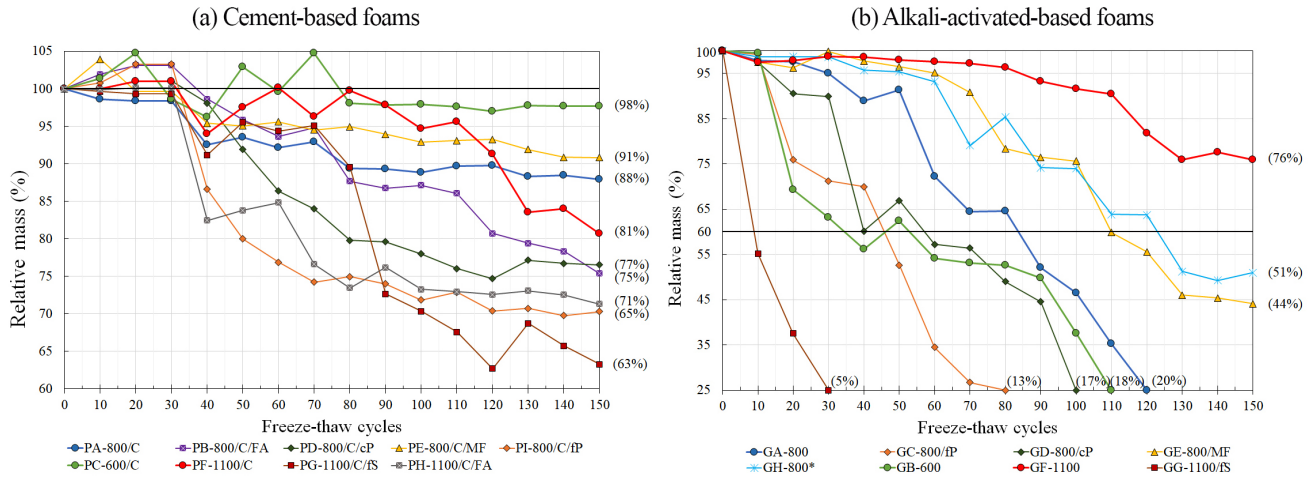

Fig. 6.2. Relative mass versus freeze-thaw cycles. Values in parenthesis represent the durability factor.

strength and higher absorption of AAFs compared to CBFs (See Table 6.1). Among CBFs, the ultra-light mix PC sustained the 150 cycles of freeze-thaw without any considerable mass loss. Mixture PA, on the other hand, underwent a 4% mass loss after 40 cycles and beyond that, its mass stayed almost constant (Figure 6.3). Contrarily, the high-density mix, PF, started to deteriorate after about 100 cycles. Figure 6.2b shows a progressive deterioration for AAFs. In contrast to cement-based foams, the lower density mixtures deteriorated faster. The ultra-light mix GB with durability factor of 18% lost 50% of its original mass after 110 cycles which can be a result of its low 28- and 90-days strength. The 800 kg/m^3 Mixture GA showed only a marginal improvement over GB with a DF equals to 20%. Whilst the deterioration of the high-density mixture GF accelerated after 110 cycles of freeze-thaw conditioning, its DF was the highest among the AAFs (76%).

Surface scaling was higher in mixtures with aggregate than the plain foams in both cement- and alkali-activated-based foams. This might be attributed to the fact that the frost damage

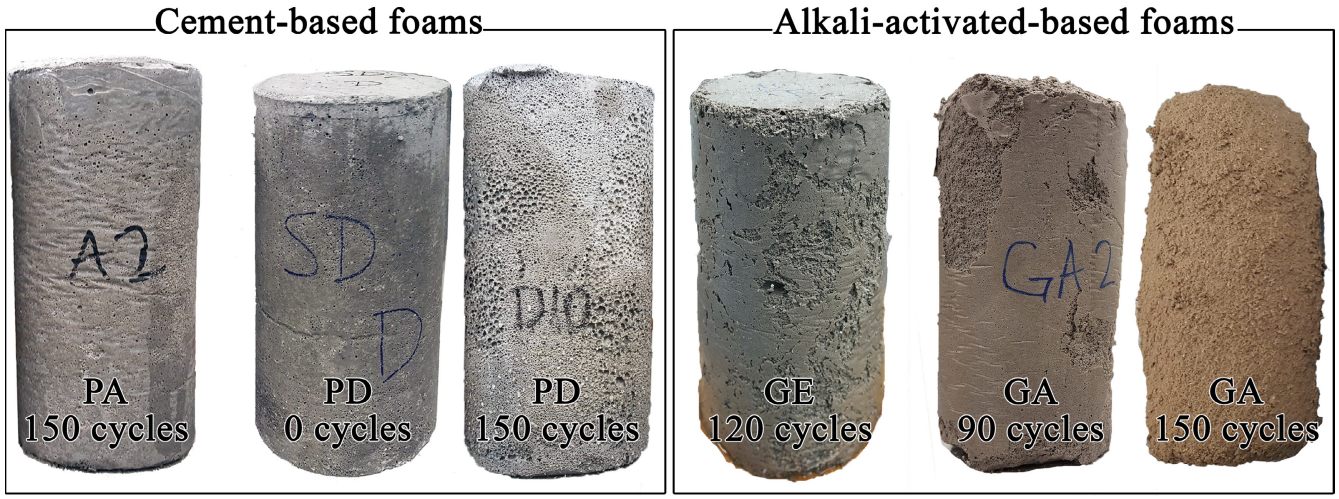

Fig. 6.3. Surface scaling of cement- and alkali-activated-based foams at different cycles of freezing and thawing.

made the surface aggregates loose and later conditioning of specimens in water, during the thawing process, washed these loose aggregate out which results in a progressive mass loss (See mix PD in Figure 6.3). Mixtures that incorporate coarse perlite (PD and GD) also had relatively better resistance to cycles of freezing and thawing when compared to mixture PI and GC with fine perlite. The higher percentage of natural sand in mixture PG and GG made them the least durable mixtures among cement- and alkali-activated-foams in this study with DF of 63% and 5% respectively. Despite being the least durable CBF, PG sustained its integrity through the 150 cycles while the low compressive strength of GG (28 days strength of 0.35 MPa) resulted in sharp deterioration and 50% mass loss in only 30 cycles.

Fibre reinforcement is known to improve the post-elastic properties of concrete after cracking [409–411]. Accordingly introducing polypropylene fibre to mixture GE resulted in DF of 44%, which is an improvement over the plain AAF, GA in the same density group with DF of

20%. Likewise, cement-based, fibre-reinforced foam PE presented a superior frost resistance (DF of 91%) compared to mix PA (DF of 88%).

As presented in Figure 6.2a, replacing cement with FA will increase scaling in CBFs. In the low-density group, mixture PB with with 40% FA replacement resulted in 14.8% reduction in DF when compared to the plain mix, PA. Similarly, in high-density group, PH (cement to FA ratio of 2.3) reduced the DF of plain mix PF by 12.3%. The same trend was observed by Tikalsky et al. [290].

6.4.2 Internal cracking

Compressive strength

Superior freeze-thaw resistance of CBFs over AAFs can also be deduced from the values of relative strength presented in Figure 6.4. While the AAFs experienced a progressive strength reduction as a result of freeze-thaw conditioning, some of CBFs ended with higher compressive strength than their 28 days strength. The same improvement in concrete properties has been reported in literature [194, 290, 388]. This is mainly due to the activation of cement and FA in CBFs during the wet curing (while thawing), leading to the formation of binding products which counteract the effect of freeze-thaw cycling [154]. On the other hand, low kinetics of the reaction of FA in AAFs, their low 28 days strength, and higher absorption are mainly responsible for their progressive freeze-thaw deterioration.

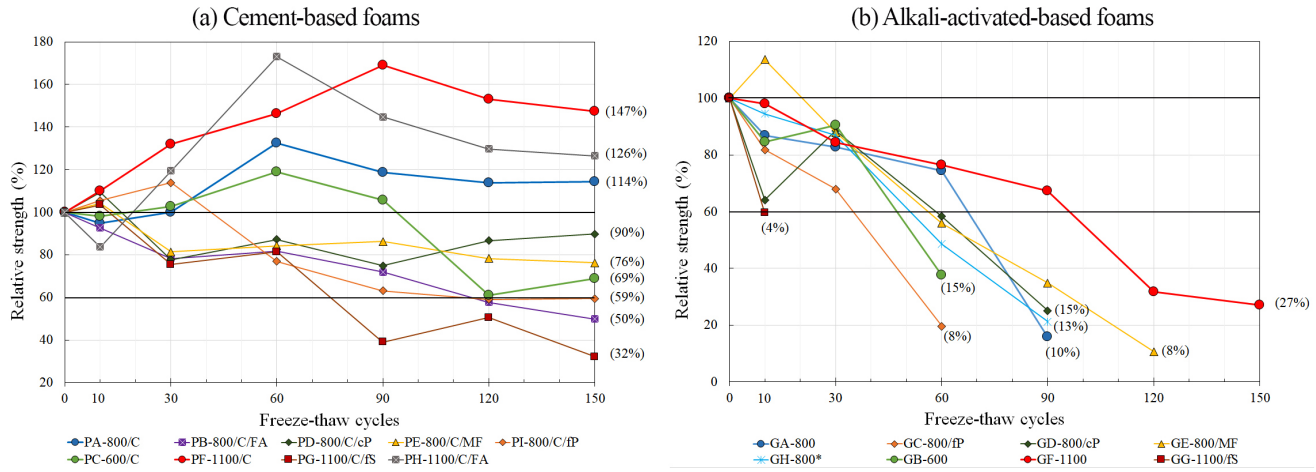

Fig. 6.4. Relative strength versus freeze-thaw cycles. Values in parenthesis represent the durability factor.

In order to consider the change in the microstructure of samples due to hydration or alkali-activation during freeze-thaw cycles, properties of conditioned freeze-thaw specimens after 60 and 150 freeze-thaw cycles are compared to that of 90 days unconditioned reference specimens. Using Equations 6.1 and 6.2, durability factors were calculated, as shown in Table 6.2. While the DF_{28d}^{150c} suggests the better durability of higher density foams, DF_{90d}^{60c} indicates otherwise. In order to calculate DF_{90d}^{60c}, the strength of specimens after 60 freeze-thaw cycles is compared to the 90-days strength of the unconditioned reference specimens. Since the freeze-thaw specimens were cured for 28 days before the start of the test, this comparison could evince the real durability of the mix. Referring to the values of DF_{90d}^{60c} reported in Table 6.2, the durability of the lightest CBF, PC, is 42% more than the lightweight mix, PA, and 157% more than the high-density mix, PF. Therefore, the heavier cement-based foams are more prone to strength loss as a result of the freeze-thaw cycling. Accordingly, a negative correlation was found between the DF_{90d}^{150c} of plain cement foams in different density groups and their relative density (correlation

coefficient of -0.82). The correlation coefficient of DF_{90d}^{60c} and relative density was also calculated as -0.99. On the contrary, the durability of AAFs is observed to reduce with density. Regarding the values of DF_{90d}^{60c}, the durability of high-density AAF, GF, is 46% and 131% more than the low-density mix GA and ultra-low-density mix, GB. This is mainly due to the low 28 days compressive strength and high absorption of GA and GB (Table 6.1).

Coarse perlite also performed better than fine perlite in both CBFs and AAFs in frost resistance. Among cement foams, PD underwent the 150 cycles of freezing and thawing with DF_{28d}^{150c} and DF_{90d}^{150c} of 90% and 61% respectively. Despite this high resistance to strength loss, the PD's durability factor is 24% less than the plain cement foam, PA, in the low-density group. On the other hand, the strength of mixture PI which contains fine perlite, increased in the first 30 cycles of conditioning, however, it started to decrease afterward and resulted in a DF_{28d}^{150c} of 59%. The freeze-thaw test on AAFs GC and GD stopped after 60 and 90 cycles respectively due to the lack of required integrity of the specimens for the compression test. However, the DF_{28d}^{150c} of GD with coarse perlite was 50% higher than the plain AAF, GA. Therefore, introducing coarse perlite improved the resistance to strength loss in AAFs. The cement and alkali-activated foam samples containing a higher percentage of natural sand were the most resistant to freeze-thaw cycling. The alkali-activated mixture GG lost its integrity after only 10 cycles of freezing and thawing. This is mainly because of the low 28 days compressive strength of GG (0.35 MPa).

Cavdar [442] studied the effect of freeze-thaw cycles on high density ($\geq 1900 kg/m^3$) fibre-reinforced aerated cement mortars. After 100 cycles, the DF_{28d}^{100c} of the control specimen was equal to 87% while that of mixtures with 0.4%, 0.8%, and 1.2% polypropylene microfibre was

measured as 88%, 89%, and 91% respectively. This shows a marginal improvement in frost resistance of fibrous ones. However, fibre reinforcement in the lightweight mixture, PE, in this study resulted in DF_{28d}^{150c} of 76% which is 38% less than PA. This is mainly because of the faster hydration of PA in wet conditioning than PE with less cement content. While the plain AAF, GA lost its integrity after 90 cycles of freezing and thawing, the fibrous mixture, GE withstood 120 cycles. It resulted in a DF_{28d}^{90c} of 35% which is a 250% improvement over that of GA. Clearly, reinforcing with microfibres does improve the freeze-thaw resistance of AAFs.

A 40% substitution of cement with FA resulting in the lightweight mixture, PB, yielded in DF_{90d}^{150c} of only 23%. This shows a 68% reduction in durability when compared to mixture PA. A 70% cement replacement with FA in high-density mixture PH resulted in a higher DF_{28d}^{150c} of 126%. However, when considering the increase in strength during the test, one will notice that the DF_{90d}^{150c} of PH is 72% less than that for plain cement foam PF in the same density group and 43% less than PB. Tikalsky et al. [290] have also noticed the marginal performance of the FA incorporated mortars in freeze-thaw test because of their less cement content, low early-age strength, and high absorption.

It is found that the durability of heat-cured specimens is slightly lower than that of moist-cured ones [443]. Moist curing produces higher air content levels with closely spaced and finely divided bubbles. This improved air-void parameters resulted in marginally higher durability factor of GA than the heat-cured mix, GH.

As discussed before, there is no standard specification as yet for controlled low strength materials used in narrow trench backfill. Following the same argument as Sections 4.4.1 and 5.4.1,

the higher and lower limits for compressive strength were selected as 8.3 and 2, respectively. After 150 cycles of freezing and thawing, all the CBFs, except PC and PG, display a strength greater than 2 and less than the maximum of 8.3 MPa. Among the AAFs, only mixture GF endure 150 cycles of conditioning with a compressive strength equals to 2.99 MPa.

Elastic behavior

The change in elastic behavior of cement- and alkali-activated-based foams during the miltiple cycles of freezing and thawing was studied by measuring their modulus of elasticity and the Poisson's ratio. The relative modulus and Poisson's ratio of CBFs and AAFs are presented in Figures 6.5 and 6.6, respectively. According to these figures and the values of durability factor in Table 6.2, inferior durability of higher density cement foams can be concluded. The only contradiction is the trend of the Poisson's ratio of mix PA which resulted in higher DF_{28d}^{150c} than that of high-density mix PF. Accordingly, relative modulus of the plain cement foams, PC, PA, and PF are found to be negatively correlated to their relative density (correlation coefficient of -0.92). DF_{90d}^{150c} in the Poisson's ratio test is also reversely correlated to the relative density with a correlation coefficient of -0.98. Similar to compressive strength, the elastic behavior of high-density AAF, GF was relatively better than the lightweight mixtures GA and GB.

Among the mixtures that incorporate aggregates and based on the values of DF_{90d}^{150c}, fine perlites in mix PI resulted in a higher increase in modulus of elasticity than coarse perlite in PD or natural sand in PG. However, higher DF_{90d}^{150c} of the Poisson's ratio in PI suggests its higher lateral strains. Contrarily, and similar to the result of the compressive strength, coarse perlite

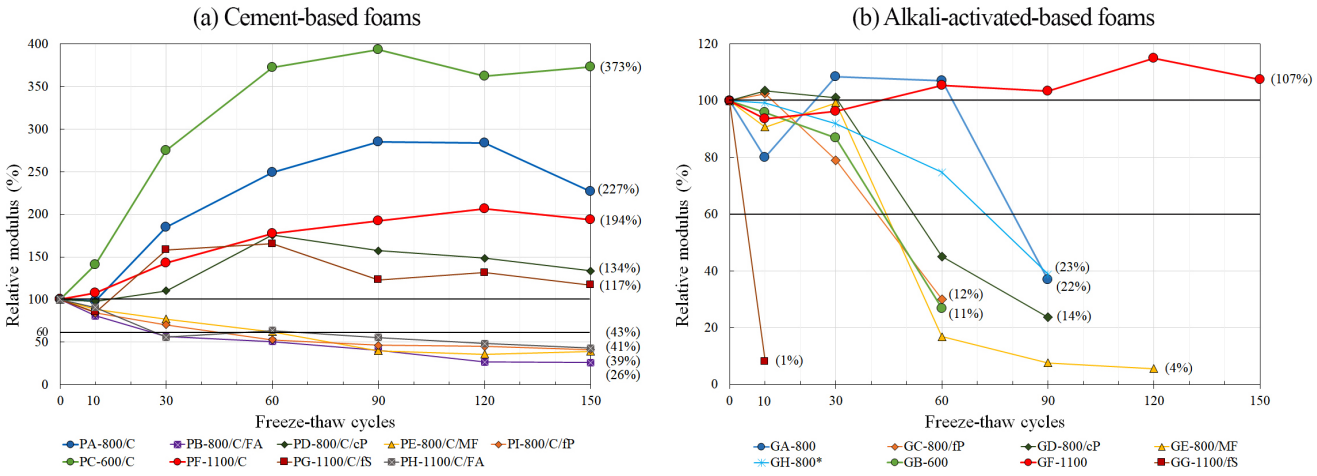

Fig. 6.5. Relative elasticity modulus versus freeze-thaw cycles. Values in parenthesis represent the durability factor.

in AAF, GD, resulted in a marginally higher DF_{90d}^{150c} than the fine perlite in GC. The fibrous mixtures PE and GE displayed an average 65% reduction in DF_{90d}^{150c} of modulus and reduced the lateral strains by 50% when compared to their corresponding plain foams, i.e PA and GA.

Similar to the relative strength, DF_{90d}^{150c} of modulus in cement foams containing FA reduced compared to the plain foam, PA. Heat curing in mix GH increased the rigidity and DF_{90d}^{150c} when compared to GA.

Figure 6.6 depicts the relative Poisson's ratio of CBFs and AAFs, respectively.

6.4.3 Cost-benefit analysis

Given the lack of a universally accepted recommendation or standard for acceptable performance of materials that enable narrow-trench reinstatement under potential freeze-thaw cycling, the durability of the different mixtures in this study was studied considering the material

Table 6.2. Durability factors of cement- and alkali-activated-based mixes.

Mix code	Compressive strength (%)			Modulus of elasticity (%)			Poisson's ratio (%)		
	DF_{28d}^{150c1}	DF_{90d}^{60c2}	DF_{90d}^{150c3}	DF_{28d}^{150c}	DF_{90d}^{60c}	DF_{90d}^{150c}	DF_{28d}^{150c}	DF_{90d}^{60c}	DF_{90d}^{150c}
Cement-based foams-LD									
PA-800/C	114	83	72	227	72	65	264	108	173
PB-800/C/FA	50	38	23	26	40	20	140	181	163
PD-800/C/cP	90	59	61	134	16	12	498	19	31
PE-800/C/MF	76	67	61	39	39	24	30	139	92
PI-800/C/fP	59	43	33	41	35	27	168	127	216
PC-600/C	69	118	68	373	38	38	114	114	237
Cement-based foams-HD									
PF-1100/C	147	46	46	194	22	24	124	13	10
PG-1100/C/fS	32	35	14	117	7	5	225	25	22
PH-1100/C/FA	126	18	13	43	27	18	244	31	55
alkali-activated-based foams-LD									
GA-800	10	46	6	22	49	10	23	14	7
GC-800/fP	8	21	8	12	16	7	10	20	8
GD-800/cP	15	56	14	14	27	8	16	27	10
GE-800/MF	8	48	7	4	12	3	6	43	3
GH-800*	6	51	6	23	53	17	67	84	53
GB-600	15	29	11	11	12	5	20	43	17
alkali-activated-based foams-HD									
GF-1100	27	67	24	107	42	43	102	60	100
GG-1100/fS	4	3	3	1	1	1	8	5	5

[1]Calculated by comparing the strength of the freeze-thaw conditioned sample after 150 cycles to the 28 days strength of the unconditioned specimen; [2]Calculated by comparing the strength of the freeze-thaw conditioned sample after 60 cycles to the 90 days strength of the unconditioned specimen; [3]Calculated by comparing the strength of the freeze-thaw conditioned sample after 150 cycles to the 90 days strength of the unconditioned specimen.

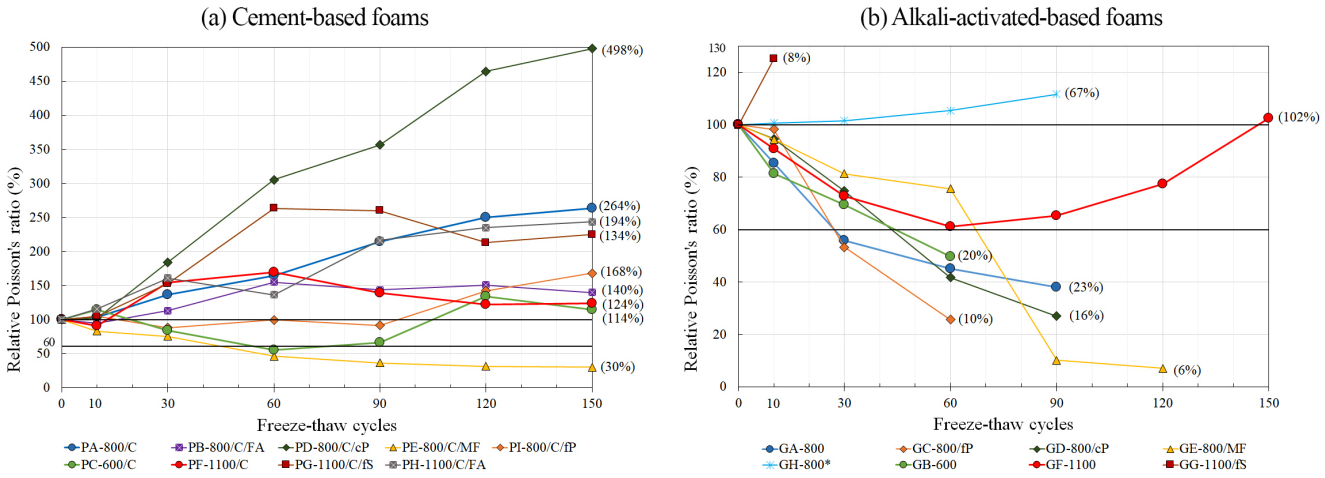

Fig. 6.6. Relative Poisson's ratio versus freeze-thaw cycles. Values in parenthesis represent the durability factor.

cost. The benefit of different CBFs and AAFs in this study is calculated as their weighted average durability in the freeze-thaw test. Similarly, the material cost of these mixtures is calculated based on the average cost quotations from the local suppliers in Alberta, Canada, and plotted against their benefit in Figure 9. This exercise aims to build a decision support system that will help select a mixture composition for future narrow-trench designers by ranking the different mixture compositions examined here, on the basis of their freeze-thaw resistance. However, it must be noted that this exercise does not consider any limits for the minimum required performance of the mixes. It is hoped that municipalities or approval authorities when using the findings from this study shall define quantitative limits for strength or elastic properties according to the specific needs of the project.

As depicted in Figure 6.7, the ultra-lightweight CBF, PC has the highest benefit and cost per benefit. However, by choosing GH over PC a 29% saving in material cost can be attained while surrendering 70% of the benefit. One with even a more limited budget might choose GB over

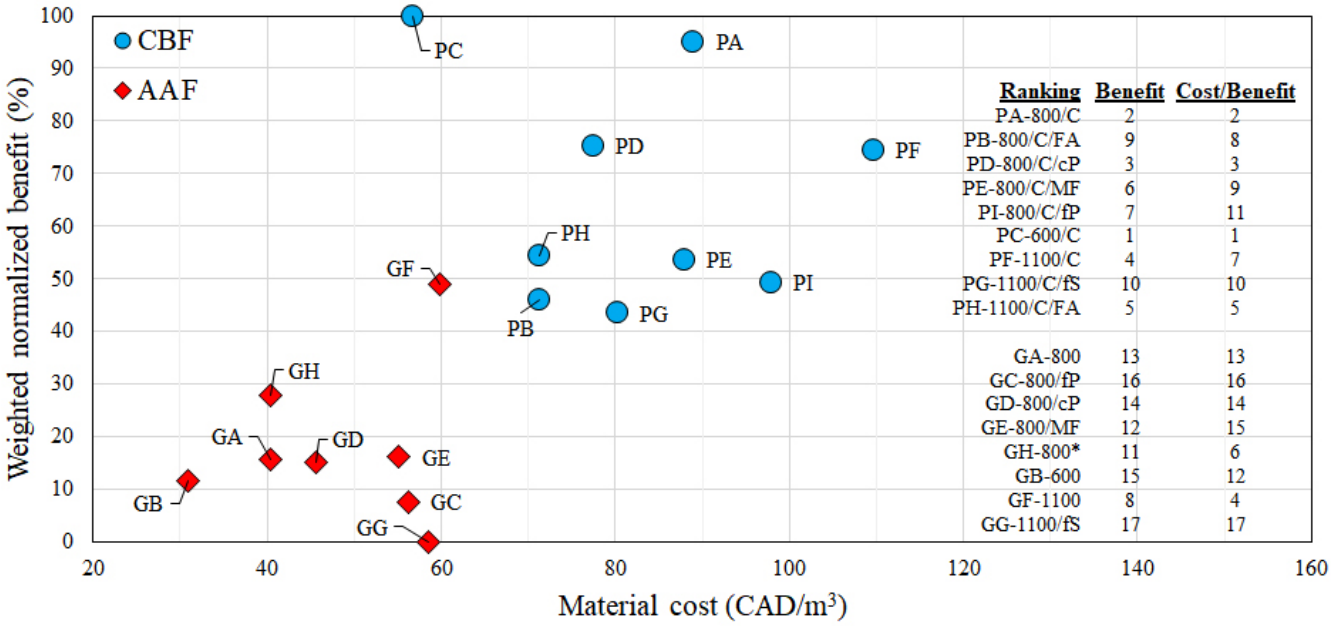

Fig. 6.7. Cost versus benefit of cement-and alkali-activated-based foams. Rankings of different mixtures based on their benefit and cost per benefit are also included in the bottom right corner of the figure.

PC which reduces the material cost by 45% but delivers 86% less benefit. While PC, GH, and GB are the "Pareto-frontiers", which means that no other mixture composition can dominate them, GG and PF seem to be the least favorable alternatives. GG delivers the minimum benefit while costing an average material cost and PF provides an average benefit with the maximum material cost.

6.5 Concluding remarks

This study was undertaken to investigate the freeze-thaw durability of cement- and alkali-activated-based foams for narrow-trench backfilling. The mixtures were cast to achieve a density between $600 - 1100\, kg/m^3$ and were examined for mass loss, compressive strength, modulus of elasticity and the Poisson's ratio at 30 cycle steps over 150 cycles of freezing and thawing. The mixtures designed in this study were ranked per their benefit-cost ratio, based on their durability factor. The results show that the low-density CBF, PC, delivers the highest benefit against its material cost that was an average. Based on the findings, the following specific conclusions may be drawn:

- Cement-based foams withstood 150 cycles of conditioning with little or no visible damage. On the other hand, the only AAF that holds its integrity during the 150 freeze and thaw cycles was the high-density mixture, GF.

- The properties of conditioned specimens were compared to those of the reference, unconditioned ones, at the age of 28 and 90 days. The results revealed that the average durability of CBFs reduces with an increase in the density. Accordingly, the durability factor, DF_{90d}^{150c} of the ultra-low-density mix PC is 11% more than for the low-density mix PA and 76% higher than for the high-density mix PF. On the other hand, the low early strength of low-density AAFs, GA and GB resulted in a progressive deterioration.

- Introducing aggregate to the foams reduced the durability when compared to the plain foams in each density group. Further, coarse perlite resulted in higher DF than fine perlite

in both cement- and alkali-activated-based foams. The higher percentage of natural sand in mixtures PG and GG reduced the 28 days compressive strength and subsequently, reduced the durability of these mixes considerably when compared to the plain foams, PF and GF.

- Although the DF_{90d}^{150c} of GE is marginally higher than GA, fibrous mixtures displayed lower durability than the plain foams in the same density group. The durability factor in mixtures incorporating FA was lower than that in the plain foams within the same density group. Additionally, curing the AAF at elevated temperature, as in mixture GH, improved the durability over the mixture GA, which was cured at room temperature.

Chapter 7

Performance Evaluation of Reinstatement Materials Inside the Narrow-Trench

This chapter aims to evaluate the performance of controlled low strength materials for narrow-trench reinstatement under the simulated traffic load and subjected to different environmental conditions. In order to fulfill this purpose, firstly, laboratory sized physical models of MT were fabricated and tested under hamburg wheel tracking device underwater and after freeze-thaw cycles. secondly, a 3D FE model was created and the effect of different traffic loading, pavement designs, temperature, trench dimensions, and reinstatement method on the stress state in the trench was investigated. Lastly, the failure potential of the reinstatement materials was evaluated by the Mohr-Coulomb failure criterion and comparing the materials' stress-to-strength ratio. This chapter concluded that double-backfilling the trench with CMA and plain grout results in higher stability in the reinstated area than the trench with CMA and sand or single

backfilling with macadam. However, the results of the numerical model revealed that the tensile failure at the bottom of the CMA layer is a concern. Moreover, debonding of the cement- or alkali-activated-based foam and AC is anticipated when backfilling the trench with CLSM.

7.1 Introduction

Cutting the pavement to install the new utility lines, like power or telecommunication cables, is a frequent activity in modern cities. However, in urban areas, the traditional open-cut method becomes time-consuming, uneconomical and disruptive to the local traffic and businesses. In contrast, narrow-trenching (NT) is known as a time- and cost-effective and environmentally friendly alternative to the traditional methods [11]. Micro-trenching (MT) is a variation of NT in urban areas wherein the cut is as narrow as 25 to 40 mm wide. The depth of the trench is usually governed by many factors including the size of the conduit, type of the pavement, frost depth and etc. Micro-trenches are normally up to 250 mm deep which makes them shallower than NT [8, 9]. MT is found to be up to 75% cheaper and 50% faster than open-cut method [11, 51]. Despite these many benefits of NT over other installation methods of infrastructures, municipalities are reluctant to accept the risks of the NT method, including the potential pavement damage. On the other hand, the shallow depth of the trench also concerns the utility owners about the stability of the installed cables and conduits.

The factors affecting the performance of the narrow-trench and its response to the traffic

or environmental loads have not been investigated. These factors include the trench dimension (width and depth), backfilling method and materials, location of the trench in the road, loading or environmental condition, pavement design of the road and etc. Due to this lack of knowledge, the current practices of narrow-trenching involve selecting the trench dimension and reinstatement materials mainly based on the availability of the equipment and materials instead of engineering the narrow-trench for the desired performance [1, 18]. Therefore, many distress was observed in the reinstated trench in different MT pilot projects in Alberta, Canada after a few months. These distress include raveling, de-bonding, settlement, damage to the asphalt pavement, and cables movement inside the trench [1, 18, 19].

In order to investigate the performance of the reinstatement materials in the narrow-trench as well as understanding their response to the traffic load, physical and numerical models of the narrow-trench were simulated and studied in this chapter. For this purpose, first, laboratory size models of the narrow-trench are manufactured and tested under a Hamburg Wheel Tracking Device (HWTD) in different environmental conditions. In order to better understand the stress distribution inside the reinstated trench and investigate the effect of different trench designs in the stress states of the trench, numerical models of the trench were developed and analyzed in the second part of this chapter.

7.2 Physical models

In order to compare the performance of the common narrow-trench backfilling methods, laboratory-scale micro-trench samples were prepared using different backfilling materials and were loaded using a wheel tracker after conditioning.

7.2.1 Specimen preparation

In order to prepare the test specimens, small physical models of the trench with dimensions of 400 $\times$ 300 $\times$ 120 mm were fabricated and tested under Hamburg Wheel Tracking Device (HWTD). The first 80 mm out of the total 120 mm height of the slab molds was filed with regular base material compacted in optimum moisture content using a laboratory roller compactor machine (Figure 7.1a). The same roller compactor was used to compact hot-mix-asphalt (HMA) layer to the thickness of 40 mm. The mix design of the HMA is presented in Table 4.6. HMA slabs were left for at least 24 hours to cool down to the room temperature and then each slab was cut into two 300 $\times$ 187.5 mm smaller slabs. A thin layer of tack coat was then applied on top of the compacted soil as shown in Figure 7.1b. Afterward, the cut HMA slabs were placed on top of the tack-coat covered soil in a way to form a 25 mm trench at the middle length of the slab as illustrated in Figure 7.1c. In the next steps, the soil was hand-dug to form an 80 mm deep trench (Figure 7.1d). Then a conduit (outer diameter of 20 mm) was laid at the bottom of the trench and secured in place by metallic clips (Figure 7.1e). The reinstatement process started by partially filling the trench up to the asphalt layer using sand or regular/foamed cement grout

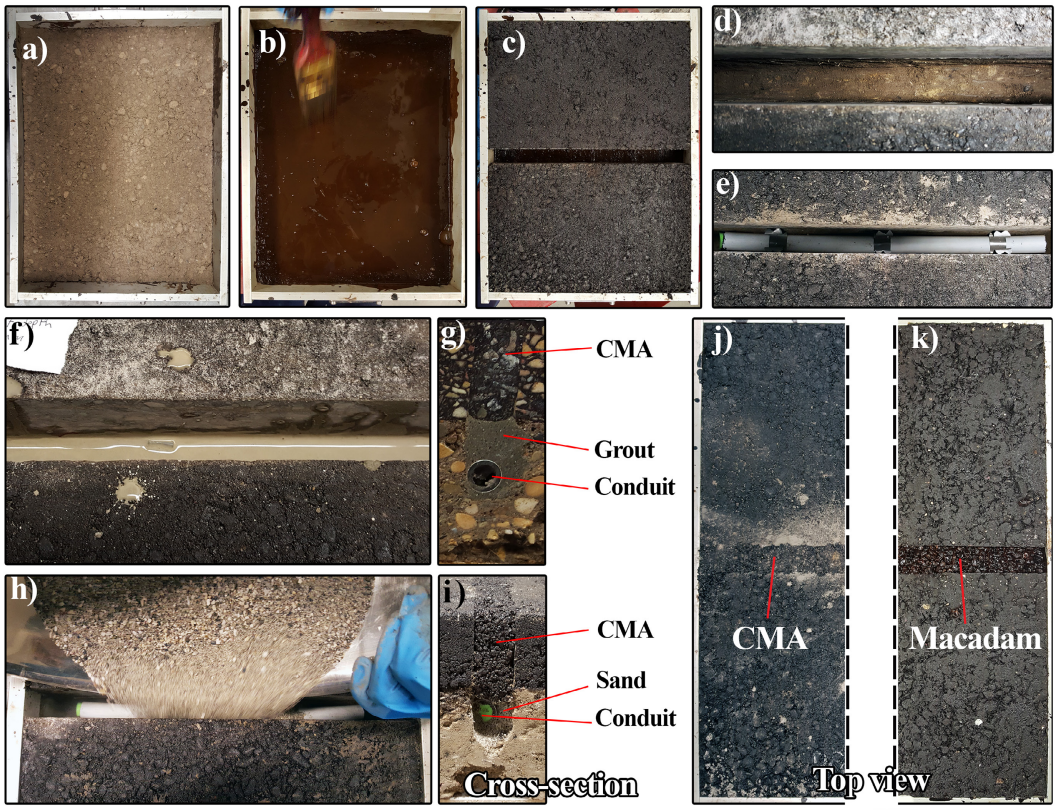

Fig. 7.1. Preparation of narrow-trench physical models.

(Figure 7.1f and h). The gradation of the sand is shown in Figure 4.2. The plain Portland cement grout had a water content of 25% which resulted in setting time of 45 min at room temperature and 28-days compressive strength of 30 MPa. The foamed-grout also had the same composition and properties as mixture PA-800/C in Chapter 4. The narrow trenches were then leveled to the top by compacting CMA-1 (introduced in Chapter 3). The final reinstated trench is shown in Figure 7.1g, i, and j.

7.2.2 Testing procedure

The performance of the trench backfilling was evaluated by measuring the rut depth at the center of the trench in the HWT test as explained in section 3.2.4. Except for one reference slab without a trench, which was tested dry without conditioning, all other tests were done in a wet condition. For this purpose, the HWT device was filled with 25 $\pm$ 1 $^{\circ}C$ water. The slabs were then placed into the device and soaked for 12 hours. Afterward, the test was started on the submerged sample and stopped after 20,000 of wheel track passes or when the rut depth reached the maximum of 12 mm (Figure 7.2a).

In order to condition the narrow-trench slabs for FT test, they were first submerged under the 25 $\pm$ 1 $^{\circ}C$ water bath, for 48 hours (Figure 7.2a) in the first cycle of freezing and thawing and 12 hours in the next cycles. Immediately after, they were put in a freezer set at -20 $\pm$ 3 $^{\circ}C$ for 24 hours (Figure 7.2b) followed by thawing at room temperature for another 24 hours. After that, the wheel tracking test was performed on the thawed samples (Figure 7.2c).

7.2.3 Results and discussion

The result of the HWT test on the physical models of narrow-trenches is presented in Figure 7.3. A rut depth of 3.1 and 5.16 mm was observed after 20,000 passes in reference slabs without trenches tested in dry and wet condition. The higher rut depth in the wet test is mainly due to the consolidation of the base soil layer. Backfilling the trench with plain cement grout and CMA on top resulted in 5.79 mm rut depth which shows a 12% increase compared to the reference slab

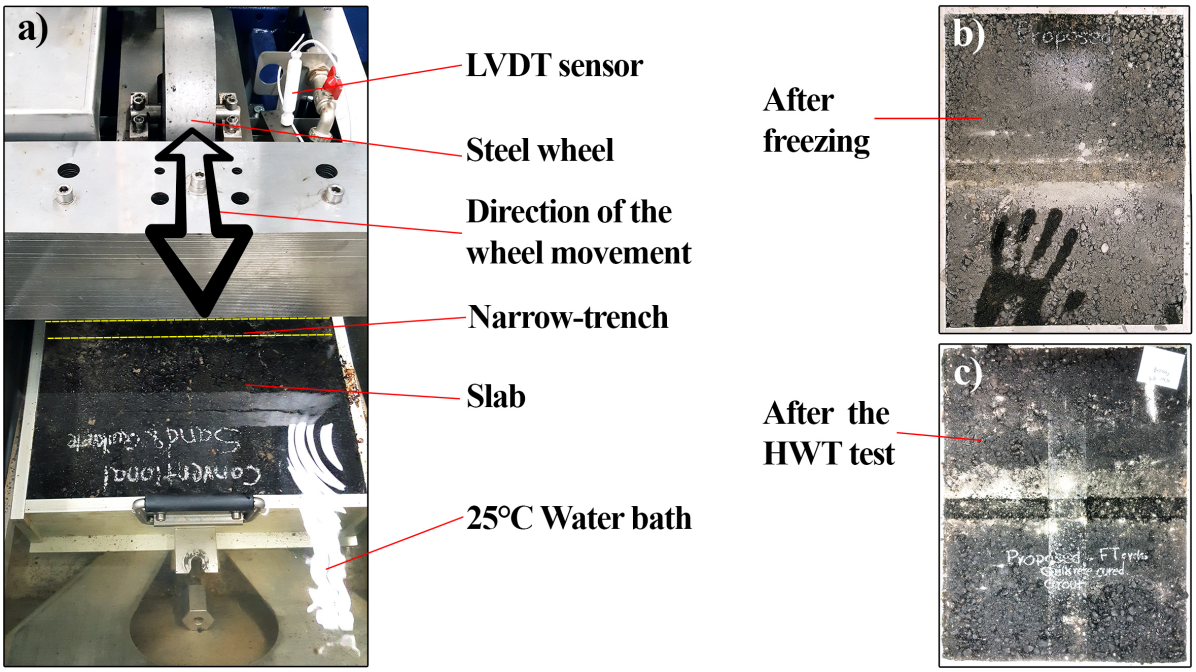

Fig. 7.2. HWT test on a physical model of narrow-trench.

without a trench. the rut depth curve of the trench reinstated with CBF and CMA follows the curve of the plain cement grout and CMA closely. So that even after 20,000 passes, the resultant rut depth was 5.98 mm, which is only 3% higher than that for plain cement grout and CMA. This confirms the applicability of CBF for replacing plain cement grout in double-backfilling of narrow-trenches. The trench with sand in the base layer and CMA on top followed the curve of the trench with plain cement grout closely up to 10,000 passes. However, the presence of water accelerated the consolidation and escape of sand particles from the trench after that point which resulted in a rut depth of 7.14 mm which is 38% higher than the reference slab without a trench. The steep rutting curve of this trench after 18,000 passes also suggests the progressive deterioration of this method of composite backfilling and confirms the observations of a real-life reinstatement with this method [1, 18]. Lastly, The single backfilling of the trench with

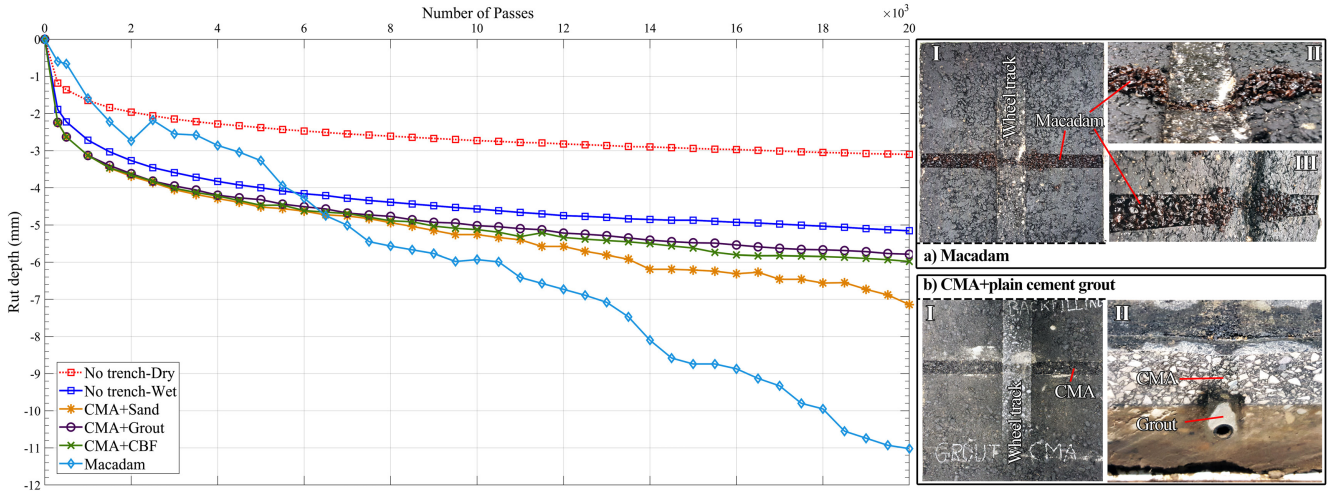

Fig. 7.3. Rut depth at the center of narrow-trench versus the number of wheel passes. The test result on the trench filled with macadam is shown in (a). (b) illustrates the HWT test result on the trench backfilled with plain cement grout and CMA.

macadam resulted in a rut depth of 11 mm at the end of the test which shows a 113% increase when compared to the rut depth of reference slab. As illustrated in Figure 7.3a, the wheel load pushed the aggregates out of the trench. In a real-life condition, the moving traffic over the trench can remove these loose aggregates from the trench and cause a progressive degradation of the reinstatement.

The performance of double-backfilling of narrow-trench with cement grout or sand at the base layer and CMA on top was also investigated by HWT test on FT conditioned samples and the results are illustrated in Figure 7.4. The test started by exposing the slabs to one cycle of freezing and thawing according to section 7.2.2 and measuring the rut depth at the center of the narrow-trench after 20,000 passes. Rut depth in the trench backfilled with plain cement grout and CMA was measured as 5.43 mm. Therefore, the effect of one FT conditioning on the rut depth of reinstated trench compared to the non-conditioned slab is negligible. Nevertheless,

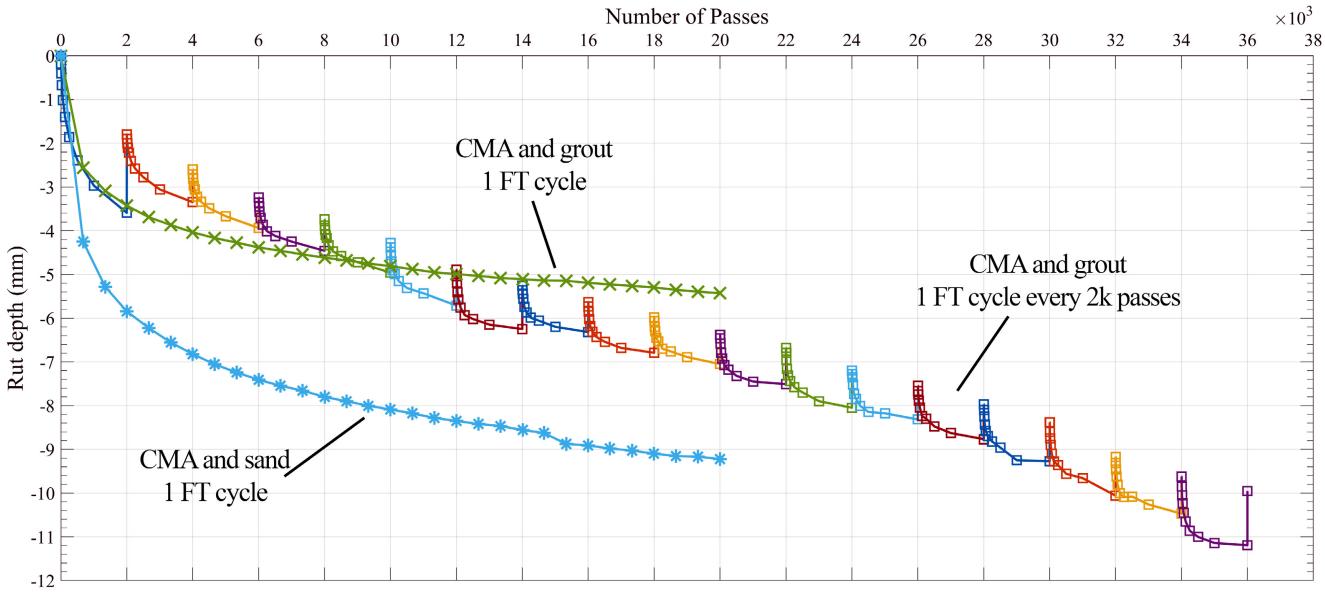

Fig. 7.4. Rut depth at the center of FT conditioned narrow-trench versus the number of wheel passes.

longitudinal micro-cracks alongside the trench was observed as depicted in Figure 7.5. Moreover, because of the pressure of the wheel as well as the frost heave in the base layer, CMA was pushed out of the trench. Rut depth after one cycle of freezing and thawing and after 20,000 passes in the trench backfilled with sand and CMA was 9.22 mm, which is 30% higher than the result of the non-conditioned trench. This proves the high FT susceptibility of backfilling with sand.

To further investigate the effect of FT cycles on the narrow-trench, a physical model of the trench filled with plain cement grout and CMA was subjected to one cycle of freezing and thawing at every 2,000 passes in HWT test and tested for a total number of 36,000 passes. As illustrated in Figure 7.4 the permanent deformation at the center of the trench after the 18th cycle of freezing, thawing, and HWT testing was 9.95 mm. The test stopped at the 19th cycle

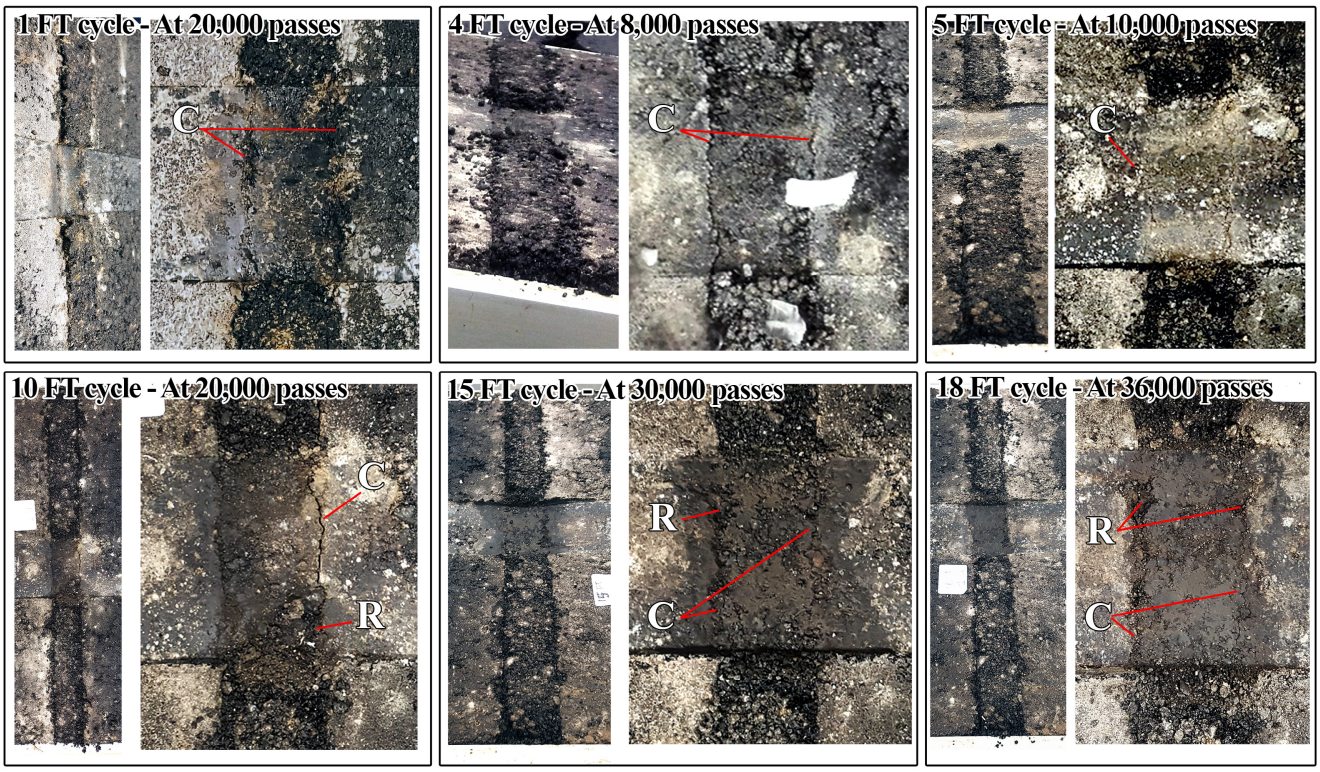

Fig. 7.5. Effect of freeze-thaw (FT) cycles on the reinstated narrow-trenches with plain cement grout and CMA.

since the rut depth reached the stop limit of 12 mm. As it can be seen in Figure 7.5, microcracks emerged alongside the trench only after 4 FT cycles and 8,000 passes. Raveling of the CMA was also observed at the 10the FT cycle, which accelerated after the 15th cycle.

Therefore, it can be concluded that using a regular or foamed cement grout could enhance the trench stability and prevent conduit movement inside the trench.

7.3 Numerical simulation

7.3.1 Model development

The commercial finite element (FE) software ABAQUS version 2018 was employed for modeling the narrow trench. Three-dimensional (3D) FE models were developed to better simulate the loading patterns of single and dual tire configurations on the narrow trench. 3D analysis of pavement systems also better reflects the complex behavior of the composite pavement system under different loading configurations [444, 445]. In order to reduce the boundary effect on the calculation, the dimensions of the FE model were selected as 1000 $\times$ 1000 $\times$ 995 mm for the single tire and 1000 $\times$ 1500 $\times$ 995 mm for dual-tire assembly as depicted in Figure 7.6.

An eight-node, linear brick element type has been successfully utilized before for analyzing the pavement response [446, 447]. To improve the rate of convergence, the eight-node linear brick reduced integration elements (C3D8R) with variable thicknesses, depending on the pavement layers, were used in this study. The generated 3D mesh was selected by trial-and-error to deliver optimal accuracy. The mesh was designed fine around the loading area and inside the narrow-trench but relatively coarse far from that, as shown in Figure 7.6.

In order to set the boundary conditions, the recommendation of Blanco et al. [38] was followed. Accordingly, the fixed boundary condition was set along the z-axis while elastic support, with the spring constant (k) of 10^9 was considered along the x- and y-axis.

At this stage of the research, it is assumed that the interfacial bond between layers never fails. Therefore, the interfaces of layers are tied together which enforces displacement and

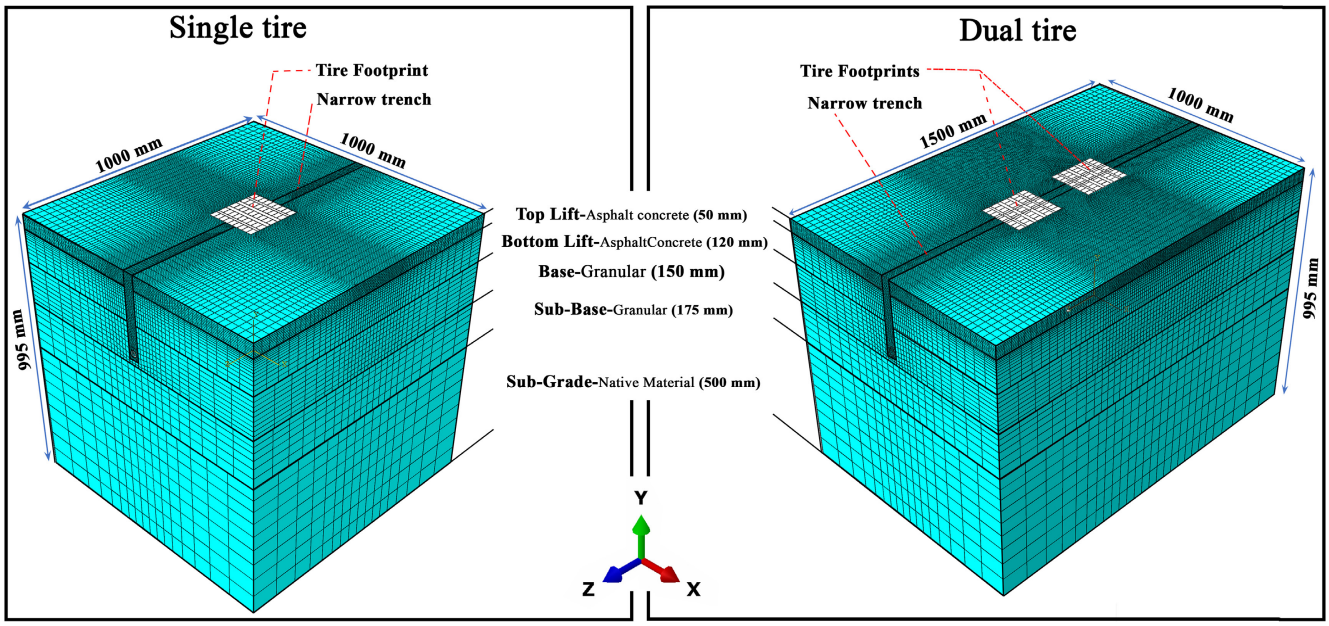

Fig. 7.6. Layout of the 3D multilayered FE models.

strain continuity at the interface. The bonding of the backfilling material to the asphalt concrete (AC) surface was later checked by comparing the interfacial shear stress to the materials' bond strength.

7.3.2 Variables considered

In order to fully investigate the stress distribution in a narrow-trench under different conditions, various variables were considered in this study as summarized in Table 7.1.

Traffic load

Blanco et al. [38] used a uniform pressure in their model to simulate the traffic load on a 150 mm wide and 700 mm deep trench. However, the pavement responses to the uniform and

Table 7.1. The variables considered in 3D modeling of the nattow-trench.

Variable	Tire assembly	Tire Location[1]	Pavement design	Temperature	Trench dimension[2]	Reinstatement design	Code
Default	Single	CT	Main road	25°C	40 × 300	Single-PA‡	DEF-TS-C
Traffic load	Single	L1T	Main road	25°C	40 × 300	Single-PA	TL-TS-L1
		L2T					TL-TS-L2
		L3T					TL-TS-L3
		CL					TL-LS-C
	Dual	CT					TL-TD-C
		CL					TL-LD-C
		L1L					TL-LD-L1
Pavement design	Single	CT	Private road	25°C	40 × 300	Single-PA	PD-TS-PR
Temperature	Single	CT	Main road	5°C	40 ×300	Single-PA	TE-TS-5
				40°C			TE-TS-40
Trench dimension	Single	CT	Main road	25°C	25 × 300	Single-PA	TD-TS-N
					55 × 300		TD-TS-W
					40 × 200		TD-TS-S
					40 × 400		TD-TS-D
Reinstatement design	Single	CT	Main road	25°C	40 × 300	Double-CMA	RD-TS-CM
						Double-HMA	RD-TS-HM

[1]Refer to Figure 7.8; [2]Cross-section dimension of the trench (mm).
‡See chapter 4 and 5 for the design and properties of the CLSM mixtures.

non-uniform contact stress distribution are known to be significantly different, especially at the layers' interface [448]. Previous works have studied the interaction of tire and flexible pavement [393, 446, 447, 449, 450]. Wang et al. [393, 449] predicted the contact stress distribution of a tire with a various wheel load of 17.8-40.2 kN and rolling condition. They concluded that the contact stress at the tire-pavement footprint are non-uniform. Moreover, while the vertical contact stress in the static condition is slightly higher than braking or free-rolling conditions, the longitudinal stress during the braking is considerably higher than others. References [446] and [447] measured the contact pressure of the wide-base and dial tire assembly for tire pressure of 720 kPa and wheel load of 38 kN. The maximum pressure was reported as 988 kPa for Dual and 956 kPa for wide-base tire measured under the center tire rib. Based on their measurement, they used a simulated tire contact area in their FE model instead of modeling the real tire-pavement interaction. Recently, Dong and Ma [450] utilized the same simplified tire contact area based on the predicted contact stresses introduced by Wang et al. [449].

In order to simplify the model, the simulated tire contact area used by references [446, 447, 450] was employed in this work. According to the study of Wang et al. [449], the stress distribution of the tire in braking condition was selected since it contributes to an assessment of the model in a more critical situation. However, due to the relatively small lateral stress, only the vertical and longitudinal stress were considered in the model. These simulated, non-uniform contact pressures are presented in Figure 7.7.

Rolling of the wheel was also simulated by considering different locations for the tire footprint at the center and around the narrow-trench as depicted in Figure 7.8.

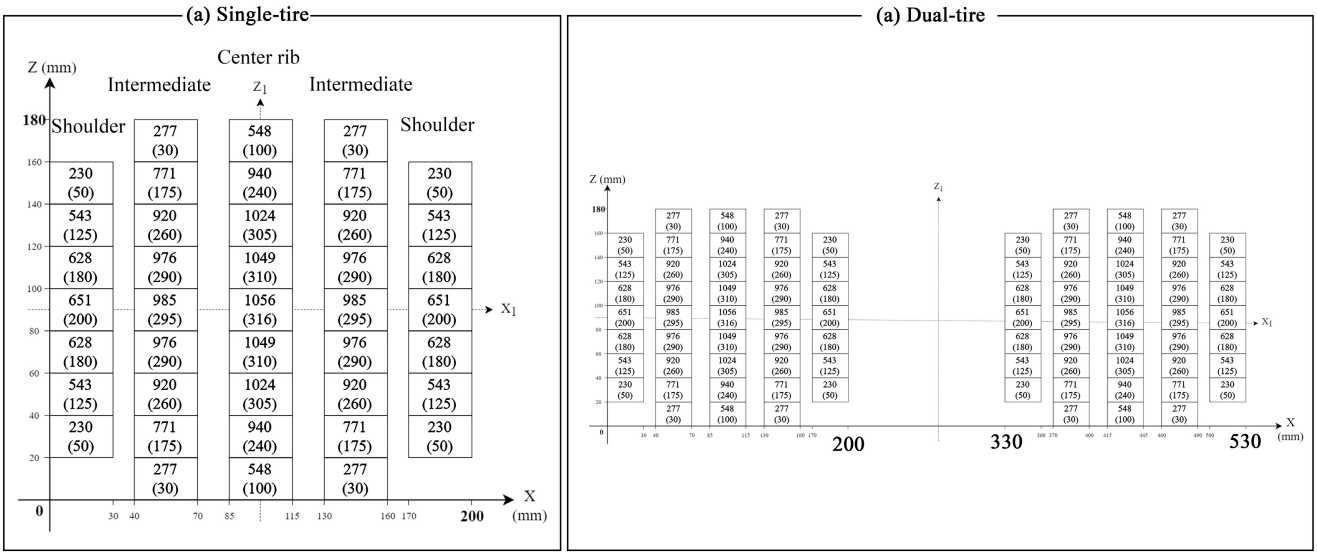

Fig. 7.7. Tire footprint dimension and non-uniform vertical and longitudinal (in parenthesis) contact pressure (kPa) for (a) single- and (b) Dual-tire assembly.

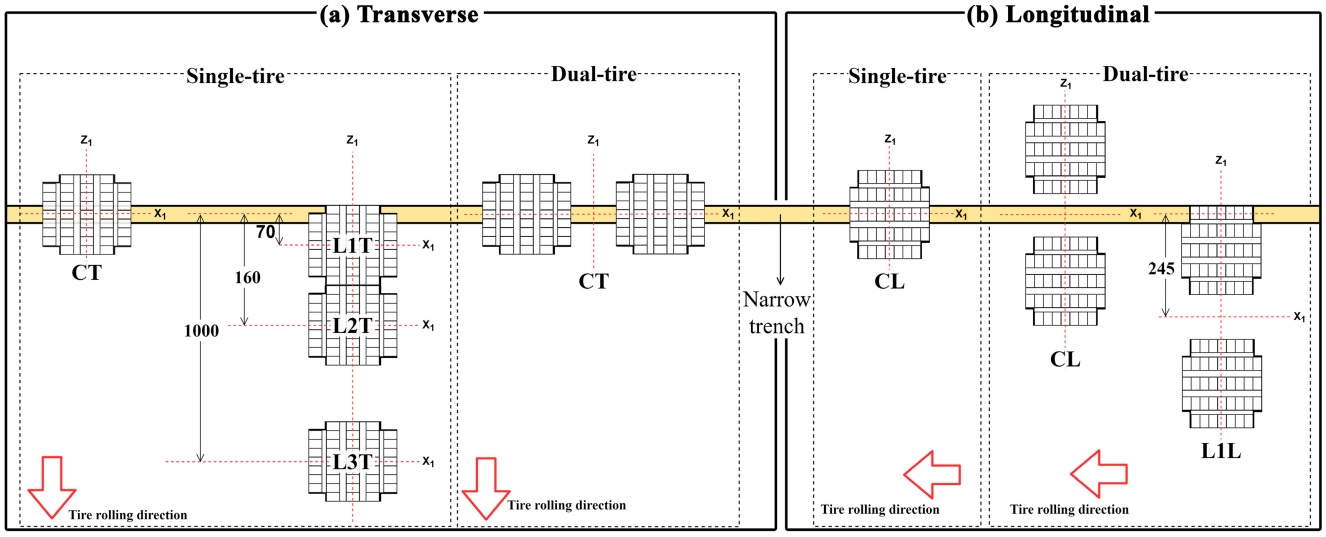

Fig. 7.8. Tire locations.

Pavement design and material properties

The pavement designs and dimensions of layers are defined based on the observations during narrow-trenching projects [19] which comply with the typical paved road construction in Alberta, Canada [451]. The default design was observed in main roads and consists of two layers of asphalt concrete on top of the granular base layer. However, coring in smaller streets or private roads revealed a single layer of asphalt concrete with an average thickness of 50 mm on top of the base layer. The layers thickness of the two aforementioned pavement designs is tabulated in Table 7.2.

Since narrow-trenches are generally excavated in older pavements with an age of several months to years, the soil can be considered as consolidated. Therefore, the soil layers are not expected to experience high-stress levels. As a result, linear-elastic behavior of the materials (defined by the modulus of elasticity and the Poisson's ratio) is considered in this work. Table 7.2 shows the properties of different pavement layers based on the works of [446, 447].

Reinstatement materials and design

According to the common practice of narrow-trenching observed in the field [19], the default trench width, and depth were selected as 40 and 300 mm, respectively. In order to further investigate the effect of trench dimension in performance of narrow-trench under the traffic load, different combinations of depth and width (from shallow to deep and narrow to wide) were considered in this study as tabulated in Table 7.1.

Table 7.2. Pavement design and material properties.

Layer	Main road	Private road	5°C		25°C		40°C	
	Depth[1]	Depth	RM[2]	PR[3]	RM	PR	RM	PR
Pavement materials								
Top lift-asphalt concrete	50	50	9155	0.22	4230	0.33	1905	0.36
Bottom lift-asphalt concrete	120	–	8930	0.23	4750	0.3	1790	0.35
Base-Granular	150	150	310	0.35	310	0.35	310	0.35
Sub-base-Granular	175	175	262	0.35	262	0.35	262	0.35
Sub-grade-Native material	500	620	200	0.3	200	0.3	200	0.3
Narrow-trench materials								
Cold-mix-asphalt	50	–	11189	0.31	2988	0.35	–	–
HDPE conduit	Figure 7.9	–	–	–	900	0.38	–	–

[1]Layer depth (mm); [2]Resilient modulus (MPa); [3]Poisson's ratio

As explained in the chapter 2, Section 2.2, single or double backfilling methods can be used for narrow-trench reinstatement. In the single backfilling method, three CBFs, namely PA, PC and PF, and three AAFs, i.e. GA, GB, and GF were considered in the model (Figure 7.9a). The elastic properties of CBFs and AAFs can be found in Figure 4.8 and 5.3, respectively.

To further investigate the effect of reinstatement method in NT performance, double backfilling of the trench with CMA or HMA was also considered. According to the discussions of Chapter 2, compaction of HMA inside the narrow trench is not practical. In practice, a small ditch of minimum 400 mm width is milled out on top of the trench and then backfilled with HMA [28]. In this research, it is assumed that the same HMA as the top lift asphalt concrete layer is used to reinstate the milled area. CMA-1, as introduced in Chapter 3 and has been successfully used in two field installations [19], was also used in the model. The elastic properties

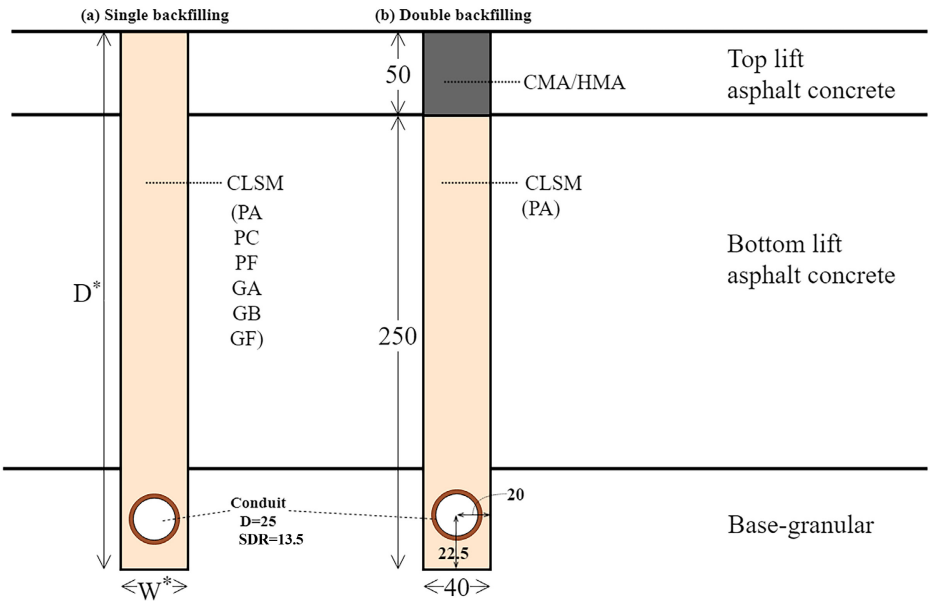

*refer to Table 7.1 for the trench dimensions.
Note: all dimensions are in mm.

Fig. 7.9. Trench design in (a) single backfilling and (b) double backfilling.

of the CMA are included in Table 7.2 according to the references [452, 453]. The cross-section of the narrow trench in the double-backfilling method is shown in 7.9b.

One of the popular methods of optical fibre installation is cable blowing through an embedded conduit inside the trench [1]. In accordance with the observations of real-life micro-trenching projects [19], an HDPE conduit with an outer diameter (OD) of 25 mm, SDR of 13.5, and elastic properties as Table 7.2 was considered at the bottom of the narrow-trench (See Figure 7.9 for illustration).

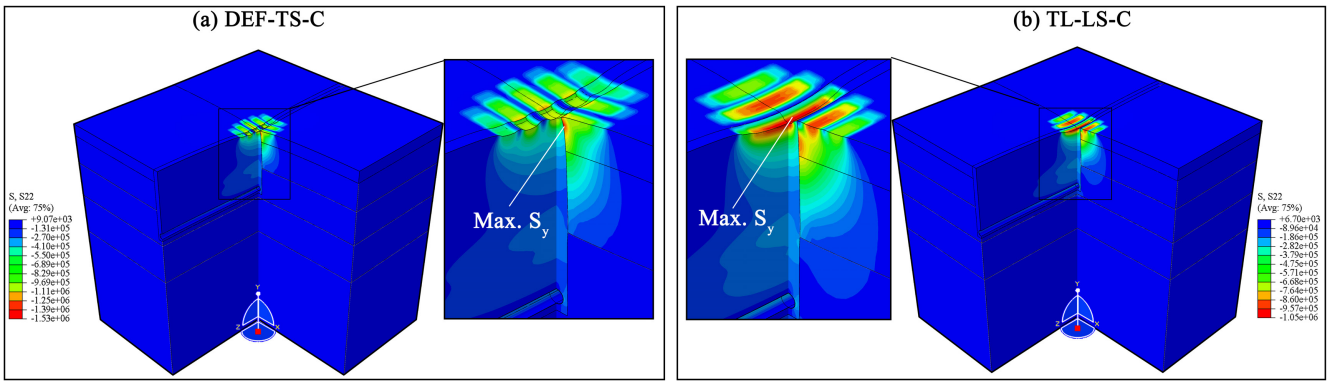

Note: The 3D model is cut along the x and z plane for better illustration of stress distribution; deformations are exaggerated 500 times to be visible in the figure.

Fig. 7.10. Normal stress (σ_y) distribution for (a) DEF-TS-C and (b) TL-LS-C.

7.3.3 Results and discussion

Tire assembly, location, and orientation

The compressive strength (σ_y) distribution in pavement layers and narrow-trench for the DEF-TS-C and TL-LS-C is shown in Figure 7.10. When the wheel is moving in the x-direction (transverse to the trench) the maximum value of σ_y and the minimum principal stress (σ_3) was recorded as -1.53 and -1.68 MPa, respectively. They both observed in the top lift asphalt layer at its interface with the trench and at the depth of 10 mm (Figure 7.10a). This is in accordance with the findings of Thom [454] where in the maximum principal stress occurs at 10 mm below the pavement surface. However, when the wheel is moving in the z-direction (longitudinal to the trench), the maximum σ_y was equal to -1.05 MPa at the surface of the narrow-trench under the central tire rib (Figure 7.10b). The σ_3, on the other hand, reached its highest compressive value of -1.24 MPa at the surface of top lift asphalt under the intermediate tire rib. Therefore, passing the trench in the transverse direction resulted in higher compressive stress in the system.

Figure 7.11 presents the effect of different tire locations and orientations (as introduced in Table 7.1) on the stress distribution in the trench. As illustrated in Fig 7.11a, σ_3, σ_y and the shear stress (τ_{xy}) increase as the tire move toward the trench and reach their maximum when the centerline of the tire is located at the center of the trench. The highest compressive principal stress was recorded as -1.38 MPa in TL-TD-C with dual-tire assembly, which is 3% higher than that of DEF-TS-C with a single tire. The maximum τ_{xy} was also equal to 0.48 MPa at the side of the trench in TL-TD-C model. During the transverse movement of the wheel over the trench, the principal tensile stress reaches its maximum value when the tire is located at L1T (Figure 7.8a). The highest principal tensile stress when the centerline of the tire is located at the center of the trench is equal to 0.25 MPa in TL-TD-C.

According to Figure 7.11I-IV, the maximum compressive principal and the maximum normal compressive stress occur at the footprint of the tire over the trench while the maximum tensile principal stress happens at the side of the trench at its mid-height (Figure 7.11I). The maximum τ_{xy} was also observed at the side of the trench and under the tire center rib at the depth of 5 mm.

Table 7.3 presents the maximum stress values in the conduit. The σ_3 and σ_y increases as the wheel moves toward the trench and reach their maximum value at the center of the narrow-trench. According to Table 7.3 dual-tire assembly causes higher stress in the conduit. Figure 7.12 illustrates the stress distribution in the conduit.

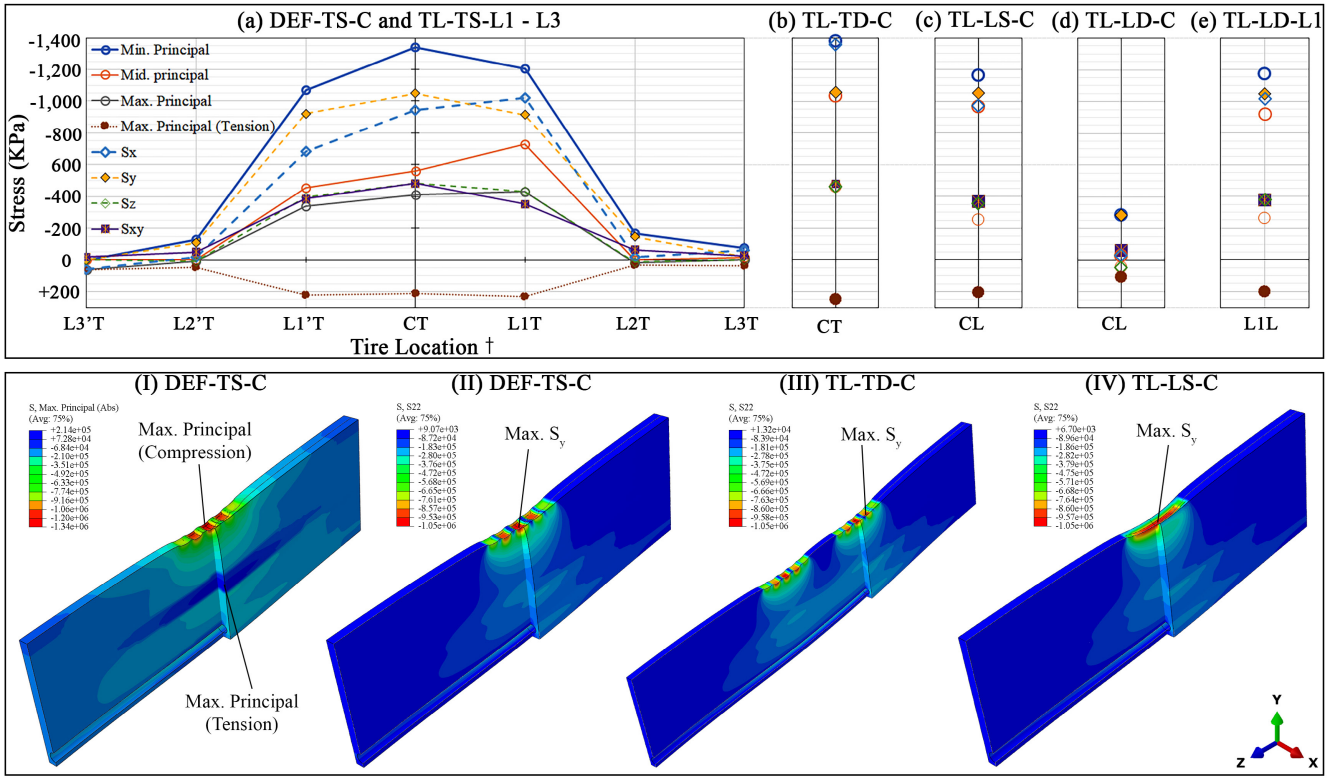

†Refer to Figure 7.8 for tire locations. L1′T,L2′T, and L3′T are respectively a reflection of L1T, L2T, and L3T over the trench centerline.

Note: The trench view is cut along the x and z plane for better illustration of stress distribution; deformations are exaggerated 500 times to be visible in the figure.

Fig. 7.11. (a)-(e) show the effect of the tire location and moving direction on the principal and direct stresses in the narrow-trench. (I)-(IV) illustrate the corresponding stress distributions.

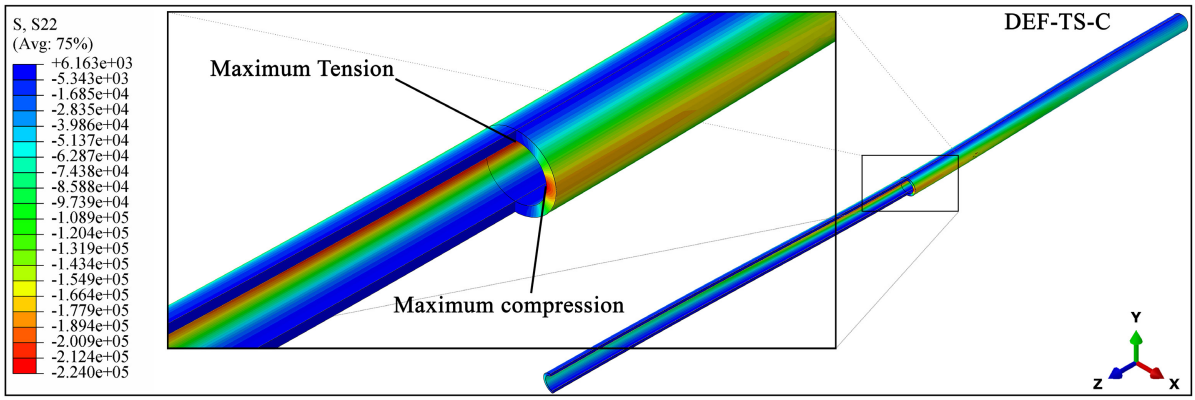

Fig. 7.12. Stress (σ_y) distribution in the conduit for DEF-TS-C.

Table 7.3. Maximum stress in the conduit due to the different tire locations and orientations.

Code[1]	Principal (σ_1:σ_2:σ_3)	Tensile principal	Normal (σ_x:σ_y:σ_z)	Shear (τ_{xy})
TL-TS-L3	-1.0 : -12.4 : -46.8	16.7	-6.1 : -31.5 : -8.3	21.3
TL-TS-L2	-2.8 : -27.4 : -122.9	39.4	-16.4 : -109.3 : -27.4	46.7
TL-TS-L1	-4.6 : -42.5 : -209.5	84.2	-9.0 : -202.5 : -43.1	57.0
DEF-TS-C	-5.2 : -50.4 : -228.7	97.3	-10.0 : -224.0 : -50.4	46.2
TL-LS-C	-4.7 : -38.9 : -201.4	79.1	-9.0 : -197.0 : -38.8	43.7
TL-TD-C	-5.8 : -62.3 : -278.2	108.9	-11.4 : -271.9 : -63.5	63.7
TL-LD-C	-5.7 : -45.1 : -251.5	94.0	-11.2 : -246.0 : -45.2	60.6
TL-LD-L1	-5.8 : -48.4 : -261.8	97.6	-10.8 : -246.3 : -46.4	85.7

[1]Refer to Table 7.1.

Pavement and trench design

The maximum stress in the narrow-trench backfill and conduit caused by the different scenarios of Table 7.1 are compared in Table 7.4 and 7.5, respectively. Among the two different pavement designs considered, the private road results in higher principal and normal stress in the trench. The trench in private road design is also experiencing 86% higher maximum tensile principal stress than the one in the main road (DEF-TS-C). Moreover, this tensile stress occurs at a shallower depth (at the bottom of the top lift AC) when compared to the DEF-TS-C model. It is worth mentioning that the lack of bottom lift asphalt in PD-TS-PR, increased the lateral stress (σ_x and σ_z) considerably. According to the data of Table 7.5, lack of bottom lift asphalt layer in PD-TS-PR resulted in a significantly higher stress transformation to the bottom of the trench and therefore, to the conduit (e.g. maximum σ_3 in PD-TS-PR is 102 % higher than that in DEF-TS-C). This can also be visually observed when comparing the distribution of the σ_y in

PD-TS-PR (illustrated in Figure 7.13) to DEF-TS-C (in Figure 7.10a and 7.11II).

Different asphalt stiffness, due to the different temperature did not influence the σ_3 or σ_y appreciably since their maximum occurs at the top of the trench. However, the absolute value of σ_1 in the trench and at 5 $^{\circ}C$ is smaller than 40 $^{\circ}C$, which results in smaller confinement pressure. At 5 $^{\circ}C$, the values of maximum tensile principal and shear stress are also higher than those measured at 25 or 40 $^{\circ}C$. However and according to Table 7.5, the transferred stress to the conduit increase with temperature.

Among the different trench widths simulated here, TD-TS-N model resulted in a slightly higher σ_3, tensile and shear stress than the normal or wide trenches. The lower values of σ_1 and σ_2 also provides smaller confinement pressure at the location of maximum stress. Besides, the stress in the conduit decrease as the width of the trench increases. In the shallow trench, principal and normal stress are slightly higher than the normal or deep trench. The tensile stress on the other hand is considerably higher (69%) in the shallower trench. The maximum shear stress in the trench also does not appreciably change with the trench depth. As expected, the stress in the conduit increase as the trench depth decrease.

Double backfilling of the narrow-trench with CLSM and CMA on top considerably reduced the maximum compressive and shear stress in the CLSM (about 70%). However, the maximum tensile stress in the CLSM and the stress state in the conduit (Table 7.5) reduced only marginally. This indicates that the stress transfer along the trench depth is not highly affected by the CMA or HMA layer. The Maximum principal stress in CMA layer is 1,413.9 kPa, which is slightly (6%) higher than that of single backfilling in DEF-TS-C model. Nevertheless, the maximum

Table 7.4. Comparison of the CLSM backfill responses due to different model variables.

Code†	Principal (σ_1:σ_2:σ_3)	Tensile principal	Normal (σ_x:σ_y:σ_z)	Shear (τ_{xy})
DEF-TS-C (kPa)	**-410.1** : **-560.6** : **-1,338.9**	**214.0**	**-944.4** : **-1,049.5** : **-481.2**	**483.0**
PD-TS-PR (%‡)	25.3 : 5.4 : 8.0	86.3	23.8 : 0.1 : 38.4	-8.7
TE-TS-5 (%)	-28.5 : -9.7 : -1.0	1.9	-5.4 : 0.3 : -6.9	21.4
TE-TS-40 (%)	34.1 : 16.2 : -2.4	-14.4	-5.3 : 0.7 : 24.4	-23.0
TD-TS-N (%)	-12.1 : -8.7 : 2.7	8.5	11.1 : -3.1 : -12.3	8.8
TD-TS-W (%)	-1.6 : -2.4 : -0.7	6.2	-6.5 : 0.4 : 8.9	5.5
TD-TS-S (%)	7.4 : 7.9 : 2.1	69.3	12.5 : 0.6 : 1.6	1.8
TD-TS-D (%)	5.5 : 5.7 : 1.2	1.2	2.3 : 0.6 : 5.3	1.8
RD-TS-CM (%)	-100.6 : -95.3 : -71.2	-3.9	-96.4 : -69.7 : -96.8	-65.2
RD-TS-HM (%)	-100.0 : -95.8 : -70.5	-4.5	-92.7 : -70.7 : -96.0	-65.7

†Refer to Table 7.1; ‡Percentile change with respect to DEF-TS-C.

principal shear stress in CMA layer is 31 % less when compared to DEF-TS-C. The maximum shear stress on the interface of the CMA and AC pavement (τ_{xy}) is also 36% less than that of DEF-TS-C.

Assessment of the reinstatement materials

Assessment criteria:

According to the above discussion, a dual-tire Assembly located transverse to a narrow (25 mm wide) and shallow (200 mm deep) trench and at its center (location CT in Figure 7.8a), in a private road and at 5 $^{\circ}C$ can result in the most critical combination of stress in the trench. This critical combination of variables given the code name CRIT- is used to simulate the stress distribution in the CLSM inside the trench and evaluate the failure potential of the reinstatement.

Table 7.5. Comparison of the conduit responses due to different model variables.

Code†	Principal (σ_1:σ_2:σ_3)	Tensile principal	Normal (σ_x:σ_y:σ_z)	Shear (τ_{xy})
DEF-TS-C	**-9.0 : -40.8 : -200.0**	**75.4**	**-9.0 : -200.0 : -40.8**	**45.8**
PD-TS-PR (%‡)	3.2 : 56.3 : 101.5	151.7	103.2 : 97.0 : 56.4	108.3
TE-TS-5 (%)	-63.4 : -11.7 : -21.0	-30.4	-28.9 : -22.5 : -11.7	-13.5
TE-TS-40 (%)	-35.4 : 16.3 : 39.7	56.2	25.3 : 36.9 : 16.3	44.9
TD-TS-N (%)	-16.7 : 32.8 : 15.7	17.0	68.9 : 11.8 : 32.8	12.8
TD-TS-W (%)	-62.1 : -40.7 : -17.8	3.8	-25.7 : -19.5 : -40.7	-3.6
TD-TS-S (%)	-35.3 : 31.8 : 35.8	426.8	30.1 : 32.9 : 31.8	45.4
TD-TS-D (%)	-62.5 : -5.9 : -19.0	-35.6	-27.8 : -20.6 : -5.9	-15.5
RD-TS-CM (%)	-49.5 : -6.0 : -3.9	-6.5	-7.0 : -5.8 : -6.0	-4.5
RD-TS-HM (%)	-49.9 : -6.7 : -4.5	-7.3	-7.6 : -6.4 : -6.7	-4.9

†Refer to Table 7.1; ‡Percentile change with respect to DEF-TS-C.

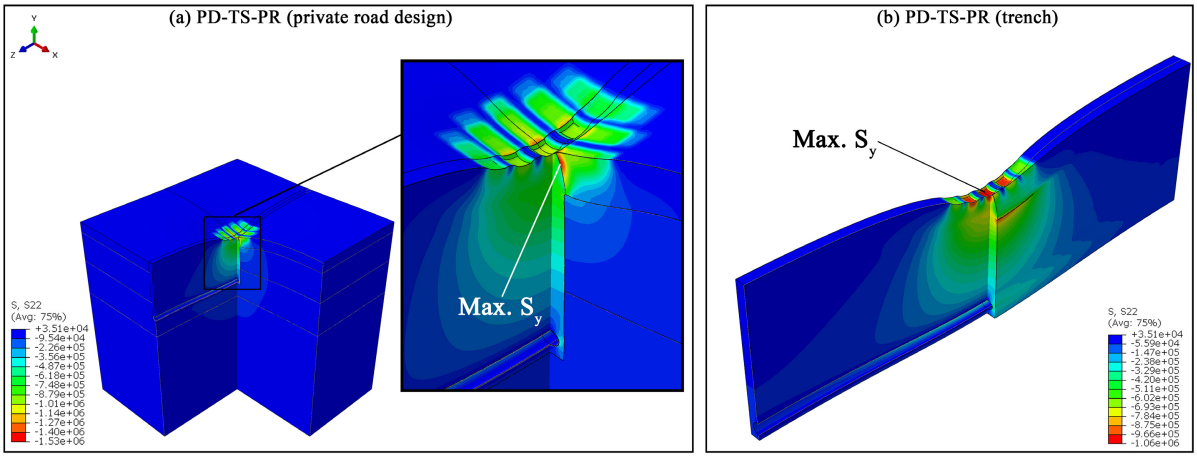

Note: The 3D model is cut along the x and z plane for better illustration of stress distribution; deformations are exaggerated 500 times to be visible in the figure.

Fig. 7.13. Stress (σ_y) distribution in the (a) private road pavement model and (b) trench backfill for PD-TS-PR.

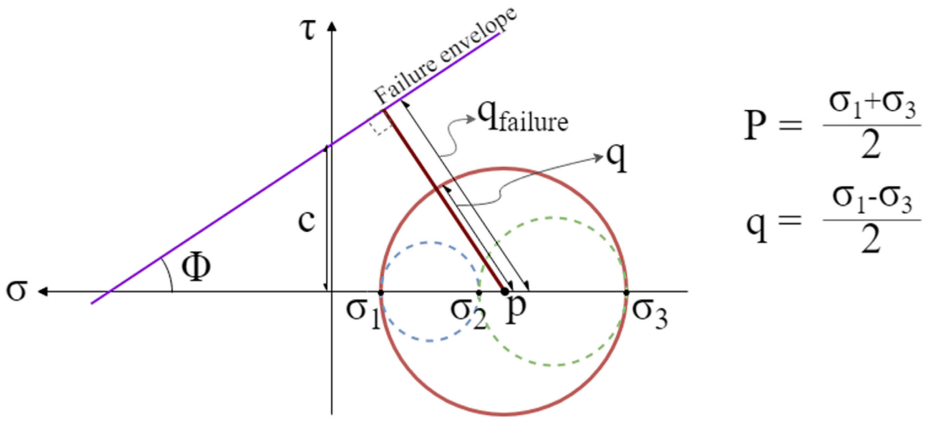

Fig. 7.14. Representations of Mohr-Coulomb failure criterion.

In order to evaluate the failure potential of the materials and due to the complex multi-dimensional stress state in the pavement and the narrow-trench, it is recommended to consider multi-axial stress states, rather than one dimensional normal or shear stress [393]. The Mohr-Coulomb failure criterion is commonly used in soil mechanics. The CLSM backfills are composed of cement particles, aggregate and air voids and therefore, are analogous to the soil. As depicted in Figure 7.14, the mohr-Coulomb failure criterion defines the stress ratio (SR) as the closeness of the stress state to the failure envelope (Equation 7.1). The factor of safety (F.S) against failure can also be defined as the inverse of the SR.

$$SR = \frac{q}{q_{failure}} = \frac{\sigma_1 - \sigma_3}{2 \times c \times cos\phi + (\sigma_1 + \sigma_3) \times sin\phi} \tag{7.1}$$

In order to define the mohr-coulomb failure envelope, the angle of friction (ϕ) and cohesive strength (c) of the CLSMs need to be determined. The values of ϕ and c are usually obtained from triaxial strength tests conducted at different confinement levels. However, in the absence

Table 7.6. The Mohr-Coulomb's failure envelope strength parameters for plain CBFs and AAFs.

Strength parameter	PA	PC	PF	GA	GB	GF
ϕ (°)	24.910	22.221	27.017	24.910	22.221	27.017
c (kPa)	1019.7	732.4	2429.2	542.5	238.5	1876.5

of triaxial test data in this research, the prediction model for friction angle of the foamed CLSMs suggested by Tiwari et al. [245] was used to estimate the value of ϕ (Equation 7.2).

$$\phi = 0.012\gamma + 15.062 \tag{7.2}$$

Where ϕ is in degree and γ is the density of the CLSM in kg/m^3.

The cohesive strength was then estimated according to the uniaxial compression test data which was provided in Chapters 4 and 5. Accordingly, the values of ϕ and c for the CLSMs considered in this chapter are calculated and tabulated in Table 7.6.

Shear stress ratio (SSR) is also defined by Equation 7.3 to evaluate the shear failure or debonding potential of the CLSM backfill and AC at their interface.

$$SSR = \frac{\tau_{xy}}{\tau_{failure}} \tag{7.3}$$

where τ_{xy} is the simulated shear stress at the interface of the trench and the top or bottom lift AC layer and $\tau_{failure}$ is the bond shear strength of the CLSM to AC in Slant shear test (SST) or flexural bond strength test (FBST), as tested in Chapters 4 and 5.

Furthermore, two more stress ratios are considered in this section. First is compressive stress

ratio (SR_C) which is the ratio of maximum compressive stress (σ_y) to the ultimate compressive strength of the CLSM (see Chapters 4 and 5 for the uniaxial compressive strength test results) and second is the tensile stress ratio (SR_T) which is defined as the ratio of maximum tensile principal stress to the ultimate uniaxial tensile strength of the CLSM. According to the reference [215], the tensile strength of foamed concrete is in the range of $20-40$ % of its compressive strength [455]. In this research and in order to be on the safe side, the tensile strength of the CLSMs is considered equal to 20% of their compressive strength.

Similarly, the failure envelope in CMA materials can be estimated according to the literature. The reference [456] proposed a cohesion value of 100 kPa and internal friction angle of 23.2 $^\circ$ for a highly workable, unaged cold-laid asphalt. In practice, CMA is heated to 60-130 $^\circ C$ before placement in the trench in order to increase its workability and compactability. This increases the strength of the CMA and accelerates its curing. Therefore, the selected failure envelope is expected to be conservative.

Results:

The simulation results of the reinstatement materials in CRIT- models are included in Table 7.7. In single backfilling method, all the CLSMs have an SR (and SR_C) less than 100% except for the alkali-activated mixture GB. This indicates their acceptable performance according to the Mohr-Coulomb criterion. Nevertheless, all the mixtures except the high-density mix PF and GF have a SR_T value higher than 100%. This unveils the potential of the tensile failure in medium- and low-density foams inside the trench. Stress distribution in PA, PC, and PF in CRIT- model is shown in Figure 7.15. As depicted in the figure, the tensile principal stress

Table 7.7. Maximum stress and the stress ratios of the CLSMs in the CRIT- and DEF- (in parenthesis) models.

CLSM	σ_1 (kPa)	σ_3 (kPa)	SR (%)	σ_y	SR_C (%)	σ_T (kPa)	SR_T (%)	τ_{xy} (kPa)	SSR-SST[1] (%)	SSR-FBST[2] (%)
Single-backfilling										
PA-800/C	-393.4	-1,755.0	49.4 (35.9)	-1,039.7	32.5 (32.8)	768.8	120.3 (33.5)	589.5	141.5 (115.9)	238.0 (195.0)
PC-600/C	-384.9	-1,750.1	63.1 (45.9)	-1,039.5	47.7 (48.4)	764.8	175.4 (48.9)	593.2	155.0 (129.0)	375.3 (312.3)
PF-1100/C	-772.6	-1,892.0	20.2 (11.9)	-1,866.8	23.5 (13.3)	848.5	53.5 (15.9)	394.2	62.5 (53.7)	113.5 (97.4)
GA-800	-235.2	-1,613.6	78.2 (59.2)	-1,032.4	60.7 (61.9)	573.2	168.6 (57.4)	647.7	137.8 (121.6)	239.0 (210.9)
GB-600	151.6	-1,384.9	135.1 (124.2)	-1,024.4	144.3 (148.1)	334.2	235.4 (405.3)	766.9	365.2 (327.0)	479.3 (429.2)
GF-1100	-651.1	-1,882.6	27.4 (35.2)	-1,381.5	22.5 (17.2)	840.4	68.6 (19.4)	470.0	64.4 (55.5)	134.6 (115.9)
Double-backfilling										
PA-800/C	-61.3	-968.5	39.7 (19.3)	-951.8	29.8 (9.9)	226.7	35.5 (32.2)	112.8	27.1 (40.3)	45.6 (67.8)
CMA	-1,123.8	-2,628.9	90.6 (61.4)	-1,196.3	–	1,539.1	–	348.8	–	–

[1]Slant shear test and [2] flexural bond strength test (See Chapters 4 and 5 for the test results).
Note: Values in parenthesis correspond to the results of DEF-TS-C model (i.e. for a 40 $\times$ 300 mm trench in a main road when a transverse single tire load located at the center of the trench at 25 $^{\circ}C$).

reaches its highest value at the bottom of the AC layer. As mentioned in the previous section, in the main road pavement design, this maximum tensile stress occurs at a higher depth (bottom of the bottom lift AC) and therefore, is about 190% less than private road pavement design. For that reason, the SR_T values of all CLSMs in DEF-TS-C model (the values in parenthesis in Table 7.7) are considerably less than 100% (except for GB).

According to the values of the SSR in Table 7.7, debonding between the CLSM backfill and AC is also a concern. As the table conveys, the SSR value of all mixtures is higher than 100% except for PF and GF which deliver a respective F.S of 1.60 and 1.55 against debonding. However, if the shear stress in the interface of the trench and AC is compared to the bonding stress in FBST, none of the CLSMs are safe against debonding failure. As depicted in Figure 7.15, the maximum shear stress is located at the top of the trench which decreases significantly with an

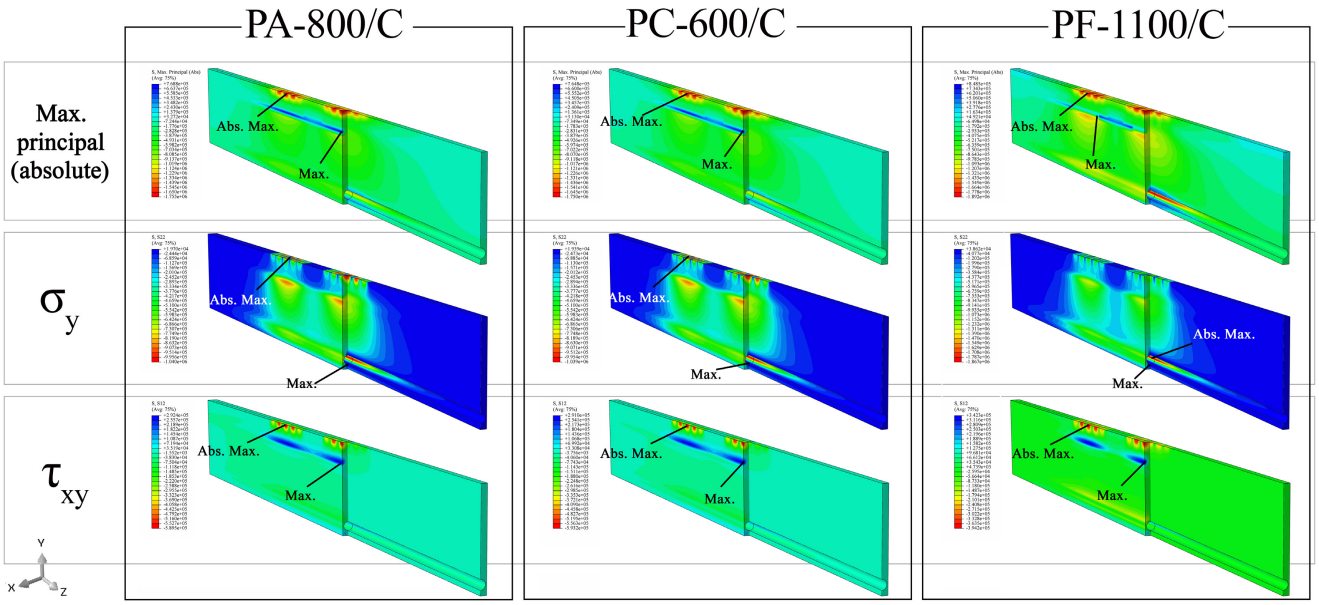

Note: The 3D model is cut along the x and z plane for better illustration of stress distribution.

Fig. 7.15. Stress distribution of the CLSM in CRIT-PA, CRIT-PC and CRIT-PF models.

increase in depth. Figure 7.16 also illustrates the distribution of SSR of CRIT-PA model. According to the figure, at the approximate depth of 10 mm, the value of SSR is equal to one (F.S = 1.0). The same argument can be made for CRIT-PC and GA. Therefore, it is essential to improve the bond strength of the CLSM to the AC at the first 10 mm of the trench depth. This can be done by replacing the top 10 mm of the CLSM with a material that provides a robust bond with AC (like specialty resins) or simply texturing the AC surface to improve its bonding to the CLSM materials.

As expected, the F.S of the CLSM materials against failure in double backfilling improved significantly when compared to the single backfilling method (see Table 7.7). However, the stress state on the CMA is higher than what was observed in CLSM in the single backfilling method. The F.S of the CMA to failure according to the Mohr-Coulomb criterion is 1.1 in CRIT-

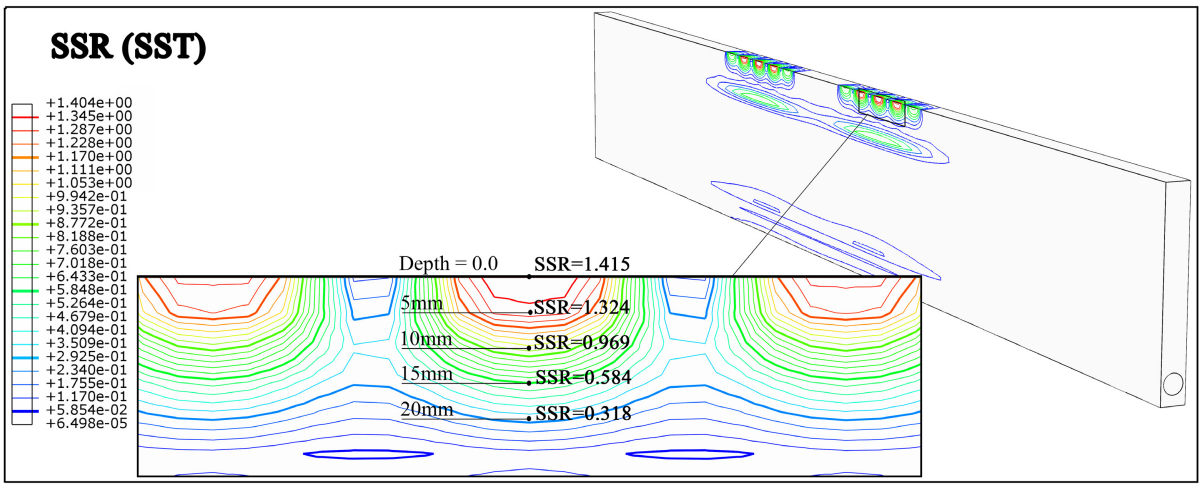

Fig. 7.16. Distribution of SSR over the trench face for the CRIT-PA model.

and 1.6 in DEF- model. The shear stress on the interface of the CMA and pavement AC is almost half of the τ_{xy} in mix PA in the single backfilling method. Therefore, it can be expected that if the pavement cut surface is cleaned and covered with a layer of tack coat before placing the CMA, debonding of the reinstatement materials and pavement AC is not a concern in the double backfilling method. Nevertheless, the maximum tensile principal stress at the bottom of the CMA is 1,539 kPa which is nearly twice the ITS of CMA-1 (see Table 3.3). According to the Figure 7.17, the σ_T is only 77.8 kPa in CMA in RD-TS-CM model. Therefore, when double-backfilling a trench in a private road, tensile failure of the CMA, and as a result, near-surface cracking can be expected when a dual-tire is passing over the trench.

According to the values of stress ratios in Table 7.7, it can be concluded that the high-density cement- and alkali-activated mixtures, PF and GF, deliver the highest F.S against failure among the CLSMs considered in this study. On the other hand, the ultra-low-density AAF, GB, is the least favourable mixture for NT backfilling because of its high stress ratios.

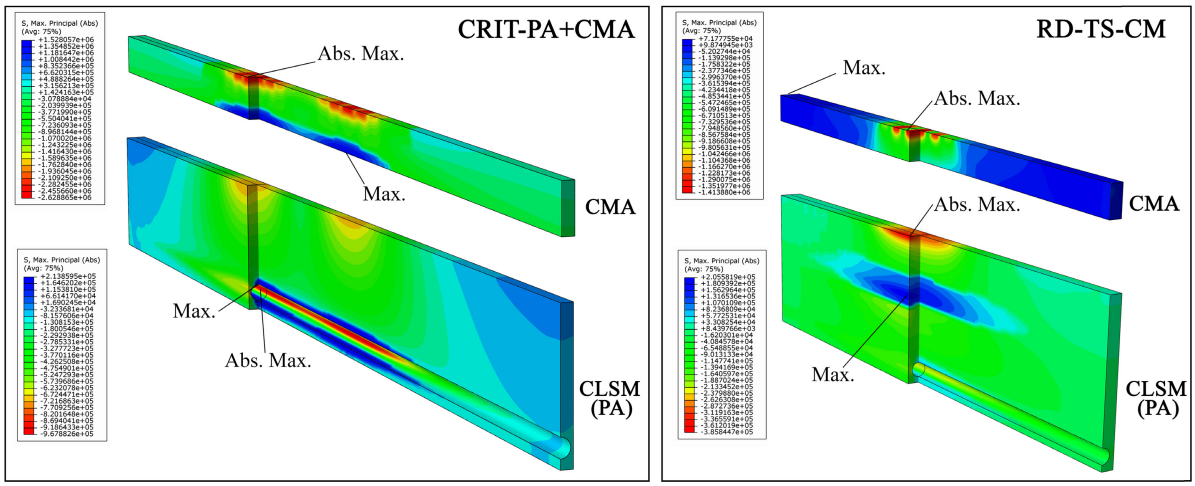

Note: The 3D model is cut along the x and z plane for better illustration of stress distribution.

Fig. 7.17. Distribution of maximum principal (absolute) stress over the trench for the CRIT-PA+CMA and RD-TS-CM models.

7.4 Concluding remarks

This chapter concludes the laboratory assessment of the NT reinstatement materials (which was presented in previous chapters) by modeling their performance inside the trench. The proposed methodology and simulated models of the narrow-trench can be used by designers or road authorities to investigate the response of the reinstated section to the traffic load and environmental conditions and set the requirement associated to the application. The following conclusions may be drawn from this study:

1. Reinstatement of the trench with CMA and plain or foamed cement grout resulted in a marginal 12% higher rut-depth when compared to the reference slab without the trench. The progressive rutting of the reinstated trench with CMA and sand or single backfilling with macadam proves the instability of these backfilling options.

2. While the rut-depth after one freeze-thaw conditioning in the trench filled with CMA and sand was 30% higher than that on an unconditioned sample, it did not have an appreciable effect on the trench filled with CMA and plain cement grout. However, after multiple freeze-thaw cycles, longitudinal cracks along the trench-AC interface as well as raveling in CMA was observed.

3. The maximum compressive principal stress in CLSM range from 385.8 kPa in RD-TS-CM model to 1,892.0 kPa in CRIT-PF model. This maximum stress in CMA layer was observed in CRIT-PA+CMA model (3,628.9 kPa). However, all the materials passed the Mohr-Coulomb failure criterion except for the low-density AAF, GB.

4. Maximum tensile stress on the CLSMs was noticed at the bottom of the AC layer and ranged from 183.3 to 848.5 kPa. Only high-density mixtures PF and GF passed the tensile failure criterion with respective F.S of 1.9 and 1.5. Tensile stress in the CMA layer is also twice its ITS which raises the possibility of tensile failure of the CMA layer in the double-backfilling method.

5. All of the CLSMs were found prone to debonding failure. According to the calculated value of SSR, the bond strength of the top 10 mm of the trench with AC needs to be improved in order to prevent debonding. Because of the low interfacial shear stress between CMA and AC layer, debonding is not a concern in the double-backfilling method.

6. The transferred stress to the conduit is not substantial (Maximum compressive stress of 272 kPa in TL-TD-C model).

Chapter 8

Time-Cost-Resource Optimization

Time-cost trade of problem is one of the principal challenges for construction project planners. On the other hand, an effective schedule is also important to eliminate waste caused by resource waiting for preceding activities to finish their work by maintaining the continuity of the crew. In such cases, traditional scheduling and planning techniques are unsatisfactory for managing repetitive construction projects. An effective schedule is important to eliminate waste caused by resource waiting for preceding activities to finish their work by maintaining the continuity of the crew. Therefore, a practical multi-objective optimization model is needed to search for possible scheduling alternative and offer a set of non-dominated solutions to the decision-makers. In this chapter, the discrete time-cost trade-off problem (DTCTP) is considered together with resource allocation and resource levelling problem (RLP). This study presents the discrete time-cost-resource optimization (DTCRO) model which together with linear scheduling model try to select starting time and the number of the crew assigned to each activity satisfying all the project constraints. To solve these problems, a non-domination based genetic algorithm (NSGA-II) is

used to search for the non-dominated solutions, taking into account the total project time, cost, and resources fluctuation as three objectives. The findings of the suggested model presented in this chapter show that adding the resource levelling capability to the available DTCTP models aside with using the benefits of linear scheduling technique provides more practical solutions in terms of resource allocation and levelling, making this research applicable to narrow-trenching projects.

8.1 Introduction

Construction planning is a fundamental and challenging aspect of construction project management. In order to achieve the project goals, careful planning and scheduling are crucial. Poor schedule can lead to significant waste as resources become idle owing to delayed completion of preceding tasks, limited availability of required resources, or other space and time constraints.

The life cycle of a construction project involves many project management challenges. Among these, the scheduling and optimization problem have received special attention [457–459]. In general, construction projects are a one-time process, therefore conducting multiple trials of the project schedule is not practical [460–462]. However, project managers can determine the optimal construction schedule by adjusting the project's timetable [461]. Scheduling enables project managers to understand and achieve their preset project management goals [461, 463]. On the other hand, generating a reliable project schedule itself is a significant objective in project

management [464]. Process control of the project would become impossible without a predetermined schedule.

Among the optimization problems, time-cost trade-offs have drawn significant attention in the construction industry. In the discrete version of the problem, the discrete time-cost tradeoff problem (DTCTP) follows a discrete and non-increasing pattern, i.e., a proportional increase in resource allocation to an activity will result in an accelerated activity. Three objectives have been defined in general for DTCTP [465]:

1. to minimize the project cost without exceeding a specified deadline (deadline problem);
2. to find the shortest project duration while meeting a given budget (budget problem); and
3. to construct a complete and efficient time-cost profile over a set of feasible project durations (time-cost curve problem).

The DTCTP was widely researched in the early 1950s under different assumptions. A restriction of the three standard scheduling optimization problems is that the description of the problem and consideration of the associated factors are rather simple and not realistic. Therefore, the produced schedules may not be well adjusted to the complex real-life construction projects in the field. An effective way to improve the practicality and flexibility of the solution is to introduce extra constraints to problem formulation. This strategy has lately been embraced by many scientists. [466, 467] tried to bring renewable resources to the traditional DTCTP. Hegazy [468] researched resource levelling optimization problems based on the constraint of peak renewable resource usage. Kolinas et al. [469] also regarded resource levelling

and resource allocation based on this constraint. Ghoddousi et al. [458] and Leu et al. [470] also looked at TCTP and resource levelling optimization problems based on the peak renewable resource usage constraint. Senouci et al. [471] dealt with both resource levelling and TCTP based on the extra peak renewable resource usage constraint by taking the anticipated resource-levelling value as a constraint.

Construction projects can be widely classified as either linear or nonlinear [457, 461]. Utility installation in gray areas, including fibre optic (FO) deployment civil works fall under the category of linear construction. As discussed in Chapter 2, NT and in particular, MT has many advantages over other methods of utility installations in urban areas. Despite all the advantages, there is no documented study which tries to manage and schedule these projects. Observation result of the four MT pilot installations and two real-life MT projects by the author [18, 19] revealed a huge saving potential in both project time and budget by optimizing the work schedule.

Linear construction projects often involve resources (e.g. crews) to do the very same job in different units (locations, segments) by moving in the project from one unit to the next [472]. Because of this frequent resource flow, it is even more essential to have an efficient schedule than the general construction projects in order to guarantee the uninterrupted use of resources between units of the repetitive project [473]. Consequently, to guarantee the work continuity, the stand-by time of the resources, waiting for preceding resources to finish their work, should be eliminated. This also benefits the project by maximizing the learning curve effect and minimizing the idle time of resources [474]. The strict application of maintaining work continuity

may, however, lead to a longer overall duration of the project. Traditional network technique (critical path method-CPM) has many disadvantages when applied to schedule linear construction projects [464, 475, 476]: first, representing a linear project requires a multitude of activities. Second, CPM does not guarantee the work continuity that can lead to crews being idle. Third, it does not show where and when a certain crew will be working on an activity, therefore, it is not efficient to visually monitor the progress of a particular crew. Therefore, a new group of scheduling methods has introduced as "linear scheduling techniques". One of the most representative of these techniques is the linear scheduling method (LSM). For transportation-type linear projects, LSM provides some advantages over CPM, including the ability to maintain construction continuity, having a concise and explanatory nature, ability to handle more comprehensive constraints, and being able to convey the rate and spatial information of the project [460–462, 477]. LSM has received increasing attention in the research community. However, it is still in the developmental stage [476].

In this chapter, an attempt is made to develop a practical procedure that searches for a near-optimum solution to linear project planning and scheduling considering project cost, duration and resource allocation and levelling, simultaneously. This procedure will provide a realistic insight for decision-makers and project planners by offering different near-optimum solutions. The Chapter begins with a short description of the advantages and shortcomings of current optimization-based and heuristic approaches. Individual improvements are then suggested to existing heuristic methods. A multi-objective optimization using the genetic algorithm (GA) technique is then described and coded. The performance of the proposed genetic algorithm

procedure is then evaluated on a real-life case study, and recommendations made.

8.2 Literature review

Classical optimization of construction projects can be categorized as resource allocation; resource levelling, and time-cost trade-off problems (TCTP) [457–459]. The primary classic objective of resource allocation is to allocate restricted resources to activities to minimize the duration [457, 459, 466, 478]. The objective of resource levelling is to make the graph of time-to-time resource usage as smooth as possible over the entire duration of the project [457, 471]. This will decrease the indirect resource management costs [458, 471] and enhance the advantages of the learning curve and the morale of employees [476]. Over the years, Researchers have used numerous analytical, heuristic and metaheuristic techniques for resource levelling. Geng et al. [479] suggested an enhanced ant colony optimization algorithm, Rieck et al.[480] introduced new linear integer model with domain reducing preprocessing methods, and Kyriklidis et al.[481] suggested a smart hybrid nature-inspired method by merging ant colony optimization and GAs. Despite the approach to optimization, most resource levelling researches are based on network-based scheduling techniques [479, 482, 483]. However, as mentioned earlier, for linear projects, CPM was discovered to be ineffective [484]. Hence, in repetitive construction projects, Elwany et al. [485] described a linear programming model for single resource allocation and levelling. The objective function was to minimize the difference between the resource usage. Georgy [463] provided a genetic algorithm to minimize absolute time-to-time variations

in total resource use as well as deviation from average total resource use throughout the project using an LSM. The objective of the adopted genetic algorithm was to solve the main deficiency of mathematical resource levelling approaches, however, it necessitated more resource usage and added variables. Lucko's study [486] was built based on an analysis of the criticality of linear schedules. The author suggested equations like the first-moment area to minimize objective function to a levelled resource profile, nevertheless, the model is complicated when the objective function exchanges. Zhang et al. [487] Proposed a line-of-balance (LOB) resource levelling algorithm that allows the number of crews in the backward control activity to be lowered until there is no backward control activity or the number of crews can not be decreased. This modification allows for consistent productivity of all tasks and provides a resource-levelled schedule. A more detailed review of resource levelling in the construction industry can be found in the works of Bhosale et al. [488] and Damci et al. [489, 490]. It is similarly essential to minimize time and cost. However, they often are negatively correlated. Therefore, it is essential to manage a trade-off between the two [458, 466, 491]. To solve this issue, TCTP is trying to find the best time-cost trade-off for the entire project. For this intent, a connection is needed between the activity's duration and cost, which is generally defined by the utility curve [459, 492, 493]. Another significant element to consider towards a reasonable time-cost trade-off is the connection between direct and indirect costs; reducing project length increases the direct costs while reducing the indirect costs of the project [494, 495]. In linear projects, the planner must consider and balance several cost and time elements related to various aspects of the projects in order to build a time- and cost-effective schedule [496]. Thus, in linear construction projects,

mathematical programming and heuristic models were used as an alternative way to solve the DTCTP. For instance, Senouci and Eldin [471] suggested a dynamic programming model to determine the time-cost profiles of repetitive projects. Their model regarded the effects of activities modes, interruptions, and delays for production activities. Because their suggested algorithm needs significant computational effort, it is only suitable for small initiatives. To resolve this issue, Computer-based artificial intelligence methods have been employed to solve the DTCTP in large-scale projects. For example, Hegazy and Wassef [497] presented a simplified CPM/LOB method to calculate the minimum total cost. Their method used a genetic algorithm and a spreadsheet template along with a specified deadline as a prerequisite. Hyari et al. [498] embraced a genetic algorithm-based strategy and the Pareto ranking process to create the optimal Pareto front. Long and Ohsato [499] presented a GA-based model aimed at minimizing both the duration and total cost of the project corresponding to different levels of the relative importance of these objectives. Ezeldin and Soliman [500] proposed a hybrid technique combining genetic algorithms with dynamic programming to solve the DTCTP under uncertainty for non-serial projects. Hegazy et al. [501] also employed an artificial intelligence technique to create a distributed scheduling system for large-scale construction. Their model combined the DTCTP with the concept of soft logic. However, their study lacks a mathematical model or a case study. Considering the aforementioned review, artificial intelligence techniques are proved to furnish a way of obtaining near-optimum solutions that require less computational effort than mathematical methods.

8.3 Problem statement

Aforementioned survey of the literature shows the lack of comprehensive models which can optimize the most important multi-objective aspects of the project (i.e. project's cost, duration and resources). Current solutions to linear project optimization generally attempt to discover the "best" solution, which corresponds to the minimum or maximum value of a single objective function that includes all different objectives. This type of optimization is a useful tool to provide insights into the nature of the problem. Nevertheless, it in normally unable to provide a trade-off between different objectives. On the contrary, the present Chapter attempts to provide a multi-objective optimization framework to simultaneously consider the project cost, time and resource optimization problems. There is no single optimal solution in multi-objective optimization with competing objectives. The interaction between objectives results in a set of compromised solutions, known as the trade-off, nondominated, non-inferior or Pareto-optimal solutions. Consideration of many objectives in the design or scheduling phase offers three significant improvements to the procedure that directly promotes the decision-making process [502]:

- A wider variety of alternatives is usually recognized with multi-objective methodology.
- More appropriate options are available for the decision-makers to make informed decisions when considering multiple objectives.
- The problem models are more realistic when multi-objectives are considered.

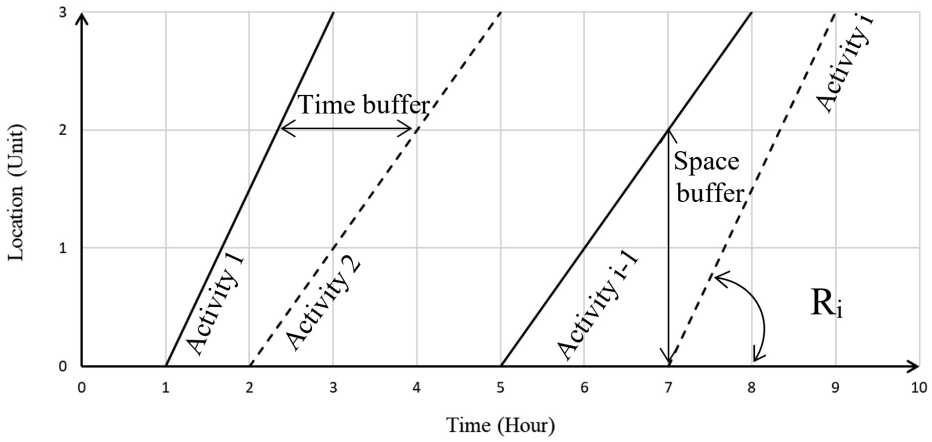

Fig. 8.1. A sample LSM schedule. Time and space buffers are also illustrated in the figure.

8.4 Background

8.4.1 Linear Scheduling Method (LSM)

LSM is intended to schedule linear construction projects containing a family of repetitive and almost identical tasks [503]. As demonstrated in Figure 8.1 it reflects a repetitive activity as a production line in a two-dimensional time and space graph. The horizontal and vertical axis represent time and location of an activity or a crew, respectively. The horizontal distance between the two lines is a graphic depiction of the time float or buffer, between the activities. Similarly, the vertical distance serves as the physical distance, or space buffer, between the activities. As stated earlier, prior studies have shown that LSM enables a better depiction of scheduling information when compared to the conventional CPM or bar charts in terms of time and space constraints, activity location, and productivity [504]. Therefore, LSM is used in this study for multi-objective optimization using LSM.

The slope of each bar in the LSM chart shows the planned rate of each activity (R_i). The productivity of the activity i (P_i), can be related to the number of crews working on that activity (C_i) and planned rate of the activity which is expressed as Equation 8.1.

$$P_i = \frac{R_i}{C_i} \tag{8.1}$$

This chapter assumes that the principles of "optimum crew size" and "natural rhythm" are also applied [505]. The principle of "Optimum crew size" implies that productivity will reduce if the crew size is different from the optimum crew size. The "natural rhythm" concept enables distinct units of manufacturing to shift the starting times of operation forward or backward by altering the number of working crews. An increase in the number of working crews will increase productivity.

8.4.2 Narrow-trenching

Narrow-trenching projects were introduced in Chapter 2 with a focus on the trenching activity. However, there are other activities in an NT project to send the telecommunication cable to the end-user. As explained, the NT process starts by cutting a narrow trench. Depending on the size of the conduit used, the trench is narrower than 20 mm wide, and up to 120-300mm deep which is usually being done by special cutting equipment with a mounted vacuum to suck the trenching dirt. The second step is the placement of cables or conduits inside the trench. After securing the cable inside the trench, the trench is ready for backfilling. In the pilot projects that

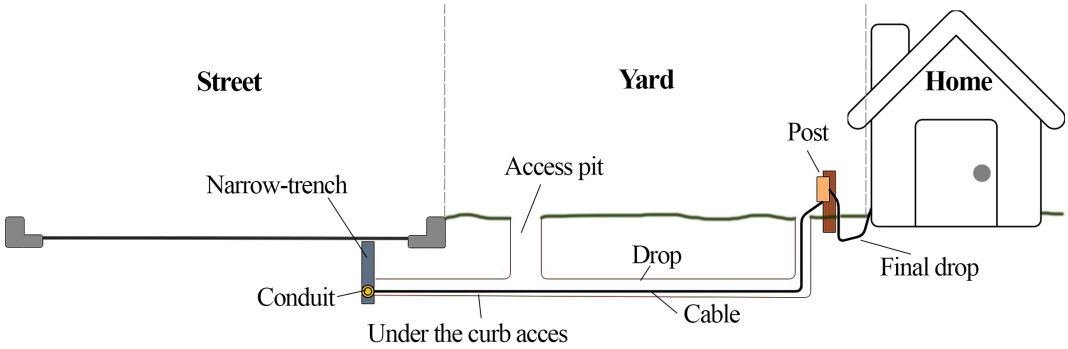

Fig. 8.2. Schematic of the lateral connections from the main trench to the end user.

studied by the author [19], the double-backfilling method was used. Therefore, the reinstatement process started by pouring cement grout up to the asphalt layer and filling the trench with cold-mix-asphalt to the top. Then, the trench was sealed by hot bitumen-based sealant. In order to send the cable to the home, an access pit and under-the curb access is being dug to access the cables inside the trench (Figure 8.2). The cable was then connected to the end-user through a drop trench to the post and lastly, the final drop to the home.

8.5 Problem formulation

An NT project is considered that consists of M activities labelled $i = 1, 2, ..., M$. Each activity needs to be repeated in N units labelled $j = 1, 2, ..., N$. Activity 1 is the only start activity and activity M is the one finish activity. Activity i is connected with its preceding activity p, $p \in P_i$, by fulfilling the precedence relation of finish to start (F.S.), start to start (S.S), or finish to finish (F.F.) with a defined time or space buffer, where P_i is the set of preceding activities of activity i. The activities are numbered from 0 to $j + 1$ in the project network, where activities 0 and $j + 1$

are "dummy" activities denoting the start and the end of the project.

The objective is to determine a set of non-dominated schedules when considering three objective functions and with satisfying both the precedence and resource constraints. Formulations of the objective function and constraints are outlined below.

8.5.1 Objective functions

It is essential to evaluate the desirability of the schedules (solutions) against a number of specific objectives. The purpose of this Chapter is to resolve a discrete time cost resource optimization (DTCRO) model using a non-dominated genetic sorting algorithm (NSGA-II) proposed by Deb et al. [506]. Accordingly, a non-dominated set of solutions with the minimum time, total cost and the sum of the square of the hourly deviations in resource histogram will be achieved, taking into account precedence relations between different activities and resource constraints in NT projects. The primary innovation in this research is to integrate impacts of resource allocation and levelling as well as time-cost trade-off in scheduling NT projects under resource constraints.

Once the number of crews and time and/or space buffer are selected for each activity, activity information will be input to the linear scheduling simulator scheme, which will produce a feasible schedule based on the given constraints. The outcome of the ensuing schedule is the project time, cost and resource usage histogram. The first objective in our DTCRO model is to minimize the project duration, which is equal to the finish time of end activity (FM) in the

project. Therefore, the total project duration (DT) is:

$$D_T = F_M \tag{8.2}$$

The second objective is to minimize total project cost. In general, the total cost of the project can be divided into direct cost and indirect cost. Direct costs are those that are directly related to the execution of activities in the project and can be calculated by:

$$DC = \sum_{i=1}^{M} \sum_{j=1}^{N} d_{ij} c_i R_{ij} \tag{8.3}$$

Where d_{ij} = duration of activity i in unit j; c_i = Unit (hourly) direct cost of activity i and R_{ij} is the number of crew working on activity i in unit j.

Project indirect cost (IC) increases linearly with the project duration [495], and thus, it can be calculated by the formula $IC = e \times DT$, where e is the daily indirect cost of the project. Since the duration optimization and resource constraint are considered in the formulation of the problem, there is no need to add any time or resource penalty cost here. Thus, the project cost (CT) can be calculated as:

$$C_T = DC + IC = \sum_{i=1}^{M} \sum_{j=1}^{N} d_{ij} c_i R_{ij} + e \times DT \tag{8.4}$$

The resource levelling objective function can be expressed in various ways. In order to reduce the fluctuation in using resources as a third objective, the proposed model considers

Minimization of the sum of the square of the hourly resource usage deviations ($Rdev_T$ in Equation 8.5). It first used by Popescu [507] and proved to provide the best average improvement in resource levelling among other objective functions studied in Damci and Polat [489].

$$Rdev_T = \sum_{k=1}^{F_M} (Rdev_k)^2 \tag{8.5}$$

Where k is the time under consideration and $Rdev_k$ is the deviation between resources required on time k and k+1.

8.5.2 Mathematical model of the proposed DTCRO

Just like DTCTP, there are three sub-problems of the DTCRO: first, the deadline problem, that minimizes total cost considering project deadline; second, the budget problem, for a given non-negative budget, tries to minimize the cost of the project; and third, the time-cost curve problem, to generate the entire time-cost trade-off profile for a project under constrained resource with discrete time-cost relationship. In this Chapter since the Pareto approach is selected for multi-objective optimization, predefining separate models for the aforementioned sub-problems are unnecessary. In other words, in the proposed DTCRO model, no limitations as a project deadline or budget are considered. Once the Pareto-front solutions are defined, it is the decision-maker who decides the best solution among the optimal, non-dominated solutions according to the specific project limitation. The model of the proposed DTCRO is formulated

as follows:

$$minD_T \tag{8.6}$$

$$minC_T \tag{8.7}$$

$$minRdev_T \tag{8.8}$$

s.t.

$$\Delta_i \geq \Delta_{imin} \qquad \forall(i) \in E \tag{8.9}$$

$$\begin{cases} f_i - \sum_{j=1}^{N} d_{ij} \geq max(f_{i'}), & \text{if } PR_{ii'} \text{ is F.S.} \\ t_i \geq max(t_{i'} + \Delta_i), & \text{if } PR_{ii'} \text{ is S.S. or F.F.} \end{cases} \qquad \forall(i, i') \in E \tag{8.10}$$

$$r_i \leq r_{imax} \tag{8.11}$$

$$0 < \sum_{j \in J_t} r_j \leq R_{max} \qquad J_t = \{j \mid f_j - d_j < t < f_j\} \tag{8.12}$$

In the above formulation, the objective functions 8.6-8.8 minimize the project time, cost and resource deviation on the X-axis which are calculated by formula 8.2-8.5. Constraint 8.9 requires

the assigned time and/or space buffer of each activity i (Δ_i) to be greater than the required buffer for that activity in that unit where E represents the set of activities. Constraint set 8.10 represents the precedence relationships (PR) between activity i and its precedents, i'. Constraint 8.11 indicates that the assigned resources to each activity cannot exceed the maximum available resources for that activity. Finally, constraint 8.12 indicates that for each time instant t, the sum of all resources on the job cannot exceed the maximum available resources. The constraint also ensures the work continuity by requiring non-zero resources at each time instant of the project.

8.5.3 Proposed GA

To search for non-dominated solutions (in this research non-dominated schedules), an elitist non-dominated sorting genetic algorithm (NSGA II) is developed for the purpose of multi-objective optimization. Genetic algorithm is capable of searching among a set of possible solutions (i.e. population) and finding the Pareto-optimal solutions efficiently at each simulation run. The NSGA II proposed by Deb et al. [506] is a modified version of the first NSGA algorithm [508], it is fast in computation, incorporates elitism, and converges better when compared to other multi-objective evolutionary algorithms [458]. The solution finding procedure with NSGA II in this study is illustrated in Figure 8.3.

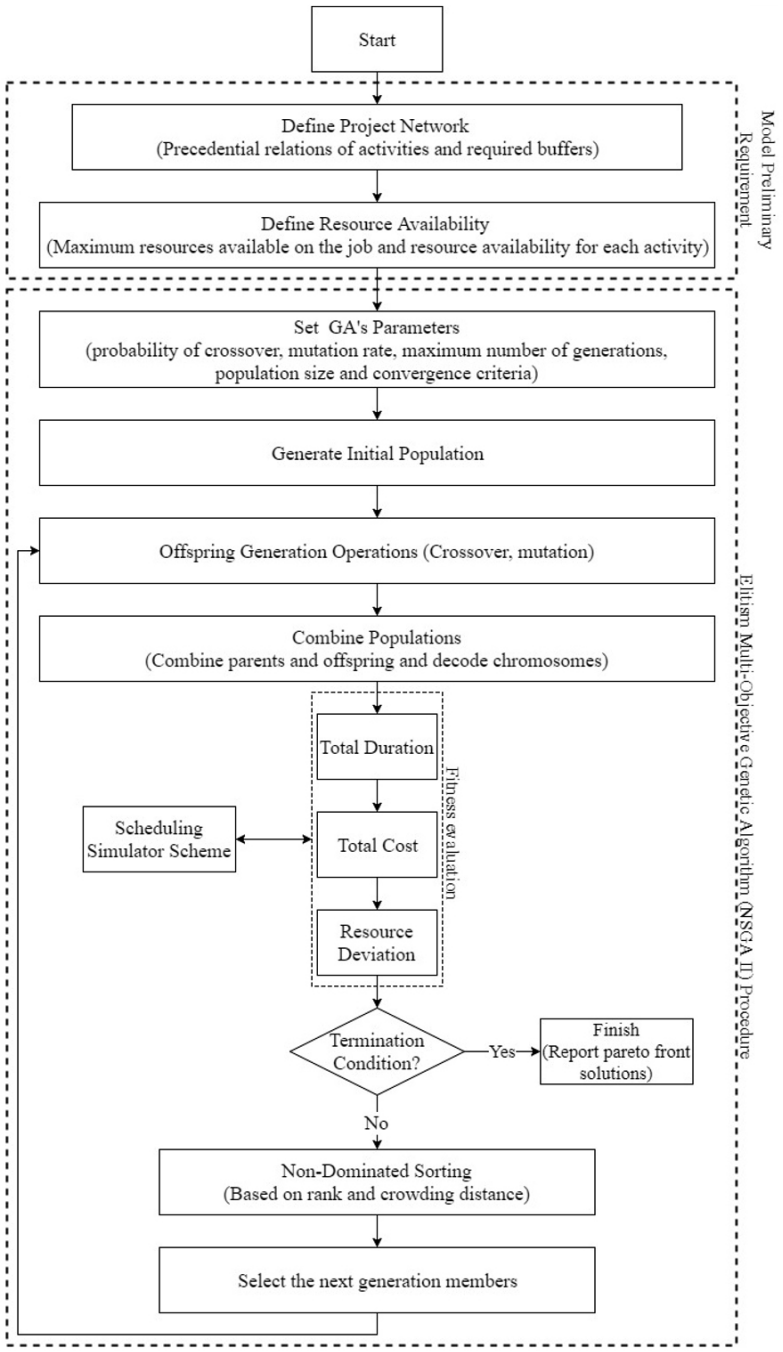

Fig. 8.3. Flowchart of the proposed DTCRO model.

8.6 Model application and discussion of the results

8.6.1 Real life implication example

The construction data gathered during four micro-trenching pilot installations in 2014 to 2016 [18] and two real-life full-size projects in 2016 and 2017 [19] is used to demonstrate how the proposed DTCRO model works in reality. As it can be seen in Figure 8.4, this case study consists of 10 activities. Table 8.1 shows the details of this case study. The backfilling method consists of filling the trench with regular Portland cement grout up to the asphalt layer and then reinstating the trench with CMA to the top. The trench is later sealed using hot sealant. We have one renewable resource and its availability is 20 labourers per day. The maximum crew of each activity is also mentioned in Table 8.1 based on the observation and experts' opinions. In this case, the indirect cost has been considered to be $65 per hour as observed during the field monitoring. The objective is to find non-dominated schedules with respect to project time, cost and deviation of resources. To increase the convergence speed of the model, sensitivity analysis has been carried out, and the tunable parameters of NSGA-II for population size, number of generation, and mutation percentage have been found to be 300, 150, and 5 respectively. It has to be mentioned that after the 213^{th} generation, Pareto front solutions did not change and convergence criteria were reached.

Figure 8.5 shows the distribution for 40 non-dominated points in the criterion space after the 200^{th} generation. The relationship between the relevant non-dominated points and the objectives of the model can be understood according to the results listed in Table 8.2. The

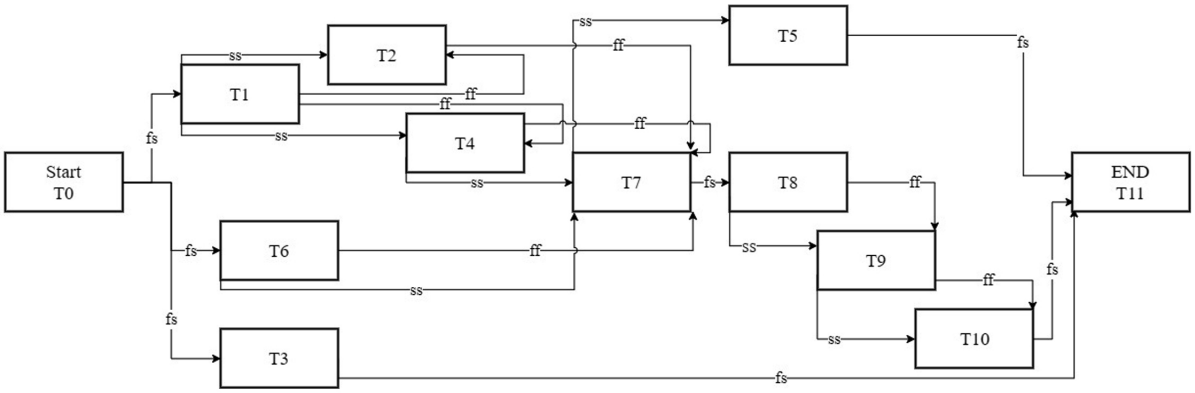

Fig. 8.4. Project network activities of the micro-trenching case study.

Table 8.1. Activity data of the micro-trenching case study used in DTCRO model [18, 19].

Activity	ID	Predecessor	Relationship	Time buffer (hr)	One crew productivity (m/hr)	Optimum crew size	Maximum available crew	Equipment cost (CAD/m)	Labor and material cost (CAD/m)
Start	T0	-	-	-	0	-	-	0	0
Digging access-pits	T1	T0	FS	0	41.56	1	10	30	30
Accessing Under-the-curb	T2	T1	SS,FF	0.5	43.17	2	3	200	80
Installing the vaults	T3	T0	FS	0	11.50	2	5	150	75
Digging drops	T4	T1	SS,FF	1	19.65	2	5	25	75
Installing final-drops	T5	T7	SS	0.5	7.31	2	5	25	75
Trenching	T6	T0	FS	0	43.61	4	1	80	140
Cabling	T7	T6,T2,T4	SS,FF	1,1,0	46.40	3	3	30	180
Grouting	T8	T7	FS	0	50.42	3	3	55	115
Asphalt backfilling	T9	T8	SS,FF	3	20.97	3	4	35	95
Applying sealant	T10	T9	SS,FF	2	40.23	2	3	10	70
End	T11	T3,T5,T10	FS	0,0,0	0	-	-	0	0

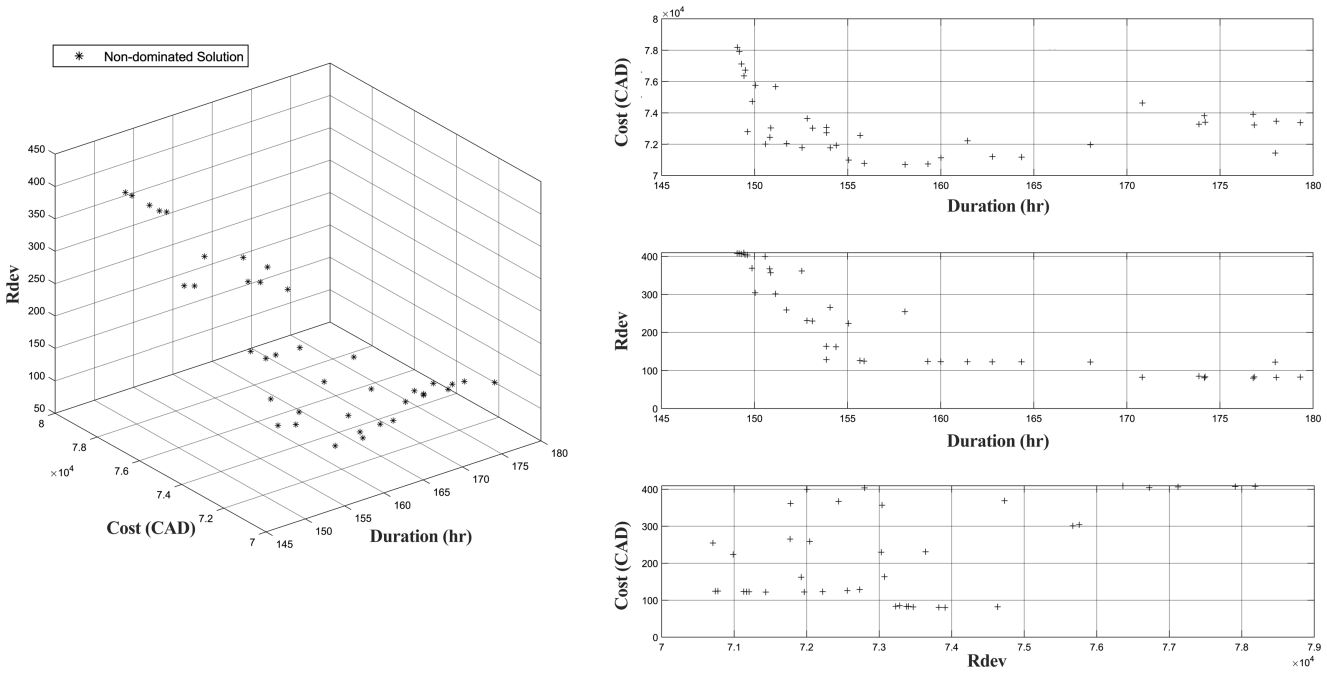

Fig. 8.5. Non-dominater solutions of the proposed DTCRO model for the micro-trenching case study.

range of time, cost and resource hourly deviation in the Pareto front solutions of the proposed DTCRO model have been 149-179 hours, 70,707-78,189 CAD and 80-410, respectively. The original schedule which has been implemented in the real-life projects resulted in the duration of 296 hours, the total cost of 132,088 CAD and $Rdev_T$ of 614 (when only considering non-idle crews). When comparing the Pareto frontier schedules of DTCRO model with the project data, the appreciable improvement in project duration, cost and resource allocation/levelling can be confirmed.

In general, with a reduction in the resource usage fluctuation ($Rdev_T$), the duration of the project has been increased. Despite there is not a solid relation between $Rdev_T$ and project cost but it can be seen that for solutions with the same duration reduction in the resource usage

Table 8.2. Results of DTCRO model for micro-trenching case study.

Solution Num.	Duration (hr)	Cost (CAD)	Rdev	Solution Num.	Duration (hr)	Cost (CAD)	Rdev
1	149	76361	410	21	161	72221	123
2	158	70707	255	22	151	72004	400
3	177	73909	80	23	153	73639	231
4	179	73377	83	24	174	73282	85
5	149	78184	408	25	163	71206	123
6	171	74632	82	26	156	70776	125
7	155	70987	224	27	149	76724	404
8	150	75758	304	28	174	73282	85
9	151	75670	301	29	152	72042	259
10	150	74729	369	30	174	73402	83
11	154	73073	163	31	160	71132	123
12	178	71436	122	32	153	73028	230
13	168	71966	122	33	153	71778	361
14	154	71772	265	34	178	73470	82
15	151	73039	357	35	156	72560	126
16	164	71173	123	36	151	72440	367
17	149	77120	407	37	159	70739	124
18	154	71925	162	38	177	73227	83
19	149	77910	407	39	150	72798	404
20	154	72731	129	40	174	73822	81

fluctuation imposes an additional cost to the project. For example, considering five solutions with an equal time of 149 days, the solution with smaller resource deviation has a greater cost value. It's important to mention the fact that we cannot interpret and conclude the results by considering only time and cost of schedules and ignoring the third aspect which is resource levelling parameter. As we can see solutions with the same time and greater cost have remained in population since they had a smaller resource moment deviation which means the smoother resource usage histogram.

Another matter that should be taken into consideration is that although the project duration in solution No.40 compared to solution No.1 has increased in a small amount (25 hr), the $Rdev_T$ has decreased significantly by almost 80%. To have a better understanding of this reduction in $Rdev_T$ we calculate the standard deviation of these two solutions. The result of this calculation is the standard deviation of 5.7 for solution No.1 and 2.9 for solution No.40. This means that most daily usage of resources in the histogram is within 2.9 of the mean for solution No.40 whereas it is almost doubled for solution No.1 which shows a higher fluctuation. Reduction in fluctuations of resource usage decreases undesirable cyclic of hiring and firing during project execution and prevents time and cost being wasted in such issues. This makes the proposed DTCRO model a more suitable tool for time-cost trade-off analysis in repetitive projects and provides more practical solutions in terms of resource allocation and levelling.

In Table 8.2, each solution is relative to a schedule which shows the starting time and the number of crew of of every activity in a project. In this study, solving the existing problems is based on an assumption that there is not any particular preference among model objectives. In

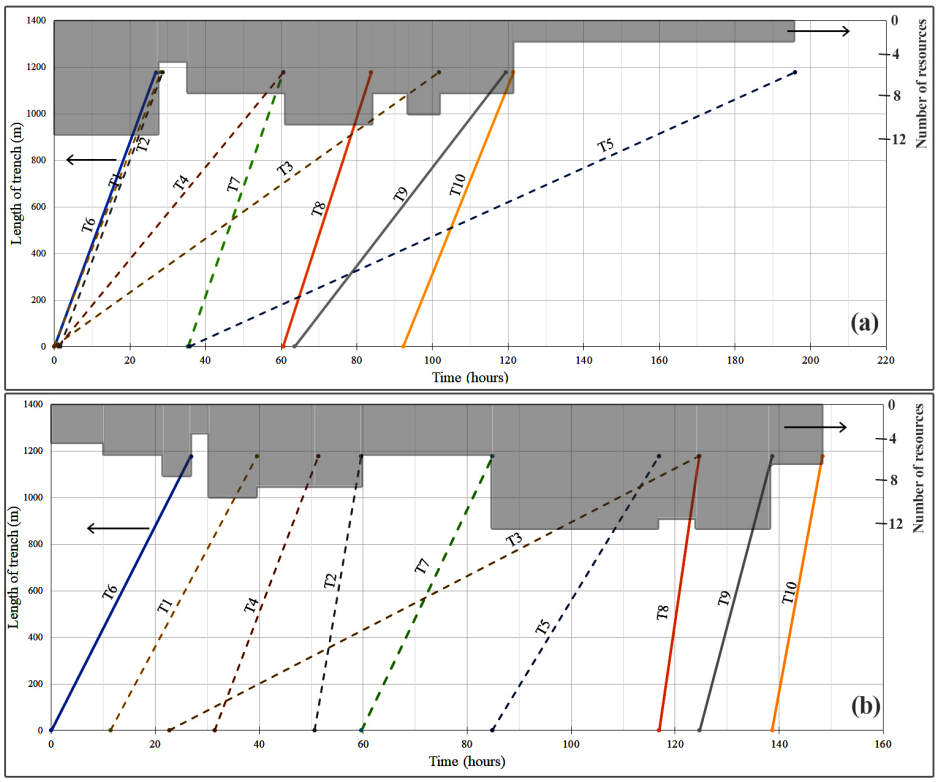

Fig. 8.6. Linear schedule graphs of (a) non-optimum solution and (b) Pareto-front solution No.1. Resource usage histograms are also presented at the top of the graphs.

real life, managers can make optimal decision in choosing the proper solution based on trade-off between time, cost and resource moment deviation for the project.

Figure 8.6 also visually compares the linear schedule graph as well as the resource usage histogram of a non-optimised schedule (Figure 8.6a) with the Pareto-frontier solution No.1 (Figure 8.6b; refer to Table 8.2). The non-optimized schedule is developed by using the minimum time buffers between activities and considering one crew assigned to each activity. As evident from the figure, the proposed model reduced the duration and $Rdev_T$ of the non-optimized schedule by 24% and 15%, respectively.

8.7 Conclusion

The two well-established scheduling problem in linear projects are the discrete time-cost trade-off and resource allocation and levelling. This Chapter aimed to simultaneously solve these two problems. Accordingly, a DTCRO model was developed to select the best combination of starting time and assignments of crews for each project activity with respect to time, cost, and resource usage histograms.

According to the characteristics of the proposed problem, the model was solved using a Pareto based multi-objective genetic algorithm NSGA-II. The model was also tested for a real size micro-trenching construction project case study with 10 activities. The data required to set up the model has been gathered from several real-life micro-trenching projects. The test non-dominated solutions of this case study not only estimate the optimal time and cost of the whole project but also the selected crew number and starting time for all of the activities. A Pareto-front solution with the minimum duration resulted in a respective saving of 49.7 and 42.2% in project's time and cost when compared to the real schedule of the project. Accordingly, the minimum cost solution resulted in 46.6% saving in project time and 46.5% in project cost. Moreover, the details of the results show that by decreasing fluctuation in resource usage histogram, the project time and cost mainly increases. This research assumed no preferences on project time, cost and resource moment deviation in the DTCRO model. Having the Pareto frontier solutions available, the manager can easily make a decision based on the project's specific preference on time, cost and resource fluctuation.

Chapter 9

Conclusions and Recommendations for Future Works

9.1 Concluding remarks

The overall civil work of NT projects was studied in this research. Reviewing the existing documentation on the topic and long-term monitoring of NT projects revealed serious concerns about the quality of materials in reinstatement. Accordingly, the present study mainly focused on evaluating the performance of three most promising narrow-trench reinstatement alternatives, namely cold-mix-asphalts, cement-based foams, and alkali-activated foams. Based on the results of the laboratory experiments, the ultra-light CBF, PC, delivers the highest benefit-to-cost ratio. Consequently, the numerical analysis suggested that double backfilling of the narrow-trench, with mixture PC in the base layer and CMA-1 in the asphalt concrete pavement layer, will guarantee both the performance and the cost-efficiency of the reinstatement.

While the narrow-trench designers and contractors can benefit from the proposed backfilling solution, it is hoped that municipalities and approval authorities can also benefit from this research by defining a detailed specification for narrow-trench reinstatement materials. Lastly, the proposed DTCRO model is expected to solve the scheduling and resource allocation problems observed in NT projects. Based on the established objectives in this study, the following detailed conclusions were drawn:

1. The first objective was met through a long-term monitoring of real-life MT projects as well as a thorough review of the literature.

    - Granual backfills like play sand are not suitable for the cold climate of Canada. A considerable cable movement, as well as settlement of the trench, was observed in the section that was filled with sand.
    - Using an improper CMA can also lead to many distresses in backfill section as raveling, settlement, and cracking due to the insufficient bonding to the pavement AC.
    - Bituminous macadam was found difficult to be applied. After a few months, progressive degradation was observed at the top of the reinstated trench.
    - While the specialty reins or grouts are expensive and not compatible with the flexible pavement, the properties of lightweight cement- or alkali-activated foams have made them a promising alternative for narrow-trench backfilling purpose.
    - Despite their potential, there is limited information on the behavior of different cement or alkali-activated substitute blends, durability properties of CLSM, especially

their F-T resistance and their Composite performance with the surrounding materials in a narrow-trench, which requires more attention.

2. The second objective was approached by laboratory testing on nine ready-to-use CMAs for their strength, rutting and moisture susceptibility.

   - The Marshall stability and flow test is effective in distinguishing rigidity of CMA materials. The average MQ value of DG CMAs is higher than OG mixtures, reflecting DG mixtures' higher stiffness and lower workability.
   - Rutting resistance of ambient-cured cold mix samples is low, and a wheel tracking test was found to be too harsh to test deformation resistance in the early life of cold mixtures. On the other hand, the accelerated curing process at 135 $^{\circ}C$ for 18 hours appears suitable to predict the eventual strength of the CMAs.
   - Despite few disparities observed, the MQ value can reflect the rutting resistance of cold mix materials. Cold mixtures with higher MQs are expected to show higher rutting resistance when tested under dry conditions in an HWT device.
   - MSI seemed to be a better indicator for moisture damage susceptibility in CMAs than SIP. CMA-3 and CMA-9 had the highest MSI and lowest TSR among DG and OG CMAs, respectively, which mark them as the most susceptible cold mixtures to moisture.

- Statistical analysis indicated that the aggregate grain size distribution has a significant effect on rutting resistance of CMAs. However, moisture susceptibility is not a function of bitumen content or grain size distribution alone; and
- Moisture susceptibility of DG CMAs is found to be strongly correlated to the percentage of fine particles, while in OG mixtures, the amount of coarse aggregates in the mix shows significant correlation with rutting and moisture susceptibility.

3. The third objective was addressed by testing on different cement- and alkali-activated foams ranging in density from 600-1100 kg/m^3. They were tested for their strength, modulus of elasticity and Poisson's ratio, drying shrinkage and coefficient of thermal expansion (CTE), and their bond performance with the asphalt concrete.

   - The compressive strength of cement-based foams is affected by the aggregate. Whereas fine perlite resulted in higher compressive strength than coarse perlite, a higher percentage of sand to cement ratio reduces the compressive strength. Both fly ash and fibre reinforcement led to an increase in the compressive strength. As expected, the modulus of elasticity followed closely the trends for the compressive strength above.
   - The drying shrinkage of cement-based foams was seen to drop with a decrease in the density. As expected, replacing the cement with fly ash and the addition of aggregates or fibres led to a substantial drop in the drying shrinkage strain.
   - The coefficient of thermal expansion (CTE) was seen to drop with a decrease in the density. A higher percentage replacement of Portland cement with fly ash reduced

the CTE significantly. Adding aggregates and fibres also led to a reduction in this coefficient.

- Between them, the slant shear test yielded a higher bond strength than the flexural bond test. The bond strength was seen to improve for an increase in the density. At early ages of curing, a smaller dosage of fly ash raised the bond strength, while a higher dosage led to its drop. This may be attributed to the rate of pozzolanic reaction. Whereas coarse perlite led to a higher bond strength, fine perlite led to a drop. No perceptible change was observed as a result of fibre addition.

- The compressive strength of alkali-activated foams is sensitive to cast density, curing temperature and aggregate type. While higher densities result in higher compressive strength, heat curing improves the strength at early ages. However, no appreciable effect was observed beyond 90 days. Among the aggregates examined here, coarse perlite outperformed fine perlite or ordinary sand. An improvement to the compressive strength resulted in an expected rise in the modulus of elasticity.

- There was a drop in drying shrinkage of AAFs with a decrease in cast density. Adding aggregates and polypropylene microfibres uniformly reduced the shrinkage strain. As well, curing at elevated temperatures resulted in lower shrinkage strain.

- The coefficient of thermal expansion drops with a decrease in the cast density. At the same time, adding aggregates and polypropylene microfibres and curing at elevated temperatures also reduced the CTE.

- The slant shear test witnessed higher bond strength than the flexural bond test. An increase in the cast density of the AAF and heat curing further increased the bond strength. Whereas adding sand to the AAF resulted in a weaker bond, neither perlite nor microfibres appear to affect the bond strength either way.

- Cement-based foams withstood 150 cycles of freeze-thaw conditioning with little or no visible damage. On the other hand, the only AAF that holds its integrity during the 150 freeze and thaw cycles was the high-density mixture, GF.

- The properties of conditioned specimens were compared to those of the reference, unconditioned ones, at the age of 28 and 90 days. The results revealed that the average durability of CBFs reduces with increase in density. Accordingly, the DF_{90d}^{150c} of the ultra-low-density mix PC is 11% more than the low-density mix PA and 76% higher than the high-density mix PF. On the other hand, the low early strength of low-density alkali-activated foams GA and GB resulted in a progressive deterioration.

- Introducing aggregate to the foams reduced the durability when compared to the plain foams in each density group. Moreover, in the compressive strength test, coarse perlite resulted in higher DF than fine perlite in both cement- and alkali-activated-based foams. The higher percentage of natural sand in mixtures PG and GG reduced the 28 days compressive strength and subsequently, reduced the durability of these mixes considerably when compared to the plain foams, PF and GF.

- Although the DF_{90d}^{150c} of GE is marginally higher than GA, fibrous mixtures displayed lower durability than the plain foams in the same density group. The durability factor in mixtures incorporating FA was lower than that in the plain foams within the same density group. Additionally, curing the AAF at elevated temperature, as in mixture GH, improved the durability over the mixture GA, which was cured at room temperature.

4. The fourth objective was met by simulating the narrow-trench with physical and numerical models.

    - Reinstatement of the trench with CMA and plain or foamed cement grout resulted in a marginal 12% higher rut-depth when compared to the reference slab without the trench. The progressive rutting of the reinstated trench with CMA and sand or single backfilling with macadam proves the instability of these backfilling options.
    - While the rut-depth after one freeze-thaw conditioning in the trench filled with CMA and sand was 30% higher than that on an unconditioned sample, it did not have an appreciable effect on the trench filled with CMA and plain cement grout. However, after multiple freeze-thaw cycles, longitudinal cracks along the trench-AC interface as well as raveling in CMA was observed.
    - The maximum compressive principal stress in CLSM range from 385.8 kPa in RD-TS-CM model to 1,892.0 kPa in CRIT-PF model. This maximum stress in CMA layer was

observed in CRIT-PA+CMA model (3,628.9 kPa). However, all the materials passed the Mohr-Coulomb failure criterion except for the low-density AAF, GB.

- Maximum tensile stress on the CLSMs was noticed at the bottom of the AC layer and ranged from 183.3 to 848.5 kPa. Only high-density mixtures PF and GF passed the tensile failure criterion with respective F.S of 1.9 and 1.5. Tensile stress in the CMA layer is also twice its ITS which raises the possibility of tensile failure of the CMA layer in the double-backfilling method.
- All of the CLSMs were found prone to debonding failure. According to the calculated value of SSR, the bond strength of the top 10 mm of the trench with AC needs to be improved in order to prevent debonding. Because of the low interfacial shear stress between CMA and AC layer, debonding is not a concern in the double-backfilling method.

5. The fifth objective was approached by developing a multi-objective decision support model based on the linear scheduling technique and non-dominated sorting genetic algorithm.

- Application of the model on a recent real-life MT project revealed its potential in scheduling and resource leveling of these projects.
- When comparing a Pareto-front solution with the minimum duration to the real schedule of the project, a respective saving of 49.7 and 42.2% in project's time and cost can be realized. Accordingly, the minimum cost solution resulted in 46.6% saving in project time and 46.5 % in project cost.

9.2 Recommendations for future works

The following recommendations are provided in the interest of future research studies:

- Microstructure and bubble analysis of the lightweight CBFs and AAFs, as one of the most important parameters affecting their properties and performance in NT application, needs to be studied in detail considering density, constituents, and stability.

- Further tests are necessary to better evaluate the bond strength of the lightweight foam to the AC substrate in real-life conditions such as testing on the freeze-thaw conditioned samples or on AC with different surface smoothness. Bond strength of CMA to HMA in the double-backfilling method also requires further attention.

- Testing the properties of the reinstatement materials under dynamic loading better reflects the loading environment inside the narrow-trench and therefore, requires further studies. While many dynamic properties of the materials (like compressive strength, modulus of elasticity, etc.) can be obtained through the existing standard test procedures, others can be tested by innovative test methods. For instance, the bond strength of the backfilling material to the AC substrate under dynamic loading can be tested through the laboratory fatigue test developed by [226]. As well, the stress rate sensitivity of the bond may be determined as per Islam et al [509].

- Triaxial compression test and failure analysis of the lightweight foams need to be studied in order to serve the performance assessment of these materials.

- The physical models of the narrow trench can be enhanced by embedding strain gauges inside the backfilled trench. It enables better the assessment of the backfill materials based on their response to the load instead of their deformation (rut-depth) under the wheel.

- Assessment of the backfill materials can be enhanced by using a more realistic FE model, considering both elastic and plastic properties of the materials, more realistic interaction between different pavement layers as well as the trench fill, and dimensional change of the reinstatement and temperature-induced loads.

- Development of a specification for narrow-trench reinstatement materials, above all cement- and alkali-activated foams, is necessary for their successful application. The specification requires to cover the testing methods and acceptance criteria in particular.

- Considering the potential of the lightweight CBFs and AAFs for use as narrow-trench backfill, full-scale trials need to be designed and tested.

Bibliography

[1] Hediyeh Vaseli. "Application of Micro-Trenching for Fiber to the Home". MA thesis. Edmonton, Alberta, Canada: University of Alberta, 2015.

[2] Sanjiv Gokhale. "Deployment of fiber optic networks through underground sewers in North America". In: *Journal of transportation engineering* 132.8 (2006), pp. 672–682.

[3] Md Hasanuzzaman. "An Investigation on Micro-Trenching Technology for FTTH Deployment". MA thesis. Edmonton, Alberta, Canada: University of Alberta, 2016.

[4] OCED. "The Development of Fixed Broadband Networks". In: *OECD Digital Economy Papers, No. 239* (2014).

[5] Alan Atalah, Choi Chang-Jin, and Keith Osburn. "Comparison study of installing fiber optic cable in university campuses using trenchless techniques relative to open cut". In: *Pipelines Division Specialty Conference*. 2002, pp. 1–17.

[6] J.K. Jeyapalan. "Solving the First Mile or FTTH Bottleneck and the Fiber Glut Using Creative Business Partnerships with Existing Utility Pipe Owners". In: *Proc. of 25th Pacific Telecommunications Council, Honolulu, Hawaii.* 2003.

[7] Majed Fedhi Alinizzi. "A Framework for Coordinating Water Distribution System and Pavement Infrastructure M&R Based on "LCCA"". MA thesis. West Lafayette, Indiana: Purdue University, 2013.

[8] City of Toronto. *Appendix X – Micro-trenching Guidelines - City of Toronto*. City of Toronto, 2018. URL: https://www.toronto.ca/wp-content/uploads/2018/05/8fad-ecs-specs-mcr-Appendix_X_Micro-trenching_Guidelines_Apr2018.pdf (visited on 03/31/2019).

[9] HAUC. *Proposed Specification for the Excavation and Reinstatement of Microtrenches in Shallow Construction and Evolved Highways [Online Document]*. The Highway Authorities and Utilities Committee (HAUC-UK), 2013. URL: http://www.pavementengineering.com.au/wp-content/uploads/2015/12/Pavement-Work-Tips.pdf.

[10] Gary Stahlbrand. *Micro Trenching; A Cost Effective Deployment Method for Open Access Networks*. Online document. 2012. URL: http://www.bbcmag.com/2012s/presentations/Stahlbrand,\%20Gary\%20\%20TeraSpan\%20Networks/BBC\%20Summit\%202012PP\%20TeraSpan.pdf.

[11] Duraline. *Recommended Procedures for Conduit Microtrenching and Restoration*. Tech. rep. Technical Bulletin: DCEB-10002. Dura-line, Knoxville, TN, USA, 2016.

[12] Shaun Trezise. *Best Practice for Installing Fiber Through Micro Trenching*. Online article. 2017. URL: https://www.ppc-online.com/blog/best-practice-for-installing-fiber-through-micro-trenching.

[13] Mike Harper. *Micro Trenching for Fibre Broadband Deployment*. Online document. 2014. URL: http://www.nextgenevents.co.uk/files/pdf/nextgen12/Mike\%20Harper.pdf.

[14] Bill Mah. *Fibre optic $1B investment will make Edmonton Canada's first gigabit society, Telus says*. Online document. 2015. URL: https://edmontonjournal.com/business/fibre-optic-1b-investment-will-make-edmonton-canadas-first-gigabit-society-telus-says.

[15] Leila Hashemian, Mohammad Rezaei, and Alireza Bayat. "Field and laboratory investigations on pavement backfilling material for micro-trenching in cold regions". In: *International Journal of Pavement Research and Technology* 10.4 (2017), pp. 333–342.

[16] Mohammad Rezaei, Leila Hashemian, Alireza Bayat, and Bryson Huculak. "Planning and Implementation of Management system for Utility Cuts." In: *Journal of Transportation Research Record* 1699 (2000), pp. 42–48.

[17] N McDonnell. "The Inside Scoop on Micro-Trenching. Broadband Properties Magazine". In: *Broadband Magazine: Game-Changing FTTH Technology* (2009), pp. 54–56.

[18] Mohammad Rezaei. *Micro-trenching projects report-company confidential report No. 2*. Technical Report. University of Alberta, Canada: University of Alberta, 2018.

[19] Mohammad Rezaei. *Micro-trenching pilot projects report-company confidential report No. 1*. Technical Report. University of Alberta, Canada, 2018.

[20] ITU. *Construction, Installation and Protection of Cables and Other Elements of Outside Plant, Micro-Trench Installation Technique*. L.49 Optical fibre cables – Guidance and installation technique. Telecommunication standardization sector of ITU, 2003. URL: https://www.itu.int/rec/T-REC-L.49-200303-I (visited on 05/31/2019).

[21] ITGI. *Board Briefing on IT Governance, 2nd edition*. IT Governance Institute, 2003. URL: https://www.oecd.org/site/ictworkshops/year/2006/37599342.pdf.

[22] W. Van Grembergen. "Introduction to the Minitrack: IT Governance and Its Mechanisms." In: *Proc., 35th Hawaii International Conference on System Sciences (HICSS), Hilton Waileoloa Village, Island of Hawaii.* 2001.

[23] Muhammad Osamah Saeed. *Determining optimal fibre-optic network architecture using bandwidth forecast, competitive market, and infrastructure-efficient models used to study last mile economics*. Citeseer, 2011.

[24] S Stojicic. "Installing Fiber Optic Cables in Sewers Maximizing the Potential of Existing Underground Infrastructure". In: *Pipelines 2002- Beneath Our Feet: Challengers and Solutions* (2002).

[25] Koen Casier, Jeroen Vanhaverbeke, Bart Lannoo, Jan Van Ooteghem, Sofie Verbrugge, Raf Meersman, et al. "Economics of FTTH: A comparative study between active and passive optical networks". In: *48th FITCE Congress*. FITCE (Forum for European ICT Professionals). 2009, pp. 35–39.

[26] Jiajia Chen, Lena Wosinska, Carmen Mas Machuca, and Monika Jaeger. "Cost vs. reliability performance study of fiber access network architectures". In: *IEEE Communications Magazine* 48.2 (2010), pp. 56–65.

[27] Manley Osbak, Hossein Akbarzadeh, Alireza Bayat, and Carrie Murray. "Investigation of horizontal directional drilling construction risks". In: *No-Dig Show* (2012), pp. 1–7.

[28] Chorus. *Deployment Standards Initiative Kelson Micro and Mini Trenching Pilot*. Tech. rep. DSI-28042011; Final. Chorus Telecom, New Zealand, 2011.

[29] Shan Solivan. "Life-cycle assessment on fiber cable construction methods". MA thesis. Stockholm, Sweden: Royal Institute of Technology, 2015.

[30] Kari A Jensen, Vernon R Schaefer, Muhannad T Suleiman, and David J White. "Characterization of utility cut pavement settlement and repair techniques". In: *Proceedings of the 2005 Mid-Continent Transportation Research Symposium, Iowa State University, Ames, Iowa*. 2005.

[31] MA Rahman, A Arulrajah, J Piratheepan, MW Bo, and MA Imteaz. "Resilient modulus and permanent deformation responses of geogrid-reinforced construction and demolition materials". In: *Journal of Materials in Civil Engineering* 26.3 (2013), pp. 512–519.

[32] Md Aminur Rahman, Monzur Imteaz, Arul Arulrajah, and Mahdi Miri Disfani. "Suitability of recycled construction and demolition aggregates as alternative pipe backfilling materials". In: *Journal of cleaner production* 66 (2014), pp. 75–84.

[33] Md A Rahman, Monzur A Imteaz, Arul Arulrajah, Mahdi M Disfani, and Suksun Horpibulsuk. "Engineering and environmental assessment of recycled construction and demolition materials used with geotextile for permeable pavements". In: *Journal of Environmental Engineering* 141.9 (2015), p. 04015019.

[34] Arul Arulrajah, MA Rahman, J Piratheepan, MW Bo, and MA Imteaz. "Evaluation of interface shear strength properties of geogrid-reinforced construction and demolition materials using a modified large-scale direct shear testing apparatus". In: *Journal of Materials in Civil Engineering* 26.5 (2013), pp. 974–982.

[35] A Arulrajah, MA Rahman, J Piratheepan, MW Bo, and MA Imteaz. "Interface shear strength testing of geogrid-reinforced construction and demolition materials". In: *Advances in Civil Engineering Materials* 2.1 (2013), pp. 189–200.

[36] Stirling-Lloyd. *Micro-Trenching Reinstatement (Technical Advice Note)*. Tech. rep. Stirling Lloyd Polychem Ltd., 2011. URL: http://www.whauc.com/site/WHAUC.

[37] David Trejo, Kevin J Folliard, and Lianxiang Du. "Sustainable development using controlled low-strength material". In: *Proceedings of International Workshop on Sustainable Development and Concrete Technology*. 2004, pp. 231–250.

[38] Ana Blanco, Pablo Pujadas, SHP Cavalaro, and Antonio Aguado. "Methodology for the design of controlled low-strength materials. Application to the backfill of narrow trenches". In: *Construction and Building Materials* 72 (2014), pp. 23–30.

[39] ACI. *ACI 229r-13: Report on Controlled Low-Strength Materials*. American Concrete Institute, 2013. ISBN: 9780870318160. URL: https://books.google.ca/books?id=7MzAnAEACAAJ.

[40] Paul Tikalsky, Mike Gaffney, and Ray Regan. "Properties of controlled low-strength material containing foundry sand". In: *ACI Structural Journal* 97.6 (2000), pp. 698–702.

[41] Tung-Chai Ling, Senthil Kumar Kaliyavaradhan, and Chi Sun Poon. "Global perspective on application of controlled low-strength material (CLSM) for trench backfilling–An overview". In: *Construction and Building Materials* 158 (2018), pp. 535–548.

[42] Tarun R Naik and Shiw S Singh. "Flowable slurry containing foundry sands". In: *Journal of Materials in Civil Engineering* 9.2 (1997), pp. 93–102.

[43] Bruce A Dockter. "Comparison of dry scrubber and class C fly ash in controlled low-strength material (CLSM) applications". In: *The Design and Application of Controlled Low-Strength Materials (Flowable Fill)*. ASTM International, 1998.

[44] Jon Kaneshiro, Stephen Navin, Luke Wendel, and Harry Snowden. "Controlled low strength material for pipeline backfill—Specifications, case histories and lessons learned". In: *Pipelines 2001: Advances in Pipelines Engineering and Construction*. 2001, pp. 1–13.

[45] Kenneth W. Trawick. "Improving Micro-Trenching: The Vision Becomes Reality." In: *Broadband Magazine* 30.6 (2009), pp. 92–93.

[46] BidNEt. *eABF Fiber Optic Cable and MicroDuct. [Installation Manual]*. Online document. Dura-Line, 2014. URL: https://www.bidnet.com/bneattachments?/427472023.pdf.

[47] R and E Contracting. *Micro Trenching Slurry Backfill 1 [Video File]*. June 2015. URL: https://www.youtube.com/watch?v=5prVpaQHICo.

[48] GM Plast. *Micro trenching urban streets [Video File]*. Sept. 2015. URL: https://www.youtube.com/watch?v=19RgzqxC11I\&t=.

[49] FastPatch DPR. *FastPatch DPR [Technical data sheet]*. 2016. URL: http://www.wilvaco.com/SecureFiles/MediaRoom/PQ_FastPatch_DPR\-Rev_1_November_2016.pdf.

[50] Elephant Armor. *Elephant Armor [Technical data sheet]*. 2017. URL: https://gotpotholes.net/wp-content/uploads/2017/02/GST-Elephant-Armor-Micro-trenching.pdf.

[51] Leila Hashemian, Vinicius Afonso Velasco Rios, and Alireza Bayat. "Laboratory Investigation of Pavement Backfilling Materials for Micro-Trenching in Cold Regions". In: *Transportation Research Record* (2018), p. 0361198118784172.

[52] BidNEt. *Fiber project from coulee dam to nespelem. [Request for proposal]*. Online document. Confederated Tribes of the Colville Reservation, 2015. URL: http://www.bidnet.com/bneattachments?/372239715.pdf.

[53] FHWA. *Materials and Procedures for Repair of Joint Seals in Portland Cement Concrete Pavements. U.S. DOT updated manual of practice*. Tech. rep. FHWA-RD-99-146. United States. Federal Highway Administration., 1999.

[54] Peter H. F. Tringham. "Joint sealants and joint design". In: *Concrete construction* (1963). URL: https://www.concreteconstruction.net/products/decorative-concrete-surfaces/joint-sealants-and-joint-design_o.

[55] B. Schultz. *How Microtrenching Cuts Fiber-Optic Cable Costs*. Online article. 2011. URL: https://www.forconstructionpros.com/equipment/attachments/article/10327940/microtrenching-for-fiber-optic-installation.

[56] GM Plast. *Micro trenching Montmeló [Video File]*. Montmelo, Spain, Nov. 2013. URL: https://www.youtube.com/watch?v=pMrPm4yS0x0\&t=.

[57] OverNet. *Micro-trenching installation from Overnet DMD [Video File]*. Skopje, Macedonia, Sept. 2014. URL: https://www.youtube.com/watch?v=snOr1l2jeqk.

[58] L De Rose and J Morris. *The influence of mix design on the properties of microcellular concrete*. Thomas Telford: London, UK, 1999.

[59] EP Kearsley and PJ Wainwright. "The effect of high fly ash content on the compressive strength of foamed concrete". In: *Cement and concrete research* 31.1 (2001), pp. 105–112.

[60] M Turner. "Fast set foamed concrete for same day reinstatement of openings in highways". In: *Proceedings of one day seminar on foamed concrete: properties, applications and latest technological developments*. Loughborough University. 2001, pp. 12–18.

[61] MR Jones and A McCarthy. "Behaviour and assessment of foamed concrete for construction applications". In: *Use of Foamed Concrete in Construction: Proceedings of the International Conference held at the University of Dundee, Scotland, UK on 5 July 2005*. Thomas Telford Publishing. 2005, pp. 61–88.

[62] I Papayianni and IA Milud. "Production of foamed concrete with high calcium fly ash". In: *Use of Foamed Concrete in Construction: Proceedings of the International Conference held at the University of Dundee, Scotland, UK on 5 July 2005*. Thomas Telford Publishing. 2005, pp. 23–27.

[63] Sagar Tandon, Maneek Guide Kumar, and Shweta Guide Goyal. "Optimization of Controlled Low Strength Material Using Spent Foundry Sand, GGBS, Fly Ash and CKD". PhD thesis. 2015.

[64] Tan Manh Do, Gyeong-O Kang, and Young-Sang Kim. "Thermal conductivity of controlled low strength material (CLSM) under various degrees of saturation using a modified pressure plate extractor apparatus-A case study for geothermal systems". In: *Applied Thermal Engineering* (2018).

[65] GJ Osborne. "Durability of Portland blast-furnace slag cement concrete". In: *Cement and Concrete Composites* 21.1 (1999), pp. 11–21.

[66] W-C Jau and D-S Tsay. "A study of the basic engineering properties of slag cement concrete and its resistance to seawater corrosion". In: *Cement and Concrete Research* 28.10 (1998), pp. 1363–1371.

[67] Tiong-Huan Wee, Daneti Saradhi Babu, T Tamilselvan, and Hwee-Sin Lim. "Air-void system of foamed concrete and its effect on mechanical properties". In: *ACI materials journal* 103.1 (2006), p. 45.

[68] KJ Byun, HW Song, SS Park, and YC Song. "Development of structural lightweight foamed concrete using polymer foam agent". In: *ICPIC-98* 9 (1998).

[69] EP Kearsley. "The use of foamcrete for affordable development in third world countries". In: *Concrete in the service of mankind: Appropriate concrete technology* 3 (2006), pp. 232–242.

[70] Zhifu Yang, Jon Huddleston, and Heather Brown. "Effects of Wood Ash on Properties of Concrete and Flowable Fill". In: *Journal of Materials Science and Chemical Engineering* 4.07 (2016), p. 101.

[71] EK Kunhanandan Nambiar and K Ramamurthy. "Influence of filler type on the properties of foam concrete". In: *Cement and concrete composites* 28.5 (2006), pp. 475–480.

[72] RS Bang, YM Ghugal, and IK Pateriya. "Strength performance of pond ash concrete". In: *International Journal Of Earth Sciences And Engineering, ISSN* (2012), pp. 0974–5904.

[73] Tan-manh Do, Young-sang Kim, and Byung-cheol Ryu. "Improvement of engineering properties of pond ash based CLSM with cementless binder and artificial aggregates made of bauxite residue". In: *International Journal of Geo-Engineering* 6.1 (2015), p. 8.

[74] Tri Ho Minh Le, Dae-Wook Park, and Jung-Woo Seo. "Evaluation of Ponded Ash as a Sustainable Backfill Material". In: *Journal of Materials in Civil Engineering* 30.8 (2018), p. 04018158.

[75] Joseph Davidovits. "Geopolymers: inorganic polymeric new materials". In: *Journal of Thermal Analysis and calorimetry* 37.8 (1991), pp. 1633–1656.

[76] Caijun Shi. "Strength, pore structure and permeability of alkali-activated slag mortars". In: *Cement and Concrete Research* 26.12 (1996), pp. 1789–1799.

[77] E Rodríguez, S Bernal, R Mejía de Gutiérrez, and F Puertas. "Alternative concrete based on alkali-activated slag". In: *Materiales de Construcción* 58.291 (2008), pp. 53–67.

[78] Huajun Zhu, Zuhua Zhang, Yingcan Zhu, and Liang Tian. "Durability of alkali-activated fly ash concrete: chloride penetration in pastes and mortars". In: *Construction and Building Materials* 65 (2014), pp. 51–59.

[79] Jose RA Goncalves, Yaman Boluk, and Vivek Bindiganavile. "Thermal properties of fibre-reinforced alkali-activated concrete in extreme temperatures". In: *Magazine of Concrete Research* 70.18 (2018), pp. 954–964.

[80] Jonathan Stolz, Yaman Boluk, and Vivek Bindiganavile. "Mechanical, thermal and acoustic properties of cellular alkali activated fly ash concrete". In: *Cement and Concrete Composites* 94 (2018), pp. 24–32.

[81] Alessandra Mobili, Alberto Belli, Chiara Giosuè, Tiziano Bellezze, and Francesca Tittarelli. "Metakaolin and fly ash alkali-activated mortars compared with cementitious mortars at the same strength class". In: *Cement and Concrete Research* 88 (2016), pp. 198–210.

[82] Caijun Shi, Della Roy, and Pavel Krivenko. *Alkali-activated cements and concretes*. CRC press, 2003.

[83] MH Maher and PN Balaguru. "Properties of flowable high-volume fly ash-cement composite". In: *Journal of Materials in Civil Engineering* 5.2 (1993), pp. 212–225.

[84] Ahmad Samadi and Richard Herbert. "Corrosiveness of Controlled Low Strength Materials vs. That of Encasement Sand". In: *New Pipeline Technologies, Security, and Safety*. 2003, pp. 514–523.

[85] CE Pierce and MC Blackwell. "Potential of scrap tire rubber as lightweight aggregate in flowable fill". In: *Waste Management* 23.3 (2003), pp. 197–208.

[86] Suhaizad Sulaiman. "Water permeability and carbonation on foamed concrete". PhD thesis. Universiti Tun Hussein Onn Malaysia, 2011.

[87] C Vipulanandan and M Neelan Kumar. "Properties of fly ash-cement cellular grouts for sliplining and backfill applications". In: *Advances in Grouting and Ground Modification*. 2000, pp. 200–214.

[88] GS Ghataora and IM Alobaidi. "Assessment of the performance of trial trenches backfilled with cementitious materials". In: *International Journal of Pavement Engineering* 1.4 (2000), pp. 297–316.

[89] Lightbuild. *Micro-trench reinstatement*. Online document. 2019. URL: http://lightbuild.co.za/docs/LightBuild-Micro-Trench-Grouting.pdf.

[90] Rudolph C Valore et al. "Cellular concretes Part 1 composition and methods of preparation". In: *Journal Proceedings*. Vol. 50. 5. 1954, pp. 773–796.

[91] Walter Harold Taylor. "Concrete technology and practice, 4/E". In: (1967).

[92] LE Brossard Perez et al. "Potential for the use of pyrolytic tar from bagasse in industry". In: *Biomass and Bioenergy* 12.5 (1997), pp. 363–366.

[93] Seung Bum Park, Eui Sik Yoon, and Burtrand I Lee. "Effects of processing and materials variations on mechanical properties of lightweight cement composites1". In: *Cement and concrete research* 29.2 (1999), pp. 193–200.

[94] Antanas Laukaitis, R Žurauskas, and J Kerien. "The effect of foam polystyrene granules on cement composite properties". In: *Cement and Concrete Composites* 27.1 (2005), pp. 41–47.

[95] DK Panesar. "Cellular concrete properties and the effect of synthetic and protein foaming agents". In: *Construction and building materials* 44 (2013), pp. 575–584.

[96] S. Nandi, Arnab Chatterjee, Prantik Samanta, and Tanushree Hansda. "Cellular Concrete & its facets of application in Civil Engineering". In: *International Journal of Engineering Research* 5.1 (2016), pp. 37–43.

[97] K Ramamurthy, EK Kunhanandan Nambiar, and G Indu Siva Ranjani. "A classification of studies on properties of foam concrete". In: *Cement and concrete composites* 31.6 (2009), pp. 388–396.

[98] Geethu Kallunkal and Elson John. "Optimization of foam concrete masonry blocks". In: *International Journal of Engineering Research and General Science* 4.5 (2016), pp. 82–106.

[99] IT Koudriashoff. "Manufacture of reinforced foam concrete roof slabs". In: *Journal Proceedings*. Vol. 46. 9. 1949, pp. 37–48.

[100] Feng Qing Zhao, Jun Qin Liu, Qian Li, and Hao Li. "Study of foamed concrete from activated ash/slag blended cement". In: *Advanced Materials Research*. Vol. 160. Trans Tech Publ. 2011, pp. 821–826.

[101] ASTM C869. "Standard Specification for Foaming Agents Used in Making Preformed Foam for Cellular Concrete". In: *ASTM International, West Conshohocken, PA* (2016).

[102] ASTM C796. "Standard Test Method for Foaming Agents for Use in Producing Cellular Concrete Using Preformed Foam". In: *ASTM International, West Conshohocken, PA* (2012).

[103] FHWA. *User guidelines for waste and by-product materials in pavement construction. U.S. DOT*. Tech. rep. FHWA-RD-97-148. United States. Federal Highway Administration., 1997.

[104] S Bouzalakos, AWL Dudeney, and BKC Chan. "Formulating and optimising the compressive strength of controlled low-strength materials containing mine tailings by mixture design and response surface methods". In: *Minerals Engineering* 53 (2013), pp. 48–56.

[105] Vahid Alizadeh, Sam Helwany, Al Ghorbanpoor, and Konstantin Sobolev. "Design and application of controlled low strength materials as a structural fill". In: *Construction and Building Materials* 53 (2014), pp. 425–431.

[106] Pablo Pujadas, Ana Blanco, S Cavalaro, and Antonio Aguado. "Performance-based procedure for the definition of controlled Low-strength mixtures". In: *Journal of Materials in Civil Engineering* 27.11 (2015), p. 06015003.

[107] NRMCA. *Guide specification for controlled low strength materials (CLSM).* National Ready Mixed Concrete Association, 2006. URL: https://www.flowablefill.org/downloads/CLSMSpecifications1.pdf.

[108] M Nehdi, Y Djebbar, and A Khan. "Neural network model for preformed-foam cellular concrete". In: *Materials Journal* 98.5 (2001), pp. 402–409.

[109] KC Brady, M Roderick Jones, and GR Watts. *Specification for foamed concrete*. Citeseer, 2001.

[110] Md Azree Othuman Mydin, Hanizam Awang, and Ahmd Farhan Roslan. "Determination of lightweight foamed concrete thermal properties integrating various additives". In: *Elixir Cement Concrete Compos* 48 (2012), pp. 9286–9291.

[111] F Batool and V Bindiganavile. "Effect of Pozzolanic Admixtures on the Fresh Properties of Cement-Based Foam". In: *Advances in Civil Engineering Materials* 5.1 (2016), pp. 263–275.

[112] M Roderick Jones, Michael J McCarthy, and Aikaterini McCarthy. "Moving fly ash utilization in concrete forward: a UK perspective". In: *Proceedings of the 2003 international ash utilisation symposium, centre for applied energy research. University of Kentucky*. 2003, pp. 20–2.

[113] Jayant D Bapat. *Mineral admixtures in cement and concrete*. CRC Press, 2012.

[114] Rafat Siddique and Mohammad Iqbal Khan. *Supplementary cementing materials*. Springer Science & Business Media, 2011.

[115] Fred C McCormick. "Ratioanl proportioning of preformed foam cellular concrete". In: *Journal Proceedings*. Vol. 64. 2. 1967, pp. 104–110.

[116] Frank M Coda, Ernst Gruenwald, Robert G Mathey, Owen Richards, Robert A Crist, WC Hansen, et al. "Guide for Cellular Concretes Above 50 pcf, and for Aggregate Concretes Above 50 pcf with Compressive Strengths Less Than 2500 psi". In: *ACI J. Proc.* 1993.

[117] ASTM C796M-12. "Standard test method for foaming agents for use in producing cellular concrete using preformed foam, Annual Book of ASTM Standards". In: *ASTM International, West Conshohocken, PA,* (2012).

[118] Simon Van Dijk. *Foamed Concrete: A Dutch View*. British Cement Association, 1991.

[119] Amarnath Yerramala and C. Ramachandrudu. "Production and properties of foamed concrete". In: *Indian Concrete Institute* (2013).

[120] EP Kearsley and HF Mostert. "Designing mix composition of foamed concrete with high fly ash contents". In: *Use of Foamed Concrete in Construction: Proceedings of the International Conference held at the University of Dundee, Scotland, UK on 5 July 2005*. Thomas Telford Publishing. 2005, pp. 29–36.

[121] EK Kunhanandan Nambiar and K Ramamurthy. "Models relating mixture composition to the density and strength of foam concrete using response surface methodology". In: *Cement and Concrete Composites* 28.9 (2006), pp. 752–760.

[122] MR Jones and A McCarthy. "Preliminary views on the potential of foamed concrete as a structural material". In: *Magazine of concrete research* 57.1 (2005), pp. 21–31.

[123] Roderick Jones, Li Zheng, Amarnath Yerramala, and Kharidu Srinivasa Rao. "Use of recycled and secondary aggregates in foamed concretes". In: *Magazine of concrete research* 64.6 (2012), pp. 513–525.

[124] She Wei, Zhang Yunsheng, and MR Jones. "Using the ultrasonic wave transmission method to study the setting behavior of foamed concrete". In: *Construction and Building Materials* 51 (2014), pp. 62–74.

[125] Kezban Ozlutas. "Behaviour of ultra-low density foamed concrete". PhD thesis. University of Dundee, 2015.

[126] T Richard, Joseph Dobogai, T Gerhardt, and W Young. "Cellular concrete-A potential load-bearing insulation for cryogenic applications?" In: *IEEE Transactions on Magnetics* 11.2 (1975), pp. 500–503.

[127] S Karl and JD Wörner. "Foamed concrete-mixing and workability". In: *Special concrete-workability and mixing*. E&FN Spon London, 1993, pp. 217–224.

[128] Sanghyeong Lim, Hyunwook Choo, Woojin Lee, and Changho Lee. "Development of controlled low strength material (CLSM) using self-cementitious fly ash". In: *19th International Conference on Soil Mechanics and Geotechnical Engineering, ICSMGE 2017*. 2017.

[129] Chao Lung Hwang, Chi Hung Chiang, Trong Phuoc Huynh, and Bo Jyun Jhang. "Evaluation of Fresh Properties of Controlled Low-Strength Material Produced from Water Treatment Sludge-Fly Ash-Slag Mixture Using Alkaline Activation". In: *Applied Mechanics and Materials*. Vol. 878. Trans Tech Publ. 2018, pp. 28–34.

[130] Tan Manh Do, Young Sang Kim, Gyeong O Kang, My Quoc Dang, and Thien Quoc Tran. "Thermal Conductivity of Controlled Low Strength Material (CLSM) Made Entirely from By-Products". In: *Key Engineering Materials*. Vol. 773. Trans Tech Publ. 2018, pp. 244–248.

[131] LK Crouch, Vernon J Dotson, Daniel A Badoe, Richard A Maxwell, Timothy R Dunn, and Alan Sparkman. "Long term study of 23 excavatable Tennessee flowable fill mixtures". In: *Journal of ASTM International* 1.6 (2004), pp. 1–11.

[132] MR Jones and A McCarthy. "Utilising unprocessed low-lime coal fly ash in foamed concrete". In: *Fuel* 84.11 (2005), pp. 1398–1409.

[133] MR Jones and A McCarthy. "Heat of hydration in foamed concrete: Effect of mix constituents and plastic density". In: *Cement and concrete research* 36.6 (2006), pp. 1032–1041.

[134] EP Kearselya. "Properties of foamed concrete as influenced by air-void parameters". In: *Concrete Beton* 101 (2002), pp. 8–14.

[135] EK Kunhanandan Nambiar and K Ramamurthy. "Shrinkage behavior of foam concrete". In: *Journal of materials in civil engineering* 21.11 (2009), pp. 631–636.

[136] Khalid Farrag. "Controlled low-strength material used around buried pipelines". In: *Transportation Research Record: Journal of the Transportation Research Board* 2251 (2011), pp. 157–164.

[137] ME Ayers, SZ Wong, and W Zaman. "Optimization of flowable fill mix proportions". In: *Special Publication* 150 (1994), pp. 15–38.

[138] T Sugama, LE Brothers, and TR Van de Putte. "Acid-resistant cements for geothermal wells: sodium silicate activated slag/fly ash blends". In: *Advances in cement research* 17.2 (2005), pp. 65–75.

[139] NK Lee and HK Lee. "Setting and mechanical properties of alkali-activated fly ash/slag concrete manufactured at room temperature". In: *Construction and Building Materials* 47 (2013), pp. 1201–1209.

[140] Tri Ho Minh Le, DW Park, JW Seo, JW Lee, and KJ Kim. "Applicability Evaluation of Ponded Ash as a Sustainable Backfill Material Using Air Foam". In: *Fourth International Conference on Sustainable Construction Materials and Technologies, Las Vegas, USA*. 2016.

[141] Subnahmanya Bhat. "Use of Coal Combustion Residues and Foundry Sands in Flowable Fill". PhD thesis. Purdue University, 1996.

[142] Chao Lung Hwang and Trong Phuoc Huynh. "Characteristics of alkali-activated controlled low-strength material derived from red mud-slag blends". In: *Key Engineering Materials*. Vol. 753. Trans Tech Publ. 2017, pp. 343–348.

[143] Angel Abelleira, Neal S Berke, and David G Pickering. "Corrosion activity of steel in cementitious controlled low-strength materials vs. that in soil". In: *The Design and Application of Controlled Low-Strength Materials (Flowable Fill)*. ASTM International, 1998.

[144] Harsh Shah. *Controlled Low Strength Material (CLSM) produced from limestone fines and other byproducts*. University of Missouri-Kansas City, 2012.

[145] ASTM C143. "Standard Test Method for Slump of Hydraulic-Cement Concrete". In: *ASTM International, West Conshohocken, PA*, (2015).

[146] ASTM C939. "Standard Test Method for Flow of Grout for Preplaced-Aggregate Concrete (Flow Cone Method)". In: *ASTM International, West Conshohocken, PA*, (2016).

[147] ASTM D6103. "Standard Test Method for Flow Consistency of Controlled Low Strength Material (CLSM)". In: *ASTM International, West Conshohocken, PA* (2017).

[148] Himanshu Tripathi, Charles E Pierce, Sarah L Gassman, and Travis W Brown. "Methods for field and laboratory measurement of flowability and setting time of controlled low-strength materials". In: *Journal of ASTM international* 1.6 (2004), pp. 1–15.

[149] AK Howard. "Flowable fill solves pipe backfilling problems". In: *Proceedings of the international conference on soil mechanics and foundation engineering-international society for soil mechanics and foundation engineering*. Vol. 3. AA BALKEMA. 1997, pp. 1609–1612.

[150] Washington Aggregates and Concrete Association. "Suggested Specifications for Controlled Density Fill". In: *Settle, Washington* (1992).

[151] ACI. *Controlled Low-Strength Materials (CLSM)*. ACI 229R-94 Report, 1994. American Concrete Institute, 1994.

[152] Jon I Mullarky. "Long term strength gain of controlled low-strength materials". In: *The design and application of controlled low-strength materials (flowable fill)*. ASTM International, 1998.

[153] David W Law, Andi Arham Adam, Thomas K Molyneaux, and Indubhushan Patnaikuni. "Durability assessment of alkali activated slag (AAS) concrete". In: *Materials and Structures* 45.9 (2012), pp. 1425–1437.

[154] Fernando Pacheco-Torgal, Joao Labrincha, Cristina Leonelli, A Palomo, and P Chindaprasit. *Handbook of alkali-activated cements, mortars and concretes*. Elsevier, 2014.

[155] Konstantin Kovler and Nicolas Roussel. "Properties of fresh and hardened concrete". In: *Cement and Concrete Research* 41.7 (2011), pp. 775–792.

[156] Laurent Josserand, Olivier Coussy, and François De Larrard. "Bleeding of concrete as an ageing consolidation process". In: *Cement and concrete research* 36.9 (2006), pp. 1603–1608.

[157] Lianxiang Du. "Laboratory investigations of controlled low-strength material". In: (2001).

[158] ASTM C940. "Standard Test Method for Expansion and Bleeding of Freshly Mixed Grouts for Preplaced-Aggregate Concrete in the Laboratory". In: *ASTM International, West Conshohocken, PA* (2016).

[159] Robert J Hoopes. "Engineering properties of air-modified controlled low-strength material". In: *The design and application of controlled low-strength materials (flowable fill)*. ASTM International, 1998.

[160] František Škvára, Josef Doležal, Pavel Svoboda, Lubomír Kopecký, Simona Pawlasová, Martin Lucuk, et al. "Concrete based on fly ash geopolymers". In: *Proceedings of 16th IBAUSIL* 1 (2006), pp. 1079–1097.

[161] Prinya Chindaprasirt, T Chareerat, and Vute Sirivivatnanon. "Workability and strength of coarse high calcium fly ash geopolymer". In: *Cement and concrete composites* 29.3 (2007), pp. 224–229.

[162] A Poulesquen, F Frizon, and D Lambertin. "Rheological behavior of alkali-activated metakaolin during geopolymerization". In: *Journal of Non-Crystalline Solids* 357.21 (2011), pp. 3565–3571.

[163] Hossein Rostami and William Brendley. "Alkali ash material: a novel fly ash-based cement". In: *Environmental science & technology* 37.15 (2003), pp. 3454–3457.

[164] Djwantoro Hardjito and B Vijaya Rangan. "Development and properties of low-calcium fly ash-based geopolymer concrete". In: (2005).

[165] C Marín-López, JL Reyes Araiza, A Manzano-Ramírez, JC Rubio Avalos, JJ Perez-Bueno, MS Muñiz-Villareal, et al. "Synthesis and characterization of a concrete based on metakaolin geopolymer". In: *Inorganic Materials* 45.12 (2009), p. 1429.

[166] Djwantoro Hardjito, Steenie E Wallah, Dody MJ Sumajouw, and B Vijaya Rangan. "On the development of fly ash-based geopolymer concrete". In: *Materials Journal* 101.6 (2004), pp. 467–472.

[167] ASTM C232. "Standard Test Method for Bleeding of Concrete". In: *ASTM International, West Conshohocken, PA* (2014).

[168] ASTM C1611. "Standard Test Method for Slump Flow of Self-Consolidating Concrete". In: *ASTM International, West Conshohocken, PA* (2018).

[169] ASTM C1610. "Standard Test Method for Static Segregation of Self-Consolidating Concrete Using Column Technique". In: *ASTM International, West Conshohocken, PA* (2017).

[170] ALDOT-452. *Sieve stability test for self-consolidating concrete ALDOT Procedures*. Tech. rep. ALDOT-452. Alabama Dept. of Transportation., 2015.

[171] RJ McLaren and NJ Balsamo. *Fly ash design manual for road and site applications. Volume 2: Slurried placement*. Tech. rep. Monroeville, PA, (USA): GAI Consultants, Inc., 1986.

[172] USACE ETL-1110-3-496. "LABORATORY SOILS TESTING". In: *U.S. Army Corps of Engineers Washington, D. C.* (1998).

[173] M Lachemi, KMA Hossain, M Shehata, and W Thaha. "Controlled low strength materials incorporating cement kiln dust from various sources". In: *Cement and Concrete Composites* 30.5 (2008), pp. 381–392.

[174] Donna L Boreck and RE Miller. "Effects of remote drop and pumpdown placement on cellular concrete". In: (1995).

[175] D Aldridge. "Introduction to foamed concrete: what, why, how?" In: *Use of Foamed Concrete in Construction: Proceedings of the International Conference held at the University of Dundee, Scotland, UK on 5 July 2005*. Thomas Telford Publishing. 2005, pp. 1–14.

[176] M Roderick Jones and Li Zheng. "Energy absorption of foamed concrete from low-velocity impacts". In: *Magazine of Concrete Research* 65.4 (2013), pp. 209–219.

[177] EK Kunhanandan Nambiar and K Ramamurthy. "Sorption characteristics of foam concrete". In: *Cement and concrete research* 37.9 (2007), pp. 1341–1347.

[178] M Roderick Jones, Kezban Ozlutas, and Li Zheng. "Stability and instability of foamed concrete". In: *Magazine of Concrete Research* 68.11 (2016), pp. 542–549.

[179] ITU. *Low impact trenching technique for FTTx networks*. L.155 Optical fibre cables – Guidance and installation technique. Telecommunication standardization sector of ITU, 2016. URL: https://www.itu.int/rec/dologin_pub.asp?lang=e\&id=T-REC-L.155-201611-I!!PDF-E\&type=items (visited on 03/31/2019).

[180] Anne Smith. "Controlled low-strength material". In: *Aberdeen's Concrete Construction* 36.5 (1991), p. 389.

[181] ASTM C403. "Standard Test Method for Time of Setting of Concrete Mixtures by Penetration Resistance". In: *ASTM International, West Conshohocken, PA* (2016).

[182] ASTM D6024. "Standard Test Method for Ball Drop on Controlled Low Strength Material (CLSM) to Determine Suitability for Load Application". In: *ASTM International, West Conshohocken, PA* (2016).

[183] Wei She, Yunsheng Zhang, MR Jones, and Panpan Guo. "In-situ monitoring the setting behavior of foamed concrete using ultrasonic pulse velocity method". In: *Journal of Wuhan University of Technology-Mater. Sci. Ed.* 28.6 (2013), pp. 1146–1154.

[184] Sanjay Kumar, Rakesh Kumar, and SP Mehrotra. "Influence of granulated blast furnace slag on the reaction, structure and properties of fly ash based geopolymer". In: *Journal of materials science* 45.3 (2010), pp. 607–615.

[185] MCHW. *Manual of contract documents for highway works (MCHW); volume 1 specification for highway works*. Series 1000, road pavements – concrete materials. Highway authorities and utilities committee, 2016. URL: http://www.standardsforhighways.co.uk/ha/standards/mchw/vol1/pdfs/MCHW\%201000.pdf (visited on 03/31/2019).

[186] WE Brewer. *The design and construction of small span bridges and culverts using controlled low strength materials (CLSM). Final report*. Tech. rep. Ohio Department of Transportation, 1992.

[187] Lorna J Gibson and Michael F Ashby. *Cellular solids: structure and properties*. Cambridge university press, 1999.

[188] CT Tam, TY Lim, R Sri Ravindrarajah, and SL Lee. "Relationship between strength and volumetric composition of moist-cured cellular concrete". In: *Magazine of Concrete Research* 39.138 (1987), pp. 12–18.

[189] Kevin J Folliard, Lianxiang Du, and David Trejo. "Effects of curing conditions on strength development of controlled low-strength material". In: *Materials Journal* 100.1 (2003), pp. 79–86.

[190] MS Hamidah, I Azmi, MRA Ruslan, K Kartini, and NM Fadhil. "Optimisation of foamed concrete mix of different sand-cement ratio and curing conditions". In: *Use of Foamed Concrete in Construction: Proceedings of the International Conference held at the University of Dundee, Scotland, UK on 5 July 2005*. Thomas Telford Publishing. 2005, pp. 37–44.

[191] EP Kearsley and P Booysens. "Reinforced foamed concrete-can it be durable?" In: *Concrete Beton* 91 (1998).

[192] G Kovalchuk, Ana Fernández-Jiménez, and A Palomo. "Alkali-activated fly ash: effect of thermal curing conditions on mechanical and microstructural development–Part II". In: *Fuel* 86.3 (2007), pp. 315–322.

[193] Peter Duxson, John L Provis, Grant C Lukey, Seth W Mallicoat, Waltraud M Kriven, and Jannie SJ Van Deventer. "Understanding the relationship between geopolymer composition, microstructure and mechanical properties". In: *Colloids and Surfaces A: Physicochemical and Engineering Aspects* 269.1-3 (2005), pp. 47–58.

[194] F Puertas, T Amat, A Fernández-Jiménez, and T Vázquez. "Mechanical and durable behaviour of alkaline cement mortars reinforced with polypropylene fibres". In: *Cement and Concrete Research* 33.12 (2003), pp. 2031–2036.

[195] A Palomo, MW Grutzeck, and MT Blanco. "Alkali-activated fly ashes: a cement for the future". In: *Cement and concrete research* 29.8 (1999), pp. 1323–1329.

[196] Mingyu Hu, Xiaomin Zhu, and Fumei Long. "Alkali-activated fly ash-based geopolymers with zeolite or bentonite as additives". In: *Cement and Concrete Composites* 31.10 (2009), pp. 762–768.

[197] Alexandre Silva De Vargas, Denise CC Dal Molin, Antonio CF Vilela, Felipe Jose Da Silva, Bruno Pavao, and Hugo Veit. "The effects of Na2O/SiO2 molar ratio, curing temperature and age on compressive strength, morphology and microstructure of alkali-activated fly ash-based geopolymers". In: *Cement and concrete composites* 33.6 (2011), pp. 653–660.

[198] T Bakharev, JG Sanjayan, and Y-B Cheng. "Effect of elevated temperature curing on properties of alkali-activated slag concrete". In: *Cement and concrete research* 29.10 (1999), pp. 1619–1625.

[199] Fareed Ahmed Memon, Muhd Fadhil Nuruddin, Samuel Demie, and Nasir Shafiq. "Effect of superplasticizer and extra water on workability and compressive strength of self-compacting geopolymer concrete". In: *Research Journal of Applied Sciences, Engineering and Technology* 4.5 (2012), pp. 407–414.

[200] Samuel Demie, Muhd Fadhil Nuruddin, Memon Fareed Ahmed, and Nasir Shafiq. "Effects of curing temperature and superplasticizer on workability and compressive strength of self-compacting geopolymer concrete". In: *2011 National Postgraduate Conference*. IEEE. 2011, pp. 1–5.

[201] F Nuruddin, Samuel Demie, FA Memon, and Nasir Shafiq. "Effect of superplasticizer and NaOH molarity on workability, compressive strength and microstructure properties of self-compacting geopolymer concrete". In: *World Academy of Science, Engineering and Technology* 75 (2011).

[202] ASTM D4832. "Standard Test Method for Preparation and Testing of Controlled Low Strength Material (CLSM) Test Cylinders". In: *ASTM International, West Conshohocken, PA* (2016).

[203] KJ Folliard, David Trejo, L Du, SA Sabol, and C Halmen. "Controlled low-strength material for backfill, utility bedding, void fill, and bridge approaches". In: *Research Interim Rep. No. NCHRP 24-12 (1)* (2001).

[204] Ronald L Larsen. "Sound uses of CLSMs in the environment". In: *Concrete International* 12.7 (1990), pp. 26–29.

[205] E Gennesseaux, T Sedran, JM Torrenti, and M Hardy. "Formulation of optimized excavatable cement treated materials using a new punching test apparatus". In: *Materials and Structures* 51.3 (2018), p. 56.

[206] G Bonnet, A Gavalda, and A Quibel. "Remblayage des tranchées, Utilisation de matériaux autocompactants (Trench filling with flowable cementitious material. State of the art)". In: *Etat des connaissances. Dossier Certu (in French)* 78 (1998).

[207] Kevin J Folliard. *Development of a recommended practice for use of controlled low-strength material in highway construction*. Vol. 597. Transportation Research Board, 2008.

[208] Caroline Morin. "Etude de l'excavabilité des matériaux traités aux liants hydrauliques pour tranchées (Study of cementitious material excavatability)". PhD thesis. Université Pierre et MarieCurie de Pari (in France), 2009.

[209] Mark C Webb, Timothy J McGrath, and Ernest T Selig. "Field test of buried pipe with CLSM backfill". In: *The design and application of controlled low-strength materials (flowable fill)*. ASTM International, 1998.

[210] HAMCIN. "A performance specification for controlled low strength material controlled density fill (CLSM-CDF)". In: *Hamilton County and the City of Cincinnati* (1996).

[211] City of Colorado Springs. *Backfill of Utility Trenches using Controlled Low Strength Materials (CLSM)*. Interim release: CLSM (to the City Standard Specifications Manual). 2017. URL: https://coloradosprings.gov/sites/default/files/section_206_-_interim_release_for_clsm_2.pdf (visited on 08/16/2018).

[212] Brewer and Associates. *Factors Governing The Removability Of Controlled Low Strength Material - Controlled Density Fill - (CLSM-CDF)*. 1991.

[213] Teruhisa Masada, Shad M. Sargand, Basel Abdalla, and J. Ludwig Figueroa. *Material Properties for Implementation of Mechanistic-Empirical (M-E) Pavement Design Procedures*. Technical Bulletin. Ohio Research Institute for Transportation & the Environment (ORITE), 2004.

[214] P Mellin. "Development of structural grade foamed concrete". PhD thesis. MSc dissertation, University of Dundee, 1999.

[215] YH Mugahed Amran, Nima Farzadnia, and AA Abang Ali. "Properties and applications of foamed concrete; a review". In: *Construction and Building Materials* 101 (2015), pp. 990–1005.

[216] Zuhua Zhang and Hao Wang. "The pore characteristics of geopolymer foam concrete and their impact on the compressive strength and modulus". In: *Frontiers in Materials* 3 (2016), p. 38.

[217] E Ivan Diaz-Loya, Erez N Allouche, and Saiprasad Vaidya. "Mechanical properties of fly-ash-based geopolymer concrete". In: *ACI materials journal* 108.3 (2011), p. 300.

[218] AASHTO T193. "Standard Method of Test for The California Bearing Ratio". In: *American Association of State Highway and Transportation Officials (AASHTO)* (2013).

[219] Frank G Burns. "Flowable fly ash backfill for buried pipelines". PhD thesis. University of North Carolina at Charlotte, 1990.

[220] Fernando Pons, John S Landwermeyer, and Larry Kerns. "Development of engineering properties for regular and quick-set flowable fill". In: *The design and application of controlled low-strength materials (flowable fill)*. ASTM International, 1998.

[221] K Lini Dev and RG Robinson. "Pond ash based controlled low strength flowable fills for geotechnical engineering applications". In: *International Journal of Geosynthetics and Ground Engineering* 1.4 (2015), p. 32.

[222] Jinsong Qian, Xiang Shu, Qiao Dong, Jianming Ling, and Baoshan Huang. "Laboratory characterization of controlled low-strength materials". In: *Materials & Design (1980-2015)* 65 (2015), pp. 806–813.

[223] Richard D Peindl, Rajaram Janardhanam, and Frank Burns. "Evaluation of flowable fly-ash backfill. I: Static loading". In: *Journal of geotechnical engineering* 118.3 (1992), pp. 449–463.

[224] AASHTO T274-82. "Standard method of test for resilient modulus of subgrade soils". In: *American Association of State Highway and Transportation Officials (AASHTO)* (1982).

[225] James W Mack, Chung Lung Wu, Scott Tarr, and Tarek Refai. "Model development and interim design procedure guidelines for ultra-thin whitetopping pavements." In: *Proceedings of the 6th international conference on concrete pavement design and rehabilitation, Indianapolis, USA* 1 (1997), pp. 231–256.

[226] Bertrand Pouteau, Jean-Maurice Balay, Armelle Chabot, and François De Larrard. "Fatigue test and mechanical study of adhesion between concrete and asphalt". In: *9th International Symposium on Concrete Roads, Istanbul, Turkey*. 2004.

[227] K Verhoeven. "Thin overlays of steel fiber reinforced concrete and continuously reinforced concrete: State-of-the-art in Belgium." In: *International conference on concrete pavement design and rehabilitation, Purdue Univ., West Lafayette, IN*. 1989, pp. 205–219.

[228] A Sainton. "Partenariat CIMbéton, SPECBEA, SNBPE pour le développement du béton de ciment dans les chaussées". In: *Revue Generale des Routes et des Aerodromes* 789 (2000), pp. 44–48.

[229] Simon Austin, Peter Robins, and Youguang Pan. "Shear bond testing of concrete repairs". In: *Cement and Concrete Research* 29.7 (1999), pp. 1067–1076.

[230] ASTM C1072-13e1. "Standard Test Methods for Measurement of Masonry Flexural Bond Strength, ASTM International". In: *ASTM International, West Conshohocken, PA* (2013).

[231] JS Wall and NG Shrive. "Factors affecting bond between new and old concrete". In: *Materials Journal* 85.2 (1988), pp. 117–125.

[232] JCT de S Clímaco and PE Regan. "Evaluation of bond strength between old and new concrete in structural repairs". In: *Magazine of Concrete Research* 53.6 (2001), pp. 377–390.

[233] Lawrence I Knab and Curtis B Spring. "Evaluation of test methods for measuring the bond strength of Portland cement based repair materials to concrete". In: *Cement, concrete and aggregates* 11.1 (1989), pp. 3–14.

[234] Amjad Mallat and Abdenour Alliche. "Mechanical investigation of two fiber-reinforced repair mortars and the repaired system". In: *Construction and building materials* 25.4 (2011), pp. 1587–1595.

[235] PJ Robins and SA Austin. "A unified failure envelope from the evaluation of concrete repair bond tests". In: *Magazine of Concrete Research* 47.170 (1995).

[236] BB Sabir, S Wild, and M O'farrell. "A water sorptivity test for martar and concrete". In: *Materials and Structures* 31.8 (1998), p. 568.

[237] EP Kearsley and PJ Wainwright. "Porosity and permeability of foamed concrete". In: *Cement and concrete research* 31.5 (2001), pp. 805–812.

[238] Lynton Cox and Simon van Dijk. "Foam concrete: a different kind of mix". In: *Concrete* 36.2 (2002).

[239] EP Kearsley and HF Mostert. "The use of foamed concrete in refractories". In: *Use of Foamed Concrete in Construction: Proceedings of the International Conference held at the University of Dundee, Scotland, UK on 5 July 2005*. Thomas Telford Publishing. 2005, pp. 89–96.

[240] N Narayanan and K Ramamurthy. "Structure and properties of aerated concrete: a review". In: *Cement and Concrete composites* 22.5 (2000), pp. 321–329.

[241] A Just and B Middendorf. "Microstructure of high-strength foam concrete". In: *Materials characterization* 60.7 (2009), pp. 741–748.

[242] EP Kearsley and PJ Wainwright. "The effect of porosity on the strength of foamed concrete". In: *Cement and concrete research* 32.2 (2002), pp. 233–239.

[243] ASTM D5084. "Standard Test Methods for Measurement of Hydraulic Conductivity of Saturated Porous Materials Using a Flexible Wall Permeameter". In: *ASTM International, West Conshohocken, PA* (2016).

[244] ASTM D2435. "Standard Test Methods for One-Dimensional Consolidation Properties of Soils Using Incremental Loading". In: *ASTM International, West Conshohocken, PA* (2011).

[245] Binod Tiwari, Beena Ajmera, Ryan Maw, Ryan Cole, Diego Villegas, and Peter Palmerson. "Mechanical properties of lightweight cellular concrete for geotechnical applications". In: *Journal of Materials in Civil Engineering* 29.7 (2017), p. 06017007.

[246] G McGovern. "Manufacture and supply of ready-mix foamed concrete". In: *One Day Awareness Seminar on Foamed Concrete: Properties, Applications and Potential, University of Dundee, Scotland*. 2000, pp. 12–25.

[247] A. McCarthy. "Thermally insulating foundations and ground slabs for sustainable housing using foamed concrete". PhD thesis. University of Dundee, 2004.

[248] Ahmad Farhan Roslan, Hanizam Awang, and Md Azree Othuman Mydin. "Effects of various additives on drying shrinkage, compressive and flexural strength of lightweight foamed concrete (LFC)". In: *Advanced Materials Research*. Vol. 626. Trans Tech Publ. 2013, pp. 594–604.

[249] Zuhua Zhang, John L Provis, Andrew Reid, and Hao Wang. "Geopolymer foam concrete: An emerging material for sustainable construction". In: *Construction and Building Materials* 56 (2014), pp. 113–127.

[250] Adam M Neville. *Properties of concrete*. Vol. 4. Longman London, 1995.

[251] P Schubert. "Shrinkage behaviour of aerated concrete". In: *Autoclaved Aerated Concrete, Moisture and Properties. Amsterdam: Elsevier* (1983), pp. 207–17.

[252] Frank Collins and Jay G Sanjayan. "Strength and shrinkage properties of alkali-activated slag concrete containing porous coarse aggregate". In: *Cement and Concrete Research* 29.4 (1999), pp. 607–610.

[253] E Douglas, A Bilodeau, and VM Malhotra. "Properties and durability of alkali-activated slag concrete". In: *Materials Journal* 89.5 (1992), pp. 509–516.

[254] K Ramamurthy and N Narayanan. "Influence of composition and curing on drying shrinkage of aerated concrete". In: *Materials and structures* 33.4 (2000), pp. 243–250.

[255] B Singh, G Ishwarya, M Gupta, and SK Bhattacharyya. "Geopolymer concrete: A review of some recent developments". In: *Construction and building materials* 85 (2015), pp. 78–90.

[256] P Kumar Mehta. "High-performance, high-volume fly ash concrete for sustainable development". In: *Proceedings of the international workshop on sustainable development and concrete technology*. Iowa State University Ames, IA, USA. 2004, pp. 3–14.

[257] S Gandham, R Seals, and Paul Foxworthy. "Phosphogypsum as a component of flowable fill". In: *Transportation Research Record: Journal of the Transportation Research Board* 1546 (1996), pp. 79–87.

[258] Douglas A Lucht. "Thermal performance of flowable fill mixtures for horizontal GSHP systems". PhD thesis. Mechanical Engineering Department, South Dakota State University, 1995.

[259] ASTM C596. "Standard Test Method for Drying Shrinkage of Mortar Containing Hydraulic Cement". In: *ASTM International, West Conshohocken, PA,* (2017).

[260] Prinya Chindaprasirt and Ubolluk Rattanasak. "Shrinkage behavior of structural foam lightweight concrete containing glycol compounds and fly ash". In: *Materials & Design* 32.2 (2011), pp. 723–727.

[261] BS EN 680:2005. "Determination of the drying shrinkage of autoclaved aerated concrete". In: *British Standards Institution (BSI), UK* (2006).

[262] Julia Shekhovtsova, Maxim Kovtun, and Elsabe P Kearsley. "Evaluation of short-and long-term properties of heat-cured alkali-activated fly ash concrete". In: *Magazine of Concrete Research* 67.16 (2015), pp. 897–905.

[263] A Castel, SJ Foster, T Ng, JG Sanjayan, and RI Gilbert. "Creep and drying shrinkage of a blended slag and low calcium fly ash geopolymer Concrete". In: *Materials and Structures* 49.5 (2016), pp. 1619–1628.

[264] Md Rashadul Islam and Rafiqul A Tarefder. "Coefficients of thermal contraction and expansion of asphalt concrete in the laboratory". In: *Journal of Materials in Civil Engineering* 27.11 (2015), p. 04015020.

[265] Michael S Mamlouk, Matthew W Witczak, Kamil E Kaloush, and Nasreen Hasan. "Determination of thermal properties of asphalt mixtures". In: *Journal of Testing and Evaluation* 33.2 (2005), pp. 118–126.

[266] Carlos R Cruz and M Gillen. "Thermal expansion of Portland cement paste, mortar and concrete at high temperatures". In: *Fire and materials* 4.2 (1980), pp. 66–70.

[267] Pongsak Choktaweekarn and Somnuk Tangtermsirikul. "A model for predicting coefficient of thermal expansion of cementitious Paste". In: *ScienceAsia* 35.1 (2009), pp. 57–63.

[268] PB Bamforth, GMN Baston, JA Berry, FP Glasser, TG Heath, CP Jackson, et al. "Cement materials for use as backfill, sealing and structural materials in geological disposal concepts. A review of current status". In: *Serco, United Kingdom, RP0618-252A* (2012).

[269] P Shah and SH Ahmad. "High Performance Concretes and Applications. 90 Tottenham Court Road". In: *London W1P 9HE* (1994), pp. 141–374.

[270] Tayfun Uygunoğlu and İlker Bekir Topçu. "Thermal expansion of self-consolidating normal and lightweight aggregate concrete at elevated temperature". In: *Construction and Building Materials* 23.9 (2009), pp. 3063–3069.

[271] RC Valore. "Foam and gas concretes". In: *Structural foams, Proceedings of a conference presented as part of the 1960 Fall Conference of the Building Research Institute. National Academy of Sciences–National Research Council, publication*. Vol. 892. 1961.

[272] Hebel. *Technical Hebel AAC properties*. 2013. URL: https://www.hebel-usa.com/en/content/technical_features_2533.php (visited on 08/16/2018).

[273] Leyla Tanaçan, Halit Yaşa Ersoy, and Ümit Arpacıoğlu. "Effect of high temperature and cooling conditions on aerated concrete properties". In: *Construction and Building Materials* 23.3 (2009), pp. 1240–1248.

[274] Adam M Neville. "Properties of Concrete, 4th". In: *London Pearson Education Limited* 443.846 (2011), p. 444.

[275] Anol K. Mukhopadhyay, Siddharth Neekhra, and Dan G. Zollinger. *Preliminary characterization of aggregate coefficient of thermal expansion and gradation for paving concrete*. Tech. rep. FHWA/TX-05/0-1700-5. United States. Federal Highway Administration., 2004.

[276] X Qian and L Zheng. "The study of thermal expansion coefficient about fly-ash aerated concrete". In: *Silicate Building Products* 90.2 (1990), pp. 1–3.

[277] Ramesh C Joshi and RP Lohita. *Fly ash in concrete: production, properties and uses*. Vol. 2. CRC Press, 1997.

[278] Zhong-he Shui, Rui Zhang, Wei Chen, and Dong-xing Xuan. "Effects of mineral admixtures on the thermal expansion properties of hardened cement paste". In: *Construction and Building Materials* 24.9 (2010), pp. 1761–1767.

[279] Jianxin Ma and Frank Dehn. "Investigations on the coefficient of thermal expansion of a low-calcium fly ash-based geopolymer concrete". In: *Structural Concrete* 18.5 (2017), pp. 781–791.

[280] Roman Loser, Beat Münch, and Pietro Lura. "A volumetric technique for measuring the coefficient of thermal expansion of hardening cement paste and mortar". In: *Cement and Concrete Research* 40.7 (2010), pp. 1138–1147.

[281] Jung Heum Yeon, Seongcheol Choi, and Moon C Won. "In situ measurement of coefficient of thermal expansion in hardening concrete and its effect on thermal stress development". In: *Construction and Building Materials* 38 (2013), pp. 306–315.

[282] Ippei Maruyama and Atsushi Teramoto. "Impact of time-dependant thermal expansion coefficient on the early-age volume changes in cement pastes". In: *Cement and Concrete Research* 41.4 (2011), pp. 380–391.

[283] Ippei Maruyama, Atsushi Teramoto, and Go Igarashi. "Strain and thermal expansion coefficients of various cement pastes during hydration at early ages". In: *Materials and structures* 47.1-2 (2014), pp. 27–37.

[284] Daniel Cusson and Ted Hoogeveen. "Measuring early-age coefficient of thermal expansion in high-performance concrete". In: *International RILEM Conference on Volume Changes of Hardening Concrete: Testing and Mitigation*. RILEM Publications SARL. 2006, pp. 321–330.

[285] M Viviani, B Glisic, and IFC Smith. "Separation of thermal and autogenous deformation at varying temperatures using optical fiber sensors". In: *Cement and Concrete Composites* 29.6 (2007), pp. 435–447.

[286] AASHTO T336. "Standard method of test for coefficient of thermal expansion of hydraulic cement concrete". In: *American Association of State Highway and Transportation Officials (AASHTO)* (2015).

[287] William C Krell. "Flowable fly ash". In: *Transportation Research Record* 1234 (1989), pp. 8–12.

[288] Tommy Edward Nantung. "Design criteria for controlled low strength materials". In: (1993).

[289] D Gress. *The Effect of Freeze-Thaw and Frost Heaving on Flowable Fill*. Tech. rep. 1996.

[290] Paul J Tikalsky, James Pospisil, and William MacDonald. "A method for assessment of the freeze–thaw resistance of preformed foam cellular concrete". In: *Cement and concrete research* 34.5 (2004), pp. 889–893.

[291] Wei She, Yi Du, Guotang Zhao, Pan Feng, Yunsheng Zhang, and Xiaoyu Cao. "Influence of coarse fly ash on the performance of foam concrete and its application in high-speed railway roadbeds". In: *Construction and Building Materials* 170 (2018), pp. 153–166.

[292] ASTM D560. "Standard Test Methods for Freezing and Thawing Compacted Soil-Cement Mixtures". In: *ASTM International, West Conshohocken, PA* (2016).

[293] F Pacheco-Torgal, Zahra Abdollahnejad, AF Camões, M Jamshidi, and Yining Ding. "Durability of alkali-activated binders: a clear advantage over Portland cement or an unproven issue?" In: *Construction and Building Materials* 30 (2012), pp. 400–405.

[294] John L Provis. "Alkali-activated materials". In: *Cement and Concrete Research* 114 (2018), pp. 40–48.

[295] Peijiang Sun and Hwai-Chung Wu. "Chemical and freeze–thaw resistance of fly ash-based inorganic mortars". In: *Fuel* 111 (2013), pp. 740–745.

[296] Zhang Yunsheng and Sun Wei. "Fly ash based geopolymer concrete". In: *Indian concrete journal* 80.1 (2006), pp. 20–24.

[297] R Janardhanatn, F Burns, and RD Peindl. "Mix design for flowable fly-ash backfill material". In: *Journal of Materials in Civil Engineering* 4.3 (1992), pp. 252–263.

[298] ASTM C666. "Standard Test Method for Resistance of Concrete to Rapid Freezing and Thawing". In: *ASTM International, West Conshohocken, PA* (2015).

[299] Shyi Min Lu, Ching Lu, Kuo Tung Tseng, Falin Chen, and Chen Liang Chen. "Energy-saving potential of the industrial sector of Taiwan". In: *Renewable and Sustainable Energy Reviews* 21 (2013), pp. 674–683.

[300] PM Jarrett, ANS Beaty, and AS Wojcik. "Cold-mix asphalt technology at temperatures below 10°C (with discussion)". In: *Association of Asphalt Paving Technologists Proceedings*. Vol. 53. 1984.

[301] D. Hendrickson and J. Braun. *Patching road beds*. US Patent App. 14/202,431. 2015. URL: https://www.google.com/patents/US20150252533.

[302] Altan Yilmaz and S Sargin. "Water effect on deteriorations of asphalt pavements". In: *Online J. of Sci. and Tech* 2.1 (2012).

[303] Yong-Rak Kim, Jun Zhang, and Hoki Ban. "Moisture damage characterization of warm-mix asphalt mixtures based on laboratory-field evaluation". In: *Construction and Building Materials* 31 (2012), pp. 204–211.

[304] John Read and David Whiteoak. *The shell bitumen handbook*. Thomas Telford, 2003.

[305] Sinan Hınıslıoğlu and Emine Ağar. "Use of waste high density polyethylene as bitumen modifier in asphalt concrete mix". In: *Materials letters* 58.3 (2004), pp. 267–271.

[306] Taher Baghaee Moghaddam, Mehrtash Soltani, and Mohamed Rehan Karim. "Experimental characterization of rutting performance of polyethylene terephthalate modified asphalt mixtures under static and dynamic loads". In: *Construction and Building Materials* 65 (2014), pp. 487–494.

[307] Qiang Li, Fujian Ni, Lei Gao, Qingquan Yuan, and Yuanjie Xiao. "Evaluating the rutting resistance of asphalt mixtures using an advanced repeated load permanent deformation test under field conditions". In: *Construction and Building Materials* 61 (2014), pp. 241–251.

[308] Matias Mario Mendez Larrain. "Analytical modeling of rutting potential of asphalt mixes using Hamburg wheel tracking device". PhD thesis. 2015.

[309] Ali Maher, Nenad Gucunski, William Yanko, and Fotina Petsi. "Evaluation of pothole patching materials". In: *Report No. FHWA NJ 2001-02*. 2001.

[310] Prithvi S Kandhal and L Allen Cooley. *Accelerated laboratory rutting tests: Evaluation of the asphalt pavement analyzer*. 508. Transportation Research Board, 2003.

[311] John T Harvey and Qing Lu. "Investigation of Conditions for Moisture Damage in Asphalt Concrete and Appropriate Laboratory Test Methods". In: *Institute of Transportation Studies* (2005).

[312] Yetkin Yildirim and Kenneth H Stokoe. "Analysis of Hamburg wheel tracking device results in relation to field performance". In: *Project Report No. 0-4185-S*. 2006.

[313] Vanessa I. Rosales-Herrera, Jolanda Prozzi, and Jorge A. Prozzi. "Mixture design and performance-based specifications for cold patching mixtures". In: *FHWA/TX-08/0-4872-2*. 2007.

[314] Anna Abela Munyagi. "Evaluation of cold asphalt patching mixes". PhD thesis. Stellenbosch: University of Stellenbosch, 2007.

[315] Min-Chih Liao, Chih-Chi Luo, Tai-Yen Wang, and Xuecheng Xie. "Developing Effective Test Methods for Evaluating Cold-Mix Asphalt Patching Materials". In: *Journal of Materials in Civil Engineering* (2016), pp. 040161081–10.

[316] J Minegishi, T Takeda, M Tatsushita, H Ohki, and S Wataya. "A study on cold mixtures for pothole repair in Tokyo". In: *The 11th International Conference on Asphalt Pavements. ISAP, Nagoya.(on CD-ROM)*. 2010.

[317] ASTM. "Standard Specification for Cold-Mixed, Cold-Laid Bituminous Paving Mixtures". In: *D4215 – 07*. Philadelphia, Pa.: ASTM, 2013.

[318] *Construction specification for cold mixed, cold laid, open and dense graded bituminous mix. OPSS 309*. Ontario Provincial Standard Specification. 2013.

[319] DA Anderson, HR THOMAS, Z Siddiqui, and DD Krivohlavek. *More effective cold, wet weather patching materials for asphalt pavements. Final report*. Tech. rep. FHWA-RD-88-001. 1988.

[320] Cheng Ling, Raquel Moraes, Daniel Swiertz, and Hussain Bahia. "Measuring the influence of aggregate coating on the workability and moisture susceptibility of cold-mix asphalt". In: *Transportation Research Record: Journal of the Transportation Research Board* 2372 (2013), pp. 46–52.

[321] K. L. Smith. *Innovative Materials and Equipment for Pavement Surface Repairs, Final Report. Volumes I and II*. Strategic Highway Research Report No. SHRP-M/UFR-91-504. Washington, D.C.: National Research Council, 1991.

[322] AASHTO. "Determining the Asphalt Binder Content of Hot Mix Asphalt (HMA) by the Ignition Method". In: *T 308-10*. 30th. Washington, D.C.: AASHTO, 2015.

[323] AASHTO. "Mechanical Analysis of Extracted Aggregate". In: *T 30-15*. Washington, D.C.: AASHTO, 2015.

[324] AASHTO. "Moisture Content of Asphalt Mixtures by Oven Method". In: *T 329-15*. Washington, D.C.: AASHTO, 2015.

[325] HU Bahia and A Stakston. "The effect of fine aggregate angularity, asphalt content and performance graded asphalts on hot mix asphalt performance". In: *Wisconsin Highway Research Program* 92 (2003), pp. 45–98.

[326] Amir Golalipour, Ehsan Jamshidi, Yunus Niazi, Zahra Afsharikia, and Mahmood Khadem. "Effect of aggregate gradation on rutting of asphalt pavements". In: *Procedia-Social and Behavioral Sciences* 53 (2012), pp. 440–449.

[327] John P Zaniewski and David Diazgranados Diaz. "Evaluation of 4.75 mm Superpave Mix Criteria for West Virginia". In: *Report*. Morgantown, West Virginia, 2004.

[328] Mesut Tigdemir, Mustafa Karasahin, and Zekai Sen. "Investigation of fatigue behaviour of asphalt concrete pavements with fuzzy-logic approach". In: *International Journal of Fatigue* 24.8 (2002), pp. 903–910.

[329] Ercan Ozgan. "Artificial neural network based modelling of the Marshall Stability of asphalt concrete". In: *Expert Systems with Applications* 38.5 (2011), pp. 6025–6030.

[330] Ahmad H Aljassar, Sayed Metwali, and Mohammed A Ali. "Effect of filler types on Marshall stability and retained strength of asphalt concrete". In: *International Journal of Pavement Engineering* 5.1 (2004), pp. 47–51.

[331] Freddy L Roberts, Prithvi S Kandhal, E Ray Brown, Dah Yinn Lee, and Thomas W Kennedy. "Hot mix asphalt materials, mixture design and construction, 2nd Ed." In: (1996).

[332] F. Hattatoglu, S. Hinislioglu, H. F. Bayata, O Ü. Bayrak, and N. Tepe. "Modeling of Marshall Quotient of Hot Mix Asphalts by Artificial Neural Networks". In: *International Conference on Engineering and Natural Sciences (ICENS)*. Macedonia, 2015.

[333] Thomas P Wilson and A Russell Romine. *Innovative materials development and testing. Volume 2: Pothole repair*. SHRP-H-353. 1993.

[334] *Porous asphalt concrete pavement, Chapter 02798*. Taipei, Taiwan: Public Construction Commission specification, 2010.

[335] ASTM. "Standard Test Method for Marshall Stability and Flow of Asphalt Mixtures". In: *D6927-15*. West Conshohocken, PA.: ASTM, 2015.

[336] Süreyya Tayfur, Halit Ozen, and Atakan Aksoy. "Investigation of rutting performance of asphalt mixtures containing polymer modifiers". In: *Construction and Building Materials* 21.2 (2007), pp. 328–337.

[337] AASHTO. "Standard Method of Test for Resistance of Compacted Hot Mix Asphalt (HMA) to Moisture-Induced Damage". In: *T 283-14*. Washington, D.C.: AASHTO, 2014.

[338] EL Dukatz Jr and RS Phillips. "The effect of air voids on the tensile strength ratio (with discussion)". In: *Association of Asphalt Paving Technologists Proc*. Vol. 56. 1987.

[339] AASHTO. "Hamburg Wheel-Track Testing of Compacted Hot Mix Asphalt (HMA)". In: *T 324-11*. Washington, D.C.: AASHTO, 2013.

[340] FHWA. *Hamburg Wheel-Tracking Device*. Bituminous Mixtures Laboratory, Federal Highway Administration, 1997.

[341] Manfred N Partl, Hussain U Bahia, Francesco Canestrari, Chantal De la Roche, Hervé Di Benedetto, Herald Piber, et al. *Advances in interlaboratory testing and evaluation of bituminous materials: state-of-the-art report of the RILEM technical committee 206-ATB*. Vol. 9. Springer Science & Business Media, 2012.

[342] Tim Aschenbrener. "Evaluation of Hamburg wheel-tracking device to predict moisture damage in hot-mix asphalt". In: *Transportation Research Record* 1492 (1995), pp. 193–201.

[343] Pedro Romero and Kevin Stuart. "Evaluating Accelerated Rut Testers". In: *Public Roads* 62.1 (1998).

[344] EBA. *Street Cold Asphalt, Preliminary Sampling and Testing Services*". EBA Engineering Consultants Ltd. <Personal communication>. 2011.

[345] AASHTO. "Theoretical maximum specific gravity (Gmm) and density of Hot Mix Asphalt (HMA)". In: *T 209-12*. Washington, D.C.: AASHTO, 2015.

[346] Selena Lavorato, Steve Manolis, Gelu Vasiliu, Bryan Hughes, Sean Zimmerman, and Ryon Reid. "Evaluation of Laboratory and Field Performance of High Performance Cold Mix Patching Material with Reduced Volatile Organic Compound Content". In: Canadian Technical Asphalt Association, CTAA, 2013.

[347] Samrat Chatterjee, Ronald P White, Andre Smit, Jolanda Prozzi, and Jorge A Prozzi. *Development of mix design and testing procedures for cold patching mixtures*. Tech. rep. FHWA/TX-05/0-4872-1. 2006.

[348] Amir Mehrara and Ali Khodaii. "Evaluation of asphalt mixtures' moisture sensitivity by dynamic creep test". In: *Journal of Materials in Civil Engineering* 23.2 (2010), pp. 212–219.

[349] Louay Mohammad, Chris Abadie, Rana Gokmen, and Anand Puppala. "Mechanistic evaluation of hydrated lime in hot-mix asphalt mixtures". In: *Transportation Research Record: Journal of the Transportation Research Board* 1723 (2000), pp. 26–36.

[350] NM Jackson and CD Baldwin. "Assessing the relative rutting susceptibility of HMA in the laboratory with the asphalt pavement analyzer". In: *International Journal of Pavement Engineering* 1.3 (2000), pp. 203–217.

[351] Emad Kassem, Eyad Masad, Robert Lytton, and Arif Chowdhury. "Influence of air voids on mechanical properties of asphalt mixtures". In: *Road Materials and Pavement Design* 12.3 (2011), pp. 493–524.

[352] Graham C. Hurley and Brian D. Prowell. *Evaluation of Evotherm for use in warm mix asphalt*. Rep. No. NCAT 06-02. 2006.

[353] Farnaz Batool and Vivek Bindiganavile. "Thermal Conductivity of Hydrated Paste in Cement-Based Foam Microstructure". In: *Advances in Civil Engineering Materials* 7.1 (2018), pp. 17–32.

[354] CSA A3000. "Cementitious Materials Compendium." In: *Canadian Standards Association, Mississauga,Ontario, Canada* (2008).

[355] Vivek Bindiganavile, Farnaz Batool, and Narayana Suresh. "Effect of fly ash on thermal properties of cement based foams evaluated by transient plane heat source". In: *Indian Concrete Journal* 86.11 (2012), p. 7.

[356] HK Lee, KM Lee, and BG Kim. "Autogenous shrinkage of high-performance concrete containing fly ash". In: *Magazine of Concrete Research* 55.6 (2003), pp. 507–515.

[357] ASTM C618-17a. "Standard specification for coal fly ash and raw or calcined natural pozzolan for use in concrete". In: *ASTM International, West Conshohocken, PA* (2017).

[358] Alexander I Kudyakov and Alexey B Steshenko. "Cement Foam Concrete with Low Shrinkage". In: *Advanced Materials Research*. Vol. 1085. Trans Tech Publ. 2015, pp. 245–249.

[359] EP Kearsley and HF Mostert. "The effect of fibre reinforcing on foamed concrete behaviour". In: *Role of Concrete In Sustainable Development: Proceedings of the International Symposium dedicated to Professor Surendra Shah, Northwestern University, USA held on 3–4 September 2003 at the University of Dundee, Scotland, UK*. Thomas Telford Publishing. 2003, pp. 557–566.

[360] Muhammad Mamun and Vivek Bindiganavile. "Sulphate resistance of fibre reinforced cement-based foams". In: *Construction and Building Materials* 25.8 (2011), pp. 3427–3442.

[361] HHK Xu, FC Eichmiller, and PR Barndt. "Effects of fiber length and volume fraction on the reinforcement of calcium phosphate cement". In: *Journal of Materials Science: Materials in Medicine* 12.1 (2001), pp. 57–65.

[362] Yiping Ma, Beirong Zhu, and Muhua Tan. "Properties of ceramic fiber reinforced cement composites". In: *Cement and concrete research* 35.2 (2005), pp. 296–300.

[363] Rosa L Santoni, Jeb S Tingle, and Steve L Webster. "Engineering properties of sand-fiber mixtures for road construction". In: *Journal of geotechnical and geoenvironmental engineering* 127.3 (2001), pp. 258–268.

[364] Sidney Mindess. *Developments in the Formulation and Reinforcement of Concrete*. Elsevier, 2014.

[365] ASTM C495. "Standard Test Method for Compressive Strength of Lightweight Insulating Concrete". In: *ASTM International, West Conshohocken, PA* (2012).

[366] ASTM C469. "Standard Test Method for Static Modulus of Elasticity and Poisson's Ratio of Concrete in Compression". In: *ASTM International, West Conshohocken, PA* (2014).

[367] ASTM C490. "Standard Practice for Use of Apparatus for the Determination of Length Change of Hardened Cement Paste, Mortar, and Concrete1". In: *ASTM International, West Conshohocken, PA* (2017).

[368] A Momayez, MR Ehsani, AA Ramezanianpour, and H Rajaie. "Comparison of methods for evaluating bond strength between concrete substrate and repair materials". In: *Cement and concrete research* 35.4 (2005), pp. 748–757.

[369] ASTM C882. "tandard Test Method for Bond Strength of Epoxy-Resin Systems Used With Concrete By Slant Shear". In: *ASTM International, West Conshohocken, PA* (2013).

[370] Muhammad Mamun and Vivek Bindiganavile. "Drop-weight impact response of fibre reinforced cement based foams". In: *International Journal of Protective Structures* 1.3 (2010), pp. 409–424.

[371] R. Barnes. *GCG 7 Foamed concrete: application and specification*. Concrete Society, Camberley, UK, 2009.

[372] Jianming Gao, Wei Sun, and Keiji Morino. "Mechanical properties of steel fiber-reinforced, high-strength, lightweight concrete". In: *Cement and Concrete Composites* 19.4 (1997), pp. 307–313.

[373] Rudolph C Valore et al. "Cellular concretes Part 2 physical properties". In: *Journal Proceedings*. Vol. 50. 6. 1954, pp. 817–836.

[374] Robert Douglas Hardy, Moo Yul Lee, and David R Bronowski. *Laboratory constitutive characterization of cellular concrete.* Tech. rep. Sandia National Laboratories, 2004.

[375] Teruhisa Masada, Shad M. Sargand, Basel Abdalla, and J. Ludwig Figueroa. *Material Properties for Implementation of Mechanistic-Empirical (M-E) Pavement Design Procedures*. Technical Bulletin. Ohio Research Institute for Transportation and the Environment (ORITE), 2004.

[376] Charles K Nmai. "New foaming agent for CLSM applications". In: *Concrete International* 19.4 (1997), pp. 44–47.

[377] Halina Ziembicka. "Effect of micropore structure on cellular concrete shrinkage". In: *cement and concrete research* 7.3 (1977), pp. 323–332.

[378] A Georgiades, CH Ftikos, and J Marinos. "Effect of micropore structure on autoclaved aerated concrete shrinkage". In: *Cement and concrete research* 21.4 (1991), pp. 655–662.

[379] Ömer Z Cebeci. "Pore structure of air-entrained hardened cement paste". In: *Cement and concrete research* 11.2 (1981), pp. 257–265.

[380] Helmut Weigler and Sieghart Karl. "Structural lightweight aggregate concrete with reduced density—lightweight aggregate foamed concrete". In: *International Journal of Cement Composites and Lightweight Concrete* 2.2 (1980), pp. 101–104.

[381] PE Regan and A Reza Arasteh. "Lightweight aggregate foamed concrete". In: *Structural Engineer* 68 (1990), pp. 167–73.

[382] Veronique Baroghel-Bouny and Ali Kheirbek. "Effect of mix-parameters on autogenous deformations of cement pastes-Microstructural interpretations". In: *Proceedings of the international RILEM Workshop, Paris*. 2000, pp. 115–141.

[383] RD Browne. "Thermal movement of concrete". In: *Concrete* 6.11 (1972), pp. 51–53.

[384] Masao Kuroda, Tomohide Watanabe, and Nariaki Terashi. "Increase of bond strength at interfacial transition zone by the use of fly ash". In: *Cement and Concrete Research* 30.2 (2000), pp. 253–258.

[385] Gengying Li. "A new way to increase the long-term bond strength of new-to-old concrete by the use of fly ash". In: *Cement and concrete research* 33.6 (2003), pp. 799–806.

[386] Thomas L Saaty. "Analytic hierarchy process". In: *Encyclopedia of Biostatistics* 1 (2005).

[387] Mohammad Rezaei and Vivek Bindiganavile. *Application of Cement-Based Foams for Narrow-Trench Backfilling*. Submitted to the journal of Road Materials and Pavement Design. 2019.

[388] Vinicius Afonso Velasco Rios, Thomas W Johnson, and Leila Hashemian. "Laboratory investigation of using foam grout as micro-trench backfilling material in cold regions". In: *TAC 2018: Innovation and Technology: Evolving Transportation-2018 Conference and Exhibition of the Transportation Association of Canada*. 2018.

[389] František Škvára, Tomáš Jílek, and Lubomír Kopeckỳ. "Geopolymer materials based on fly ash". In: *Ceram.-Silik* 49.3 (2005), pp. 195–204.

[390] Shao-dong Wang. "Review of recent research on alkali-activated concrete in China". In: *Magazine of concrete research* 43.154 (1991), pp. 29–35.

[391] John L Provis and Jannie SJ Van Deventer. *Alkali activated materials: state-of-the-art report, RILEM TC 224-AAM*. Vol. 13. Springer Science & Business Media, 2013.

[392] Vivek Bindiganavile, Jose RA Goncalves, and Yaman Boluk. "Crack Growth Resistance in Fibre Reinforced Geopolymer Concrete Exposed to Sustained Extreme Temperatures". In: *Key Engineering Materials*. Vol. 711. Trans Tech Publ. 2016, pp. 511–518.

[393] Hao Wang. "Analysis of tire-pavement interaction and pavement responses using a decoupled modeling approach". PhD thesis. University of Illinois at Urbana-Champaign, 2011.

[394] Giulia Masi, William DA Rickard, Les Vickers, Maria Chiara Bignozzi, and Arie Van Riessen. "A comparison between different foaming methods for the synthesis of light weight geopolymers". In: *Ceramics International* 40.9 (2014), pp. 13891–13902.

[395] Kiatsuda Somna, Chai Jaturapitakkul, Puangrat Kajitvichyanukul, and Prinya Chindaprasirt. "NaOH-activated ground fly ash geopolymer cured at ambient temperature". In: *Fuel* 90.6 (2011), pp. 2118–2124.

[396] R Arellano Aguilar, O Burciaga Díaz, and JI Escalante García. "Lightweight concretes of activated metakaolin-fly ash binders, with blast furnace slag aggregates". In: *Construction and building materials* 24.7 (2010), pp. 1166–1175.

[397] J Wongpa, K Kiattikomol, C Jaturapitakkul, and P Chindaprasirt. "Compressive strength, modulus of elasticity, and water permeability of inorganic polymer concrete". In: *Materials & Design* 31.10 (2010), pp. 4748–4754.

[398] A Nazari, F Pacheco-Torgal, A Cevik, and JG Sanjayan. "Prediction of the compressive strength of alkali-activated geopolymeric concrete binders by neuro-fuzzy modeling: a case studys". In: *Handbook of Alkali-Activated Cements, Mortars and Concretes*. Elsevier, 2015, pp. 217–233.

[399] Mehrzad Mohabbi Yadollahi, Ahmet Benli, and Ramazan Demirboğa. "The effects of silica modulus and aging on compressive strength of pumice-based geopolymer composites". In: *Construction and Building Materials* 94 (2015), pp. 767–774.

[400] Ross P Williams and Arie Van Riessen. "Determination of the reactive component of fly ashes for geopolymer production using XRF and XRD". In: *Fuel* 89.12 (2010), pp. 3683–3692.

[401] Jadambaa Temuujin, Arie van Riessen, and KJD MacKenzie. "Preparation and characterisation of fly ash based geopolymer mortars". In: *Construction and Building Materials* 24.10 (2010), pp. 1906–1910.

[402] Zuhua Zhang, John L Provis, Andrew Reid, and Hao Wang. "Mechanical, thermal insulation, thermal resistance and acoustic absorption properties of geopolymer foam concrete". In: *Cement and Concrete Composites* 62 (2015), pp. 97–105.

[403] Ze Liu, Ning-ning Shao, Dong-min Wang, Jun-feng Qin, Tian-yong Huang, Wei Song, et al. "Fabrication and properties of foam geopolymer using circulating fluidized bed combustion fly ash". In: *International Journal of Minerals, Metallurgy, and Materials* 21.1 (2014), pp. 89–94.

[404] Keun-Hyeok Yang, Kyung-Ho Lee, Jin-Kyu Song, and Min-Ho Gong. "Properties and sustainability of alkali-activated slag foamed concrete". In: *Journal of Cleaner Production* 68 (2014), pp. 226–233.

[405] Monita Olivia and Hamid Nikraz. "Properties of fly ash geopolymer concrete designed by Taguchi method". In: *Materials & Design (1980-2015)* 36 (2012), pp. 191–198.

[406] Ana M Fernandez-Jimenez, Angel Palomo, and Cecilio Lopez-Hombrados. "Engineering properties of alkali-activated fly ash concrete". In: *ACI Materials Journal* 103.2 (2006), p. 106.

[407] Michael Yong Jing Liu, U Johnson Alengaram, Mohd Zamin Jumaat, and Kim Hung Mo. "Evaluation of thermal conductivity, mechanical and transport properties of lightweight aggregate foamed geopolymer concrete". In: *Energy and Buildings* 72 (2014), pp. 238–245.

[408] Thang T Nguyen, Ha H Bui, Tuan D Ngo, Giang D Nguyen, Markus U Kreher, and Felix Darve. "A micromechanical investigation for the effects of pore size and its distribution on geopolymer foam concrete under uniaxial compression". In: *Engineering Fracture Mechanics* 209 (2019), pp. 228–244.

[409] Ehsan Mohseni. "Assessment of Na2SiO3 to NaOH ratio impact on the performance of polypropylene fiber-reinforced geopolymer composites". In: *Construction and Building Materials* 186 (2018), pp. 904–911.

[410] J Clarke, C Peaston, and N Swannell. "Guidance on the use of Macro-synthetic-fiber reinforced Concrete". In: *The Concrete Society* 65 (2007), pp. 1–2.

[411] Vahid Afroughsabet and Togay Ozbakkaloglu. "Mechanical and durability properties of high-strength concrete containing steel and polypropylene fibers". In: *Construction and building materials* 94 (2015), pp. 73–82.

[412] Prinya Chindaprasirt and Ubolluk Rattanasak. "Synthesis of polypropylene fiber/high-calcium fly ash geopolymer with outdoor heat exposure". In: *Clean Technologies and Environmental Policy* 19.7 (2017), pp. 1985–1992.

[413] Alan E Richardson. "Compressive strength of concrete with polypropylene fibre additions". In: *Structural survey* 24.2 (2006), pp. 138–153.

[414] K Vijai, R Kumutha, and BG Vishnuram. "Properties of glass fibre reinforced geopolymer concrete composites". In: (2012).

[415] H Mazaheripour, S Ghanbarpour, SH Mirmoradi, and I Hosseinpour. "The effect of polypropylene fibers on the properties of fresh and hardened lightweight self-compacting concrete". In: *Construction and Building Materials* 25.1 (2011), pp. 351–358.

[416] Teruhisa Masada, Shad M Sargand, Basel Abdalla, and J Ludwig Figueroa. *Material properties for implementation of mechanistic-empirical (ME) pavement design procedures*. Tech. rep. 2004.

[417] Zahra Abdollahnejad, Zuhua Zhang, Hao Wang, and Mohammad Mastali. "Comparative study on the drying shrinkage and mechanical properties of geopolymer foam concrete incorporating different dosages of fiber, sand and foam agents". In: *High Tech Concrete: Where Technology and Engineering Meet*. Springer, 2018, pp. 42–48.

[418] Ailar Hajimohammadi, Tuan Ngo, and Alireza Kashani. "Sustainable one-part geopolymer foams with glass fines versus sand as aggregates". In: *Construction and Building Materials* 171 (2018), pp. 223–231.

[419] Charoenchai Ridtirud, Prinya Chindaprasirt, and Kedsarin Pimraksa. "Factors affecting the shrinkage of fly ash geopolymers". In: *International Journal of Minerals, Metallurgy, and Materials* 18.1 (2011), pp. 100–104.

[420] Steenie Wallah and B Vijaya Rangan. "Low-calcium fly ash-based geopolymer concrete: long-term properties". In: (2006).

[421] Steenie Edward Wallah. "Drying shrinkage of heat-cured fly ash-based geopolymer concrete". In: *Modern Applied Science* 3.12 (2009), pp. 14–21.

[422] Anol K Mukhopadhyay, Siddharth Neekhra, and Dan G Zollinger. "Preliminary characterization of aggregate coefficient of thermal expansion and gradation for paving concrete". In: (2004).

[423] Shuguang Hu, Hongxi Wang, Gaozhan Zhang, and Qingjun Ding. "Bonding and abrasion resistance of geopolymeric repair material made with steel slag". In: *Cement and concrete composites* 30.3 (2008), pp. 239–244.

[424] Huajun Zhu, Zuhua Zhang, Fenggan Deng, and Yalong Cao. "The effects of phase changes on the bonding property of geopolymer to hydrated cement". In: *Construction and Building Materials* 48 (2013), pp. 124–130.

[425] Zahra Abdollahnejad, F Pacheco-Torgal, T Félix, W Tahri, and J Barroso Aguiar. "Mix design, properties and cost analysis of fly ash-based geopolymer foam". In: *Construction and Building Materials* 80 (2015), pp. 18–30.

[426] O Senbu and E Kamada. "Mechanism of frost deterioration of ACC, advances in autoclaved aerated concrete". In: *3rd RILEM International Symposium on Autoclaved Aerated Concrete, Odense, Demark*. 1992, pp. 153–156.

[427] S. Aroni. *Autoclaved aerated concrete: Properties, testing, and design: RILEM recommended practice.* Tech. rep. RILEM Technical Committee 78-MCA., and 51-ALC. London: E and FN Spon, 1993.

[428] CA Roulet. "Expansion of aerated concrete due to frost−Determination of critical saturation". In: *Proceedings Autoclaved Aerated Concrete, Moisture and Properties. Amsterdam: Elsevier* (1983), pp. 157–69.

[429] E Kamada, Y Koh, and M Tapata. "Frost deterioration of cellular concrete". In: *3rd International Conference on the Durability of Building Materials and Components, Espoo, Finland*. Vol. 3. 1984, pp. 372–382.

[430] Erfan A Amiri, James R Craig, and Barret L Kurylyk. "A theoretical extension of the soil freezing curve paradigm". In: *Advances in water resources* 111 (2018), pp. 319–328.

[431] SİMGE Andolsun. "A study on material properties of autoclaved aerated concrete (AAC) and its complementary wall elements: their compatibility in contemporary and historical wall sections." MA thesis. Department of Architecture, Middle East Technical University, 2006.

[432] Frederick Measham Lea and Perter C Hewlett. *Lea's chemistry of cement and concrete*. Amold Press, London, 1998. Chap. 7.

[433] O. Senbu and E. Kamada. "Mechanism and evaluation method of frost deterioration of cellular concrete, durability of building materials and components". In: *J.M. Baker, P.J. Nixon, A.J. Majumdar, H. Davies (Eds.), Proceedings of the Fifth International Conference*. 1990, pp. 241–246.

[434] Agnes Nagy. "Determination of E-modulus of young concrete with nondestructive method". In: *Journal of materials in civil engineering* 9.1 (1997), pp. 15–20.

[435] Byung Jae Lee, Seong-Hoon Kee, Taekeun Oh, and Yun-Yong Kim. "Effect of cylinder size on the modulus of elasticity and compressive strength of concrete from static and dynamic tests". In: *Advances in Materials Science and Engineering* 2015 (2015).

[436] O Bortnovsky, K Dvorakova, P Roubicek, J Bousek, Z Prudkova, and P Baxa. "Development, properties and production of geopolymers based on secondary raw materials". In: *Alkali activated materials–research, production and utilization 3rd conference, Prague, Czech Republic*. 2007, pp. 83–96.

[437] R Slavik, V Bednarik, M Vondruska, and A Nemec. "Preparation of geopolymer from fluidized bed combustion bottom ash". In: *Journal of Materials Processing Technology* 200.1-3 (2008), pp. 265–270.

[438] Robert Brooks, Mozhgan Bahadory, Fernando Tovia, and Hossein Rostami. "Properties of alkali-activated fly ash: high performance to lightweight". In: *International journal of sustainable engineering* 3.3 (2010), pp. 211–218.

[439] Yawei Fu, Liangcai Cai, and Wu Yonggen. "Freeze–thaw cycle test and damage mechanics models of alkali-activated slag concrete". In: *Construction and Building Materials* 25.7 (2011), pp. 3144–3148.

[440] J Shi. "Response of geopolymer concrete to environmental loads". PhD thesis. PhD Thesis, Louisiana Tech University Ruston, LA, 2012.

[441] Tarja Häkkinen. *Properties of alkali-activated slag concrete*. Valtion teknillinen tutkimuskeskus. Betoni-ja silikaattitekniikan laboratorio, 1986.

[442] Ahmet Çavdar. "Investigation of freeze–thaw effects on mechanical properties of fiber reinforced cement mortars". In: *Composites Part B: Engineering* 58 (2014), pp. 463–472.

[443] Peter M Gifford and Jack E Gillott. "Freeze-thaw durability of activated blast furnace slag cement concrete". In: *Materials Journal* 93.3 (1996), pp. 242–245.

[444] KD Hjelmstad, J Kim, and QH Zuo. "Finite element procedures for three-dimensional pavement analysis". In: *Proceedings of the 1997 Airfield Pavement Conference*. ASCE. 1997.

[445] Jiwon Kim and William G Buttlar. "Analysis of reflective crack control system involving reinforcing grid over base-isolating interlayer mixture". In: *Journal of Transportation Engineering* 128.4 (2002), pp. 375–384.

[446] PJ Yoo, Imad L Al-Qadi, MA Elseifi, and I Janajreh. "Flexible pavement responses to different loading amplitudes considering layer interface condition and lateral shear forces". In: *The International Journal of Pavement Engineering* 7.1 (2006), pp. 73–86.

[447] Imad L Al-Qadi, Pyeong Jun Yoo, Mostafa A Elseifi, and Susan Nelson. "Creep behavior of hot-mix asphalt due to heavy vehicular tire loading". In: *Journal of engineering mechanics* 135.11 (2009), pp. 1265–1273.

[448] Raj V Siddharthan, Jian Yao, and Peter E Sebaaly. "Pavement strain from moving dynamic 3D load distribution". In: *Journal of Transportation Engineering* 124.6 (1998), pp. 557–566.

[449] Hao Wang, Imad L Al-Qadi, and Ilinca Stanciulescu. "Simulation of tyre–pavement interaction for predicting contact stresses at static and various rolling conditions". In: *International Journal of Pavement Engineering* 13.4 (2012), pp. 310–321.

[450] Zejiao Dong and Xianyong Ma. "Analytical solutions of asphalt pavement responses under moving loads with arbitrary non-uniform tire contact pressure and irregular tire imprint". In: *Road Materials and Pavement Design* 19.8 (2018), pp. 1887–1903.

[451] Morrison Hershfield Limited. "Guidelines on Valuations of Tangible Capital Assets for PSAB 3150". In: *Alberta Municipal Affairs, Edmonton, Alberta* (2008).

[452] Ahmed I Nassar, Mahmoud Khashaa Mohammed, Nicholas Thom, and Tony Parry. "Mechanical, durability and microstructure properties of Cold Asphalt Emulsion Mixtures with different types of filler". In: *Construction and Building Materials* 114 (2016), pp. 352–363.

[453] F Allou, M Takarli, F Dubois, C Petit, and J Absi. "Numerical finite element formulation of the 3D linear viscoelastic material model: Complex Poisson's ratio of bituminous mixtures". In: *Archives of Civil and Mechanical Engineering* 15.4 (2015), pp. 1138–1148.

[454] NH Thom. *How Long Does a Long-Life Pavement Last*. Tech. rep. NCPE 03/1. University of Nottingham, 2003.

[455] Sergey Averyanov. "Analysis of construction experience of using lightweight cellular concrete as a subbase material". MA thesis. University of Waterloo, 2018.

[456] Cindy K Estakhri and Joe W Button. "Test methods for evaluation of cold-applied bituminous patching mixtures". In: *Transportation research record* 1590.1 (1997), pp. 10–16.

[457] T Warren Liao, PJ Egbelu, BR Sarker, and SS Leu. "Metaheuristics for project and construction management–A state-of-the-art review". In: *Automation in construction* 20.5 (2011), pp. 491–505.

[458] Parviz Ghoddousi, Ehsan Eshtehardian, Shirin Jooybanpour, and Ashtad Javanmardi. "Multi-mode resource-constrained discrete time–cost-resource optimization in project scheduling using non-dominated sorting genetic algorithm". In: *Automation in construction* 30 (2013), pp. 216–227.

[459] Bryan Christopher Que. "Incorporating practicability into genetic algorithm-based time-cost optimization". In: *Journal of construction engineering and management* 128.2 (2002), pp. 139–143.

[460] MC Vorster, Yvan J Beliveau, and T Bafna. "Linear scheduling and visualization". In: *Transportation Research Record* 1351 (1992).

[461] Sameh Monir El-Sayegh. "Linear construction planning model (LCPM): A new model for planning, and scheduling linear construction projects." In: (1999).

[462] Raj Kapur Shah. "A new approach for automation of location-based earthwork scheduling in road construction projects". In: *Automation in construction* 43 (2014), pp. 156–169.

[463] Maged E Georgy. "Evolutionary resource scheduler for linear projects". In: *Automation in Construction* 17.5 (2008), pp. 573–583.

[464] Atilla Damci, David Arditi, and Gul Polat. "Resource leveling in line-of-balance scheduling". In: *Computer-Aided Civil and Infrastructure Engineering* 28.9 (2013), pp. 679–692.

[465] Mario Vanhoucke and Dieter Debels. "The discrete time/cost trade-off problem: extensions and heuristic procedures". In: *Journal of Scheduling* 10.4-5 (2007), pp. 311–326.

[466] Po-Han Chen and Haijie Weng. "A two-phase GA model for resource-constrained project scheduling". In: *Automation in Construction* 18.4 (2009), pp. 485–498.

[467] Peng Wuliang and Wang Chengen. "A multi-mode resource-constrained discrete time–cost tradeoff problem and its genetic algorithm based solution". In: *International Journal of Project Management* 27.6 (2009), pp. 600–609.

[468] Tarek Hegazy. "Optimization of resource allocation and leveling using genetic algorithms". In: *Journal of construction engineering and management* 125.3 (1999), pp. 167–175.

[469] Georgios K Koulinas and Konstantinos P Anagnostopoulos. "Construction resource allocation and leveling using a threshold accepting–Based hyperheuristic algorithm". In: *Journal of construction engineering and management* 138.7 (2011), pp. 854–863.

[470] Sou-Sen Leu and Chung-Huei Yang. "GA-based multicriteria optimal model for construction scheduling". In: *Journal of construction engineering and management* 125.6 (1999), pp. 420–427.

[471] Ahmed B Senouci and Neil N Eldin. "Use of genetic algorithms in resource scheduling of construction projects". In: *Journal of Construction Engineering and Management* 130.6 (2004), pp. 869–877.

[472] Mario Vanhoucke. "Work continuity constraints in project scheduling". In: *Journal of Construction Engineering and Management* 132.1 (2006), pp. 14–25.

[473] Robert B Harris and Photios G Ioannou. "Scheduling projects with repeating activities". In: *Journal of construction engineering and management* 124.4 (1998), pp. 269–278.

[474] George S Birrell. "Construction planning—beyond the critical path". In: *Journal of the Construction Division* 106.3 (1980), pp. 389–407.

[475] David Arditi and M Zeki Albulak. "Line-of-balance scheduling in pavement construction". In: *Journal of Construction Engineering and Management* 112.3 (1986), pp. 411–424.

[476] Yuanjie Tang, Rengkui Liu, Futian Wang, Quanxin Sun, and Amr A Kandil. "Scheduling optimization of linear schedule with constraint programming". In: *Computer-Aided Civil and Infrastructure Engineering* 33.2 (2018), pp. 124–151.

[477] Yuanjie Tang, Rengkui Liu, and Quanxin Sun. "Schedule control model for linear projects based on linear scheduling method and constraint programming". In: *Automation in construction* 37 (2014), pp. 22–37.

[478] Erik Leuven Demeulemeester and Willy S Herroelen. *Project scheduling: a research handbook*. Vol. 49. Springer Science & Business Media, 2006.

[479] Jin-qiang Geng, Li-ping Weng, and Si-hong Liu. "An improved ant colony optimization algorithm for nonlinear resource-leveling problems". In: *Computers & Mathematics with Applications* 61.8 (2011), pp. 2300–2305.

[480] Julia Rieck, Jürgen Zimmermann, and Thorsten Gather. "Mixed-integer linear programming for resource leveling problems". In: *European Journal of Operational Research* 221.1 (2012), pp. 27–37.

[481] Christos Kyriklidis, Vassilios Vassiliadis, Konstantinos Kirytopoulos, and Georgios Dounias. "Hybrid nature-inspired intelligence for the resource leveling problem". In: *Operational Research* 14.3 (2014), pp. 387–407.

[482] MA Younis and B Saad. "Optimal resource leveling of multi-resource projects". In: *Computers & industrial engineering* 31.1-2 (1996), pp. 1–4.

[483] Jose Luis Ponz-Tienda, Víctor Yepes, Eugenio Pellicer, and Joaquin Moreno-Flores. "The resource leveling problem with multiple resources using an adaptive genetic algorithm". In: *Automation in Construction* 29 (2013), pp. 161–172.

[484] I-Tung Yang and Chi-Yi Chang. "Stochastic resource-constrained scheduling for repetitive construction projects with uncertain supply of resources and funding". In: *International Journal of Project Management* 23.7 (2005), pp. 546–553.

[485] MH Elwany, IE Korish, M Aly Barakat, and SM Hafez. "Resource smoothening in repetitive projects". In: *Computers & industrial engineering* 35.3-4 (1998), pp. 415–418.

[486] Gunnar Lucko. "Integrating efficient resource optimization and linear schedule analysis with singularity functions". In: *Journal of Construction Engineering and Management* 137.1 (2010), pp. 45–55.

[487] Lihui Zhang, Yaping Tang, and Jianxun Qi. "Resource leveling based on backward controlling activity in line of balance". In: *Mathematical Problems in Engineering* 2017 (2017).

[488] V Bhosale, SS Shastri, and MA Khandare. "A Review of Genetic Algorithm used for optimizing scheduling of Resource Constraint construction projects". In: *International Research Journal of Engineering and Technology* 4.5 (2017), pp. 2869–2872.

[489] Atilla Damci and Gul Polat. "Impacts of different objective functions on resource leveling in construction projects: a case study". In: *Journal of civil engineering and management* 20.4 (2014), pp. 537–547.

[490] Atilla Damci, David Arditi, and Gul Polat. "Impacts of different objective functions on resource leveling in Line-of-Balance scheduling". In: *KSCE Journal of Civil Engineering* 20.1 (2016), pp. 58–67.

[491] Jan Węglarz, Joanna Józefowska, Marek Mika, and Grzegorz Waligóra. "Project scheduling with finite or infinite number of activity processing modes–A survey". In: *European Journal of operational research* 208.3 (2011), pp. 177–205.

[492] BM Baker. "Cost/time trade-off analysis for the critical path method: A derivation of the network flow approach". In: *Journal of the Operational Research Society* 48.12 (1997), pp. 1241–1244.

[493] Heng Li and Peter Love. "Using improved genetic algorithms to facilitate time-cost optimization". In: *Journal of Construction Engineering and management* 123.3 (1997), pp. 233–237.

[494] Hojjat Adeli and Asim Karim. "Scheduling/cost optimization and neural dynamics model for construction". In: *Journal of Construction Engineering and Management* 123.4 (1997), pp. 450–458.

[495] Saleh A Mubarak. *Construction project scheduling and control*. John Wiley & Sons, 2015.

[496] Pandelis G Ipsilandis. "Multiobjective linear programming model for scheduling linear repetitive projects". In: *Journal of Construction Engineering and Management* 133.6 (2007), pp. 417–424.

[497] Tarek Hegazy and Nagib Wassef. "Cost optimization in projects with repetitive nonserial activities". In: *Journal of Construction Engineering and Management* 127.3 (2001), pp. 183–191.

[498] Khalied Hesham Hyari, Khaled El-Rayes, and Mohammad El-Mashaleh. "Automated trade-off between time and cost in planning repetitive construction projects". In: *Construction Management and Economics* 27.8 (2009), pp. 749–761.

[499] Luong Duc Long and Ario Ohsato. "A genetic algorithm-based method for scheduling repetitive construction projects". In: *Automation in Construction* 18.4 (2009), pp. 499–511.

[500] A Samer Ezeldin and Ahmed Soliman. "Hybrid time-cost optimization of nonserial repetitive construction projects". In: *Journal of Construction Engineering and Management* 135.1 (2009), pp. 42–55.

[501] Tarek Hegazy, Ahmed Elhakeem, and Emad Elbeltagi. "Distributed scheduling model for infrastructure networks". In: *Journal of Construction Engineering and Management* 130.2 (2004), pp. 160–167.

[502] Jared L Cohon. *Multiobjective programming and planning*. Vol. 140. Courier Corporation, 2004.

[503] Jimmie W Hinze. *Construction planning and scheduling*. Pearson Higher Ed, 2011.

[504] Rene A Yamin and David J Harmelink. "Comparison of linear scheduling model (LSM) and critical path method (CPM)". In: *Journal of Construction Engineering and Management* 127.5 (2001), pp. 374–381.

[505] David Arditi, Onur B Tokdemir, and Kangsuk Suh. "Challenges in line-of-balance scheduling". In: *Journal of construction engineering and management* 128.6 (2002), pp. 545–556.

[506] Kalyanmoy Deb, Amrit Pratap, Sameer Agarwal, and TAMT Meyarivan. "A fast and elitist multiobjective genetic algorithm: NSGA-II". In: *IEEE transactions on evolutionary computation* 6.2 (2002), pp. 182–197.

[507] Calin Popescu and John D Borcherding. *How to use CPM in practice*. Department of Civil Engineering, University of Texas at Austin, 1975.

[508] DD Goldberg. "Genetic Algorithms in Search, Optimization, and Machine Learning Genetic Algorithms in Search, Optimization, and Machine Learning, 1989". In: *IEEJ Transactions on Electronics, Information and Systems* 126.7 (2006), pp. 857–864.

[509] Md Toihidul Islam, Rachel Chan, and Vivek Bindiganavile. "Stress rate sensitivity of stone masonry units bound with fibre reinforced hydraulic lime mortar". In: *Materials and structures* 45.5 (2012), pp. 765–776.